A MODULATED-ENERGY-DISSIPATION MANIPULATOR AND APPLICATION TO SUPPRESSING HUMAN ARM TREMOR

by

SCOTT MARCIL MAXWELL

B. S. in Mechanical Engineering, University of California, Davis (1984)

S.M. in Mechanical Engineering, University of California, Davis (1986)

S.M. in Management, Massachusetts Institute of Technology (1990)

SUBMITTED TO THE DEPARTMENT OF
MECHANICAL ENGINEERING
IN PARTIAL FULFILLMENT OF THE REQUIREMENTS
FOR THE DEGREE OF

DOCTOR OF PHILOSOPHY

at the

MASSACHUSETTS INSTITUTE OF TECHNOLOGY

JUNE 1990

Signature of Author_____
Department of Mechanical Engineering
May 17, 1990

Certified by_____
Michael J. Rosen
Thesis Supervisor

Accepted by_____
Ain A. Sonin
Chairman, Department Committee on Graduate Studies

A MODULATED-ENERGY-DISSIPATION MANIPULATOR AND APPLICATION TO SUPPRESSING HUMAN ARM TREMOR

by

SCOTT MARCIL MAXWELL

Submitted to the Department of Mechanical Engineering on May 17, 1990 in partial fulfillment of the requirements for the Degree of Doctor of Philosophy

Abstract

This program of analysis, design, and research contributes theoretically and experimentally to the development of controlled orthotics meant to reduce the difficulty encountered by tremor-disabled individuals in performing the tasks of daily living. Prior studies have shown that application of damping across joints of the human arm reduces pathological tremor. This research expands our progress toward effective functional tremor management through the development and testing of a novel six degree-of-freedom modulated-energy-dissipation (MED) manipulator for use as an orthosis simulator. The manipulator linkage design is a 6R serial link device. The three distal degrees of freedom are arranged in the form of a novel gimbal configuration. Two of the proximal degrees of freedom are mechanically coupled through a four bar mechanism providing, in effect, two rotations and a near-prismatic joint. This design was driven largely by our goal of building a system with a diagonal Jacobian matrix to provide end-point force-velocity colinearity. The manipulandum applies its 6-dof load at a single point of attachment to the human forearm. The orthosis simulator system incorporates the MED manipulator, control electronics, control software run on a PC/AT computer, a display for target tracking experiments, and a specially designed subject support chair. Theoretical contributions include the development of a general theory for modulated-energy-dissipation spatial devices (manipulators). Initial experimental results have been obtained from two tremor-impaired subjects and one able-bodied subject.

Thesis Supervisor: Dr. Michael J. Rosen
Title: Principal Research Scientist

Members of the Thesis Committee

Dr. M.J. Rosen (Chairman)
Principal Research Scientist
Department of Mechanical Engineering

Dr. W.K. Durfee
Associate Professor of Mechanical Engineering
Department of Mechanical Engineering

Dr. W.C. Flowers
Professor of Mechanical Engineering
Department of Mechanical Engineering

Dr. H. West
Soderberg Assistant Professor of Mechanical Engineering
Department of Mechanical Engineering

Acknowledgements

Many individuals have signifigantly contributed to the work presented in this thesis. I am greatly appreciative of all their hard work, support (even enthusiasm at times), and guidance over the course of this project.

Mike Rosen, my thesis advisor and committee chairman, gave me a very long rope from which to develop my professional skills in an individual manner. His respect and confidence in my work gave me inspiration from which to try new ideas. Mike always had six ideas to solve a technical problem and his input substantially guided my thoughts. Financially, Mike's support allowed me to work on this research without worry about funding the next semester.

Each member of my thesis committee; Will Durfee, Woody Flowers, and Harry West; was helpful in all aspects of this project. They gave me their time, but more importantly their thoughts and critiques, from which this project was partially formed.

Neville Hogan's ideas on controlling impedance directions helped shape the development of MED manipulator theory. The Teaching Assistantship he gave me was a wonderful opportunity to understand his physical system insights while helping fund my first semester at MIT.

Dr. Mindy Aisen, from the Burke Rehabilitation Center, found the subjects for our human subject experiments and donated her time to help determine the efficacy of the MED arm in managing tremor.

Norm Berube built most of the manipulator hardware, spending 12, 14 or 16 hours a day for three months to help see this project to completion. Norm's good nature, advice, and comments not only added to my project's development, but also added to my life at M.I.T. Norm taught me manufacturing methods that simplified the development of the MED manipulator and added significantly to my design knowledge. Norm is not only a good machinist, but he also has a terrific physical insight. I can only hope that more mechanical engineering students are exposed to Norm.

Bob Samuel donated his time to help complete the machining of the manipulandum. Bob has helped me throughout this project to better understand design and machining.

Mike Rosen's "tremor group" helped me significantly throughout the years. Dov Adelstein was always there to help when I needed it. Dov either knew exactly what I needed or where to find it. Steve Beringhause helped develop some of the C programs used in the MED arm and became a good friend along the way. Ivan Baiges developed the spectral analysis software used in the tracking experiments and Sheila Eglowstein helped transport and set up the equipment for the human subject experiments.

A number of undergraduate research assistants have assisted throughout the project. Stacy Ho developed most of the electronics for the manipulator, helped calibrate the force/torque sensor and potentiometers, and helped during the human subject experiments. Stacy is the most dilligent worker I have ever seen (including graduate students) and I am very thankful that he chose to work on this project. Jessie Wong was also very helpful in all aspects of this project. She developed the set of limb-coupling cuffs, performed experiments, designed a number of attachment handles for the one-degree-of-freedom

testbed, and helped with photography. Mohnjit Jolly designed and built part of the housing for the electronics box, Ed Lovelace designed and built the first one-degree-of-freedom testbed, and Susan Huang designed a low-inertia kinematic linkage for studying human tremor.

Ralph Burgess was instrumental in troubleshooting our electronic circuits. Whenever we had trouble in the development of the circuitry, Ralph always had an idea of what was wrong and how to fix it.

Karl Ousterhaut helped me think through the force/torque sensor design. His strain gage installation kit and personal instruction saved me many hours.

Crispin Miller's instruction on making limb-couplers with orthoplast was a fantastic help to this project. Bruce Kay and Denis Ragoon helped me perform TRACK experiments. Ted Clancy was very helpful with an array of ideas and help in the last year of this project. And Pete, Keta, Pat, Mike, Eric, Don, John, Andy, Bob, and the rest of the researchers that have passed (or are passing) through "the lab" in the past four years each had a hand in this thesis directly or indirectly.

I have had a number of officemates (Tripp, Grace, Jeff, George, Scott, Dan, Sue, and Dennis) while at MIT. Each has added to my enjoyment of the MIT experience.

The office staff; Marie, Pat, Elizabeth, and Sylvia; ably helped keet the office in order and the material orders flowing. Marie, especially, has been a wonderful friend over the the years.

Visiting the administrative staff office of Bill, John, Maureen, and Marie proved to be a great work break. They always had a smile to share. All for one and one for all!

Jane Hoffman, my bride-to-be, has put up with a very large pain-in-the-neck over the last two years. She has been a relentless inspiration that yes, someday, this project would be completed. Her help in the last month pulling this document together has been tremendous. I look forward with great anticipation to our years together.

Finally my family, especially my mother, has been a great source of strength for me over the years. I could never begin to recount the number of times I have been inspired by her confidence and leadership. And to my sister, Sarah, the score is 4-2. Keep working!

Thank-you, everyone, for all your help

Scott M. Maxwell

This work was performed in the Evelyn E. and Eric P. Newman Laboratory for Biomechanics and Human Rehabilitation. It was funded by The Department of Education NIDRR grant number H133E80024 and the Burke Rehabilitation Center, White Plains, NY.

Contents

List of Figures

List of Tables

Nomenclature

$\mathbf{m}$:	The 6 x 1 vector of potentiometer angular position measurements
$\dot{\mathbf{m}}$:	The 6 x 1 vector of potentiometer angular velocity measurements
$\mathbf{q}$:	The 6 x 1 vector of manipulator joint angular positions
$\dot{\mathbf{q}}$:	The 6 x 1 vector of manipulator joint angular velocities
τ:	The 6 x 1 vector of manipulator joint torques
$\mathbf{v}$:	The 6 x 1 vector of manipulator endpoint velocities
$\mathbf{A_i}$:	The 4 x 4 Denavit-Hartenberg transformation matrix between coordinate system i-1 and Coordinate System i
$\mathbf{T_6}$:	The 4 x 4 transformation between the world coordinate system and the manipulator endpoint coordinate system
$\mathbf{J}$:	The 6 x 6 manipulator jacobian matrix
$\mathbf{J_a}$:	The 6 x 6 jacobian matrix between endpoint space and actuator space
$\mathbf{C}$:	The 6 x 6 coupling matrix between the joint space and the actuator space
τ_m:	The 6 x 1 vector of particle brake torques
$\mathbf{v_m}$:	The 6 x 1 vecor of particle brake velocities
$\mathbf{f}$:	The 6 x 1 vector of manipulator endpoint forces
$\mathbf{f_h}$:	The 6 x 1 vector forces the human imparts on the manipulator endpoint
$\mathbf{B}$:	The 6 x 6 diagonal matrix of viscous damping terms
$\mathbf{B_m}$:	The 6 x 6 diagonal matrix of viscous damping terms
$\mathbf{K}$:	(6 x 8) Force/torque sensor calibration matrix
C:	(8 x 6) Force/torque sensor calibration sensitivity matrix
$\mathbf{W}$:	(6 x 1) Force/torque sensor electronics Wheatsone bridge output voltage vector
$\mathbf{Fs}$:	(6 x 1) Vector of applied loads to force/torque sensor
R^2:	Coefficient of determination

b_1: Least squares regression slope estimator

b_0: Least squares regression offset estimator

b_2: Velocity calibration parameter

G_p: Analog electronics position gain

G_d: Analog electronics velocity gain

m_1-m_6: Potentiometer angles

K_x: Stiffness of the manipulator in the X direction (world coordinates)

K_y: Stiffness of the manipulator in the Y direction (world coordinates)

K_z: Stiffness of the manipulator in the Z direction (world coordinates)

m_e: Effective mass of manipulator endpoint

M: Mass

g: Acceleration due to gravity

t(t): The target signal as a function of time.

r(t): The response signal as a function of time.

$G_{tt}(f)$: The auto-power spectra of the target signal.

$G_{rr}(f)$: The auto-power spectra of the response signal.

$G_{tr}(f)$: The cross-power density between the target and response signals.

$H_{tr}(f)$: The transfer function between the input target and the output response signals.

f_c: The maximum frequency content of the target signal.

$\Delta r(t)$: The residual portion of the response not linearly related to the input target.

$G_{\Delta r \Delta r}(f)$: The auto-power spectra for the residual portion of the response.

$\hat{r}(t)$: The portion of the response signal linearly related to the target signal.

$\gamma_{tr}^2(f)$: The coherence between the target signal and the response signal.

T(f): The tremor spectrum.

T: The integrated tremor.

R: The signal to noise ratio, comparing purposeful response with tremor.

Chapter 1

Introduction

This document describes the development and use of a six-degree-of-freedom manipulator using modulated energy-dissipation (MED) actuators[1]. The specific use described here, tremor research, was the impetus behind the funding for the device; however, the device was developed to be used more generally for many types of human limb studies including neurological and musculoskeletal assessment and rehabilitation.

The MED manipulator is part of a broader research program lead by Dr. Rosen which includes the design and evaluation of practical devices for enhancing motor performance of tremor-disabled people, and development of methods for instrumented clinical assessment and differential diagnosis. This system will make a contribution to both lines of work in future research.

Specific Research Objectives

This research had three major objectives:

1) Develop a theoretical method for analysis of MED manipulator designs;

2) Design, fabricate, and evaluate a six degree-of-freedom orthosis simulator system; and

3) Test three human subjects to demonstrate that the MED manipulator can be used in a clinical setting and to generate preliminary experimental results.

---

1 Modulated energy-dissipation (MED) is the name we have chosen to use for computer-controlled brakes. Other researchers, notably those in the vehicle suspension area (Karnopp, 1982; Margolis, 1982), have used the term semi-active for similar devices.

Commonly, an engineer will be given specific design criteria along different design dimensions (eg. size, weight, power consumption, etc.). This project began without any such criteria. As far as we knew, no six-degree-of-freedom device existed which would come close to accomplishing the goals of this research. We borrowed heavily from previous Newman Lab research in the area of prosthesis design (Abul-Haj, 1987; Mansfield, 1988) and other devices for tremor loading (Adelstein, 1981, 1989), and past research in exoskeletal systems (discussed in chapter 2) to help develop the criteria which would be useful to us. We also developed a one-degree-of-freedom testbed (discussed in chapter 2) to assist in our development of the 6 DOF system. Finally, we developed mathematical and physical ("erector set") models to help guide our design. In the end, however, we made some decisions based on "engineering judgement."

In practical terms, the MED manipulator has been very successful to date. We tested three subjects on the device and then left the system with our colleagues at the Burke Rehabilitation Center in White Plains, New York. They used the system clinically for approximately two hours per day during a two month period. The system completed the study without technical attention. We considered this a success even before seeing the results of the study.

Research Overview and Thesis Organization

Tremor

Complete clinical (Findley and Capildeo, 1984; Desmedt, 1978) and theoretical (Adelstein, 1981; Adelstein, 1989) discussions of tremor are given elsewhere. Here, we delve into the subject only enough to explain the motivation behind the MED manipulator development.

Rosen (1986) estimates that over three quarters of a million people in the United States are significantly functionally impaired by intention tremor due to adventitious and

inherited neurological conditions. These include Multiple Sclerosis, Joseph's Disease, Friedreich's Ataxia, familial essential tremors, and sequelae of head injuries resulting in lesions of the cerebellum or brain stem. Tremor-disabled people often have sufficient strength and voluntary control that they would be capable of independent performance of activities of daily living were it not for the degradation of their movements by rhythmic involuntary muscle activity. The functional handicap which can result from intention tremor is due, of course, to the reduction of accuracy it entails. At worst, the amplitude of the tremor oscillations can be comparable to the magnitude of intended movements which are therefore completely obscured. Pathological tremor has been measured to have a peak magnitude in the 2-4 hertz frequency band (measured at the wrist by Adelstein and Rosen, 1981)[1].

Most of the tremor research conducted to date has been directed either toward identification of tremor mechanisms or clinical tremor management. Identification experiments have been performed using energy storing passive devices (Joyce and Rack, 1974; Robson, 1959; Vilis and Hore, 1977) and active devices simulating energy storing passive devices (Adelstein and Rosen, 1984, 1987) in an attempt to test the hypothesis that tremors are due to a biomechanical resonance (second order mass-spring-damper) model. These investigators reasoned that the biomechanical resonant peak will shift if an inertia or a spring to ground is added to the free limb segment in one-degree-of-freedom tremor experiments.

Tremor management research in our lab has confirmed the hypothesis that application of energy-absorbing loads across tremor-affected joints can produce a significant selective reduction of tremor amplitude. Results from one (Dunfee, 1979) and two (Beringhause, 1988) degree-of-freedom experiments have shown that viscous damping reduces tremor amplitude in pursuit tracking tasks without significant attenuation

---

1 This paragraph has been directly taken from or paraphrased from prior research papers and proposals of Dr. Rosen.

of purposeful movements. Before the development of the MED manipulator, full-arm functional tests could not be performed because there was no safe device capable of applying controllable loads in six-degrees-of-freedom. The research described in this document extends past work in three ways:

1) It is directed toward identifying and managing tremor in six degrees of freedom;

2) it is more theory-based than previous work directed at orthosis design, and

3) it includes a novel linkage design based upon the theory developed.

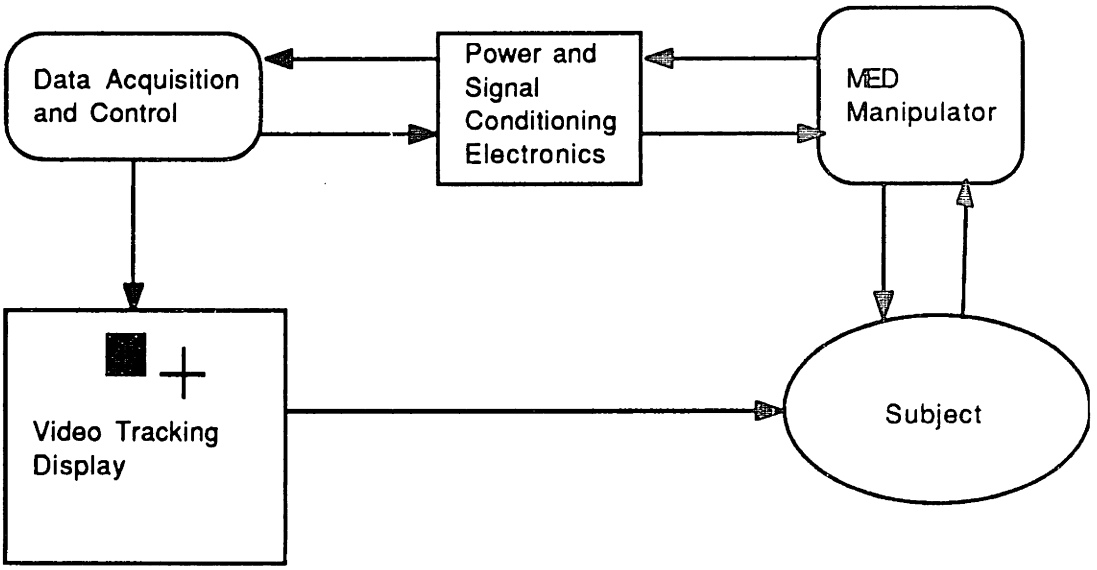

Figure #1-1

Simulator Design Issues

MED manipulator design issues are discussed in Chapters 2 and 3. An overview of the final system is shown in Figure 1-1. A taxonomy of possible orthosis simulator designs was formulated to identify research questions and design choices. Although most questions have to do with standard details of mechanical design and control, others require novel approaches to theoretical and empirical issues which have not previously been

addressed. Particularly important are issues of mechanical coupling between the human limb and the manipulator, and multi-degree-of-freedom MED device limitations vis-a-vis active devices.

Manipulators with active actuators have a more general load simulation capacity including the ability to simulate the more limited performance of MED actuators. This is achieved, however, at the cost of much greater risk of injury to human subjects. Work has been undertaken, and is discussed in Chapter 3, to determine the theoretical limitations of spatial devices using MED actuators. Our analysis indicates that only particular MED designs will result in manipulators with desirable properties.

Chapter 4 presents the final multi-degree-of-freedom system and chapter 5 discusses the calibration and verification tests which were performed on the manipulator. As shown in Figure 1-1, the simulator includes a PC/AT-computer-controlled MED manipulator, a subject support chair, and a video tracking display. The resistance level of the energy dissipating actuator connected to each of the six axes of movement is actively controlled.

The manipulator design is a 6R (six revolute joint) device with the last three joints configured in a gimballed arrangement. This, combined with coupling of the second and third joints with a novel r-2r linkage results in force-velocity colinearity (when a force is applied to the manipulator endpoint the manipulator moves in the direction of the force). The actuators chosen were magnetic particle brakes, which have the advantages over other candidates that they are easily controllable and obtainable, and are relatively inexpensive.

Manipulator sensors include potentiometers at each of the actuators. The potentiometer signals are differentiated by analog electronics resulting in approximate velocity signals. A six degree-of-freedom force/torque sensor at the manipulator end point was custom built for this application, but incorporates the cross design strain element geometry proven to work well by others.

Chapter 5 discusses the details of potentiometer and force sensor calibration as well as a more general system characterization.

Experimental Evaluation

Chapters 6, 7 and 8 discuss the human subject experimental protocol, data analysis methods and experimental results. The human subject testing included abstract and functional components. In the abstract tests, subjects were tested with a number of different damping loads using two degree of freedom computer representations of a pseudo-randomly moving target icon and a response icon which was controlled by the position of the subject's hand. The Subject attempted to follow the target icon with the response icon as the target icon moved about the computer screen. Tremor and voluntary performance measures based on spectral analysis were used to determine the best of the strategies tested (Riley and Rosen, 1987). The qualitative tests involved tasks the subject found most difficult, such as drinking from a full glass or eating soup with a spoon.

Three subjects were tested in the experiments, one normal and two tremor impaired. Although this does not provide statistically significant results, the resulting data suggest enough research directions which look promising and should be statistically verified.

Accomplishments and Future Work

Chapter nine recapitulates the thesis discussing the specific accomplishments for this work and suggestions for future research directions.

Chapter 2
Design Issues

This chapter develops a framework for the MED manipulator design issues. Although systems have been developed in the past which connect to the human arm, this prior work did not develop a sufficient foundation which we could adapt to our problem. In this chapter we:

1) review past devices which connected to the human arm;
2) develop a criteria for design evaluation;
3) analyze methods of applying loads to the human arm;
4) develop a taxonomy of possible device structures; and
5) perform a component technology assessment.

Review of Research on Mechanical Devices Coupled to the Human Arm

Before developing a framework to identify the important design issues, we undertook a search of past references on subjects pertaining to humans interacting with manipulators. We found a substantial body of literature on devices which move in one or two degrees of freedom, but found few devices which allowed the human arm a full six degrees of freedom. We grouped these devices with three or more degrees of freedom into three major classifications-- controlled orthotic devices, man amplifiers (which some researchers are now calling "extenders"), and telemanipulators. Although these three areas are distinct application areas, they have much in common. The most mechanically complex

devices in each domain are linkages which kinematically follow the movement of the arm[1] while applying controlled loads to it[2].

Low Order Devices

The number of one, two, or three degree of freedom devices which kinesthetically couple to the human arm is quite large. A good review of these devices is given by Adelstein (1989). Some of the simple one-degree-of-freedom devices have been commercialized in the rehabilitative exercise market. These devices are discussed by McGory (1990).

Higher Order Devices

In the controlled orthotic area, our research shows that there were two major studies performed in the 1960's. The first major study was at Case Western Reserve (then Case Institute of Technology). The Case research team performed a very complete and extensive study (Corell and Wijnschenk, 1964). The project produced a five-degree-of-freedom controlled orthosis, the Arm-Aid, which was used as a research tool for studies into orthotic and prosthetic systems. The Arm-Aid was used mainly to augment the reduced functional capabilities of paralyzed human limbs. The Arm-Aid manipulated the paralyzed or partially paralyzed human arm in five degrees of freedom (It was an exoskeletal robot which moved where the computer-controller instructed it to move). The Arm-Aid was conceived as an essential first step in a program meant to lead to the recovery of movements for paralyzed or otherwise disabled patients. From an engineering point of view, the researchers considered the performance of the Arm-Aid a success. The project consumed substantial effort, involving fourteen graduate students, six consultants, and five faculty

---

1 We do not mean to imply causality here.

2 We use the term "controlled loads" loosely here. We could not find references which quantitatively discussed how well the devices could control the loading.

members at the Case Institute of Technology. Over the course of the project seven masters theses and one Ph.D. thesis were derived.

The second major controlled orthosis project was conducted at the Rancho Los Amigos Hospital (Nickel, 1964; Karchak and Allen, 1968). The Rancho Electric arm was similar to the Case Institute Arm-Aid. While the Arm-Aid remained a research project, the electric arm was developed into a commercial product. It was sold in a kit with a fitting manual so that specially trained or skilled technicians were not required.

Other controlled orthosis studies have been conducted on the lower extremity (see,for example, Vukobratovic et al. 1975). These studies are very similar to the upper extremity studies in that the aim of the controlled orthosis is to restore motion to a paralyzed limb.

Man amplifiers, now called Extenders (Kazerooni, 1989 gives a good history and current review of these devices) are devices that amplified the load capability of the human body. They are intended to follow the motion of the human body, measure the forces applied by the human, and apply proportional, amplified forces to the environment. Theoretically, a man wearing a man amplifier device could do tremendous lifting and moving tasks. The major thrust of the man amplifier research came from a group led by Mosher at General electric in the 1950's and early 1960's (see, for example, Johnson and Corliss, 1967; Gray and Pieper, 1973). Mosher developed a hydraulic man amplifier with ten degrees of freedom in each arm-hand combination. This design, which they called the powered exoskeleton, even had fingers[3].

Finally, teleoperators are robotic devices whose motion is controlled by an operator at a distance. In order to communicate the motion commands to the remote robotic device at the distance, the early teleoperators were built in geometrically identical pairs. The human operator would move one linkage, the master, and the joint positions and velocities

---

3 The freedom of the fingers is not included in the ten degrees-of-freedom.

would be measured and commanded to the other identical linkage, the slave. Some teleoperators (for example, Fornof and Thornton, 1973; Vykukal, King, and Vallotton 1973) were built with master and slave geometry of the master and slave devices being identical to the human arm. With this geometry, the human operator is able to insert his arm into the master linkage and the joint motion of the human arm is therefore transfered to the motion of the slave. Vykukal (Vykukal, 1971) suggested that a good application of a modified version of his master-slave manipulator might be for the damping of tremor and other forms of rehabilitation.

As shown by the citations above, many of the major research projects took place in the 1950's, 60's, and early 70's and was then discontinued. The Case project and the General Electric man amplifier project probably were not continued because they reached the limits of the then existing technology (although Leifer, 1981, suggests that the Case Institute line of research evolved to yield robots which were physically isolated from the user. That is, the current rehabilitative robots do not move the human's arm, they simply assist the human.) We attribute the decline of exoskeletal masters in the telemanipulator area to two technological innovations-- the inexpensive microprocessor and the algorithm by Whitney (1969) which allowed the microprocessor to calculate the joint velocities needed for a given end point velocity. Because of Whitney's innovations the master and slave telemanipulator no longer needed to have the same geometrical structure. The human could maneuver the endpoint of the master telemanipulator and the microprocessor would measure the master joint velocities, calculate the master endpoint velocities, and then calculate the slave joint velocities so that the slave endpoint had the same (or scaled) end point velocities as the master endpoint. If the master needed kinesthetic coupling then a similar calculation could be performed so that the force feedback to the end of the master is equal to the force (of some proportion of the force) measured at the slave. Another possible reason for this research being shut down is that the researchers may have moved

into conventional robotics research. Robotics research was expanding greatly at that time because of the innovations mentioned above as well as some further actuator innovations.

The research areas discussed above, especially the teleoperator area (now called telepresence[4]) and man-amplifier area, have heated up again in the last few years (possibly because of increased government funding) and research reports are beginning to trickle into the public domain (Kazerooni, 1989; also see Adelstein, 1989, for a short review of the telepresence literature).

We have investigated the geometries of the devices discussed above as well as current clinical orthoses. The designs of past researchers seemed to suit their specific endeavors but none address the complete issue of loading in six directions safely. The literature search did, however, help us begin thinking through the design issues and help develop the design criteria discussed below.

---

4 The term telepresence is meant to include any or all of the sensations a human might perceive which make the human believe he is present in some reality which is artificially created.

Criteria for Design Evaluation

As we began development of the MED manipulator, we realized that it may share many of the design criteria for a future *wearable* orthosis. We undertook the analysis necessary to determine a set of design criteria for each of these design projects so that we could steer the MED manipulator project as much as possible toward the design necessary for a wearable orthosis.

Table 2-1 lists the system design considerations for both the present MED manipulator research tool project and the future wearable orthosis project. While the criteria for latter would be nice to incorporate in the present project (and were incorporated where we felt the "cost" was low compared with the advantages), the criteria for completing our project were a small subset of the ultimate criteria.

The criteria for design evaluation have been grouped into the eight areas listed under the "Research Tool" heading in Table 2-1. A discussion of each follows.

Table #2-1

System Design Considerations

Research Tool	Future, Wearable Orthosis
Functional Issues	
• Safety	• Safety
• Control	• Control
• Workspace	• Workspace
• Reliability	• Reliability
• Cost	• Cost
Cosmesis issues	
• Size	• Size
• Weight	• Weight
	• Color
	• Feel
	• Shape
• Noise	• Noise
Biomechanical issues	
• Tissue impedance	• Tissue impedance
	• Blood Flow
	• Pressure Points
	• Tissue Damage
	• Heat Dissipation
	• Perspiration Dissipation
Human factor issues	
	• Washability
	• Calibration
• Maintenance	• Maintenance
	• Fatigue
	• Donning and doffing ease
	• Washability

Safety

Safety is the single most important issue in the development of any device which interacts with humans. Many professional societies emphasize safety is the engineer's foremost responsibility (Whitbeck, 1987). The National Society of Professional Engineers (NSPE) Code of Ethics, for instance, states " Engineers shall hold paramount the safety, health and welfare of the public in the performance of their professional duties."[5]

Rahimi (1984) introduced the idea of energy barrier analysis (EBA) to help model potential safety problems in robotic systems. EBA is predicated on the idea that energy is the dominant variable affecting human injury. If the energy transfered to the human is at too high a level, the human is injured through a variety of possible mechanisms including electrocution in the electrical energy domain or impaling in the mechanical energy domain. Safety can be assured if the energy transfered to the human is kept below the level of energy needed to produce injury. As Figure 2-1 shows, we can evaluate the safety of a particular system by analyzing the sources of energy in the system and the means of controlling the energy in the system.

---

5 As an aside, it should be noted that the public's acceptance of a safe product is presently only slightly greater than a more risky product (Otway and Haastrup, 1989). This may be why managers, trained to think in terms of profit or net present value, do not put as great an emphasis on safety as some might like (for instance, Nader, 1967). In our estimation, one result is that researchers are not considering the ultimate safety of their devices at the inception of the project. Many devices seem to make the transition to the commercial market without being completely safe.

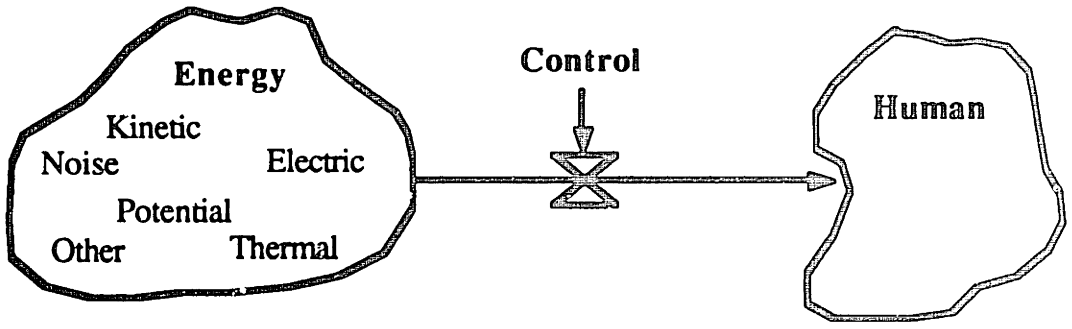

Figure #2-1. Diagram of simple energy barrier analysis.

If the energy in the system is high enough to cause potential injury to the human, failure of the energy control mechanism may result in injury. The simplest mode of control "failure" is caused by the system operator improperly using the system. This occurs often in systems with complex operator interfaces (Gibson-Harris, 1987; Schultz, 1987).

Another mode of controller failure results when computers are controlling the transfer of energy to the system. Controller failure, or even simple computer calculation errors, can lead to injury. Work has increased in the last few years on designing more reliable computer-based controllers (see, for example, Krishna and Shin, 1987; Woolnough, 1988). But, even with very reliable, redundant computers, failure problems can exist. Take for example the Intel Corporation 80386 microprocessor chip. In April, 1987, after it had sold more than 100,000 chips, Intel discovered that under specific sets of operating conditions the 80386 chip produced some incorrect multiplications ("Faults and Failures", 1987). In its next generation chip, the 80486, Intel again found defects after shipping the chip ("Chip by Intel Contains Flaw In Calculating", 1989). If one of these chips controlled energy interactions with humans, it might have allowed critical injuries to occur.

Even if the hardware is working flawlessly, small flaws in software have on occasion caused humans who interact with them to be maimed and killed. Many examples of software failure and concern about software failure are described in the 1987 *Wall Street Journal* article, "As Complexity Rises, Tiny Flaws in Software Pose a Growing Threat". In one case a computer-controlled radiation therapy machine's software bug killed a patient (the machine delivered too high a dose). In another case cited in the article:

> "Two years before the first launch of the space shuttle, a programmer changed the timing on some shuttle software by 1/30th of a second. Unknown to the National Aeronautics and Space Administration, that minuscule change introduced a 1-in-67 chance that the shuttle's five on-board computers wouldn't work in sync. Twenty minutes before launch in April 1981, the bug appeared, the computers couldn't communicate and NASA scrubbed the flight.
>
> NASA says that thousands of hours of testing hadn't uncovered the bug."

Even a control system as simple as opening and closing subway doors has had reliability problems. The New York Times reports ("Subway Door Problem No Open and Shut Case") that in 1986 the New York Transit Authority reported 121 cases of "door opening enroute" (D.O.E.). Luckily, no one was seriously injured that year by these control system failures (although previous years have found injured and even dead subway riders because of inadvertent door openings).

Cybex, a company which manufactures one-degree-of-freedom dynamometers for therapeutic exercise, "is convinced that the combination of high speed and high force capabilities in active systems is not acceptably safe for patient care" ("The Case Against Active Robotics"). Industrial robot safety systems require keeping humans out of the

workspace of the robot to reduce the possibility of injury if the robot has a malfunction. More specifically on this issue, Thomas Deringer of IBM Corporation states

> "Anyone willing to crawl into a cage with today's third-generation robotic systems that have six, seven, or eight degrees of freedom...with the power ON, is out of their mind.
>
> A ten-cent resistor failure on a control card deep down inside the most sophisticated controller can scramble your sunny-side-ups!" (Deringer, 1984).

There are however, *active* one-degree-of-freedom musculoskeletal testing and rehabilitation systems on the market (McGory, 1989). How do the companies making these systems justify the use of these devices in intimate connection with humans? McGory suggests redundant angle sensors help prevent failure due to sensor error. Also, if preset range of motion limits or speed limits are exceeded, the software will shut down the system. A more fail-safe system of mechanical limits are in place if the computer controller fails (the probability of mechanical limit stop failure is much lower than the probability of computer or electronic system failure).

Unfortunately, while increasing the number of axes on a device increases the usefulness, it also reduces the safety of the device. Mechanical limit stops, devices which mechanically limit the range of motion a given axis can move through in the event of controller failure, work well for one-degree-of-freedom systems, but lose their effectiveness as the number of degrees of freedom in the system controlled by a computer increase. Limit stops on a one-degree-of-freedom revolute system, for instance, will still allow movement in an arc in the event of controller error. If the human arm is placed in an orientation which guarantees both that the human arm joints will not be injured if the device moves anywhere between the limit stops (eg. no human arm hyperextension occurs) and the device cannot impale the human if it moves anywhere between the mechanical limit stops, then the device can be considered safe.

For a more flexible two-degree-of freedom system, limit stops on each axis will allow motion anywhere in a surface if the controller fails. Placing the human arm so that the joints will not be injured and preventing human-device contact injuries is much harder than in the one degree-of-freedom case. For a three degree of freedom system, motion is limited to a volume, creating even less safety with mechanical limit stops. In general, for n degrees of freedom motion is limited to n space. This suggests that human arm connected to a six-degree-of-freedom industrial robot is not safe just because limit stops are installed on each axis.

The safety argument was the primary motivation for our decision to use computer-controlled brakes instead of active actuators in the MED Manipulator. The brakes have only the capability to *absorb* energy, thereby satisfying the energy barrier analysis criteria.

Control

The second most important issue in the the development of the MED manipulator is the system performance, that is controllability of the device. If the device can generate the load profiles required of it, the device will be said to meet this requirement. The first control algorithm we anticipated using was that required to produce simple viscous resistance, i.e., where the force output is proportional to the velocity input. We anticipate future load profiles will include any of the broad range of dissipative loads dependent on the state and inputs of the system (force as a function of position, velocity, acceleration, and/or force).

Workspace

The manipulator workspace should be large enough so that the device allows the human are movements which are needed for activities of daily living (grooming, eating, etc.). The manipulator should provide this workspace while not obstruction vision (the subject needs to see what he is doing).

The above list of issues was not quantitatively developed because we had no idea exactly what could be developed until we investigated each issue in detail. In the end there were some complex tradeoffs associated with the criteria (many cannot be codified). Our initial hope was to push each dimension as far as possible. Although this does not result in quantifiable evaluation of our final design, the final design gives a benchmark for evaluations on future designs.

Table 2-1 lists the criteria which might be used for a future *wearable* orthosis. This table may not be complete and may contain considerations which are not necessary for future designs. They are included here to help guide future research into wearable orthoses.

Reliability and Maintenance

Reliability and maintenance are two issues that must be considered at all phases of the design. Reliability assures the system will get the greatest possible use and ease of maintenance both increases reliability and increases the life of the device. While it might be acceptable to develop a laboratory research tool that has maintenance and reliability difficulties, the design decisions which permitted them might propagate into future commercial orthosis designs[6] with resulting consumer dissatisfaction.

Cost

The budget for this project was small compared with the magnitude of the project. We had to make do without many of the expensive components (encoders, molded plastics,

---

6 Sound engineering is important from the initial stages of a project, especially graduate student projects, because there is no continuity of the technical personnel (students graduate). A new graduate student may believe that a given design has been given a "seal of approval" by the design faculty signalled by the graduation of the student who produced the design (a student who produces a "bad" design should not graduate until the design is improved). Also, many designs which are "bad" in the early stages may propogate because the device is not put though extensive reliability testing, and therefore may not fail until later stages, creating a greater design change cost.

parallel processing boards for the computer, and etc.) we would have liked to design into the device. This cost constraint produced an inexpensive device which did not sacrifice controllability, reliability, or maintainability.

Size, weight, noise

Finally, the MED manipulator needed to be contained in a reasonable package size, and within weight, and noise constraints so that it could be transportable and not intimidate our experimental subjects (a very serious consideration).

Applying Loads to the Human Arm

Modelling of the Human Arm

Before undertaking the development of a device which attached to the human arm, we performed a literature search to determine arm geometry, range of motion of different joints, maximal torques at each joint, and issues involved in applying loads to the arm such as tissue impedance, impeding blood flow, and nerve or tissue damage.

Figure 2-2 shows the joint symbols which will be used in this and later chapters to describe linkages. Figure 2-3a and 2-3b shows a very simple seven-degree-of-freedom model of the human arm from the shoulder (scapulo-humeral) joint through the wrist (radio-carpal and mid-carpal) joint using the symbols of Figure 2-2. Figure 2-3a is more physiologically oriented while Figure 2-3b is more mechanism oriented. We have greatly simplified the actual arm, first by eliminating clavicular and hand joints and second by simplifying the true movement of each joint.

The clavicular motion was eliminated from consideration because we felt we could do an adequate job of restricting shoulder motion in our early system tests. The motion of the fingers and thumbs were eliminated because this motion is a micro-manipulation problem which could be investigated as a separate research project. If the micro-

manipulation research ended up developing a device, we believe we could merge the two devices resulting in a complete-arm system.

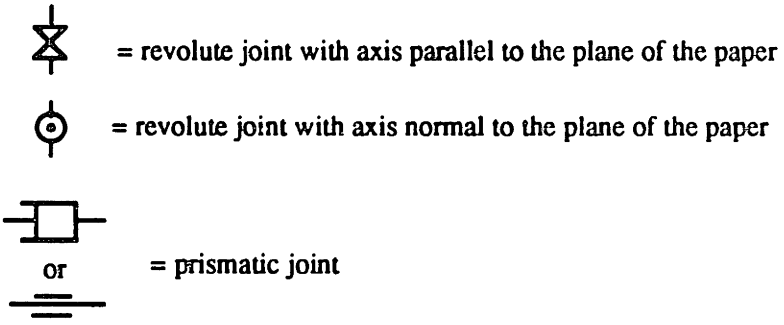

Figure #2-2. Definition of linkage symbols

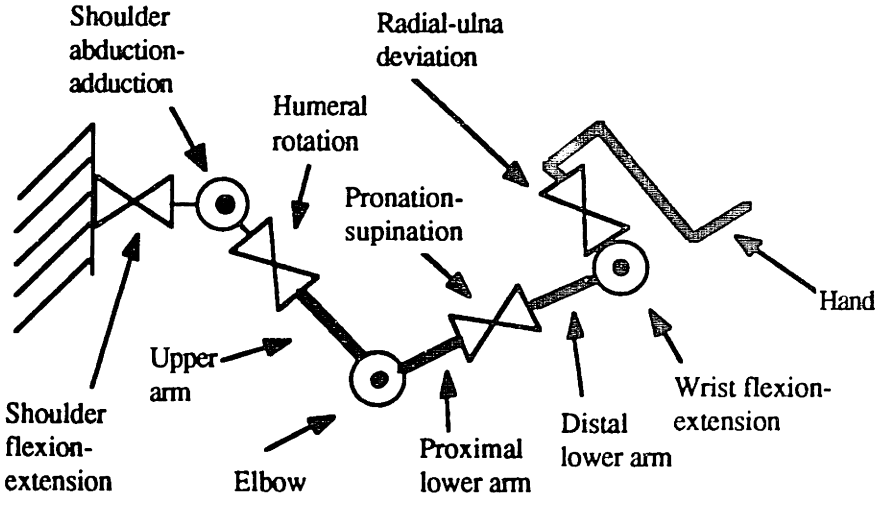

Figure #2-3a. Human arm model

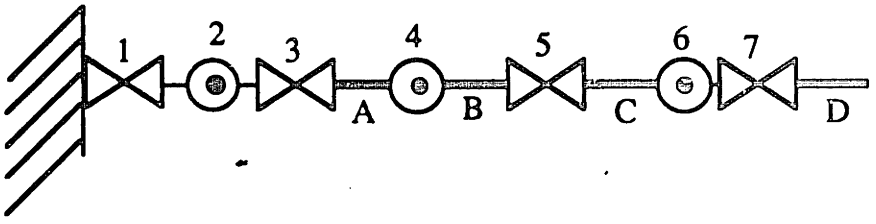

Figure 2-3b. Simple geometric model of human arm

Axes 1,2, and 3 of Figure 2-3 represent the shoulder adduction-abduction, flexion-extension, and humeral rotation; axis 4 represents the elbow flexion-extension; axis 5 represents ulnar-radial rotation (pronation-supination); and axes 6 and 7 represent the wrist flexion-extension and radial/ulnar deviation. (For a complete discussion on joint physiology see Kapandji (1982).) A, B, C, and D in the figure represent the upper arm, proximal lower arm, distal lower arm, and hand, respectively. These are the locations on the human arm to which we can physically connect our device (discussed later).

Holerbach (1985) developed the Denavit-Hartenberg parameters (Denavit and Hartenberg, 1955) for the human arm "manipulator" of Figure 2-3. These parameters are given in Table 2-2. The parameters are useful for future work on this project if the researcher wishes to calculate the human arm Jacobian matrix or coordinate transform matrices.

Table #2-2
Denavit-Hartenberg parameters for the human arm model

i	a_i	d_i	α_i
1	0	0	$+\pi/2$
2	0	0	$-\pi/2$
3	0	d3	$+\pi/2$
4	0	0	$-\pi/2$
5	0	d5	$+\pi/2$
6	0	0	$-\pi/2$
7	0	0	0

Characteristics of the human arm model (lengths, widths, circumferences, range of motions, and strength) were investigated using the Humanscale™ system (Diffrient, Tilley,

and Bardagjy, 1974; Diffrient, Tilley, and Harman, 1981). These parameter values were used to quantify the range-of-motion and load requirements for the MED manipulator.

Impedance Model of the human arm

Another area which required investigation was the mechanics of transfering loads through human flesh. The ultimate goal was to produce a stiff connection between the human skeleton and the manipulator. Manipulator control over the human limb movement is reduced as this stiffness is lowered. The best possible design would transfer the load directly to the bone; this would produce a very stiff connection. Unfortunately, practical methods do not allow permeating the soft tissues.

Many studies have determined static, elastic properties of the skin, subcutaneous tissue, and muscle (see, for example, Nyborg, 1975; Simonson et. al., 1949; Oomens et. al., 1983; Phillips and Johnson, 1981). Others have experimentally determined the dynamic reactions of human flesh to loads (see, for example, Von Gierke et. al. 1952; Franke, 1951). The most relevant study was performed by Bennett (1971-1974). Bennet's who attached prosthetic devices to human limbs (transfering loads of soft tissue) while preventing lesions, cysts, plugs, abrasions, etc.

From our literature search, we developed a very simple model, i.e., a set of idealizations and an experimental paradigm. It is meant to help determine the best method of mechanically connecting to the human arm, i.e., the method which produces the greatest stiffness without injuring or causing pain to the human subject. The stiffness model we used is shown in Figure 2-4 for an individual human limb segment. The model assumes the bone and limb cuff are infinitely stiff, the tissue is homogeneous, and any piece of tissue is linearly elastic to compression but cannot hold shear load. Although these simplifications are not exactly correct, the model describes the behavior we want to analyze, and is conservative in the sense that it exaggerates the unacceptably high compliance of the soft tissue layers in shear.

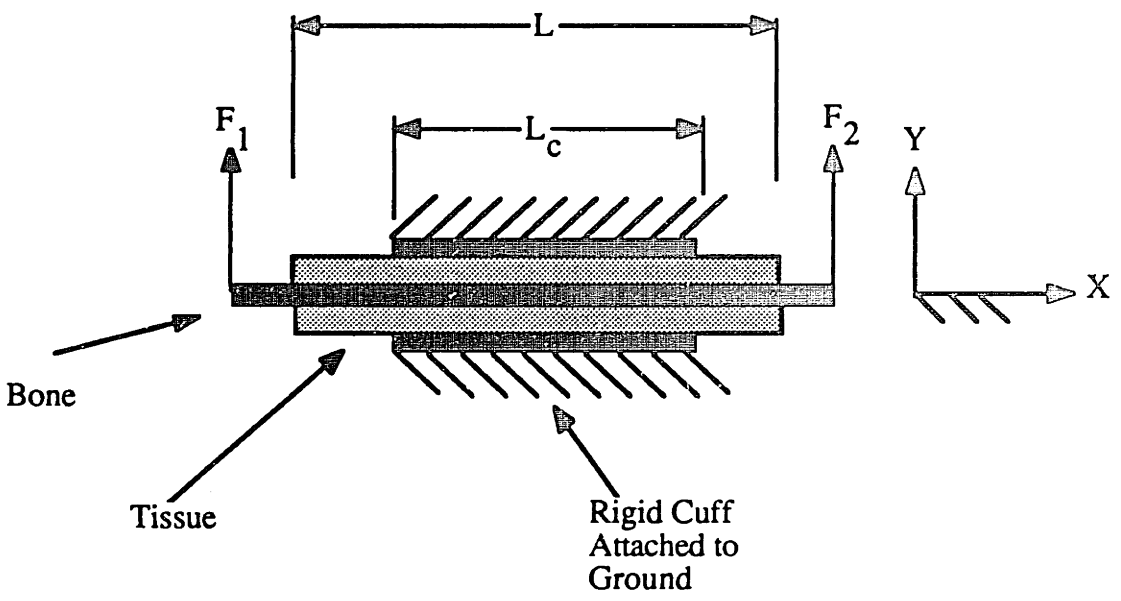

Figure #2-4. Tissue model

L = The limb segment length

L_c = The limb cuff length

Assume the tissue has static impedance per length (stiffness density) k(x) uniform throughout the segment. We would like to find the total stiffness for a force in the Y or, equivalently, Z direction. The total stiffness is $k(x)L_c$, i.e. the longer the cuff, the stiffer the connection to ground. The stiffness along the X direction has no meaning in this model because of our assumption that shear stiffness is zero. While the stiffness in the X direction is not zero, it is difficult to model the system in this direction. We suspect that the longer length will produce a higher stiffness in the X direction but will not have as great an influence as it does in the Y or Z directions.

Like the stiffness in the X direction, rotational stiffness about the long axis (x axis) is zero because of our assumed zero shear stiffness. In actuality, rotational stiffness would

be very low if the skeleton were shaped like a cylinder, but it increases as the underlying geometry increases in rotational asymmetry (e.g., the rotational stiffness is quite high, while for the upper arm the long axis rotational stiffness is quite low).

The rotational stiffness in the Y and Z direction approximated using the model as $\frac{k(x)L_c^3}{12}$ (this equation was easily be derived using basic mechanics) . Notice that again the greater the length of the cuff, L_c, the higher the stiffness.

The above results indicate that the longer the limb coupling cuff, the stiffer the connection between the cuff and the bone. Although these models are not predictive in an absolute sense, they do help guide the design by confirming the intuitive notion that the longest length cuffs are the best for our stiffness criteria.

Development of Limb-Coupling Cuffs

Another design task was the development of a set of limb-coupling cuffs (limb couplers) which we could use to transfer loads between the mechanically well-defined MED manipulator and the mechanically complicated human arm.

Referring to Figure 2-3, the possible attachment sites for the MED manipulator are:

- the upper arm,
- the proximal end of lower arm (B),
- the distal end of lower arm (C), or
- the hand (D).

Candidate Materials

We investigated possible materials and the commercial clinical methods of attaching splints to the human limb (see, for example, Tenney and Lisak, 1986; American Academy of Orthopaedic Surgeons, 1975; Redford, 1980).

Showers and Strunck (1985) give a very good overview of sheet plastics and their applications in orthotics and prosthetics. Orthoplast, the material we ultimately chose for our application, is used very frequently in orthotic applications. Many use the material because it can be formed directly on the patient and is easily adjusted with a heat gun after construction. One drawback of the material, however, is its shorter life expectancy than other, more durable sheet plastics. We chose to use Orthoplast because it is easily obtainable, easily molded, and the laboratory has had good success with it in past research.

Another possibility we considered was limb coupler designs that are adjustable to fit different size arms. We felt that an adjustable liner would make a single cuff capable of fitting many individuals. A number of the lining material investigated are discussed below:

Conforfoam

Confor™foam is a medium density, open-celled, visco-elastic polyurethane foam sold by Specialty Composites Corporation of Newark, Delaware. The manufacturer sells the foam with varying visco-elastic parameters. The open-celled nature of the foam helps the foam dissipate moisture from perspiration.

Air Bladder

The idea of the air bladder is to have an inflatable inner bladder that would conform to the shape of the limb segment. A number of shoe manufacturers have recently used this idea. Reebok International Ltd., for instance, has recently introduced a of basketball shoes called the Pump. The shoe's lining and tongue have an air bladder system that allows the wearer to pump air into the heel and midfoot for a custom fit. The pressure can be adjusted by squeezing a basketball-shaped button on the tongue of the shoe.

Injectable foam, closed cell foam, cotton sock

Finally, other lining materials were considered including an injectable foam, closed cell foam, or cotton.

In the end we decided that any lining material would unacceptably reduce the stiffness of the limb coupler connection to the bone. As a result, we developed limb couplers without a lining material, custom fit for each subject.

Final Limb Coupler Design

A number of limb couplers for different limb segments were built and evaluated by undergraduate research assistant Jessie Wong. For a complete description of this line of

research see her B.S. thesis (Wong 1990). Figures 2-5 and 2-6 show a few of the many limb couplers built.

Wong found that the limb coupler of Figure 2-6 was the best limb coupler design at transfering all six load directions to the bone of the arm. This limb coupler crosses and immobilizes the joints of the wrist. While the immobilized wrist reduces the human arm's workspace, the design reduces the complexity of our project by reducing the number of degrees of freedom of the arm and gives a simple, stiff connection between the manipulator and the human arm.

Experiments

Stiffness experiments were performed by Wong on the limb coupler of Figure 2-6 to determine its stiffness properties in the translational directions. The set-up for the stiffness experiments is shown in Figures 2-7 and 2-8. The stiffness experiments were performed with a Barry Wright Corporation FSG-120A 6-axis force sensor and Phase II brand dial indicators with a 1 inch range and .001 inch graduation. The dial indicator was attached to three bony prominences of the arm and hand; the olecranon process (proximal end of ulna), the Slyloid Process (distal end of ulna), and the proximal end of the third proximal phalanx (proximal end of a bone in the middle finger).

The compliance of the arm changes with changing muscle activity level (a high level of muscle activation will result in less compliance than a flaccid muscle). Because the muscles will be active when pushing on the resisting MED manipulator, Wong tested the arm by having the subject apply the load to the force sensor and the displacement was measured (another possibility would have been to test the flaccid muscle stiffness by immobilizing the human arm and applying a force to it while asking the subject to relax).

Experiments were performed on three male subjects. Example plots of the results are shown in Figures 2-10, 2-11, and 2-12 for Subject A in the X, Y, and Z directions and

tabular data is shown in Table 2-3. The X, Y, and Z directions are defined by figure 2-9 for Wong's stiffness tests.

The stiffness tests were useful in a number of ways. First, as the representative plots show, the stiffness is fairly linear with force in the force range chosen. Second, as Table 2-3 shows, the order of magnitude of the stiffness for all subjects in all directions is approximately the same. While this result is not statistically significant, the results do suggest that the tissue and limp coupler cuff impedance is of the same order of magnitude across subjects. Finally, the plots are useful to compare future generations of limb couplers with this baseline to determine how such added conveniences as air bladders change the stiffness.

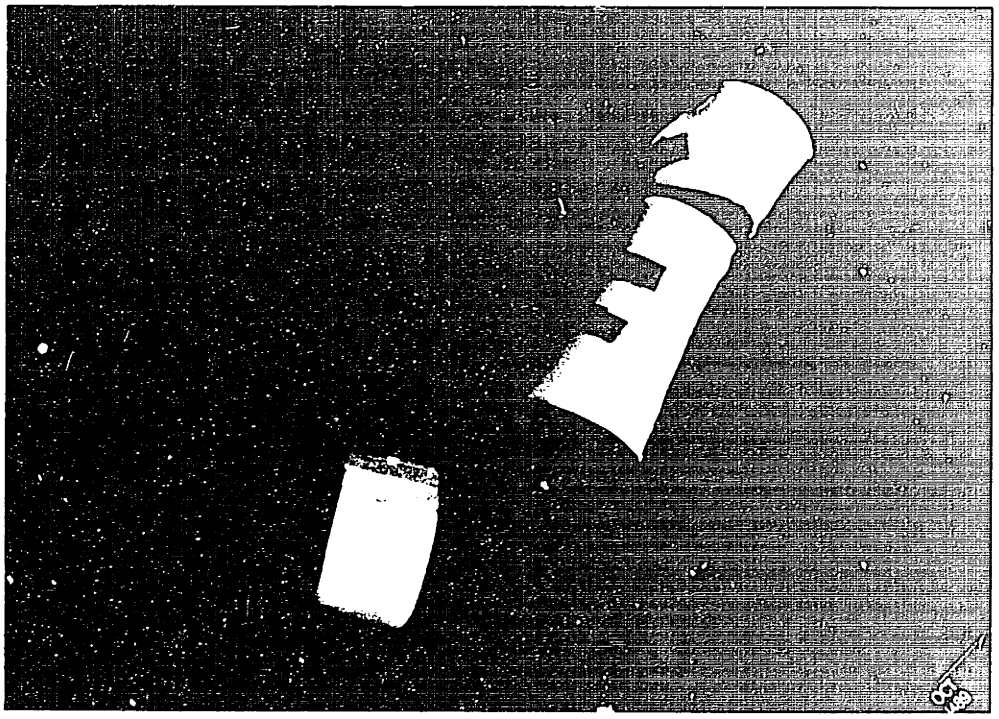

Figure #2-5. Limb coupler set

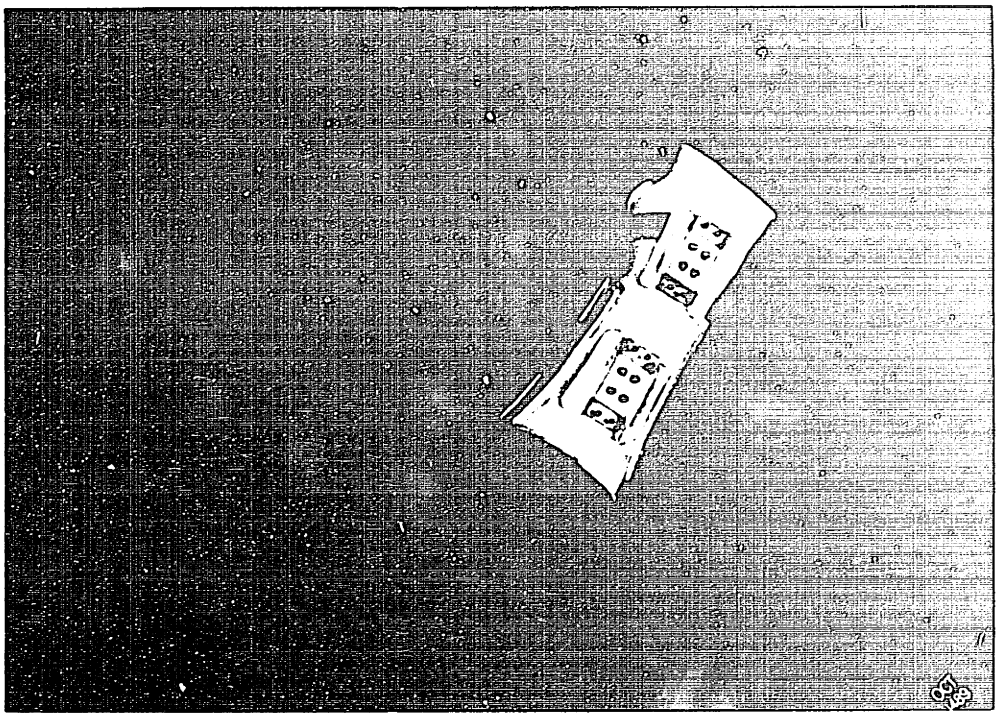

Figure #2-6a. Connection side of final limb coupler design

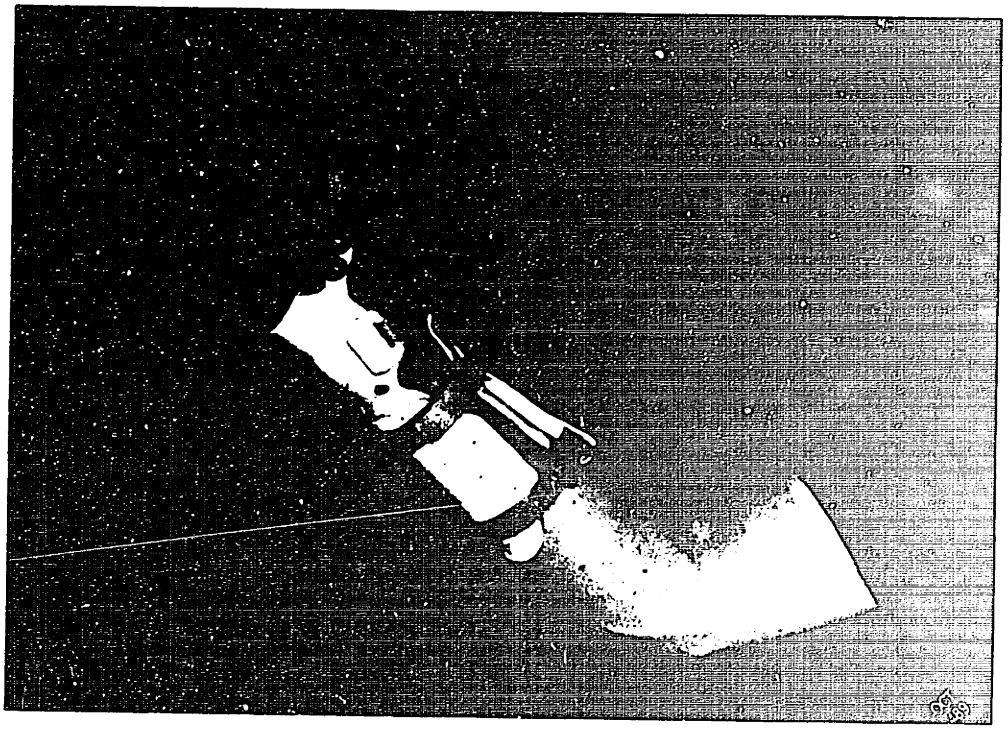

Figure #2-6b. Open side of final limb coupler design

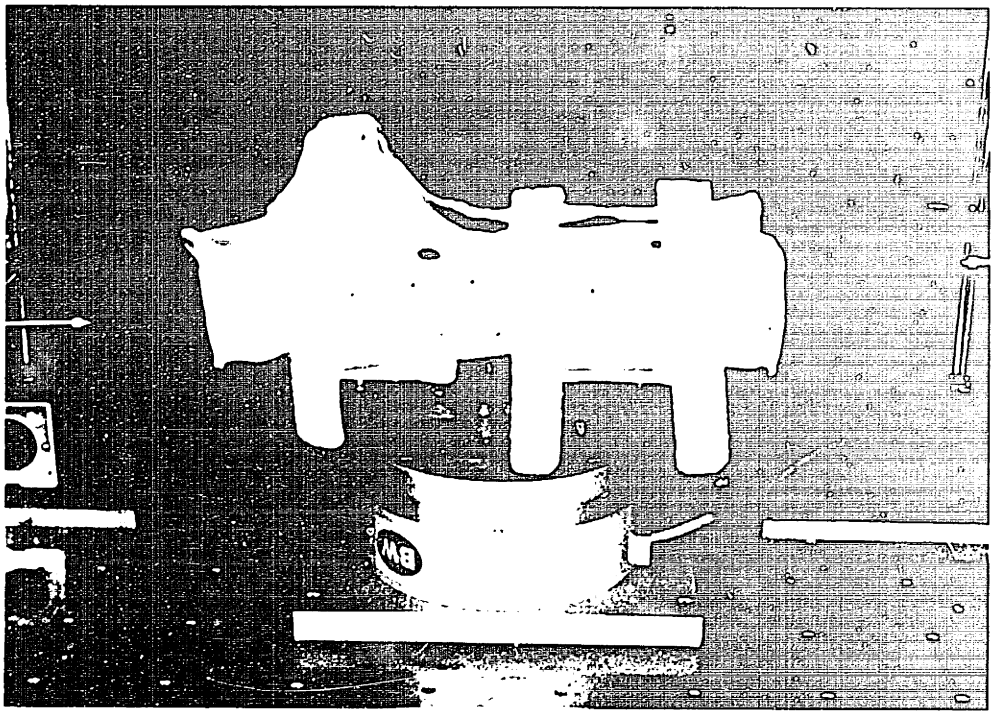

Figure #2-7. Experimental set-up for stiffness experiments

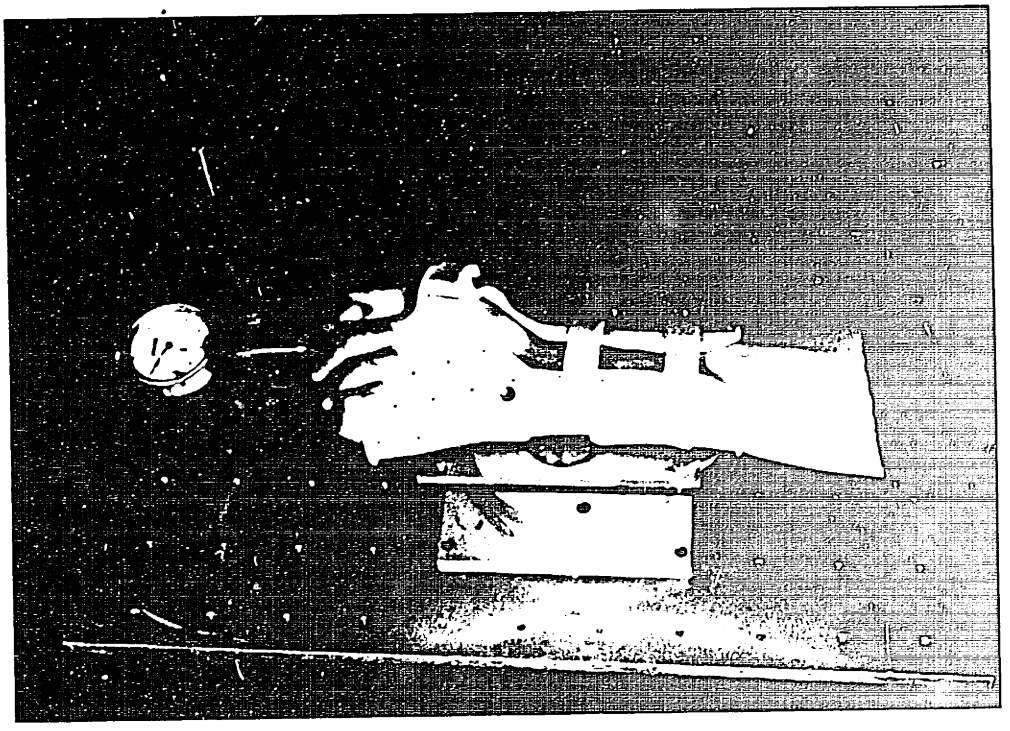

Figure #2-8. Top view of stiffness experiment

Side View of Experiment

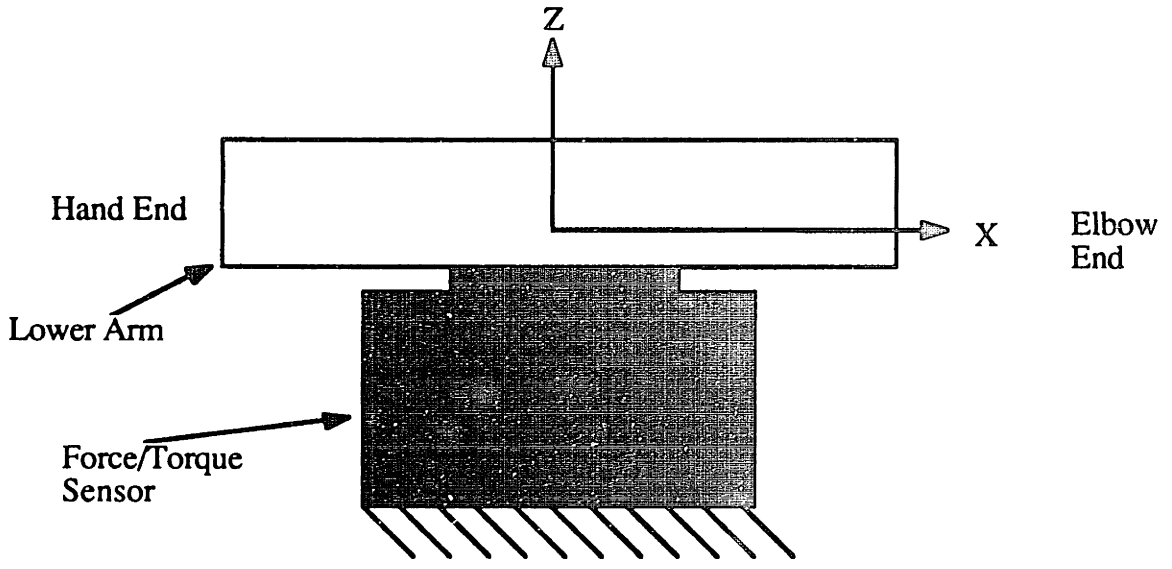

Figure #2-9. Stiffness experiments axis definitions.

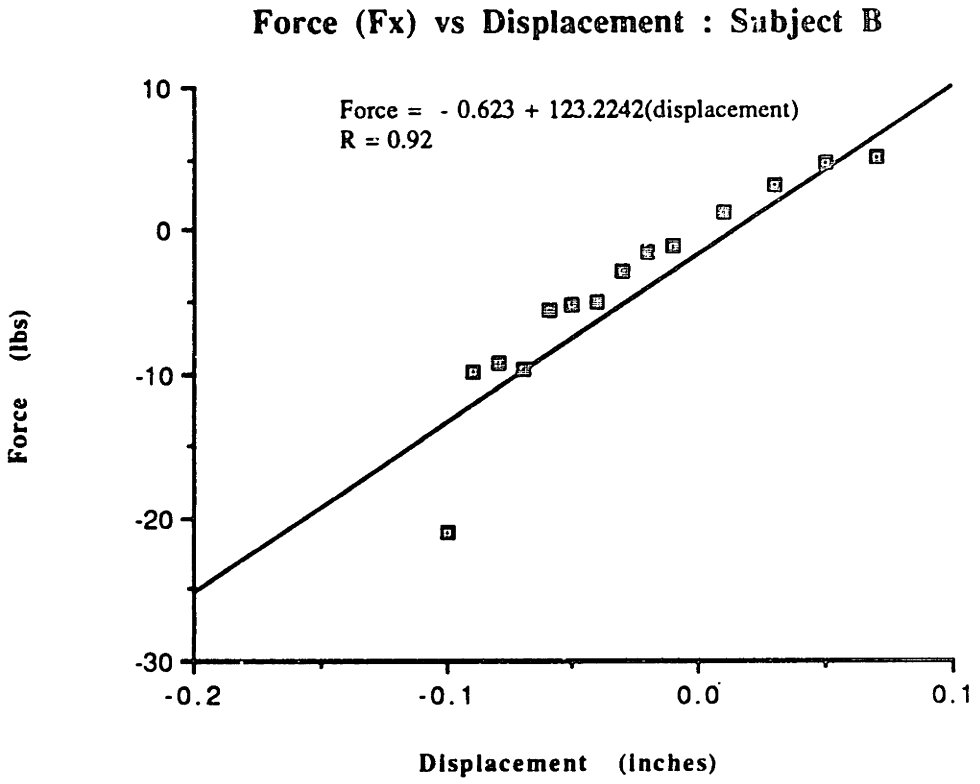

Figure #2-10. Force vs. displacement for subject B in the X direction

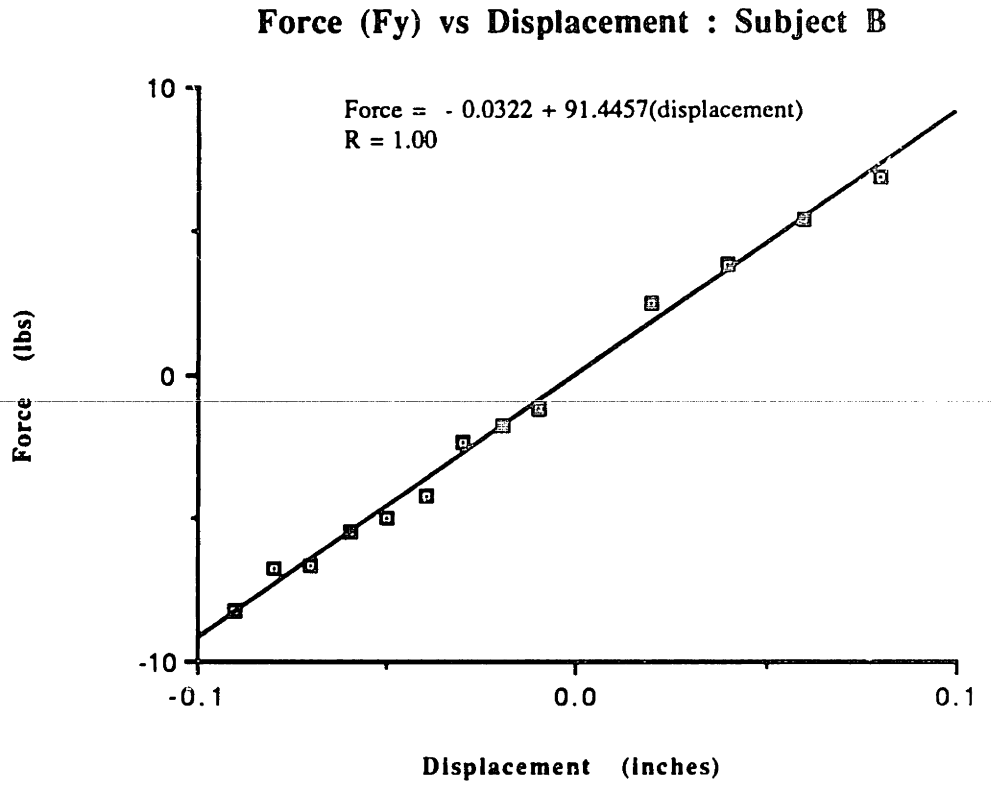

Figure #2-11. Force vs. displacement for subject B in the Y direction

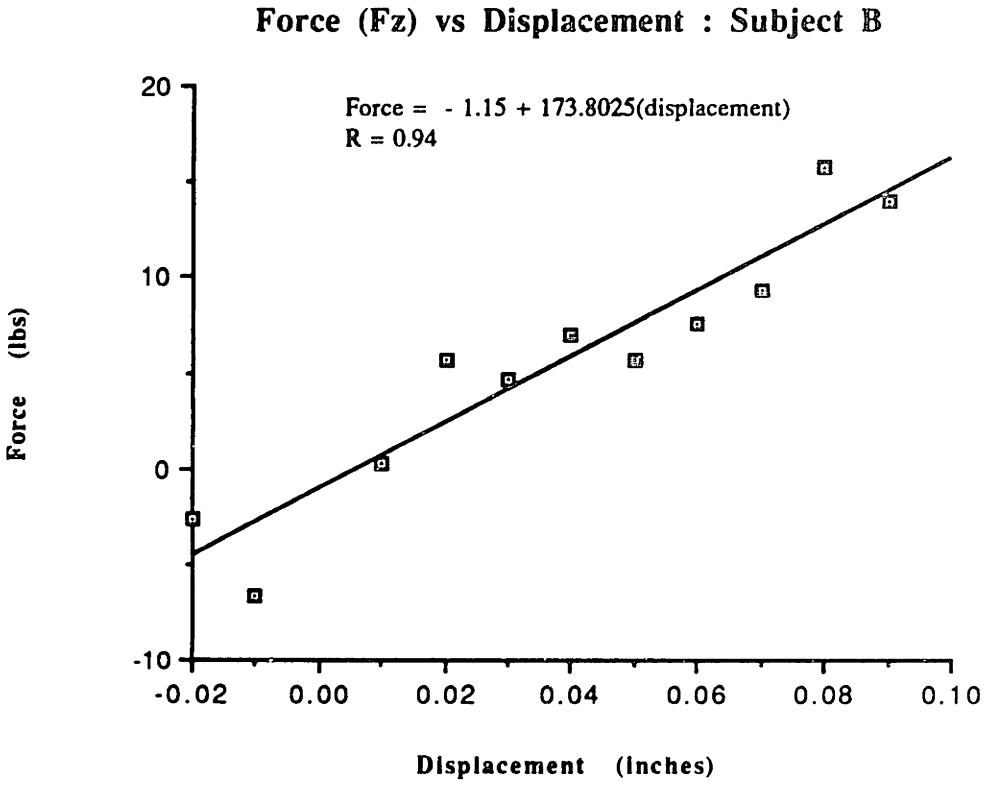

Figure #2-12. Force vs. displacement for subject B in the Z direction

Table 2-3
Results of Stiffness Experiments
(lbs/in)

Force Direction	Subject A	Subject B	Subject C
X	$K_x = 106.30$	$K_x = 123.22$	$K_x = 102.41$
Y	$K_y = 92.19$	$K_y = 91.45$	$K_y = 154.70$
Z	$K_z = 391.29$	$K_z = 173.8$	$K_z = 221.27$

Taxonomy of Possible Devices

In this section we discuss some of the technical and hardware issues we evaluated before developing the MED manipulator. To assist in structuring the problem, we investigated both the structure of the device and the component technology.

Device Structure

This discussion entails a discussion of all possible loading methods and then a narrowing of these methods to the most feasible. Figure 2-13 shows a breakdown of possible methods of load application to the human arm. As the figure shows, limb loading can be grouped into two very broad categories, methods having no physical connection to the limb and methods having physical connections.

The latter methods have many possibilities. These include loads applied using controlled magnetic fields and electrostatic fields as well as using newton-euler law relationships to produce a force (moment) by changing linear momentum (angular momentum) of of the combined subject and device. This latter method might involve such ideas as accelerating masses or using directed air jets (Colgate, 1983).

While the application areas of controlled magnetic and electrostatic fields are not practical for technical reasons (very large fields are needed to produce the magnitudes of loading we are looking for) the methods using newton-euler relationships may have some promise. In general, however, Colgate (1983) forsaw many control difficulties for either of these methods.

Although load application via physical realizations, they have many physical possibilities, they can be subdivided into two classes, those including connections which are tensile only (eg. cables) and connections which are both tensile and compressive (eg. linkages). A tensile device could be pictured as a series of cables connected to the subject on one end and to actuators on the other end. By connecting them in particular geometric patterns (Atkinson, Bond, and Wilson; 1977), they can produce loads in all directions. A

tensile and compressive device could be pictured as any possible geometry of linkages including robots.

The only practical method for applying loads which could be developed into a (near) future wearable orthosis was a linkage device. These devices have developed a high degree of sophistication in the area of robotics, and applying this type of device was very feasible.

Figure #2-13
Methods of Load Application

Linkage Structural Possibilities

As has been consistent throughout this document, the emerging technology forces us to develop a lexicon. We continue this development here. There are many different types of linkage devices (manipulanda) from which to decide. In order to facilitate the discussion of alternative load application structures, we developed three classifications: **coincident, semi-coincident**, and **non-coincident** as shown in Figures 2-14, 2-15, and 2-16.

A coincident manipulandum is defined here as an exoskeleton whose the axes are coincident with the axes of the human arm. Semi-coincident manipulanda have one or more axes are not coincident with the human joint axes. Finally, non-coincident manipulanda have an axis structure completely different from the structure of the human arm.

With any of the manipulator structures -- coincident, semi-coincident, and non-coincident -- the base of the manipulator can be connected to either the human body or to ground. The former connection affords a greater portability of the device while the latter connection allows for mechanical simplicity in the base and looser specifications on the total weight of the manipulator.

The major disadvantage of coincident and semi-coincident manipulanda is difficulty of alignment. Although Figure 2-3 shows a human arm mechanism with simple revolute joints, their axis of rotation actually change with position, activation level of the muscles (compression of cartilage), and external load on the limb. Also, every individual has different body parameters such as bone and muscle shapes and sizes. This produces a construction difficulty because of the customization that must be done for each manipulandum. Simply put, it is nearly impossible to design a a linkage which is perfectly coincident with the human arm joints (this alignment problem may be absorbed by the soft tissue compliance).

The non-coincident manipulandum also has deficiencies. The manipulator must be built so that it moves in the same workspace as the human arm but it stays out of its way. This problem does not exist with the coincident manipulandum.

We chose to move forward with the non-coincident manipulandum. The decision was made mostly because we could use the non-coincident manipulandum without needing to adjust it to different human arm geometries.

West (1986) has worked out a general mathematical method for analyzing braced manipulators, i.e. manipulators which have one or more linkages attached to them. This method could possibly be applied to different manipulator structures for analysis. The manipulator structure we use is developed mathematically in the next chapter in connection with an analysis on different linkage types with MED actuators connected to the human at a single point. It will be shown that in order to have force-velocity colinearity at the end of the human arm, we need to have a specific manipulator structure.

Analysis can be made more complex by considering multiple manipulators connected across one or more joints in any of the coincident, semi-coincident, or non-coincident manners. We leave the many possibilities to the reader's imagination.

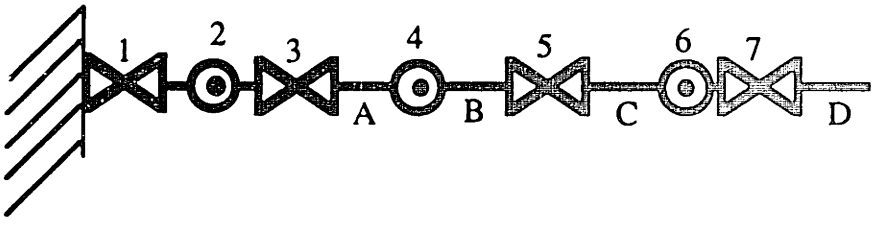

Figure #2-14. Coincident manipulator (exoskeleton)

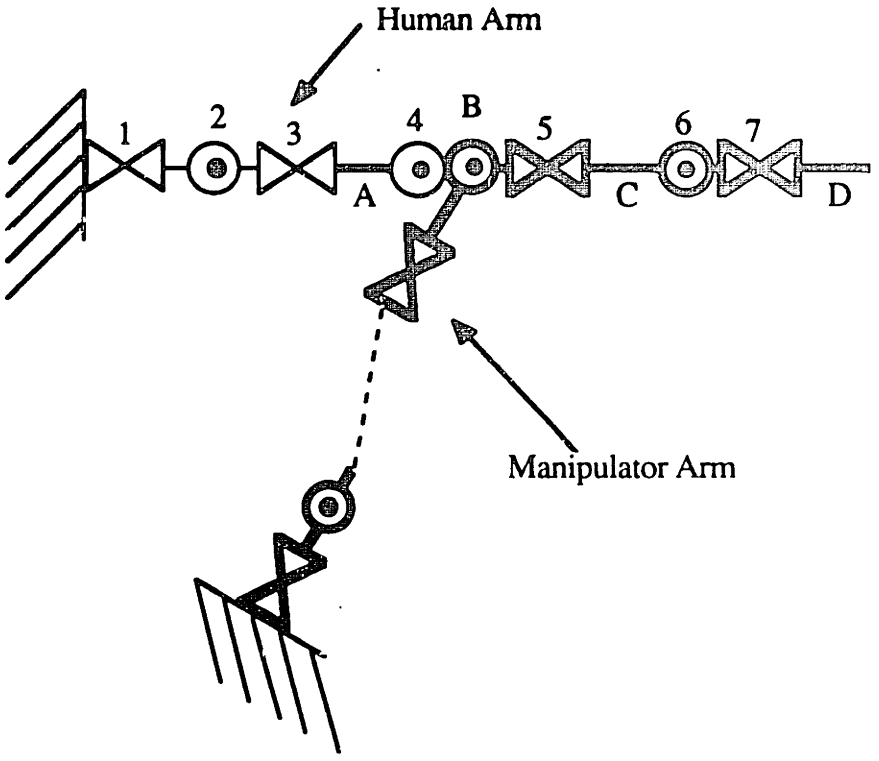

Figure #2-15. Semi-coincident manipulator

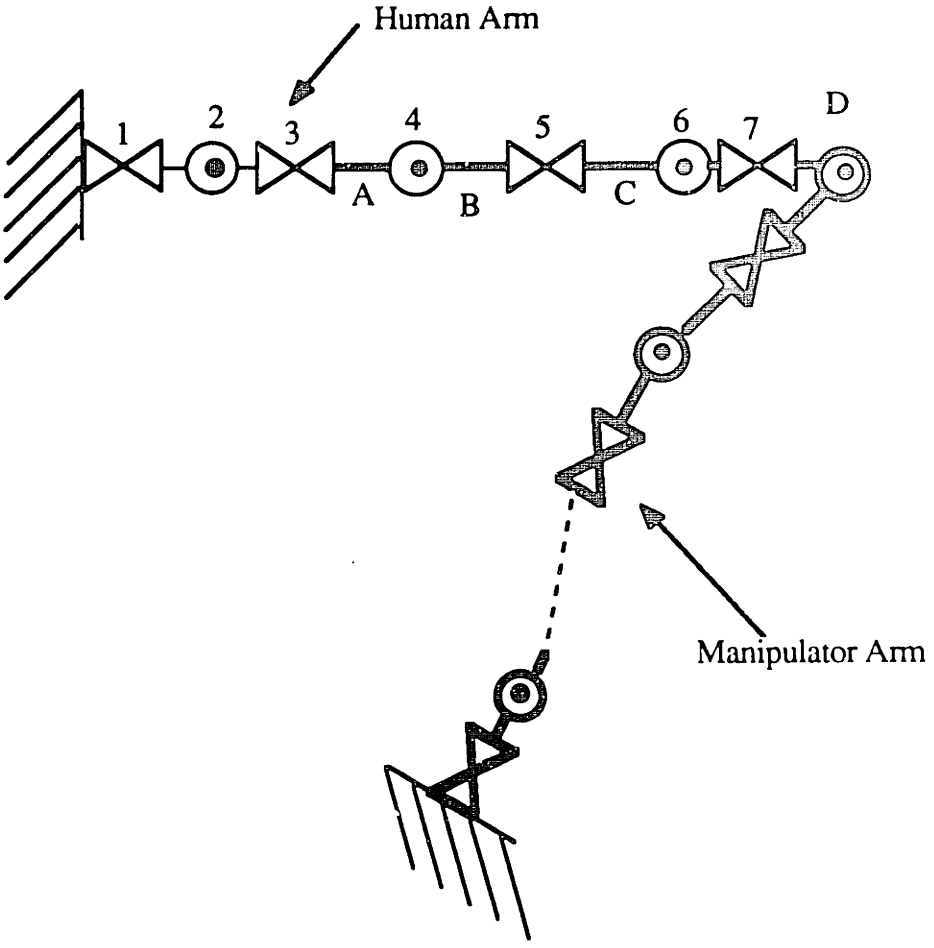

Figure #2-16. Non-coincident manipulator

Component Technology Assessment

To better understand the possible components, a technology assessment was undertaken. The objective of the assessment was to determine the best components for uses in the MED manipulator design. Four areas were investigated:

- actuators,
- transmissions
- sensors, and
- materials.

The ideal manipulator design would be infinitely stiff, have zero mass, use no power, make no noise, be invisible and completely safe, cost nothing to manufacture, and have controllable impedance levels ranging from zero to infinity. Although this is unrealizable, we need to keep the ideal in mind during component evaluation.

Actuators

Virtually any type of brake can be made computer controllable. In this section we discuss some of the practical actuator possibilities including motors, hydraulic systems, and particle brakes. Desirable characteristics for MED actuators are:

- High power output/weight ratio (power density)
- Low power output/power input ratio (efficiency)
- Ease of control
- Low power-off friction
- High inherent control bandwidth
- No need for transmission
- Simple to implement
- Proven dependability
- Low cost

Electric Motors

Good discussions of electric motors are given elsewhere (see Chesmond, 1982; Kenjo and Nagamori, 1985). Here we discuss the use of electric motors as MED actuators. A diagramatic representation of a permanent magnet DC motor is shown in Figure 2-17. Motors are usually controlled by controlling the excitation voltage, e, or current, i. To make the motor behave only in an energy dissipation mode we could still control e or i, or we could use the motor's inherent passive braking property[7]. The motor can act like a controlled viscous brake by controlling the armature resistance, R. This can be accomplished in one of a number of ways including switching the output lines through a resistor network or connecting the output lines through the collector-emmiter of a transistor and controlling the motor current by means of the transistor base current. If the resistor network is chosen, a practical method of changing resistances, called an R-2R network (Sheingold, 1980) can be copied from digital to analog converters.

Another method for using electric motors as brakes is using a separately excited dc motor (shown schematically in Figure 2-18). With this motor, the controlled brake would have its output leads shorted together; then, the field current, i_f, changes the braking torque. While the permanent magnet design results in a higher efficiency than the field current design, the field current design may result in better controllability.

Electric motors have two drawbacks as MED actuators. First, most dc motors produce their highest power and efficiency at relatively high speed and low torque, requiring a gear reducer for most applications involving manipulators. Second, the power density of electric motors is very low as compared to other MED actuators discussed below. Even direct drive torque motors (motors which do not need gear reducers for some applications) have very low power density.

---

7 The passive braking property of motors is evident when the output wires of a permanent magnet DC motor are shorted together. When this occurs, the motor acts like a viscous load to an applied torque.

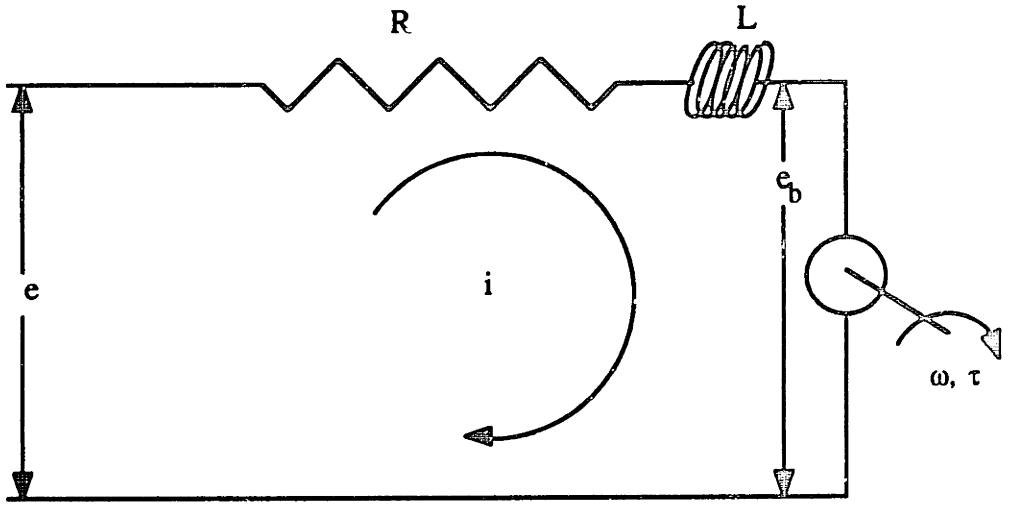

Figure #2-17. Simple model of permanent magnet electric motor

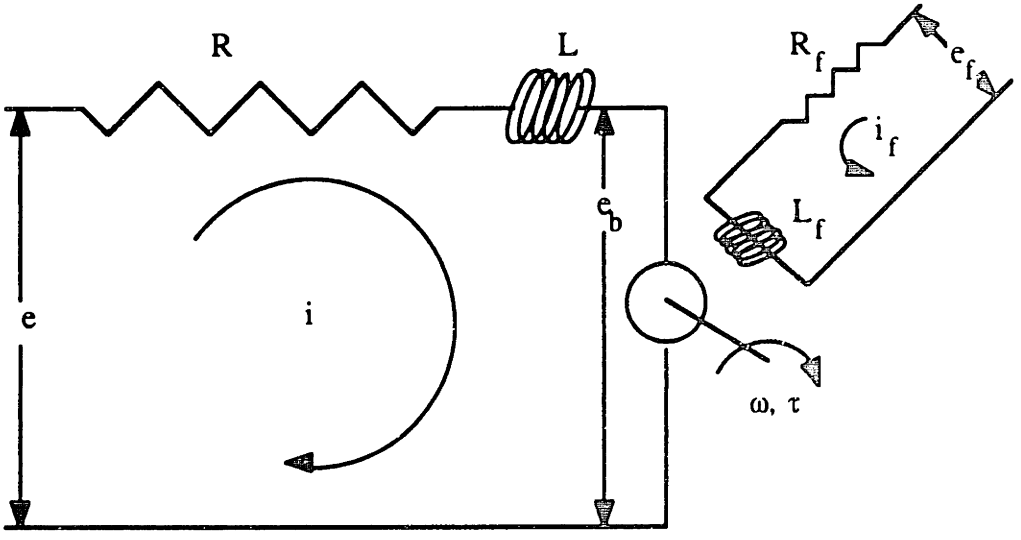

Figure #2-18. Simple model of a separately excited dc motor

An interesting design incorporating a motor is available on the commercial human rehabilitation market, developed originally by Cybex Corporation, which includes an electric motor coupled to a worm and worm wheel (Figure 2-19). The worm wheel is connected to the user's arm or leg and the human attempts to rotate the wheel. The small motor slowly turns the worm in response to a drive signal originating in measured user-produced torque. The human feels the the worm wheel turn in the direction he is pushing so that it feels like a resistive load. In this application the electric motor exists to help backdrive the normally non-backdrivable worm gear arrangement. All of the energy is dissipated in the gears, i.e., both the motor and the human do positive work. The motor has such a low power capability, however, that it is not capable of driving the worm wheel with much power.

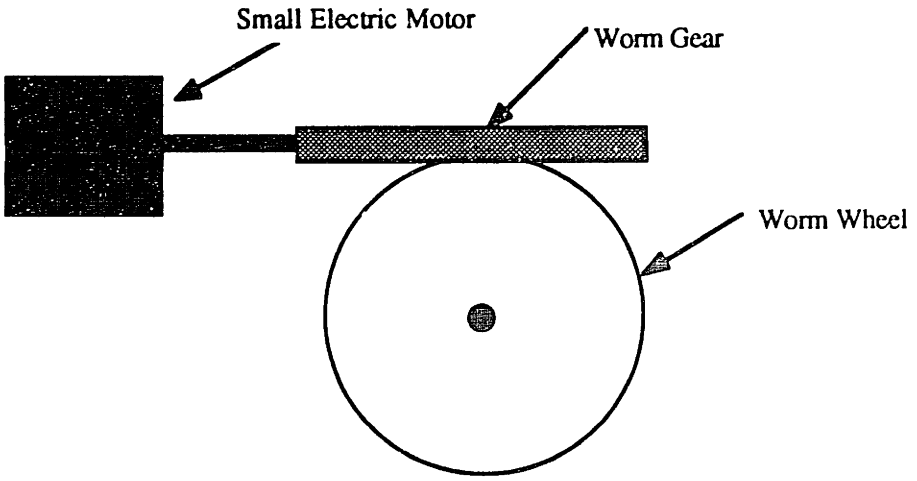

Figure #2-19. Cybex MED actuator design

Hydraulic Actuators

As with electric motors, discussions on hydraulic system actuators can be found elsewhere (see, for example, Machine Design, September 18, 1986). The most straightforward method for using hydraulic actuators as MED actuators is by resisting the flow of hydraulic fluid.

A traditional means doing so is shown in Figure 2-20. As the piston moves in the direction X, the fluid is forced in the direction of the arrows through the valve. By changing the valve resistance, the brake torque is increased or decreased. The diagram shows a translational actuator as a representative sample of the many translational and rotational fluid actuators available with application to robotics.

Hydraulic actuators are easily controlled, but they also have some negative aspects associated with them. They are very expensive because of the expensive controlled valve and they have a low power density compared with other MED actuator types.

Another hydraulic method under development is to control the viscosity of the hydraulic fluid. Electro-rheological fluids (fluid viscosity changes in an electric field) are under investigation by a number of researchers including Dr. Frank E. Filisco at the University of Michigan. As far as we know, the development of rheologic fluids has not resulted in commercially available MED actuators.

Pneumatic actuators come in the same basic configurations as the hydraulic systems. Although the air in the pneumatic actuators is lighter than the oil in the hydraulic system, the added compliance of the pneumatic system is too high to be considered for this application.

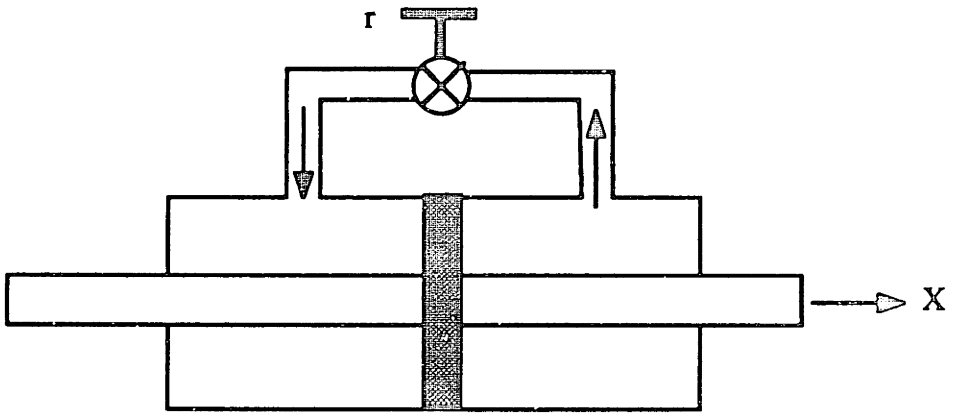

Figure #2-20. Translational hydraulic actuator

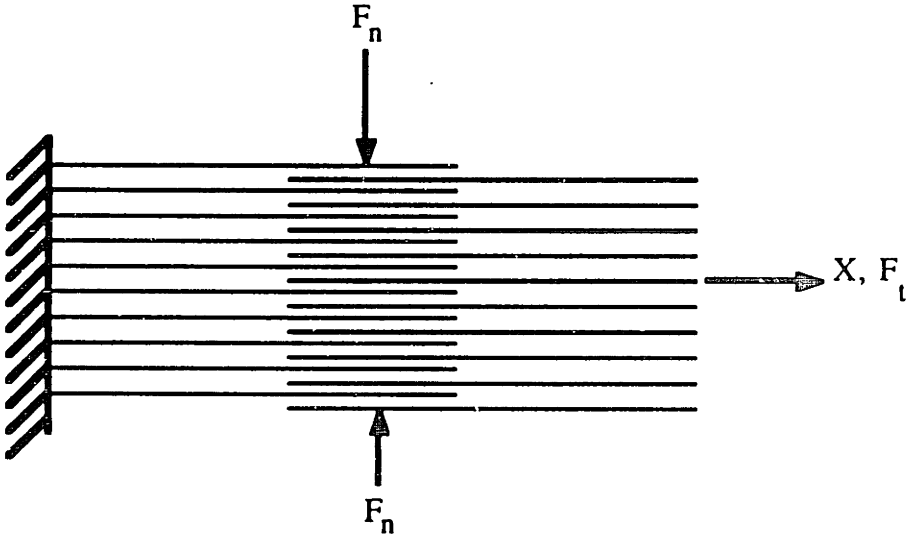

Figure #2-21. Principle of mylar brake design

Mylar Brake

A novel mylar sheet brake was designed by Hunt (1985). The concept behind this brake, shown schematically in Figure 2-21[8], was that a small normal force, F_n, on a stack of mylar film will resist an extremely high tangential force, F_t, attempting to pull apart the sheets of mylar film. This concept proved to be worthwhile in a completely passive test rig, but has yet to be connected to an active normal force generator.

Particle Brake

Finally, particle brakes were considered. Magnetic particle brakes (Figure 2-22) have a coil that, when energized, produces a magnetic field which forms chains of powdered magnetic particles. The chains of particles resist the motion of the disc attached to the brake's output shaft, producing a resistive torque which is approximately proportional to the current in the coil. Magnetic particle brakes were chosen as the actuator to use in our application mainly because of their simplicity, reliability, low cost, power density, and ease of computer control. They do, however, need gear reducers in our application.

One difficulty with most of the above MED actuators is the passive, power off, mechanical energy dissipation that occurs due to friction. This friction as well as the friction in the manipulator drive train and joints and inertial loading can not be eliminated with MED actuators. The passive properties of the MED manipulator set the lower impedance limits on the device. One possible remedy to this problem is to employ a low power active actuator in parallel with the MED actuator that compensates for the parasitic power-off impedance. A design such as this has been developed in one degree of freedom by Smith (1988) and was extended to three-degrees-of-freedom by Russo and Tadros at

---

8 The schematic representation is of a translational brake. The actual application was a rotational brake.

MIT. We felt that the additional components would unduly complicate the present design without adding benefits presently known to be important.

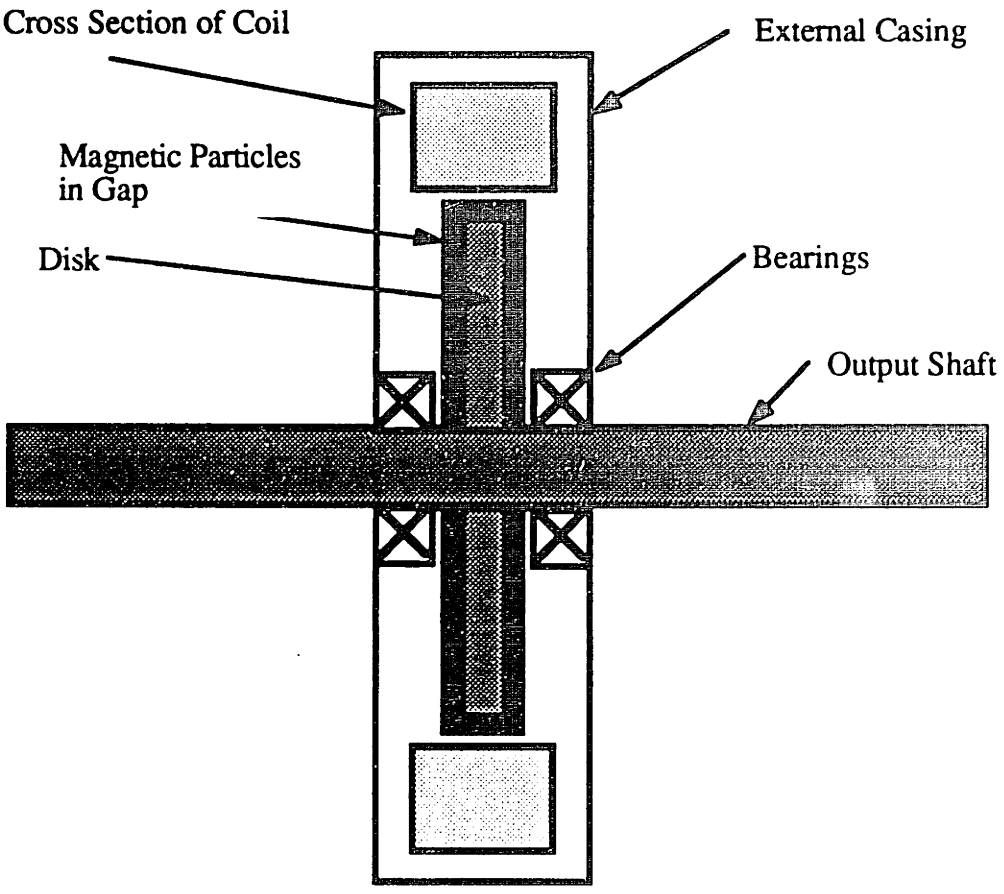

Figure 2-22. Diagram of particle brake

Transmissions

A variety of transmissions are on the market. This section discusses the drives we most seriously considered for our application, harmonic drives, gears, and cable drives.

Desirable transmission characteristics for use in a MED manipulator are:

- Low weight
- High stiffness
- Low backlash
- High level of backdrivability
- High efficiency (Low friction)
- Simple to implement
- Low cost

Harmonic drives

Harmonic drives are an attractive choice due to their compactness, complete absence of backlash, and high torque capability for their size and weight. On the negative side, they are difficult to backdrive, lacking in stiffness in the zero output torque region, and expensive.

Gears

Excellent discussions of types and relative merits gear trains are provided elsewhere (for example, Mansfield, 1988; Spotts, 1985; Shigley and Mitchell, 1983). Briefly, gears are fairly high in inertia, have backlash, and are fairly expensive applications requiring for high precision and high power. As Mansfield (1988) notes, gears can be made to perform near backlash free, but they are expensive and require precise alignment resulting in more expense.

Cable drives (tendon drives)

Cable drives are compact, lightweight, provide power transmission over distances, backlash free, stiff, and inexpensive. Cable drives have been used in a number of MIT

applications recently (for example Townsend, 1988; Dipietro, 1988) as well as more generally (Bejczy and Salisbury,1980; TRAX, 1986; Takase et. al., 1974). Townsend (1988) reports from his theoretical development that the efficiency of cable drives increases the higher the cable drive stiffness, the lower the tension difference between the two cables, and the lower the number of transmission stages. He further reports that pulley eccentricity causes torque ripple caused by changing the effective radius. Dipietro (1988) and the Wire Rope Users Manual (1981) give very useful information on cable drive design. While we do not believe cable drives have been completely evaluated in robot manipulators, they have proved reliable in elevators, airplanes, automobiles, cranes, computer plotters, and an assortment of other applications.

We chose to use cables in our design because they were low weight, stiff, backlash free, backdrivable, efficient, simple to implement, and had low cost. In short, they seemed to be the ideal transmission.

Sensors

The MED manipulator requires two types of sensors, a position sensor for each joint/actuator and a force/torque sensor to measure the six loads applied between the manipulator end point and the limb coupler.

Desirable sensor characteristics for all sensors are:

- Low weight
- Compact
- High accuracy
- High reliability
- Simple to implement
- Low cost

Position Sensor

A large number of technologies exist which will transduce angles, the most common of which are potentiometers, resolvers, and optical encoders. These sensors are discussed in this section.

Position measurement can be made at the actuators, at the joints or at the endpoint. Only position measurement at the actuators or joints is discussed here. For active actuators in robotic systems, researchers have found that mounting the sensors on the motor produces a much more robust controller. This type of mounting does however, reduce the precision of the endpoint position calculation because of backlash, slip, and compliance between the actuator and the manipulator joint. Some researchers have used two sets of sensors to alleviate this problem, one set at the actuators and another at the joints.

Resolvers provide high resolution, linearity, and ruggedness (they are often used in military applications). They are however, larger than potentiometers or encoders, more expensive, and more difficult to interface to computers (commercially available boards do not exist to interface resolvers to computers).

Optical encoders are smaller, accurate devices, but, as with resolvers, they are larger in size than potentiometers, more expensive, vibration sensitive, and harder to interface to computers.

Potentiometers are small, lightweight, easy to interface to computers, and inexpensive. However, potentiometers may have limited accuracy and are sensitive to dust and electromagnetic and mechanical disturbances (EMI, shock, vibration). For our application, we used potentiometers primarily because of cost considerations.

To measure velocity in a potentiometer position circuit, the position output can be differentiated using either analog or digital techniques, or a tachometer can be added to the system. To keep the device simple and light, a differentiation circuit was used to derive velocity from the potentiometer position sensor.

Force/Torque

Any Force/Torque sensor consists of three parts: an elastic element which deforms under loading, a sensing element which senses the elastic element deformation, and an electrical circuit which converts the sensing element output into a signal suitable for computer interfacing.

The many different geometries of elastic elements indicate the many possible methods of measuring force and torque. Design of the force/torque transducer elastic element is largely driven by desired load capacity, load directions, transducer stiffness, transducer natural frequency (fast response time), and required sensitivity to loading in order to attain the desired characteristics described above. It is desirable that the detector-transducer be as sensitive as possible (maximum output per unit input load should be obtained). This would seem to require an elastic member that deflects considerably under load, i.e., as low a value of K as possible. Novel elastic element geometries have been developed, however, so that the transducer can be mechanically stiff while retaining sensitivity.

One issue which needed to be resolved is whether to measure the torques at the joints of the manipulator and compute the forces and torques at the endpoint of the manipulator (see Luh et. al., 1983; Asada and Youcef-Toumi, 1987) or whether to measure all loads at the endpoint of the manipulator. We chose the latter because the former may result in better joint control, it cannot measure the inertial and friction loading between the joints and the endpoint of the manipulator and is therefore less accurate than direct measurement as a means of determining endpoint force and torque.

Many designs of multi-axis strain gage dynamometers have been described in the literature (see, for example, Beckwith and Buck, 1982; Ono and Hatamura, 1986; Chaplin, Lueders, and Zhao, 1987; Watson and Drake, 1978; Molland, 1978; Goodwin, 1975; Millward and Rossiter, 1983; Regan and Reuber, 1985; Girard, D., 1986; Quinn and

Mote, 1988; Ewald, 1979; Dubois, 1981; Tani, Hatamura, and Nagao, 1983, Wunderly and Hull, 1987, Hull and Davis, 1981; Shaw, 1984). Six-degree-of-freedom force/torque sensors are also available commercially for prices generally above $5,000 (see, for example, Lord Corporation, JR^3, or Barry Wright Corporation references).

Sensing elements range from the exotic sensors such as capacitive sensors (Brookes-Smithe and Colls, 1939; Carter et. al., 1945; Hetenyi, 1950A) and inductive sensors (Langer, 1943); to more commonly used piezoelectric sensors (Ripperger, 1954; Mark and Goldsmith, 1955) and piezoresistive sensors (Mason and Thurston, 1957) to the most commonly used metalic resistive sensors (Perry and Lissner, 1962).

Use of some form of bridge circuit is the most common method for connecting passive transducers to computer equipment in making up a measuring system. Of all the possible configurations, the Wheatstone resistance bridge (Wheatstone, 1843) is used most often. Wheatstone bridge circuits consist of four resistance arms with a source of energy and an amplifier. Measurements may be accomplished either by balancing the bridge by making measureable adjustments in one or more bridge arms until the voltage across the bridge is zero, or by determining the magnitude of unbalance from the amplifier output. Typical resistance transducers using a circuit of this kind may include resistance thermometers, thermistors, or resistance-type strain gages.

For our application, discussed in detail in Chapter 4, we decided on the proven resistive foil gages mounted on a common cross design elastic element. This design proved to be compact, low cost, reliable, and easily implementable.

Materials

The requirements that the manipulator be stiff but light can best be can be achieved with both a good geometric design and stiff, lightweight material. The composite materials we chose for our design are as advanced as possible without losing manufacturing simplicity. Composite materials are present in almost every competitive sport and other orthosis applications (Schwartz, 1984). Examples of these applications include bicycles, kayaks, lightweight aircraft, oars, water skis and golf clubs. Our initial assumption was that if these commercial products are using advanced composites, then they should be sufficiently developed for our design. In the MED manipulator system, we use prefabricated graphite epoxy composite tubing and machined aluminum parts. Thompson and Sung (1985) found favorable results using graphite epoxy composite over steel.

One-Degree-of-Freedom Testbed

After determining that a particle brake, belt drive, potentiometer, and strain gage load cell system were the components which best satisfied our design criteria, we developed a one-degree-of-freedom test bed to both determine how well the components performed their function and to use for developing sensing and control electronics development. The test bed underwent a few stages of development, beginning as part of an MIT Bachelors Thesis (Lovelace, 1988) and ending up as a stand-alone one-degree-of-freedom orthosis simulator as part of another Bachelors Thesis (Wong, 1990). The design is discussed in more detail in the two citations and describe briefly below.

The overall design, shown in Figure 2-23, contains a Placid Industries magnetic particle brake, a Helipot potentiometer, and Omega Engineering Strain Gages. The B115P 24 Volt particle brake has a rated torque of 115 inch-lbs at a rated current of .333 Amps, a maximum speed of 1800 RPM, and a de-energized drag[9] of 25 ounce-inches. Potentiometers were chosen as the position sensors for this application and velocity was derived by differentiating the position signal. Helipot model 6186-R5K L1.0 B604M potentiometers were chosen for this application. These conductive plastic 5KΩ potentiometers have a manufacturers specification of 1% linearity over their near-360 degree range of operation. The potentiometers connect to the output shaft through PIC Designs No-Slip series timing belts and pulleys. The double aramid fiber core timing belts are designed and manufactured to be backlash free, operate without lubrication, and to be very quiet during operation. A torque sensor was built with Omega Engineering Model HBM 120XY21 strain gages were chosen because of their low-cost and ease of purchase. Each strain gage backing sheet comes with two strain gages mounted in a 90 degrees rosette (the stain gages are mounted 90 degrees relative to one another). The final torque

---

9 De-energized drag is the power off "Coulomb" friction torque resulting from seals and residual magnetism.

sensor required two rosettes to measure the torque while electrically eliminating the sensitivity to other load directions.

Figures 2-24 and 2-25 show the one-degree-of-freedom system with the covers removed. In Figure 2-24, the torque-sensing strain gages are barely visible on the neck of the output shaft. In Figure 2-25, the potentiometer and belt assembly can be seen attached to the output shaft of the particle brake.

Figures 2-26 and 2-27 show the torque sensor calibration set-up, designed by undergraduate research assistant Stacy Ho, and some low level graphics software developed for this application. The calibration apparatus applied a pure torque to the output shaft of the testbed using weights and pulleys. The graphics software shown in Figure 2-27 shows real time bar graphs of the output shaft position, the torque measured from the torque sensor, and the torque command output from the computer.

The testbed was used to help develop an understanding of the components and develop electronics to interface them to a computer.

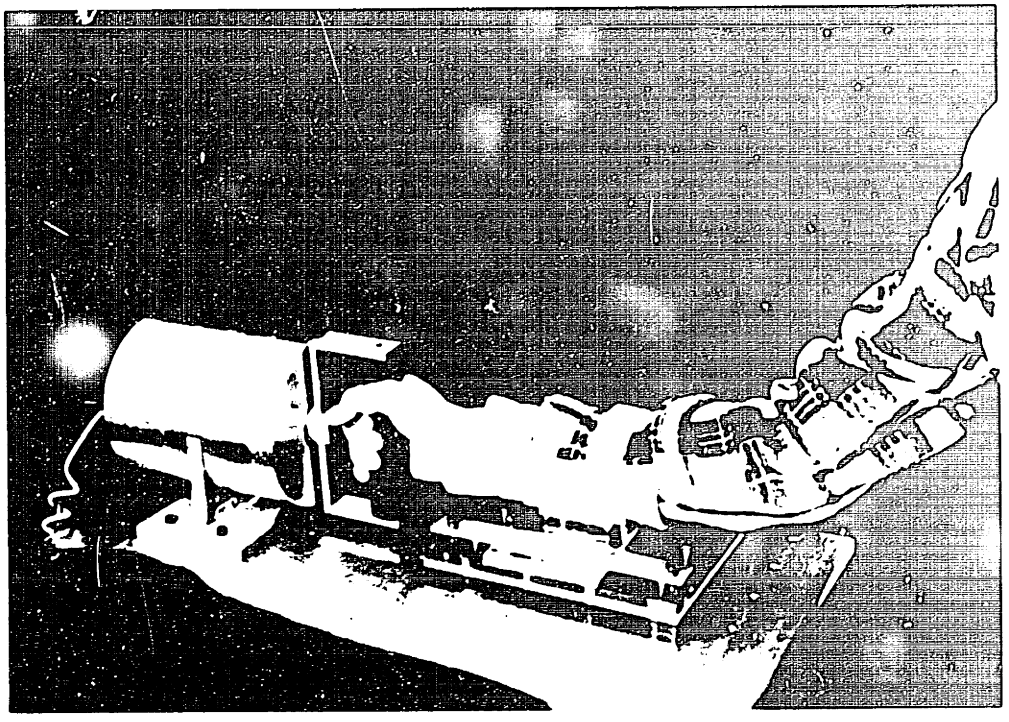

Figure #2-23. One-degree-of-freedom testbed

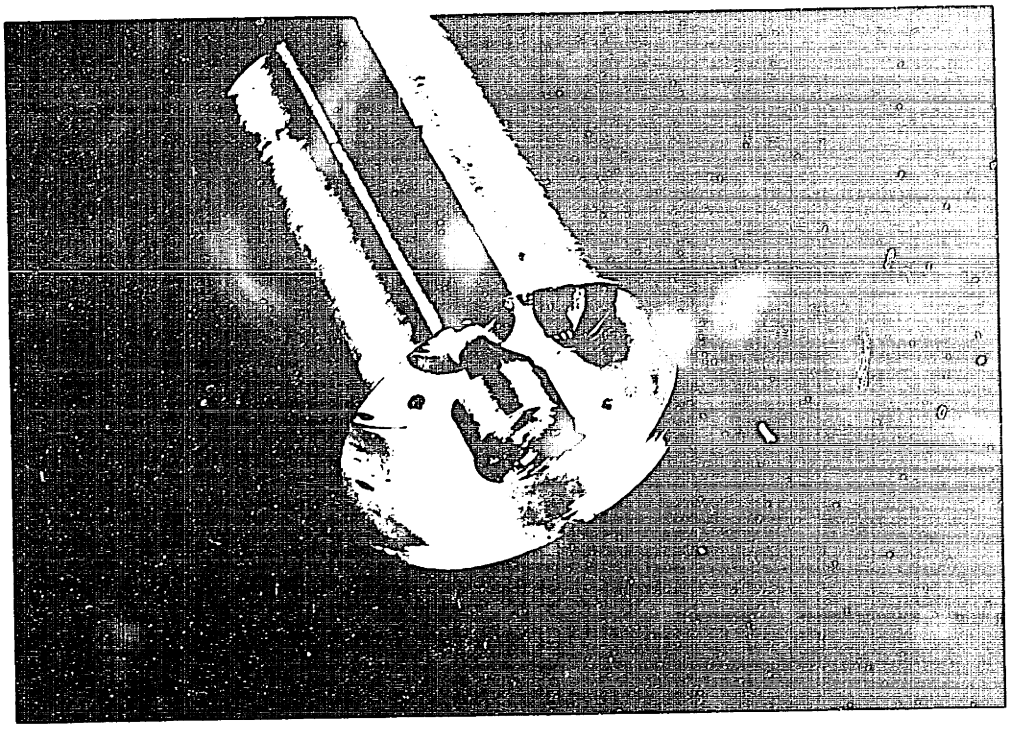

Figure #2-24. Open front end of one-degree-of-freedom testbed

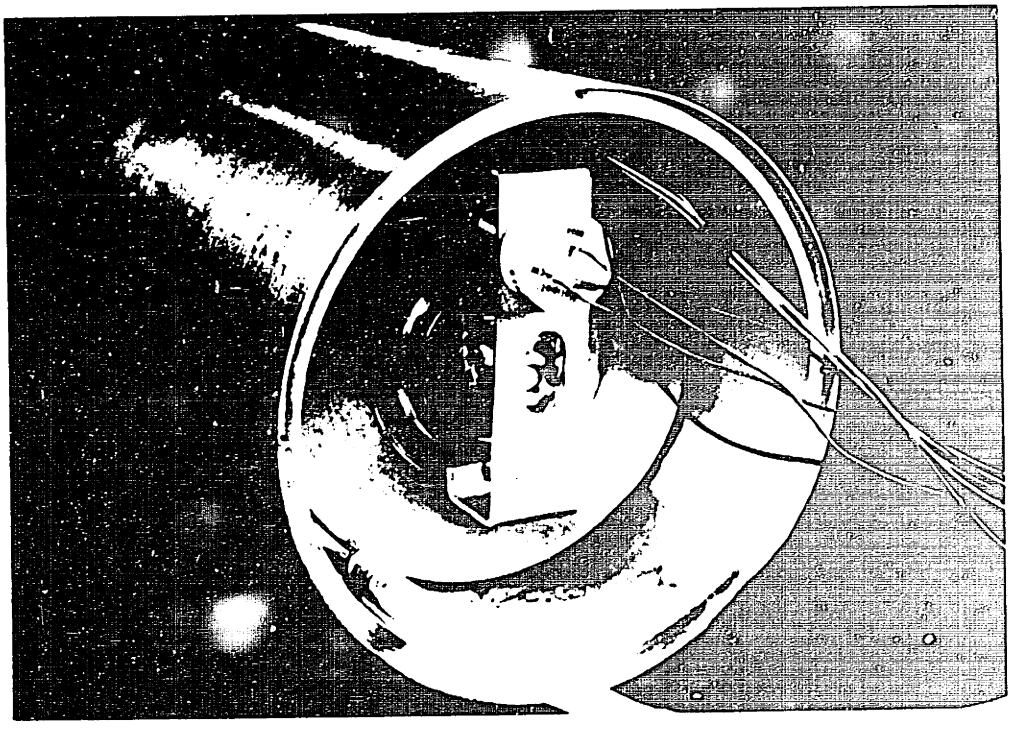

Figure #2-25. Open back end of one-degree-of-freedom testbed

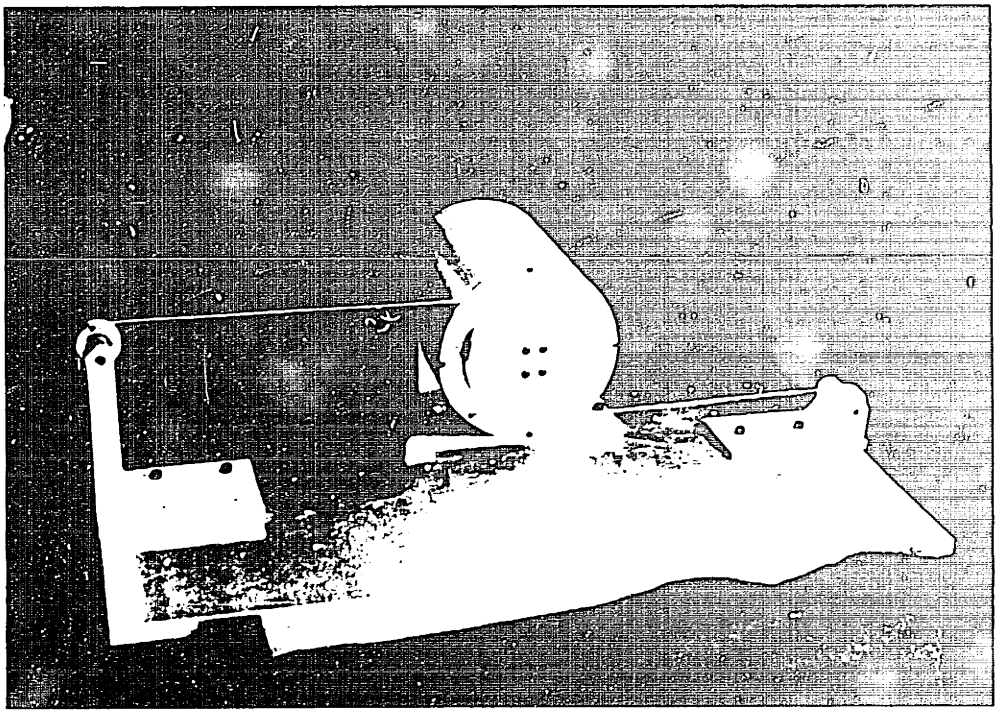

Figure #2-26. Torque sensor calibration apparatus

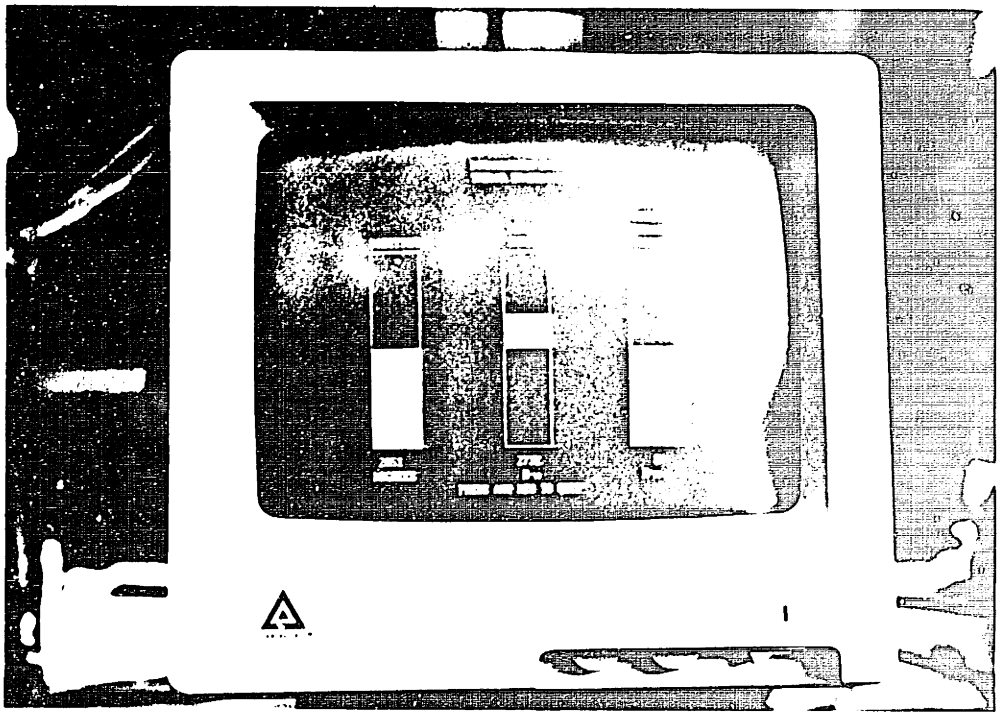

Figure #2-27. Computer graphics for one-degree-of-freedom

Chapter 3

Design Theory

This chapter develops mathematically some of the issues involved in building a linkage with MED actuators. The chapter covers five general areas. In the chapter we

1) Determine the passive stiffness, intertial, and friction requirements of the MED manipulator,
2) Develop a general theory of MED manipulators, and
3) Use the theoretical results to discuss possible linkage designs.

Our research budget dictated that very simple analysis was to be performed on the device. If the resources were present, we could perform very sophisticated computer simulations of static and dynamic behavior of the manipulator. In the end, however, we felt that our simple models guided our design sufficiently and left us with good general purpose tools from which to analyze both MED manipulators and, more generally, active robot applications.

Physical System Limitations

MED actuators are a subset of the more general active actuators. This section looks at some of the inherent physical limitations that exist with MED manipulators which, in some cases, do not exist in active manipulators.

Mass and Stiffness Requirements

We model the ideal MED manipulator in one-degree-of-freedom as shown in Figure 3-1. The MED actuator is modelled as a viscous damper with an adjustable damping parameter, b. The ideal linkage has zero mass, zero compliance, and zero

passive friction in the joints. The Bode plot assymptote for this ideal MED manipulator is shown in Figure 3-2. The assymptote has a slope of negative one[1].

Figure 3-3 shows a more practical model for the MED manipulator in one-degree-of-freedom. This model has added mass to the ideal model, but we continue to assume zero compliance in the system. The assymptotic Bode plot for this model is shown in Figure 3-4. Now we have two assymptotes. At low frequencies (below b/m radians/second) the plot looks like the ideal plot of Figure 3-2 while at higher frequencies the assymptote has a slope of negative two. This plot shows that the system model of Figure 3-3 behaves like an ideal viscous damper at low frequencies and like a mass at high frequencies. As long as our excitation frequency is well below b/m radians/second, this model behaves like the Ideal model.

This conclusion sets a maximum limit on our mass. We would like the system to behave like a damper up to a maximum of 60 radians/second (9.5 Hz)[2]. In order for this model to act like a damper up to 60 rad/sec, b/m must be much greater than 60 or, equivalently, m must be less than b/60. More generally, in order for the system of Figure 3-3 to behave like a viscous damper,

$$m << \frac{b_{min}}{\omega_{max}}. \qquad (3\text{-}1)$$

Where b_{min} is the minimum level of damping expected out of the system, and ω_{max} is the maximum excitation frequency.

Figure 3-5 illustrates another simple model of a single-degree-of-freedom manipulator. This model has zero mass but nonzero compliance. The Bode assymptotes for this model are plotted in Figure 3-6. As can be seen from the plot, this model behaves like a viscous damper for k/b greater than the maximum excitation frequency and like a

---

1 The vertical axis on the Bode plot is not in the units of decibels as sometimes seen. To convert to decibels, multiply the vertical axis values by 20. The slope in this case becomes -20 db.

2 Pathological tremor is seen is the 2-4 Hz. frequency band. The system behaving like a viscous damper up to 9.5 Hz. should be sufficient to make the device "feel" viscous in the tremor band.

spring otherwise. More generally, in order for the system of Figure 3-5 to behave like a viscous damper,

$$K >> b_{max}\omega_{max}. \tag{3-2}$$

Where b_{max} is the maximum viscous damping expected out of the system.

Models of greater complexity can be developed for this system, but all will lead to the same conclusion: The stiffness of the manipulator should very large and the mass of the manipulator should be very small.

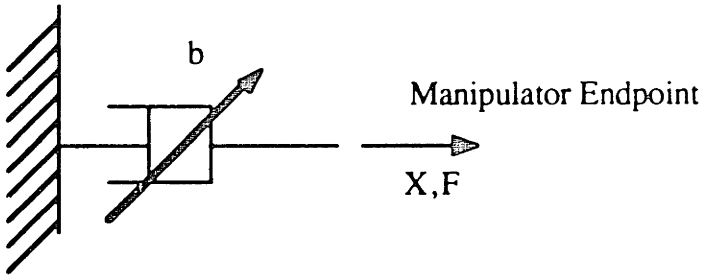

Figure #3-1. Ideal MED manipulator model

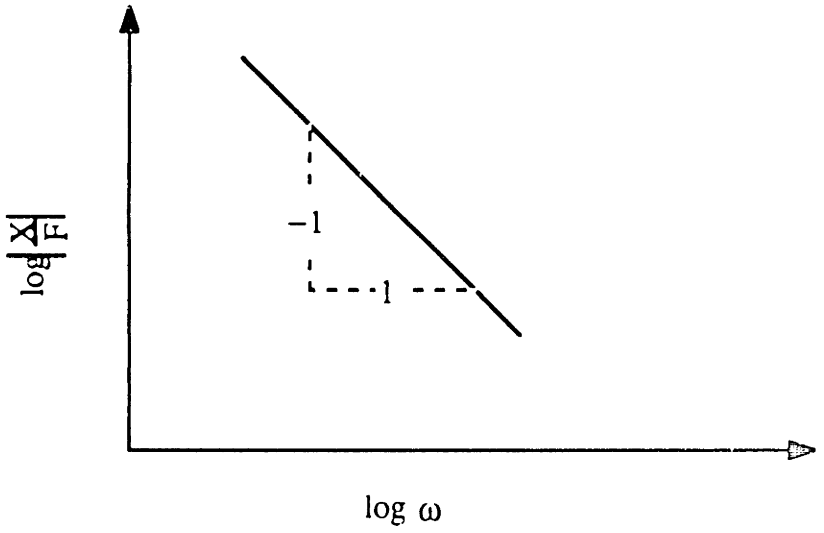

Figure #3-2. Bode plot assymptotes for ideal MED manipulator model

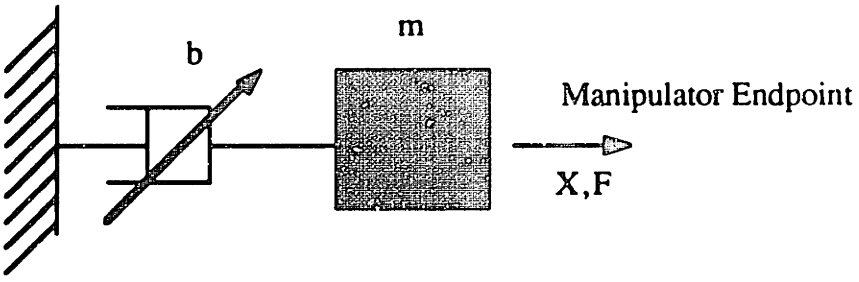

Figure #3-3. Dynamic system model of manipulator (assuming zero compliance)

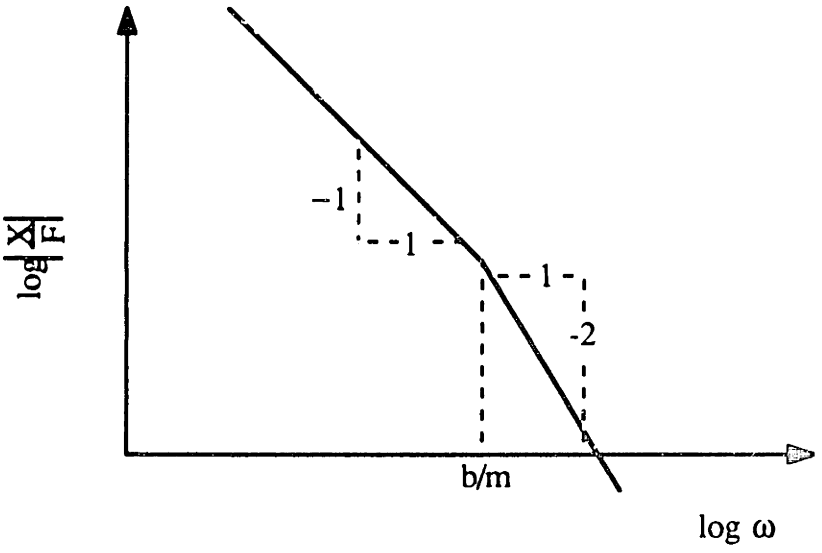

Figure #3-4. Bode plot assymptotes for zero compliance model

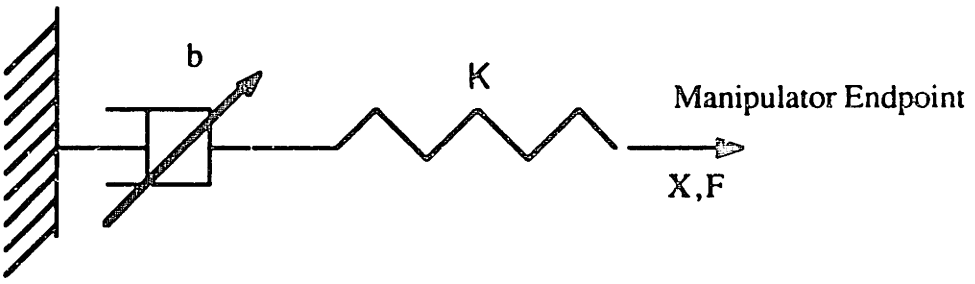

Figure #3-5. Dynamic system model of manipulator (assuming zero mass)

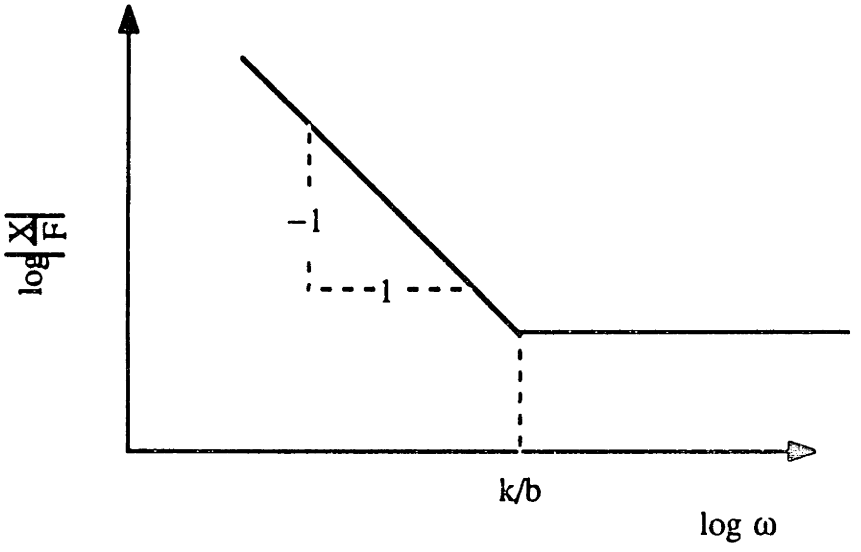

Figure #3-6. Bode plot assymptotes for zero mass model

Optimal Placement of Counterbalance Mass

In order for the human connected to the endpoint of the manipulator not to feel the weight of the manipulator mass, a method of countering the effects of gravity must be be implemented. Traditionally robots have been counterbalanced with either springs or masses. Springs do not add to the passive mass of the manipulator but are more difficult to use as a perfect balance. Counterbalance masses were chosen for this particular application mostly because of the simplicity of design and adjustment. While increasing the inertia of the device, the counterbalance mass also has useful effects of reducing the inertial coupling effects between manipulator joints.

Figure 3-7 shows a simple one-degree-of-freedom counterbalance model. We assume for simplicity that the point mass of link, m, and the length of the link, l, are fixed by the design and we have freedom to choose counterbalance length, d, and mass, m_c. In order for the link to counterbalance

$$ml = dm_c. \tag{3-3}$$

Given parameters of mass, m, and length, l, we would like to find the parameters of counterbalance length, d, and mass, m_c, such that the inertia of the link is minimized. The total inertia about the pivot is

$$I = ml^2 + m_c d^2. \tag{3-4}$$

From equation 3-3

$$m_c = \frac{ml}{d}. \tag{3-5}$$

So, combining 3-4 and 3-5,

$$I = ml^2 + mld \tag{3-6}$$

which is minimized by setting d = 0. Putting d = 0 into 3-5 and we get $m_c = \infty$.

This derivation suggests that to minimize the counterbalanced link inertia, we should make the counterbalance distance as small as possible and the counterbalance mass

correspondingly large. In the limit, d = 0 and $m_c = \infty$, we have no added inertial to the link.

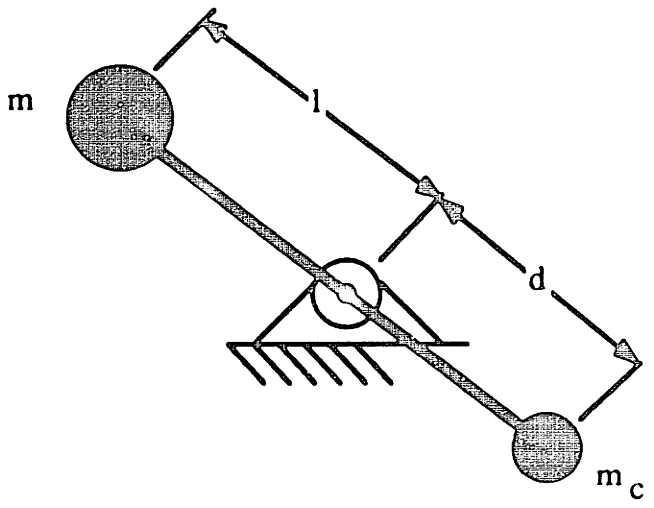

Figure #3-7. One degree of freedom counterbalance model

The two-degree-of-freedom counterbalance model of Figure 3-8 is more difficult to analyze. Now it the counterbalance mass for link 2, m_{c2}, were infinite, the moment of inertia about link 1 would be infinite. This problem can be broken into two steps. First, set the counterbalance length and mass for the second link, d_2 and m_{c2}. After this is accomplished, the second link center of mass is at the end of the first link and the problem drops down to the one-degree-of-freedom problem of Figure 3-7. In the limit, the link 1 counterbalance length will go to zero, $d_1 = 0$, and the counterbalance mass will go to infinity, $m_{c2} = \infty$.

By looking at the counterbalance problem in this way, we can break down the problem into a problem of optimizing the placement of the link 2 counterbalance mass so that the inertia of pivot 2 motion plus the inertia of pivot 1 motion is minimized. Performing this optimization, we get $d_2 = l_2$ and $m_{c2} = m$. In summary, for the minimum

total inertia of pivots 1 and 2, we set the counterbalance lengths $d_1 = 0$ and $d_2 = l$, and the counterbalance masses $m_{c1} = \infty$ and $m_{c2} = m$.

In our final manipulator design (discussed in Chapter 4), which had m = 3.5 lbs and l = 22.56 inches, we ended up with the counterbalance lengths $d_2 = l/2$ and $d_1 = l/3$ for practical reasons. This result produces an interesting result for how an endpoint mass propagates through the system. In our manipulator, for every unit of mass at the endpoint we need two units of mass m_{c2} and six units of mass m_{c1}. In total, every unit of mass at the endpoint adds nine units of mass to the total manipulator mass.

Counterbalance models for more degrees of freedom have been developed for our manipulator by Undergraduate Research Assistant Susan Huang (1989). Huang's results suggest that this simple two-degree-of-freedom model is sophisticated enough to develop a manipulator with all its practical restraints. In general, for pivots other than the most proximal place the counterbalance mass at a distance of approximately the same dimensions of the original link. For the most proximal pivots, put the mass as close as practically possible to the pivot and make it of a high mass.

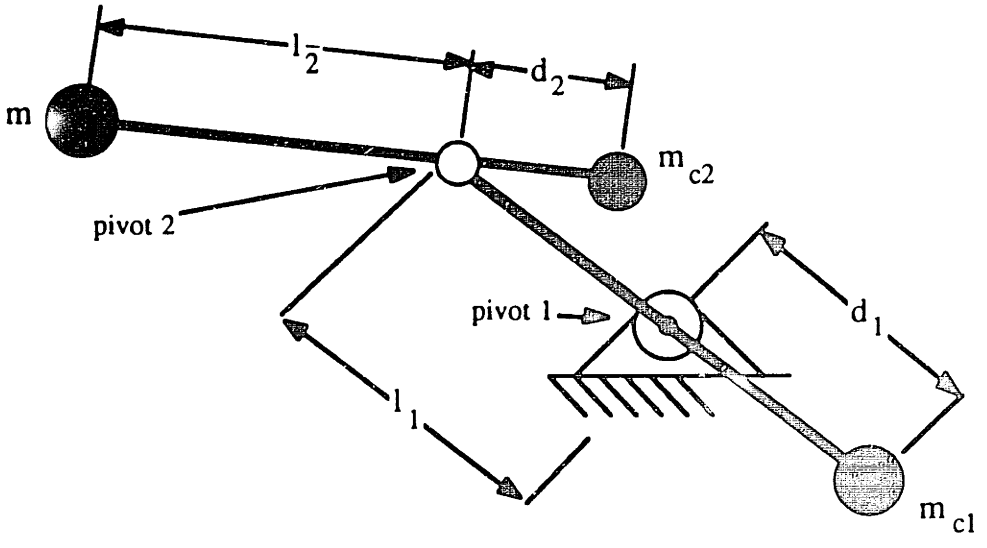

Figure #3-8. Two degree of freedom counterbalance model

Passive System Friction Effects

In order to discuss how passive manipulator friction upsets the control of a MED manipulator, consider the case of force-velocity colinearity for the simple two-degree-of-freedom cartesian manipulator of Figure 3-9. Assume that a MED actuator is connected to each of the translational axes of movement so that the damping parameters b_x and b_y can be controlled. Now suppose a human pushes[3] on the manipulator endpoint in the direction $\mathbf{f_h}$ of Figure 3-9 and the manipulator moves in the direction v. Under what conditions, we can ask, do the force and velocity become colinear for all force directions? To answer this, we can break the problem up into a joint-space reaction to the force, $\mathbf{f_h}$, and then recombine the joint velocities to get the endpoint velocity.

As with all models in this research, the cartesian manipulator model is simplified by assuming a quasi-static movement (ie: neglect the mass of the linkage). This can be accomplished by moving the endpoint of the manipulator very slowly or by building the manipulator out of lightweight materials.

If we push with force $\mathbf{f_h}$, then the X MED actuator sees force f_x and the Y MED actuator sees force f_y. The joints have reaction velocities

$$v_x = \frac{f_x}{b_x} = \frac{|\mathbf{f_h}|}{b_x} \cos \phi \tag{3-7}$$

$$v_y = \frac{f_y}{b_y} = \frac{|\mathbf{f_h}|}{b_y} \sin \phi \tag{3-8}$$

3 We have not been careful about assigning causality in our derivations. The reader will find that we change causality depending on the particular situation.

Combining the individual velocities and setting $b_x = b_y = b$ to get the endpoint velocity,

$$|v| = \sqrt{v_x^2 + v_y^2} = \frac{|f_h|}{b} \tag{3-9}$$

$$\alpha = \text{atan}\left(\frac{v_y}{v_x}\right) = \text{atan}\left(\tan\phi\right) = \phi \tag{3-10}$$

This results shows that viscous damping in a cartesian manipulator results in inherent force-velocity colinearity as long as the damping parameters in both directions are equal.

Figure 3-11 shows the effect of passive coulomb friction in the joints of the manipulator. A cartesian manipulator with coulomb friction f_x in the X direction MED actuator or joint and f_y in the Y direction produces a constant passive force magnitude and direction for movement in each quadrant. Only in the velocity direction along one of the joint axes or directly along the combined coulomb friction direction does coulomb friction result in force-velocity colinearity. The passive friction effect gets worse if we consider stiction[4].

What can be done to reduce the problems caused by coulomb friction? The effect may not be a problem. The passive effect is small if the passive coulomb force magnitudes are small compared with the force magnitude of the MED actuators. If passive system friction is a problem the effect could be partially offset by controlling the MED actuator to introduce an artificial coulomb force in one of the directions so that the force stays colinear with the velocity. This solution keeps the force-velocity colinearity but does not reduce the coulomb friction which may have negative effects in human motion studies. Another alternative is to add small active actuators, such as motors, to eliminate the

---

4 In stiction, the static coefficient of friction is higher than the dynamic coefficient of friction.

coulomb friction. In our design, discussed in chapter 4, we did not have difficulties with passive friction.

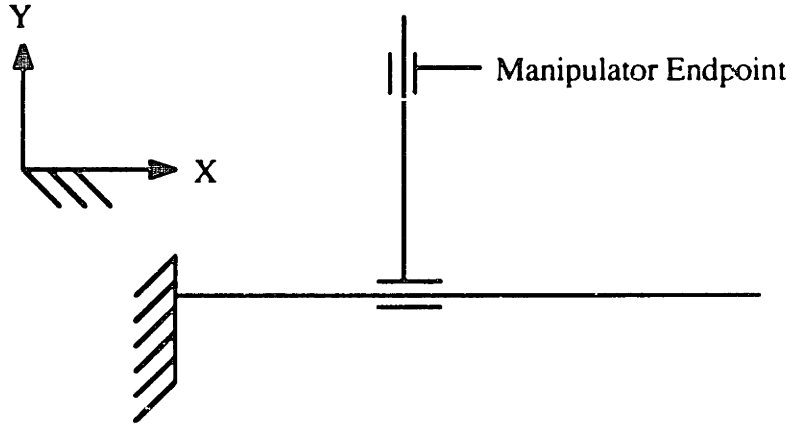

Figure #3-9. Two-degree-of-freedom cartesian manipulator

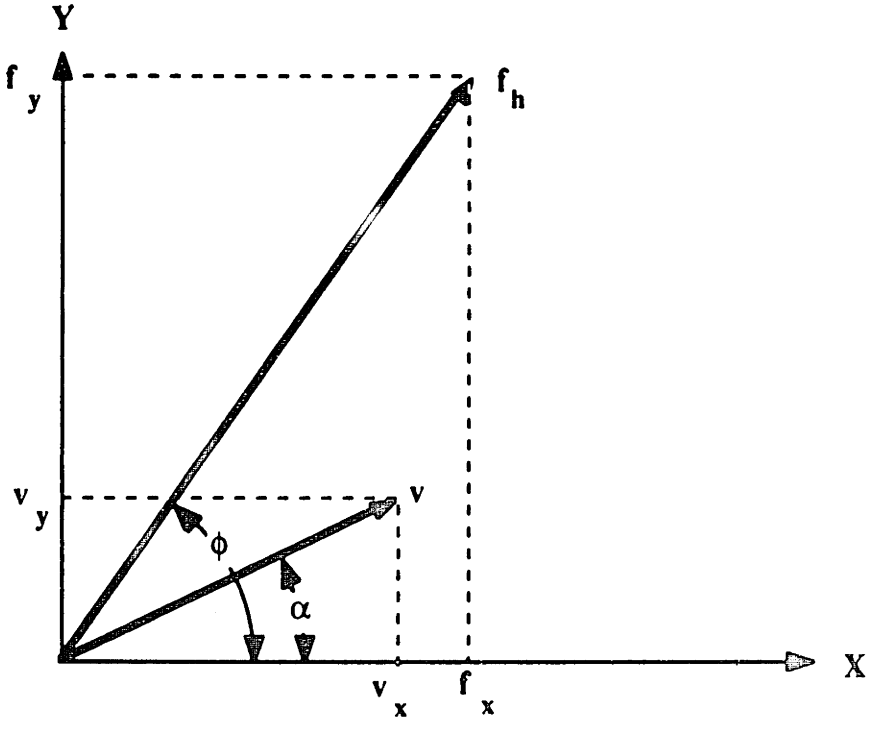

Figure #3-10. Direction of applied force and velocity at manipulator endpoint

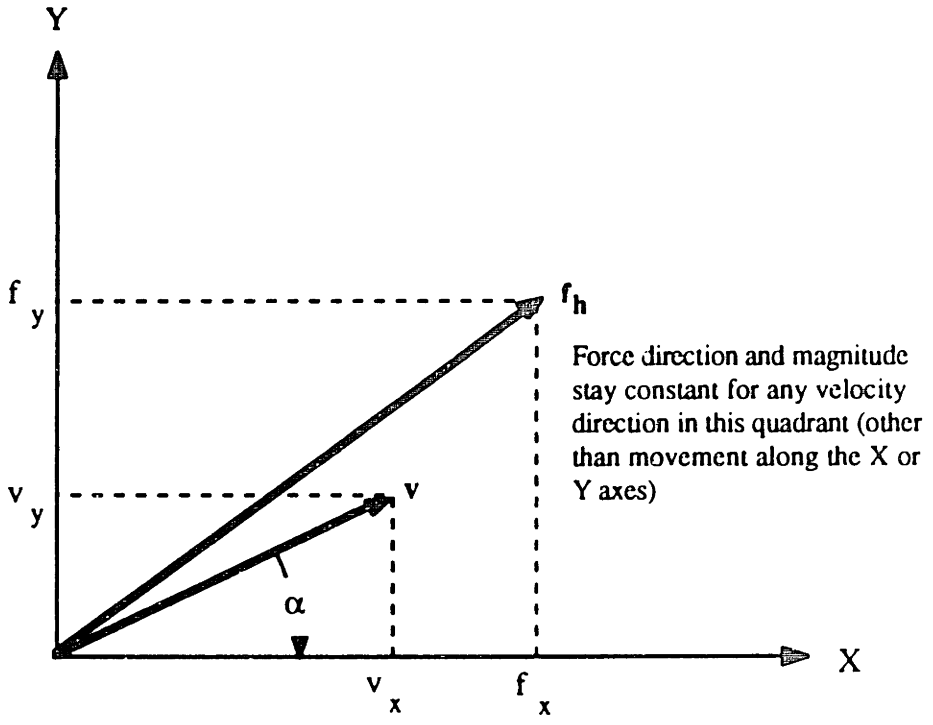

Figure #3-11. Direction of applied force and velocity with passive Coulomb friction.

General Theory of MED manipulators

The discussion above on the cartesian manipulator begins to give a flavor of the more general theory of MED manipulators discussed in this section. The analysis below discusses the idea of a general energy absorbing manipulator and then develops two subset cases, human joint space damping and endpoint space damping.

General Energy Absorbing Case

The most general equation for energy dissipation at the endpoint of a manipulator is that the power the manipulator is producing in its mechanical interaction with the environment is negative. That is,

$$\mathbf{f}^t\mathbf{v} \leq 0 \tag{3-11}$$

where $\mathbf{f}^t$ is the transpose of the 6 x 1 column vector of forces the manipulator endpoint is imparting on the environment and $\mathbf{v}$ is the velocity of the manipulator endpoint.

Figure 3-12 gives a two degree of freedom visual representation of this equation. If the manipulator endpoint is moving in the direction $\mathbf{v}$, then, for an energy dissipating manipulator, the manipulator force needs to be within the 180 degree arc shown. It would be an interesting device that could control the direction of the force anywhere within this range because it would be inherently safe (because it can only dissipate energy) and could simulate many of the physical interactions a human has with his environment. For instance, the frictionless wall of Figure 3-13 has a force range of 90 degrees in order for the human's finger to move in the same direction.

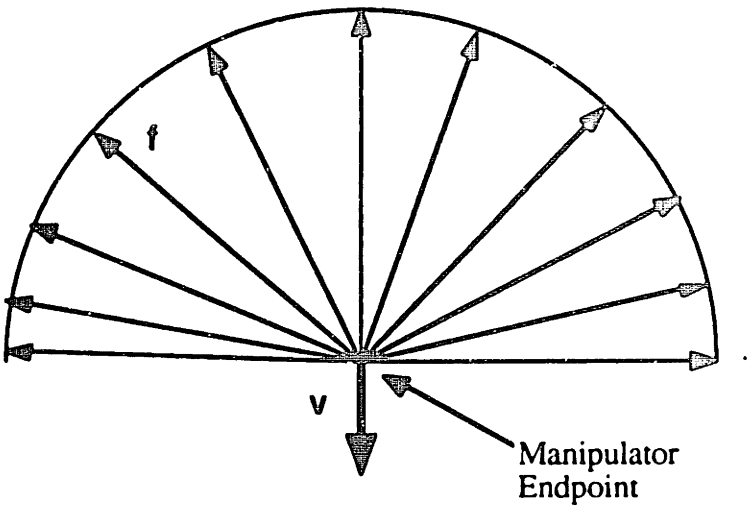

Figure #3-12. Energy dissipating manipulator endpoint

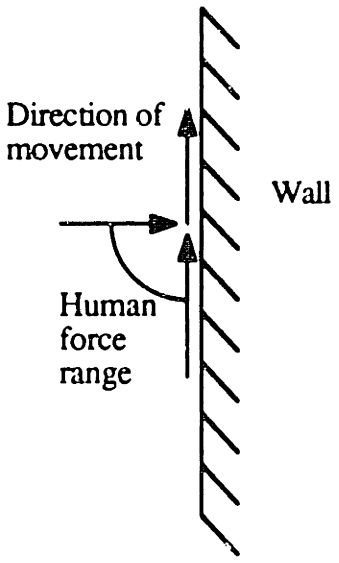

Figure #3-13. Human interaction with a wall

Subsets of General Endpoint Energy Dissipation

Two of the many subsets that exist from the general energy dissipating case are human joint space tremor reduction and endpoint force-velocity colinearity. We define force-velocity in terms of translational colinearity and rotational colinearity. Translational colinearity has the manipulator endpoint translation in the same direction as the force the human applies to the manipulator. Similarly, rotational colinearity has the manipulator endpoint rotation in the same direction as the torque the human applies to the manipulator.

These subsets are two of the more interesting cases for use as tremor reduction devices. Human joint space damping is the damping of each joint's motion. Most previous tremor studies have been performed in one-degree-of-freedom loading the motion of one joint. Loading the complete human arm in joint space can be thought of as attaching a MED actuator to each of the human arm joints (in actual practice, however, this may not be our actual manipulator structure). Force-velocity colinearity, discussed earlier and illustrated in Figure 3-14, is simply resisting the movement of the endpoint of the human arm so that the human arm endpoint force is in the direction of the endpoint velocity. While we thought the idea of human joint space control was an interesting idea, we felt early on that we should attempt to make the MED manipulator so that it could perform force-velocity colinearity.

Figure #3-14. Illustration of force-velocity colinearity

Stapleton (1982) was the first researcher we know of to work on the concept of force-velocity colinearity with a viscous damping device. Her concept was to incorporate passive viscous dampers on a commercially available orthotic feeder. She believed that a person has a difficult time controlling the trajectory of a device which has large directional differences between applied velocity and resisted force. She concluded that, for the geometry she studied, "the best damping characteristics would be obtained with a restraint of equal length links, a reach of approximately twice that of the arm, and variable continuous rotational viscous dampers (MED actuators) with feedback control providing positional and directional information."

While it has not been quantitatively proven that a non-colinear device will degrade purposeful motion more than a colinear device, we performed a very simple qualitative experiment to test Stapleton's hypothesis. Adelstein set up his two-degree-of-freedom manipulandum (Adelstein, 1989) so that we could vary the angle of non colinearity a subject felt during a straight line trajectory task. We found that both of the two able-bodied subjects tested felt they were able to stay closer to their desired trajectory as we reduced the non-colinearity angle. We found that approximately 10 degrees was the non-colinear angle at which the subjects felt their trajectory tracking performance was reduced.

While force-velocity colinearity may be needed so that purposeful movement is not degraded, this method of control may not be best from the standpoint of tremor reduction. Some movement physiology research suggests that humans control the endpoint stiffness of their arms and that the stiffness is different in different directions (see, for example, Hogan, 1980, 1985; Mussa-Ivaldi, Hogan, and Bizzi, 1985). If one of the mechanisms for tremor is caused by the stiffness magnitude (such as a biomechanical resonance) then we may want to have an energy dissipating field that is not isotropic (non force-velocity colinear). While a full research study should be performed on tracking performance during

non-isotropic loading, we felt our simple experiment, along with our intuition, justified our intention of requiring our manipulator to be force-velocity colinear.

Equation Development

This section develops the equations necessary to determine how well a given manipulator linkage geometry can control the endpoint force direction given an input endpoint velocity or, equivalently, how well the linkage can control the endpoint velocity direction given an input force. We begin with the general transformation relationship between the manipulator endpoint position, $\mathbf{x}$, and the vector of joint positions, $\mathbf{q}$

$$\mathbf{x} = f(\mathbf{q}). \tag{3-11}$$

Differentiating both sides of equation 3-11, we get the relationship between the endpoint velocity, $\mathbf{v}$, and the joint velocity, $\dot{\mathbf{q}}$

$$\mathbf{v} = \mathbf{J}\,\dot{\mathbf{q}} \tag{3-12}$$

where $\mathbf{J}$ is the configuration dependent Jacobian matrix. From the relationship between endpoint velocity and joint velocity, we can derive the relationship between endpoint force, $\mathbf{f}$, and joint force, τ, for a zero mass linkage. We begin by setting the energy output of the joints equal to the energy output of the endpoint:

$$\mathbf{v}^t\mathbf{f} = \dot{\mathbf{q}}^t\tau. \tag{3-13}$$

Combining 3-12 with 3-13, we get

$$\dot{\mathbf{q}}^t\mathbf{J}^t\mathbf{f} = \dot{\mathbf{q}}^t\tau \tag{3-14}$$

which can only be true if

$$\mathbf{J}^t\mathbf{f} = \tau. \tag{3-15}$$

Equations 3-12 and 3-15 are well known equations in the field of robotics that can be derived in a number ways.

If the actuators are not mounted on the joints, we need to consider the coupling between the actuator space and the joint space. Two cases exist which we derive separately. First, we derive the case when the number of actuators equals the number of

joints in the manipulator. Second, we will look into the possibility of actuator redundancy, when the number of actuators is greater than the number of joints.

Non-Redundant Actuators

If the number of joints equals the number of actuators, we can easily derive the equations

$$\dot{\mathbf{q}} = \mathbf{C}\mathbf{v}_\mathbf{m} \tag{3-16}$$

and

$$\mathbf{C}^t\boldsymbol{\tau} = \boldsymbol{\tau}_\mathbf{m} \tag{3-17}$$

where $\mathbf{C}$ is the coupling matrix between the joint space and the actuator space, $\mathbf{v}_\mathbf{m}$ is the actuator velocity vector, and $\boldsymbol{\tau}_\mathbf{m}$ is the vector of actuator forces. We can now combine equations 3-12 and 3-16 and equations 3-15 and 3-17 to get the relationship between endpoint space and actuator space

$$\mathbf{v} = \mathbf{J}\mathbf{C}\mathbf{v}_\mathbf{m} \tag{3-18}$$

and

$$\mathbf{C}^t\mathbf{J}^t\mathbf{f} = \boldsymbol{\tau}_\mathbf{m}. \tag{3-19}$$

Finally, define the Jacobian between endpoint space and actuator space as

$$\mathbf{J}_\mathbf{a} = \mathbf{J}\mathbf{C} \tag{3-20}$$

which results in (combining 3-20 with 3-18 and 3-19)

$$\mathbf{v} = \mathbf{J}_\mathbf{a}\mathbf{v}_\mathbf{m} \tag{3-21}$$

and

$$\mathbf{J}_\mathbf{a}^t\mathbf{f} = \boldsymbol{\tau}_\mathbf{m}. \tag{3-22}$$

For any MED actuator,

$$f = bv \tag{3-23}$$

where f is the force[5] the actuator puts on the environment, v is the velocity of the actuator, and b is the damping parameter. For a MED actuator the damping parameter, b, is controllable but must remain negative to satisfy the energy absorbtion requirement.

We can represent the relationship between all the actuator forces and velocities with the matrix equation

$$\tau_m = \mathbf{B_m} v_m \tag{3-24}$$

which can just as easily be written

$$v_m = \mathbf{B_m}^{-1} \tau_m \tag{3-25}$$

where $\mathbf{B_m}$ is the diagonal actuator damping matrix. In the 6 x 6 case, for example,

$$\mathbf{B_m} = \begin{bmatrix} b_1 & 0 & 0 & 0 & 0 & 0 \\ 0 & b_2 & 0 & 0 & 0 & 0 \\ 0 & 0 & b_3 & 0 & 0 & 0 \\ 0 & 0 & 0 & b_4 & 0 & 0 \\ 0 & 0 & 0 & 0 & b_5 & 0 \\ 0 & 0 & 0 & 0 & 0 & b_6 \end{bmatrix}. \tag{3-26}$$

This result should be carefully studied because it is the major difference between MED actuators and active actuators. With active actuators equation 3-23 can be made to be true, but it is a subset of the possible control methods. With ideal MED actuators, equation 3-23 is always true given the assumptions of low mass and high stiffness and $\mathbf{B_m}$ is always diagonal with negative, but controllable, diagonal element values.

---

5 We use the terms force and velocity very loosely. These terms are meant to represent the translational terms as well as the rotational terms torque and angular velocity.

Using the building block equations we developed above, we can now put together the relationship between force and velocity at the end of the manipulator arm. Beginning with equation 3-21,

$$\mathbf{v} = \mathbf{J_a v_m} \tag{3-21}$$

and, using 3-25 to substitute for $\mathbf{v_m}$,

$$\mathbf{v} = \mathbf{J_a B_m^{-1} \tau_m}. \tag{3-27}$$

Finally, using 3-22 to substitute for τ_m,

$$\mathbf{v} = \mathbf{J_a B_m^{-1} J_a^t f}. \tag{3-28}$$

This equation gives the relationship between manipulator endpoint force and velocity for a given actuator velocity and is the damping equivalent of salisbury's (1980) well known equation for stiffness.

Equation 3-28 can be decomposed for a better understanding. First, the actuator Jacobian matrix, $\mathbf{J_a}$, can be represented by its column vectors, $\mathbf{j_i}$, where

$$\mathbf{J_a} = \begin{bmatrix} \uparrow & \uparrow & \uparrow & \uparrow & \uparrow & \uparrow \\ \mathbf{j_1} & \mathbf{j_2} & . & . & . & \mathbf{j_n} \\ \downarrow & \downarrow & \downarrow & \downarrow & \downarrow & \downarrow \end{bmatrix}. \tag{3-29}$$

As can be interpreted from equation 3-21, each of the column vectors represents the direction of motion when its corresponding actuator is moving in the positive direction. Equation 3-28 can now be decomposed into the form

$$\mathbf{v} = \sum_{i=1}^{n} \left(\frac{1}{b_i} \mathbf{j_1} \mathbf{j_1^t f} \right). \tag{3-30}$$

Equation 3-30 can be interpreted very easily. First, each of the data sets in the summation reflects the contribution of one actuator. Next, looking at the data set from the right hand side, $\mathbf{f}$ is the force the manipulator imparts on the environment. $\mathbf{j}_i^t\mathbf{f}$ is a scalar representing the torque output from the i^{th} MED actuator which, when added to all the other actuator torques, produces the force, $\mathbf{f}$. $\frac{1}{b_i}\mathbf{j}_i^t\mathbf{f}$ is a scalar representing the velocity of the i^{th} actuator resulting from the torque applied to the actuator. Finally, the complete data set, $\frac{1}{b_i}\mathbf{j}_i\mathbf{j}_i^t\mathbf{f}$, is an endpoint velocity (magnitude and direction) resulting from the velocity of the i^{th} actuator.

Redundant Actuators

Now, what changes if we have actuator redundancy? If the number of actuators is greater than the number of joints then it is difficult to justify equations 3-16 and 3-17 because the non-square coupling matrix can only be developed in its alternative form since $\mathbf{C}$ is no longer unique

$$\mathbf{C}^{-1}\dot{\mathbf{q}} = \mathbf{v}_m \tag{3-31}$$

$$\tau = \mathbf{C}^{-t}\tau_m \tag{3-32}$$

The way we are writing the equations may appear that we are suggesting the inversion of a non-square matrix, but this is not the case. The components of the matrix are identified in the inverted form. For the derivation in the case of redundant actuators, we use equations 3-12 and 3-15 in their alternative forms

$$\dot{\mathbf{q}} = \mathbf{J}^{-1}\mathbf{v} \tag{3-33}$$

and

$$\mathbf{f} = \mathbf{J}^{-t}\tau. \tag{3-34}$$

Notice that for this derivation to work the joint-space Jacobian matrix must be non-singular.

Now, we can combine 3-31 with 3-33 and 3-32 with 3-34 to get

$$\mathbf{v_m} = \mathbf{C^{-1}J^{-1}v} \tag{3-35}$$

and

$$\mathbf{f} = \mathbf{J^{-t}C^{-t}\tau_m}. \tag{3-36}$$

By setting

$$\mathbf{J_a^{-1}} = \mathbf{C^{-1}J^{-1}} \tag{3-37}$$

and

$$\mathbf{J_a^{-t}} = \mathbf{J^{-t}C^{-t}} \tag{3-38}$$

equations 3-35 and 3-36 become

$$\mathbf{v_m} = \mathbf{J_a^{-1}v} \tag{3-39}$$

and

$$\mathbf{f} = \mathbf{J_a^{-t}\tau_m} \tag{3-40}$$

Now, we can derive the equation for redundant actuators. We begin with equation 3-40 and substitute for τ_m using equation 3-24 to get

$$\mathbf{f} = \mathbf{J_a^{-t}B_m v_m}. \tag{3-41}$$

Finally, using equation 3-39 to substitute for **vm**, we get

$$\mathbf{f} = \mathbf{J_a^{-t}B_m J_a^{-1}v}. \tag{3-42}$$

On the surface, equations 3-28 and 3-42 seem to be inversely related, suggesting our derivations are correct. In practice, however, we would usually use the equation which best suits the situation and in some situations only one of the methods can be used. For instance, equation 3-28 was derived assuming non-redundant actuators and works for the singular Jacobian case. Also, equation 3-42 is derived for the case of redundant actuators and only works only for a non-singular Jacobian matrix.

As with equation 3-28, we can decompose equation 3-42 into parts. First, the inverse actuator Jacobian matrix transpose, $\mathbf{J_a}^{-t}$, can be represented by its column vectors, $\mathbf{j^f_i}$, where

$$\mathbf{J_a}^{-t} = \begin{bmatrix} \uparrow & \uparrow & \uparrow & \uparrow & \uparrow & \uparrow \\ \mathbf{j^f_1} & \mathbf{j^f_2} & . & . & . & \mathbf{j^f_n} \\ \downarrow & \downarrow & \downarrow & \downarrow & \downarrow & \downarrow \end{bmatrix}. \tag{3-43}$$

As can be interpreted from equation 3-40, each of the column vectors represents the direction of the endpoint force when its corresponding actuator is producing a torque. This vector direction is much more difficult to visualize than the column vector interpretation of 3-39.

Equation 3-42 can now be decomposed into the form

$$\mathbf{f} = \sum_{i=1}^{n} \left(b_i \, \mathbf{j}^f_i \, \mathbf{j}^{ft}_i \, \mathbf{v} \right) \tag{3-44}$$

Like equation 3-30, equation 3-44 can be interpreted very easily. First, each of the data sets in the summation reflects the input of one actuator torque. Next, looking at the data set from the right hand side, $\mathbf{v}$, is the velocity of the endpoint of the manipulator. $\mathbf{j}^{ft}_i \, \mathbf{v}$ is a scalar representing the velocity of the i^{th} actuator due to the endpoint velocity. $b_i \, \mathbf{j}^{ft}_i \, \mathbf{v}$ is the torque output from the MED actuator due to the angular velocity. Finally, the complete data set, $b_i \, \mathbf{j}^f_i \, \mathbf{j}^{ft}_i \, \mathbf{v}$, is the endpoint force contribution from the i^{th} MED actuator torque. We give an example interpretation of this equation in the section on force-velocity colinearity.

Human Joint Space Tremor Reduction Theory

In this section, we look at the special case of human joint damping. In human joint damping, we would like

$$\tau = b\omega \tag{3-45}$$

where τ is the torque output from the joint, ω is the angular velocity of the joint, and b is the adjustable, but positive damping parameter (the damping parameter is positive because the human joint is producing energy to be dissipated by our device). Now, we go through the analysis of equations 3-24 to 3-28 for our human arm linkage to get

$$\mathbf{v} = \mathbf{J_h B_h^{-1} J_h^t f_h} \tag{3-46}$$

Where $\mathbf{v}$ is the velocity of the human endpoint, $\mathbf{f_h}$ is the force the human endpoint imparts on the environment, $\mathbf{J_h}$ is the human arm Jacobian matrix between endpoint space and joint space, and $\mathbf{B_h^{-1}}$ is the diagonal human arm damping matrix (the terms of the matrix are positive but adjustable).

We assume that we do not have redundant actuators and can accomplish this if we can make a MED manipulator such that equation 3-46 can be set equal to equation 3-28 (the equation for a non-redundant med manipulator). That is, setting the velocity of the human arm endpoint equal to the manipulator endpoint velocity,

$$\mathbf{v} = \mathbf{J_h B_h^{-1} J_h^t f_h} = \mathbf{J_a B_m^{-1} J_a^t f}. \tag{3-47}$$

Note that the force the human imparts on the manipulator endpoint, $\mathbf{f_h}$, is the negative of the force the manipulator imparts on the human endpoint, $\mathbf{f}$, so

$$\mathbf{-J_h B_h^{-1} J_h^t f} = \mathbf{J_a B_m^{-1} J_a^t f} \tag{3-48}$$

which can be reduced to

$$\mathbf{J_h(-B_h^{-1})J_h^t} = \mathbf{J_a B_m^{-1} J_a^t} \tag{3-49}$$

A sufficient condition for equation 3-49 to be true is the case where $\mathbf{J_h} = \mathbf{J_a}$ and the Jacobian matrix non-singular[6]. This is the simple case of a coincident exoskeleton with a connection at the hand (and the human arm restricted to a maximum of six-degrees-of-freedom) . But is this a necessary condition? We have not produced an answer to this question. Assuming $\mathbf{J_a}$ is not singular, we can rearrange 3-49 to get

$$\mathbf{B_m}^{-1} = \mathbf{J_a}^{-1}\mathbf{J_h}(-\mathbf{B_h}^{-1})\mathbf{J_h}^{t}\mathbf{J_a}^{-t}. \tag{3-50}$$

This equation has the general form

$$\mathbf{A} = \mathbf{C}^{t}\mathbf{B}\,\mathbf{C} \tag{3-51}$$

Where **A** and **B** are diagonal with negative elements. A sufficient solution to this problem is a diagonal **C** matrix which is the identity matrix for $\mathbf{J_h} = \mathbf{J_a}$. Other solutions may be possible, but we have not solved them.

Endpoint Force-Velocity Colinearity

The case of endpoint force-velocity colinearity can be derived using a similar method as the human endpoint case. After we have used this development, we give example uses of equations 3-30 and 3-44 to give us a physical understanding of the MED manipulator problem.

Force-velocity colinearity can be written mathematically as

$$\mathbf{f} = \mathbf{B_e}\mathbf{v} \tag{3-52}$$

or, equivalently,

$$\mathbf{f_h} = -\mathbf{B_e}\mathbf{v}. \tag{3-53}$$

---

6 In practice, the human arm joints produce a minimum of seven degrees of freedom producing a singular Jacobian matrix. The assumption of a non singular Jacobian works if we assume either one or more joints is fixed with a brace or the manipulator connects to the arm at a point more proximal than the human hand.

Equation 3-52 can just as easily be written

$$\mathbf{v} = \mathbb{B}_e^{-1} \tag{3-54}$$

$\mathbf{f_h}$, $\mathbf{f}$, and $\mathbf{v}$ have been defined earlier and

$$\mathbf{B}_e = \begin{bmatrix} b_t & 0 & 0 & 0 & 0 & 0 \\ 0 & b_t & 0 & 0 & 0 & 0 \\ 0 & 0 & b_t & 0 & 0 & 0 \\ 0 & 0 & 0 & b_r & 0 & 0 \\ 0 & 0 & 0 & 0 & b_r & 0 \\ 0 & 0 & 0 & 0 & 0 & b_r \end{bmatrix}. \tag{3-55}$$

The $\mathbf{B_e}$ matrix has one term for translational movement, b_t, and one term for rotational movement, b_r. This is the colinearity condition. For the manipulator to be dissipating energy, both b_t and b_r must be negative.

Now, we want to find the conditions for which we can achieve force-velocity colinearity for a MED manipulator. If we can achieve this special case, we can take equation 3-28 and substitute 3-54 in for v, we get

$$\mathbf{B}_e^{-1}\mathbf{f} = \mathbf{J}_a\mathbf{B}_m^{-1}\mathbf{J}_a^t\mathbf{f} \tag{3-56}$$

which can be reduced to

$$\mathbf{B}_e^{-1} = \mathbf{J}_a\mathbf{B}_m^{-1}\mathbf{J}_a^t. \tag{3-57}$$

If the left side of the equation equals the right side of the equation, then we can always achieve force-velocity colinearity. Equation 3-57 is similar to the result by Salisbury (1980) for the case of stiffness control in active robots.

Equation 3-57 has the same general form as equation 3-51. Here, a sufficient solution is $\mathbf{J_a}$ diagonal. A less restrictive condition is for the upper 3 x 3 partition of matrix $\mathbf{J_a}$ can be in any orthogonal coordinate system (representing the velocity components of damping) and the lower 3 x 3 partition of matrix $\mathbf{J_a}$ can be in any orthoganol coordinate system. This translates to the upper 3 x 3 partition matrix of $\mathbf{J_a}$

having orthogonal columns and the lower 3 x 3 partition matrix of $\mathbf{J_a}$ having orthogonal columns for $\mathbf{J_a}$ in any orthogonal coordinate system.

Examples

In this section we develop simple examples for the use of equations 3-30 and 3-44. We begin with equation 3-30 and the trivial single-degree-of-freedom translational linkage of Figure 3-15. By inspection, we can see that the manipulator with move in the Y direction for

$$0 < \vartheta < 180 \text{ degrees}$$

and will move in the -Y direction for

$$180 < \vartheta < 360 \text{ degrees.}$$

There are only two directions of force-velocity colinearity, when $\vartheta = 90$ degrees and when $\vartheta = 270$ degrees.

We believe it is instructive to work through this example using equation 3-30 so the reader can get a physical interpretation. First, because there is only one axis, equation 3-30 becomes

$$\mathbf{v} = \frac{1}{b}\,\mathbf{j}\,\mathbf{j}^t\,\mathbf{f_h} \tag{3-58}$$

if we assume b is positive and controllable and we remember $\mathbf{f} = -\mathbf{f_h}$. The Jacobian vector is along the Y direction,

$$\mathbf{j}^t = [0\ 1] \tag{3-59}$$

and the force vector

$$\mathbf{f_h}^t = [-f\cos\vartheta \quad -f\sin\vartheta] \tag{3-60}$$

where f is the magnitude of $\mathbf{f_h}$.

Now, starting with the right hand side of equation 3-58,

$$\mathbf{j}^t\mathbf{f_h} = -f\sin\vartheta \tag{3-61}$$

which is simply the component of the force which the MED actuator feels.

Next,

$$\frac{1}{b} j^t f_h = \frac{f}{b} \sin\vartheta \tag{3-62}$$

is the velocity of the MED actuator due to the force of 3-61. Finally,

$$v = \frac{1}{b} j j^t f_h = \begin{bmatrix} 0 & \frac{f}{b} \sin\vartheta \end{bmatrix} \tag{3-63}$$

is the velocity of the endpoint due to MED actuator velocity of 3-62. We can see by examining 3-60 and 3-63 that the force and velocity are only colinear when $\cos\vartheta = 0$. This occurs for ϑ equals 90 degrees and 270 degrees.

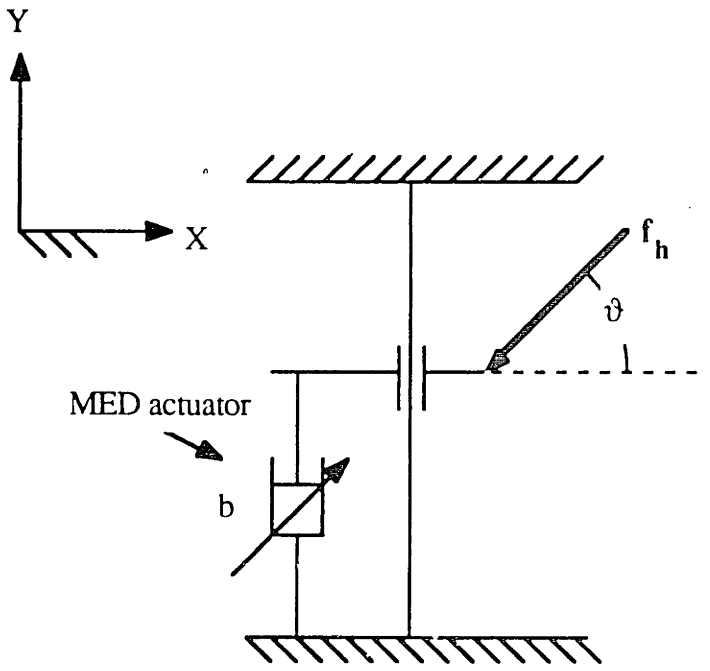

Figure 3-15. One-degree-of-freedom translational MED manipulator

A slightly more complex system is shown in Figure 3-16 which is the same manipulator analyzed earlier from Figure 3-9. We discuss the physical intuition for this example here. Figure 3-17 gives a visual interpretation of equation 3-30. The vector $\mathbf{f_h}$ is the force applied to the end of the manipulator by the human and the vectors $\mathbf{j_1}$ and $\mathbf{j_2}$ are the movements of the endpoint of the manipulator due to movements of the MED actuators 1 and 2 (Jacobian directions). The $\mathbf{f_h}$ force produces a force in the $-\mathbf{j_1}$ direction for actuator 1 and $-\mathbf{j_2}$ direction for actuator 2. Actuator 1 responds with any velocity magnitude (adjustable by adjusting b1) in the direction $-\mathbf{j_1}$ and actuator 2 responds with any velocity magnitude in the $-\mathbf{j_2}$ direction. This shows that the manipulator velocity due to the force vector shown can be anywhere in the third quadrant of the diagram, including the direction of the force for $b_1 = b_2$ (as shown earlier in the chapter). Thinking through this diagram for all force directions should convince the reader that in any direction the force and velocity can be made colinear by adjusting $b_1 = b_2$. This result comes about because of the orthogonality of the Jacobian vectors $\mathbf{j_1}$ and $\mathbf{j_2}$. Next we look at two manipulators which do not have this orthogonality property and determine their resulting deficiencies.

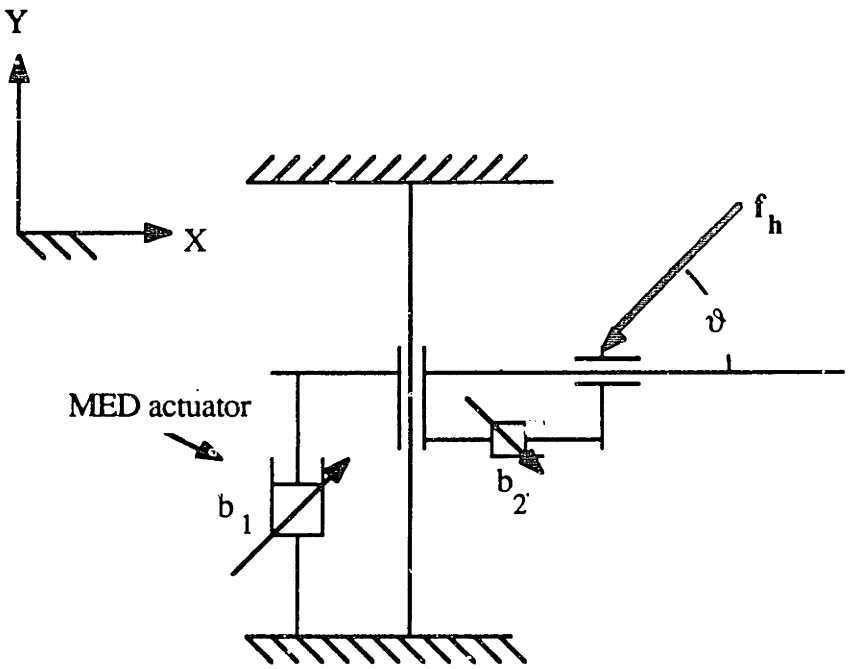

Figure #3-16. Two-degree-of-freedom cartesian manipulator

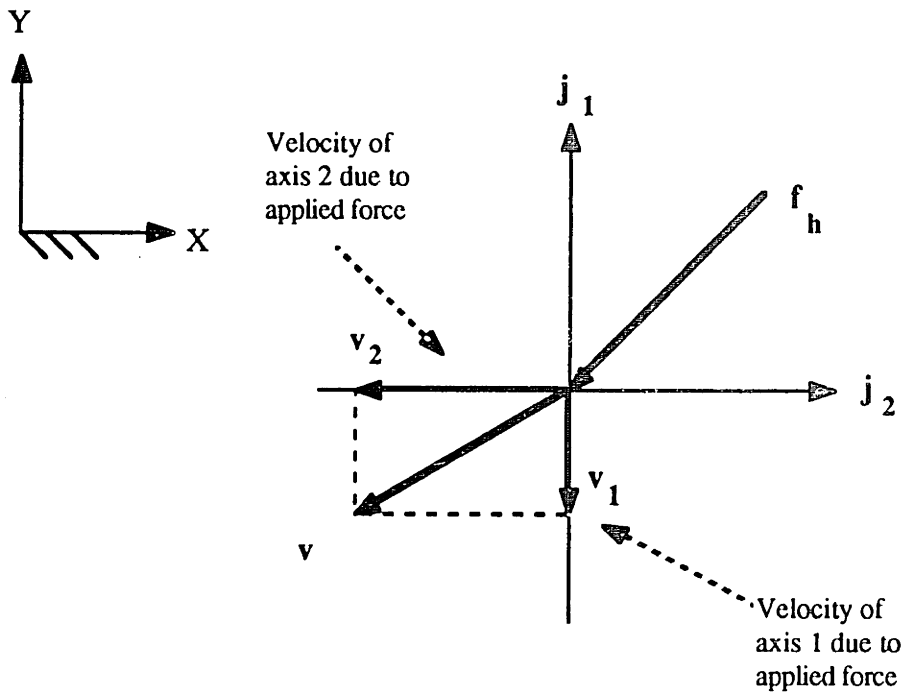

Figure #3-17. Jacobian vectors for the cartesian manipulator

Figure 3-18 illustrates a simple two degree of freedom revolute manipulator with MED actuators on axis 1 (between ground and link 1) and axis 2 (between link 1 and link 2). The paths of motion at the end of the manipulator show the movement of the manipulator endpoint if either axis 1 or axis 2 had movement. Figure 3-19 shows the Jacobian vectors for the manipulator in the approximate orientation of Figure 3-18. The Jacobian vectors are tangent to the path of movement for each axis and change with manipulator orientation. Figure 3-19 also shows a force applied to the endpoint of the manipulator and the resulting velocities of the endpoint due to the MED actuator velocities (remember the magnitude is controllable, the direction is not). In the force direction shown the manipulator can move in any direction between the $-\mathbf{j}_1$ vector and the $-\mathbf{j}_2$ vector inclusive. This suggests we are capable of force velocity colinearity for the force direction shown.

If the human pushes in another direction, however, this result may not be present. Figure 3-20, for instance, illustrates a direction for which the endpoint velocity can only be between the $\mathbf{j}_1$ vector and the $-\mathbf{j}_2$ vector inclusive, depending on our damping parameter control. The force direction is not within this bound; therefore, force-velocity colinearity is not possible for this force direction.

The directions of force-velocity colinearity capability for the given manipulator orientation is shown in Figure 3-21. Force-velocity colinearity is possible in the odd numbered areas and not possible in the even numbered areas. The dashed lines separating the areas are the lines perpendicular to the Jacobian vectors $\mathbf{j}_1$ and $\mathbf{j}_2$.

Papadopoulos (1987) produced similar results for this two-degree-of-freedom linkage applied to bicycle pedalling. In his study, however, he was interested in actuators which only produce energy and cannot absorb energy. Also, he only analyzed this specific case, and did not develop the general case.

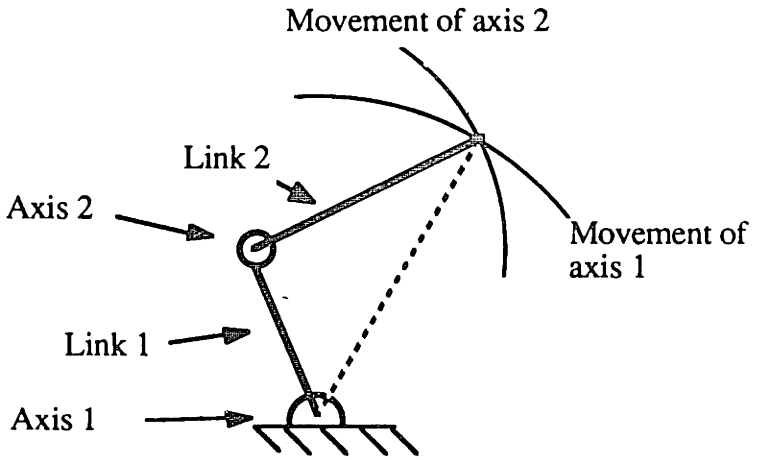

Figure 3-18. Two-degree-of-freedom revolute manipulator

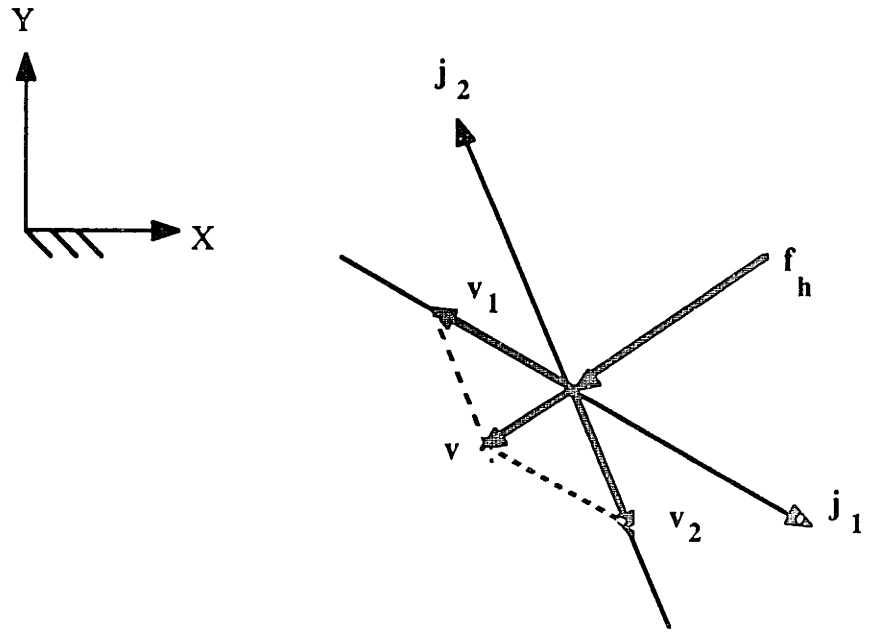

Figure 3-19. Diagram of movement directions for force direction 1

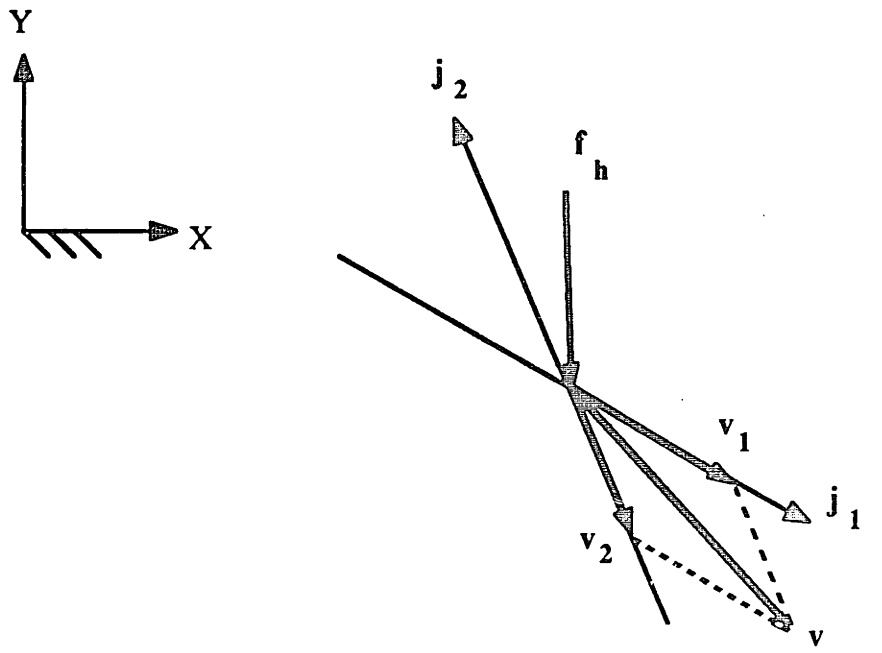

Figure 3-20. Diagram of movement directions for force direction 2

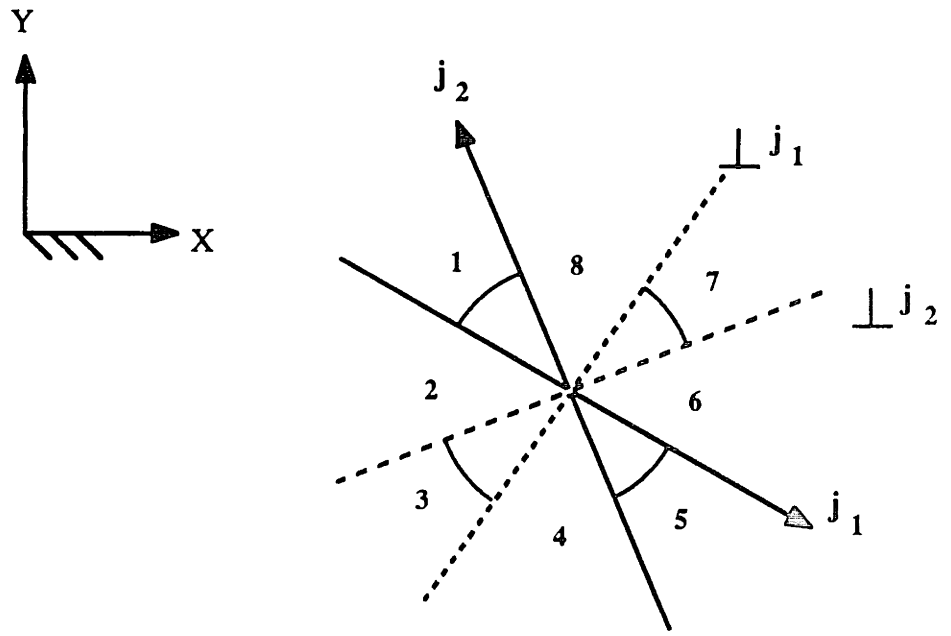

Figure 3-21. Regions of force-velocity colinearity for revolute manipulator

Figure 3-22 shows another common revolute axis manipulator. This manipulator has coupled axes, however. The MED actuators for this manipulator are mounted between ground and link 1 and between ground and link A for actuators 1 and two, respectively. Also shown in the diagram are the arcs produces if either actuator one or actuator two moves in the orientation shown. Note that for the orientation shown, the Jacobian vectors (tangent to the axes of movement at the endpoint of the manipulator) are very nearly perpendicular. This is not the case for other orientations of this manipulator linkage.

The regions of colinearity for the coupled revolute axis manipulator are shown in Figure 3-23. Note that the regions of non-colinearity are small in this case. This is because the Jacobian vectors are nearly colinear. In general, as the Jacobian vectors become closer to orthoganal, the regions of non-colinearity become smaller.

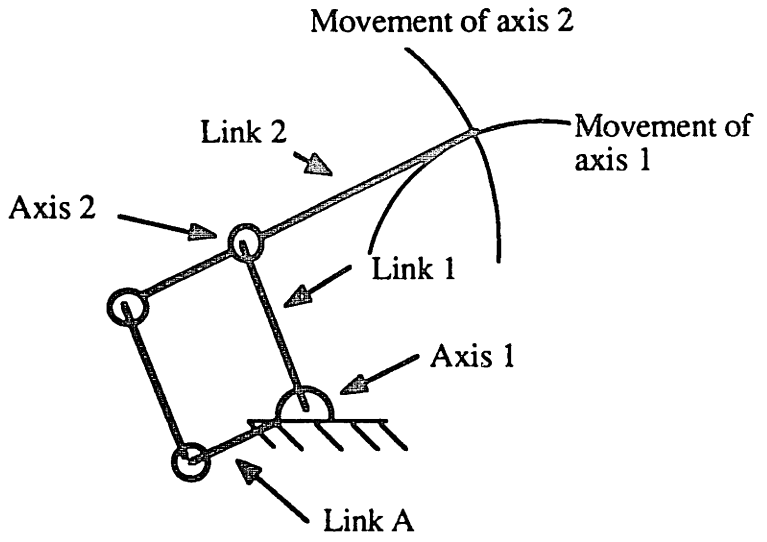

Figure 3-22. Coupled axis revolute manipulator

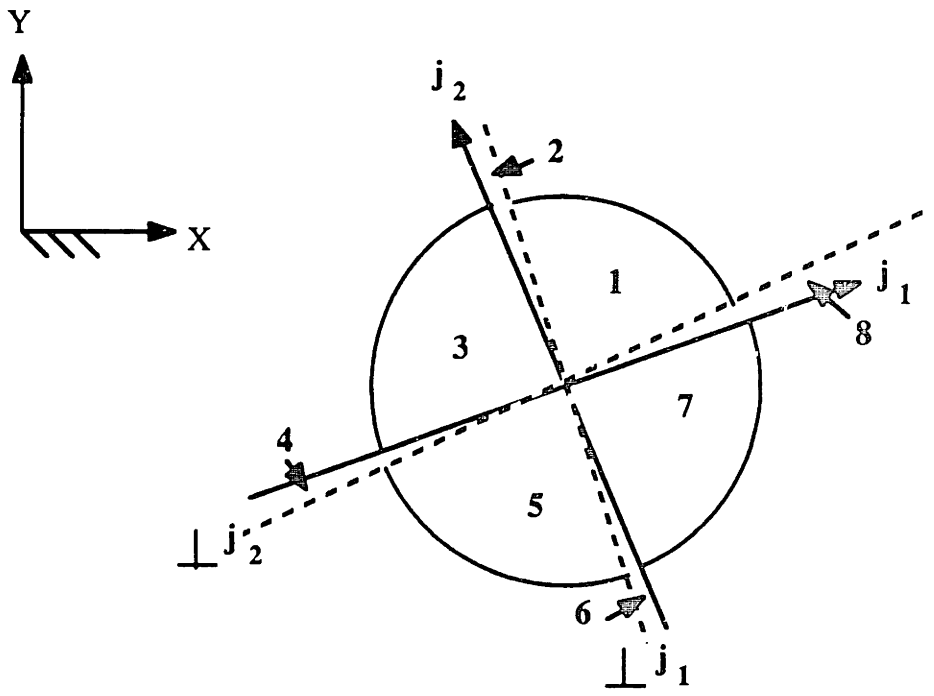

Figure #3-23. Regions of colinearity for coupled axis revolute manipulator

Next, we discuss the use of equation 3-44 on the redundant-actuator cartesian manipulator of figure 3-24 (a similar coupled manipulator was developed with springs by Hogan, 1980). This is the same manipulator as that of Figure 3-16 with an added, redundant, third actuator. The actuator is attached to a push-pull cable wrapped around a pulley (although it is not possible in the configuration shown, consider both the cable an the pulley to work in both tension and compression). Using equation 3-44, we consider the effects of an applied endpoint velocity, $\mathbf{v}$, as shown in Figure 3-25. Each of the actuators can respond with a force which is in the opposite direction of the hand force direction shown. Finally, each force is added to produce the total endpoint force which is in the opposite direction of the hand force, $\mathbf{f_h}$. For this velocity direction, the manipulator is capable of producing a load which results in a human force in any direction between the $\mathbf{j_3^f}$ Jacobian force vector direction and the $-\mathbf{j_2^f}$ Jacobian force vector direction.

In general, adding redundant actuators increases the range of the force-velocity non-colinearity angle. Redundant actuators can be used with linkages which are incapable of producing force velocity colinearity. The redundant actuators can be designed into the system so that the linkage can then produce force-velocity colinear loads.

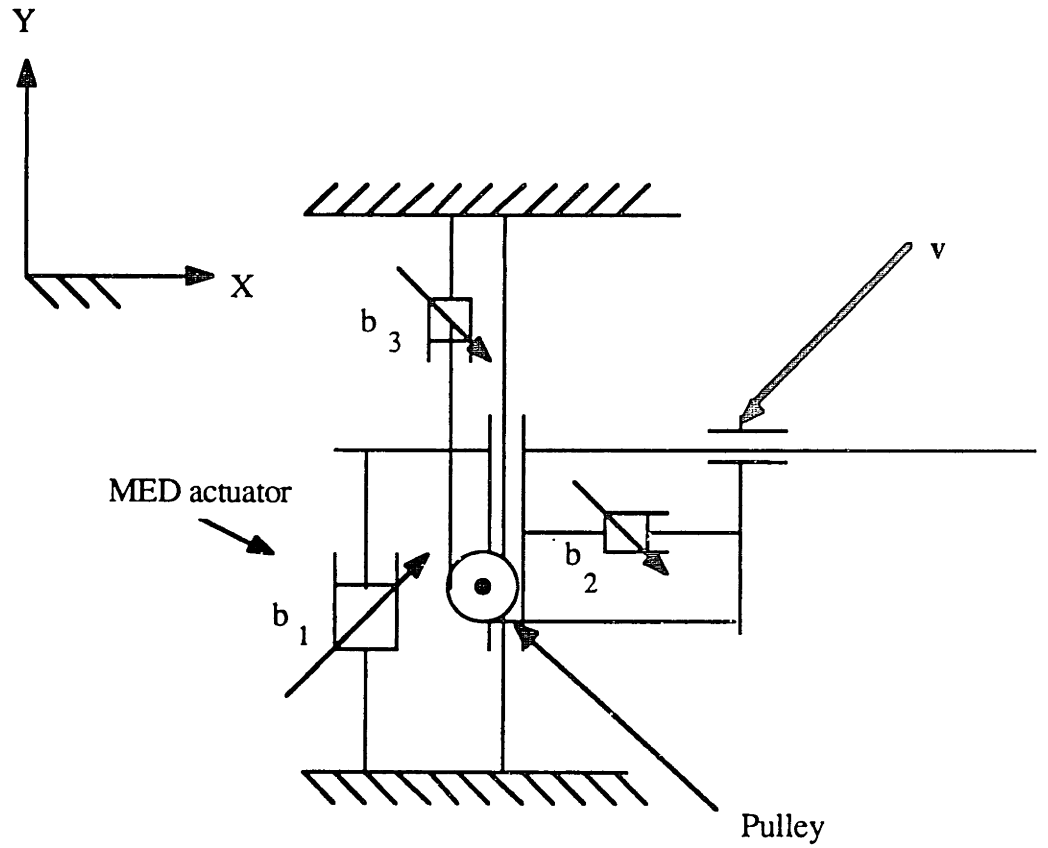

Figure 3-24. Redundant actuator cartesian manipulator

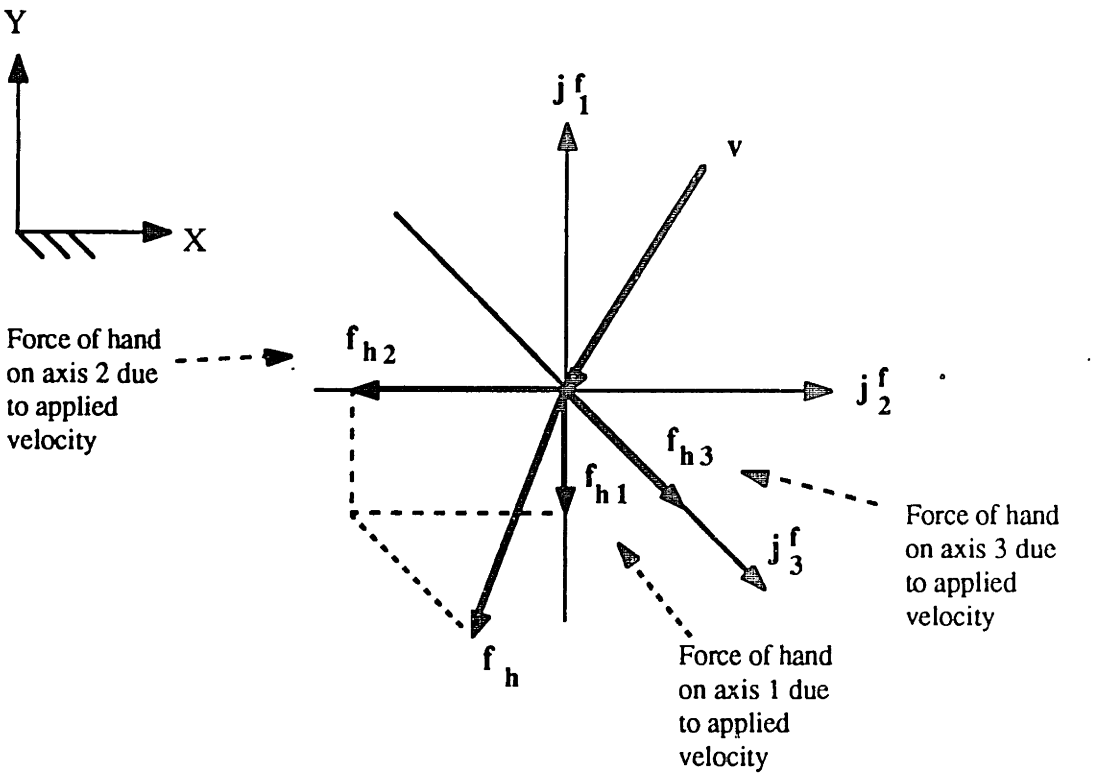

Figure 3-25. Diagram of force direction for coupled cartesian manipulator

General Energy Dissipation Case

We have returned full circle to the case of controlling the manipulator in a general energy dissipating case. We believe the discussion above is enough to convince the reader that no discrete set of energy dissipating actuators can be controlled to produced the general energy dissipation function. To produce this general device, we believe active actuators must be used. If the designer wants to make certain the energy levels never produce injury, he can incorporate a method of energy flow control. Energy flow control basically amounts to taking the energy from the axes which are absorbing it and redistributing it to the axes which are energy producing. This is a very difficult-to-implement concept, and could involve electrical energy flow, hydraulic energy flow, or energy flow from some other energetic domain.

Linkage Development

Designing the manipulator linkage was a challenging task. The goals of the manipulator design seemed somewhat unrealistic, especially the attempt to make the device force-velocity colinear. Many revolute robot manipulators are on the market but few, if any, could have their active actuators replaced with MED actuators and have resulting force-velocity colinearity. The easiest manipulator with orthogonal mapping between the actuator apace and the endpoint space (the force-velocity colinear condition) would be, in three-degrees-of-freedom, a cartesian manipulator (see Figure 3-26). But, as Vijaykumar,Tsai, and Waldron (1985) point out, "rotating joints can achieve workspaces with smaller structural volumes as compared to sliding joints and this is one of the principal reasons why revolute joints have been more popular with robot manufacturers." Also, it turns out that the effective mass at the endpoint of a cartesian manipulator is much greater than a revolute manipulator with similar workspaces.

Another possibility is the spherical coordinate manipulator of Figure 3-27. With the MED actuators mounted on the joints, this manipulator can always produce force-velocity colinear motion at the endpoint because there is an orthogonal mapping between the endpoint space and the actuator space. This manipulator still has one prismatic joint, however.

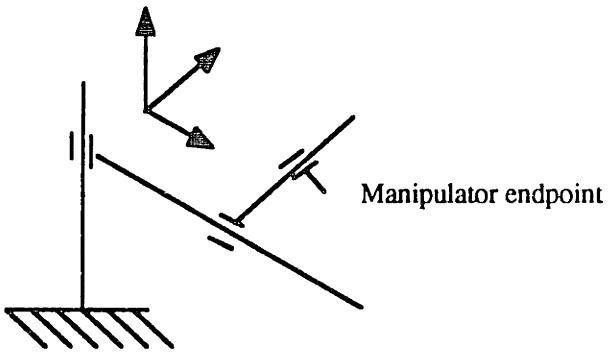

Figure #3-26. 3-dof cartesian manipulator

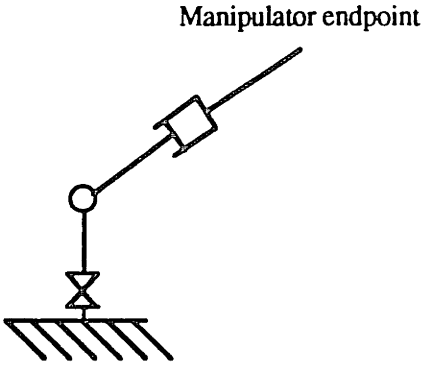

Figure #3-27. 3-dof spherical coordinate system manipulator

The design of the final manipulator received a tremendous advance when we realized there was a method that would give us the prismatic motion with revolute joints, so that we could achieve the configuration of Figure 3-27 without prismatic joints. This method is diagrammed in Figure 3-28. In the diagram, the upper pulley is fixed to the upper arm and the lower arm is free to rotate with respect to both the upper and lower pulleys. The lower pulley is fixed to mechanical ground (in the actual linkage, the lower pulley is connected to the previous link). The connection between the upper pulley and the lower pulley could be made with any of a number of drives including belts, chains, or cables. The key to the system's endpoint moving in a straight line is the ratio of upper pulley to lower pulley diameters equal to 1/2 and the lower link length equalling the upper link length.

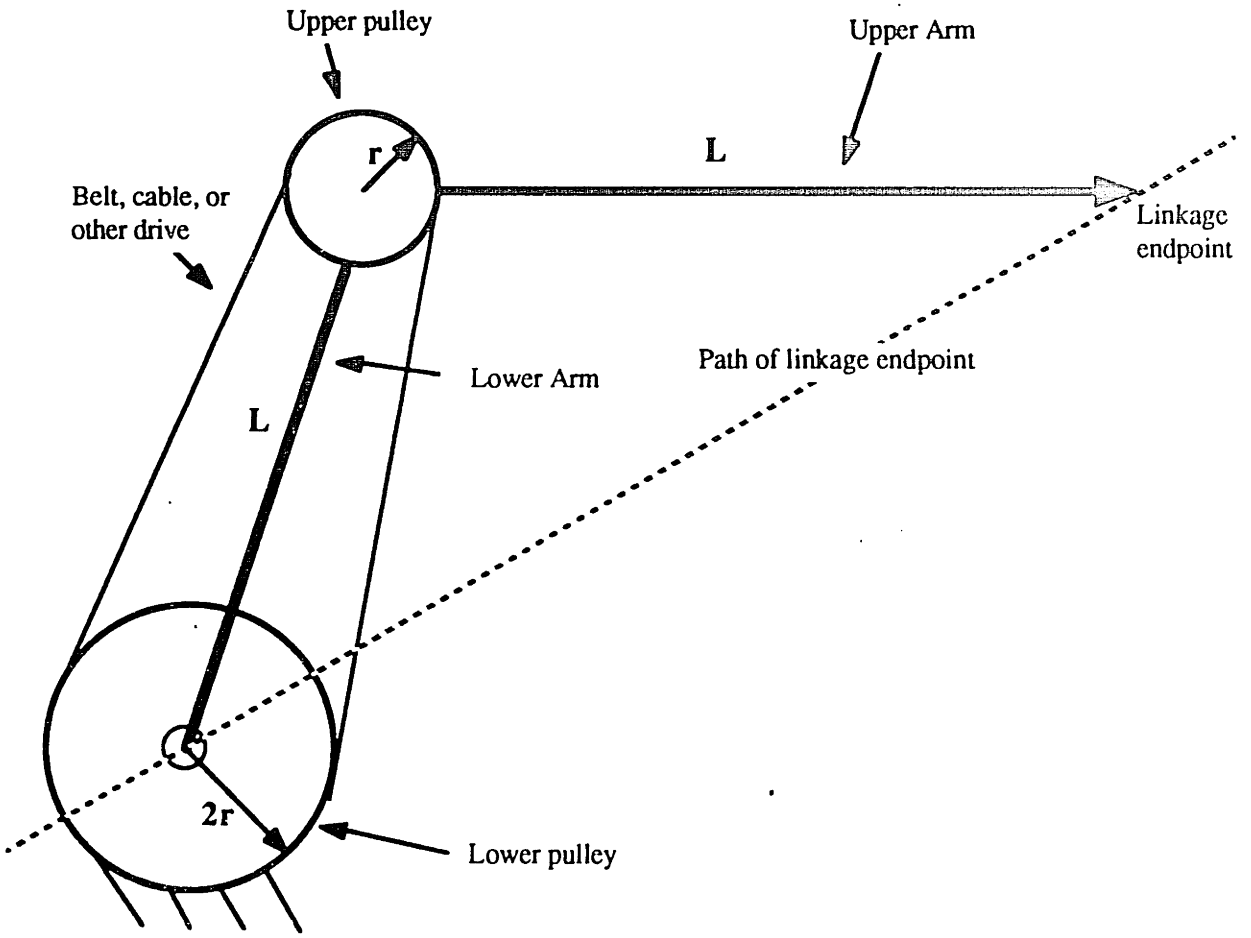

Figure #3-28. Diagram of coupled revolute axes resulting in translational movement

This design has some practical limitations. The most difficult limitation is the making the system rotationally stiff. The simple model of Figure 3-29 illustrates the rotational stiffness condition for a drive with a preloaded belt[7]. The rotational stiffness of the upper pulley in this model is the stiffness of the belt times the radius of the small pulley squared. The rotational stiffness can be increased by increasing the cross sectional area of the belt, changing the belt to a material with a higher coefficient of elasticity, or increasing the radius of the upper pulley.

Increasing the stiffness has many practical problems. The radius of the pulley has size limitations. The pulley adds mass to the system and the lower pulley must be twice the size of the upper pulley. The area of the belt is a function of the thickness of the belt and the width of the belt. The belt has a thickness limitation because the strain in the belt caused by the curvature of the upper pulley must not cause fatigue failure. Finally, the stiffest materials on the market are fiber reinforced timing belts or steel (or titanium) belts or chains, with chains having the added advantage that the thickness limitation is not present (they do not bend around a sprocket, the links rotate about the pins).

After weighing the alternatives, steel belts and chains were fully investigated, but the results were somewhat dissapointing. The steel belts, besides being expensive at approximately $300-$400/belt in small quantities, would not produce a practical system. The problems included the need for large pulleys, a high initial tension in the belt, and a belt that would be very thick. The chain could do the job, but the resulting system would have backlash and a chordal speed variation[8]. Although either system could be designed into the system, neither system was elegant.

---

7 The assumption here is that the preload is high enough so that the low force side of the belt never drops to zero force (never becomes slack).

8 Some chain drive systems have been developed which have three belts and sprockets which are out of phase with each other. These designs are intended to reduce the backlash and decrease the chordal speed variation. For a more complete discussion of practical chain drives see Shigley and Mitchell (1983).

Another drive system investigated was the rack-and-pinion system of Figure 3-30. The pulleys (or sprockets) have been replaced with pinions which have a pitch diameter ratio of 1/2 and the belt (or chain) has been replaced with a rack. This system is very similar to the belt drive system except that the rack can be made to be very stiff (it does not nced to rotate around a pulley). This system does have drawbacks, however. The system has backlash and the system design is complicated by the floating rack which must have a mechanism designed to keep it the correct distance away from the center of the pulleys.

The drive system which turned out to be the system we chose for the final design is the four bar linkage design diagrammed in Figure 3-31 and shown as part of the final implementation in Figure 3-32. This structure is simple and can be made very stiff. This linkage structure does have a nonlinear transmission ratio, but the ratio stays within a very small error. A spreadsheet analysis was performed on this linkage, varying the link length r, the ratio of the upper link r to the lower link (shown in the figure as 2r), and the upper arm angle θ. The key parameter of interest is the angle of deviation defined as the angle between the ideal straight line motion and the line between the base, point O, and the endpoint of the linkage. The results indicate that increasing r moves the linkage more toward the ideal transmission ratio and changing the ratio between the upper link and the lower link has some effect on the outcome, but the overall effect is not positive. In all, the four bar linkage is a quite simple, stiff solution to the transmission problem[9].

The final design has r = 5 inches, the lower link has a length of 10 inches, and the link length, l, is 22.56 inches. The transmission ratio is within $\pm$ 10% of the ideal ratio, 2, for upper link angle, θ, between -40 and 15 degrees. Further, the maximum angle of deviation is less than two degrees for θ between -50 and +40 degrees.

---

9 A cardboard model was made for the advisors with "physical intuition" to verify the analytical spreadsheet analysis.

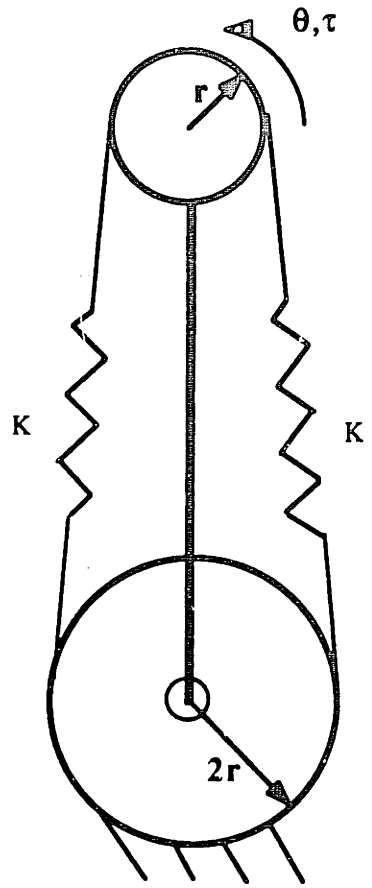

$$\tau = K R^2 \theta$$

Figure #3-29. Stiffness model of r-2r linkage

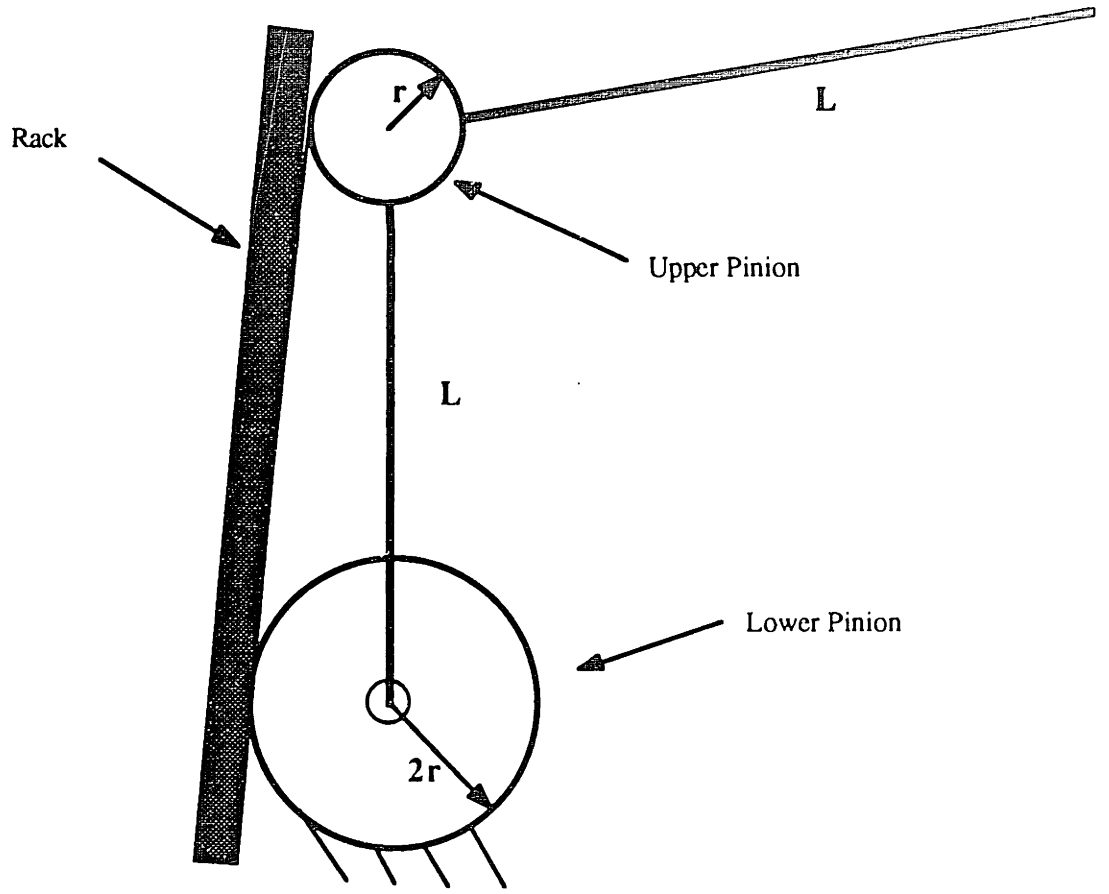

Figure #3-30. Rack and pinion drive design

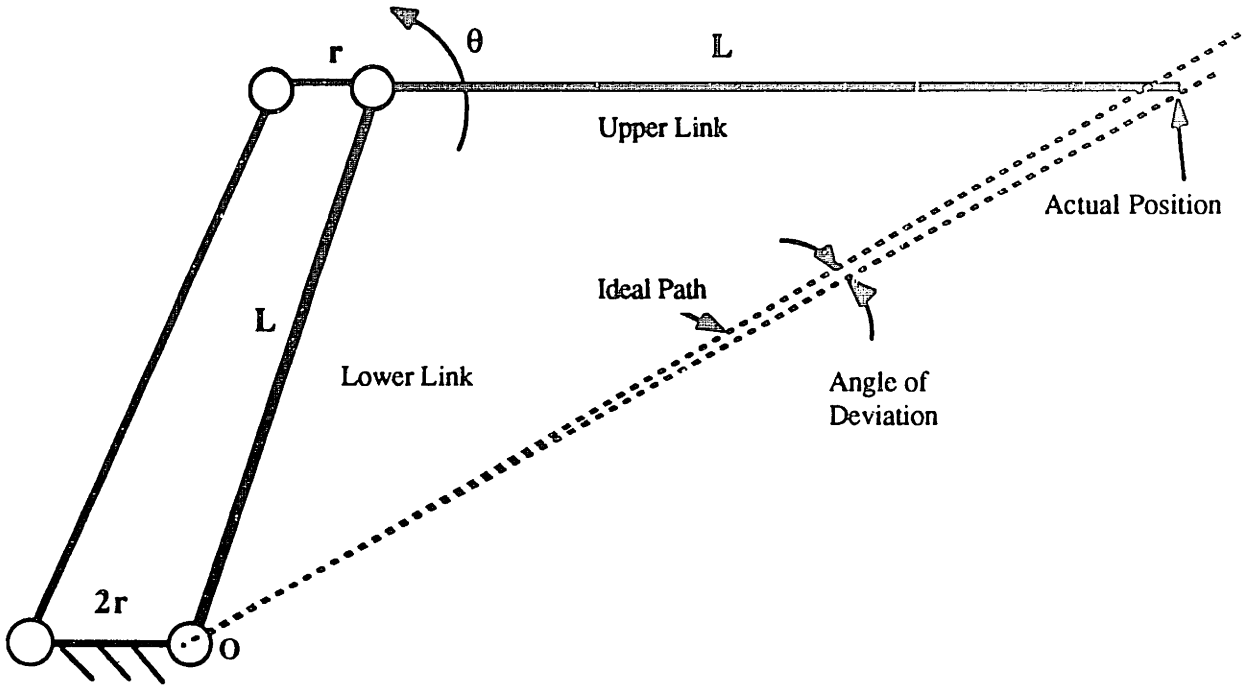

Figure #3-31. r-2r linkage design

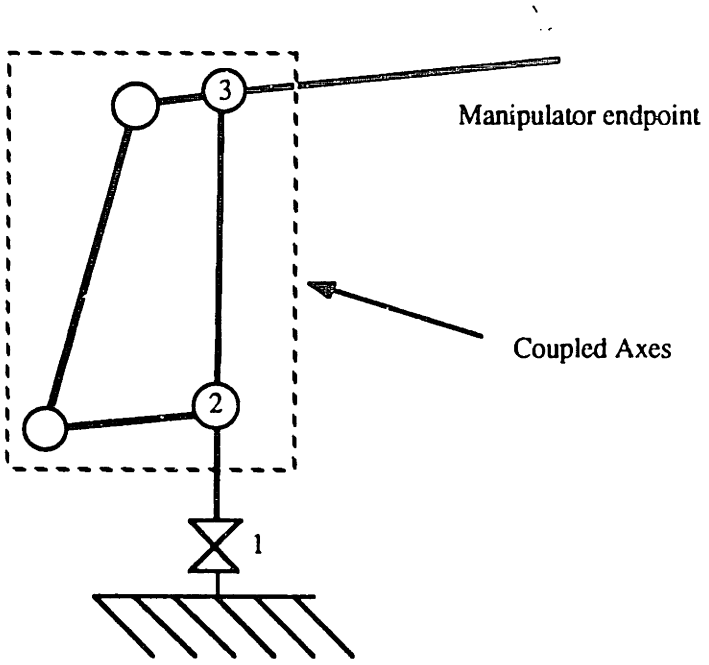

Figure #3-32. Diagram of first three axes

Gimballed Wrist

Most of the more recent commercial 6 dof robot manipulators have the last three joint axes intersecting at one point. This seems to be done mostly to reduce the computational complexity of the wrist-partitioned kinematics and dynamics (Peiper, 1968; Paul, Renaud, and Stevenson, 1983; Hollerbach, 1983). We aimed to take the simplicity one step further, with the endpoint of the manipulator at the point where the last three axes intersect, making a gimballed endpoint.

Two possible link geometries were considered, shown in Figures 3-33 and 3-34. The gimbal geometry of Figure 3-33 is the method used for most gimbals. Axis 4 produces a roll of the endpoint while axis 5 produces a yaw and 6 a pitch. The Figure 3-34 alternative is somewhat more complex. Axis 4 is the same as in the first alternative, but linkage A,B,C,D,E,F now is used to produce the pitch and axis six 6 produces the yaw of the endpoint.

The pitch linkage is designed as two parallelograms with links C and E kept parallel to link A and links D, B, and F kept parallel to each other. The total effect of the linkage is that link F rotates about the imaginary manipulator endpoint (the imaginary endpoint is at the intersection of the rotations of axes 4, 5, and 6).

Each alternative was investigated with the objective being a lightweight, low cost, easily manufacturable design. The most difficult section of design alternative one, pictured in Figure 3-33, is axis 6. This section must be designed so that the center of the axis coincides with the center of the limb coupler cuff. That is, the axis must be out of the way of the arm. Figures 3-35, 3-36, and 3-37 are a sample of the designs considered for axis 6. They are discussed in turn.

Design concept A is pictured in Figure 3-35 with the side view pictured above the front view. The limb coupler cuff attaches to the force/torque sensor, which in turn attaches to the rotating member. The partial spur gear attaches to the rotating member and drives the spur gear which is connected to the output shaft of the particle brake. The

rotating member is held by a set of cam followers which restrict its motion to a rotation. The potentiometer measures the rotation of the spur gear shaft via a belt and pulley assembly.

Design concept B is shown in Figure 3-36 in only the side view (the front view is similar to concept A's). In this concept, the particle brake is mounted perpendicular to the axis 6 rotation. The rotating member drives the particle brake through the combination of spur gears and the bevel gears. The rotating member is again restricted to rotation by cam followers and the potentiometer again measures the rotation of the shaft through a belt and pulley arrangement.

Figure 3-37 illustrates design concept C, again shown only in side view. The assembly is very similar to concept A, with the cable drive replacing the spur gears. Again, cam followers support the rotating member and the potentiometer measures rotation.

Design alternative two (Figure 3-34) also had many candidate designs. One alternative is to use belts instead of linkages. Figure 3-38 illustrates a design alternative with belts. Other concepts included variations on link placement, link lengths, material, actuator and potentiometer placement, and counterbalance technique.

Many concepts were investigated involving both gimballed wrist alternatives. The outcome of the investigation was that none of the concepts for alternative one came close to those of alternative two's advantages. Alternative two's basic advantage is weight at the endpoint. All the alternative one concepts had much more weight at the end of the manipulator than the concepts of alternative two. Because the mass propagates due to counterbalancing, the extra weight of alternative number one would make the manipulator have a much greater passive inertia.

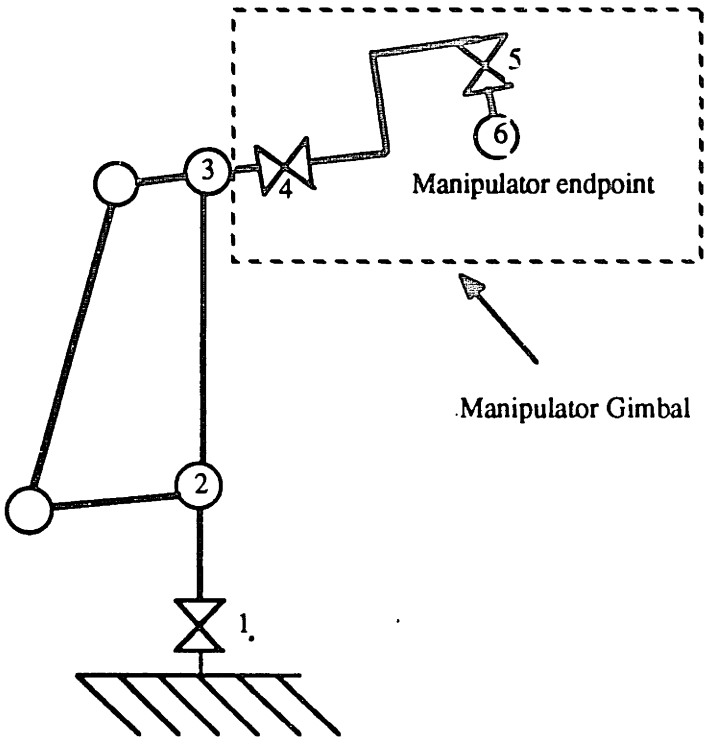

Figure 3-33. Possible gimballed wrist alternative 1

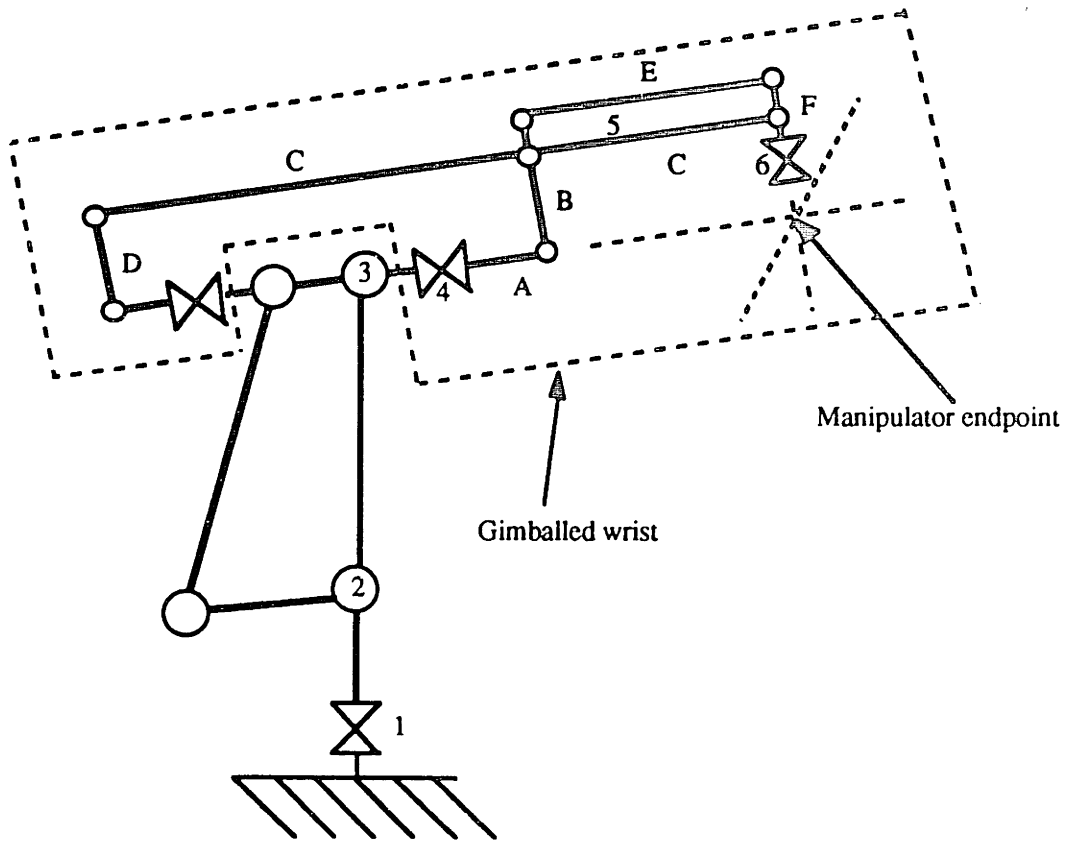

Figure #3-34. Possible gimballed wrist alternative 2

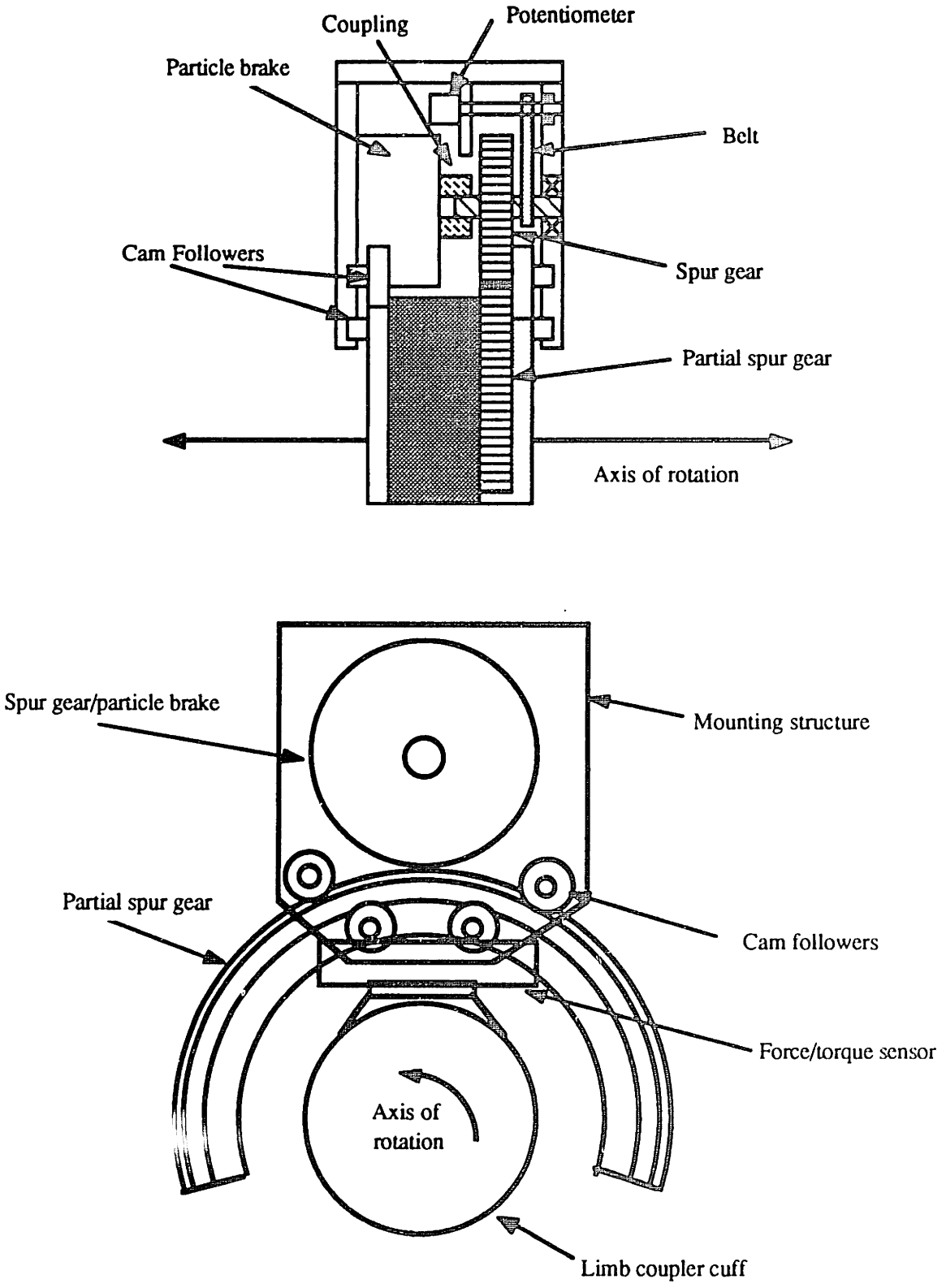

Figure #3-35. Axis #6 concept A

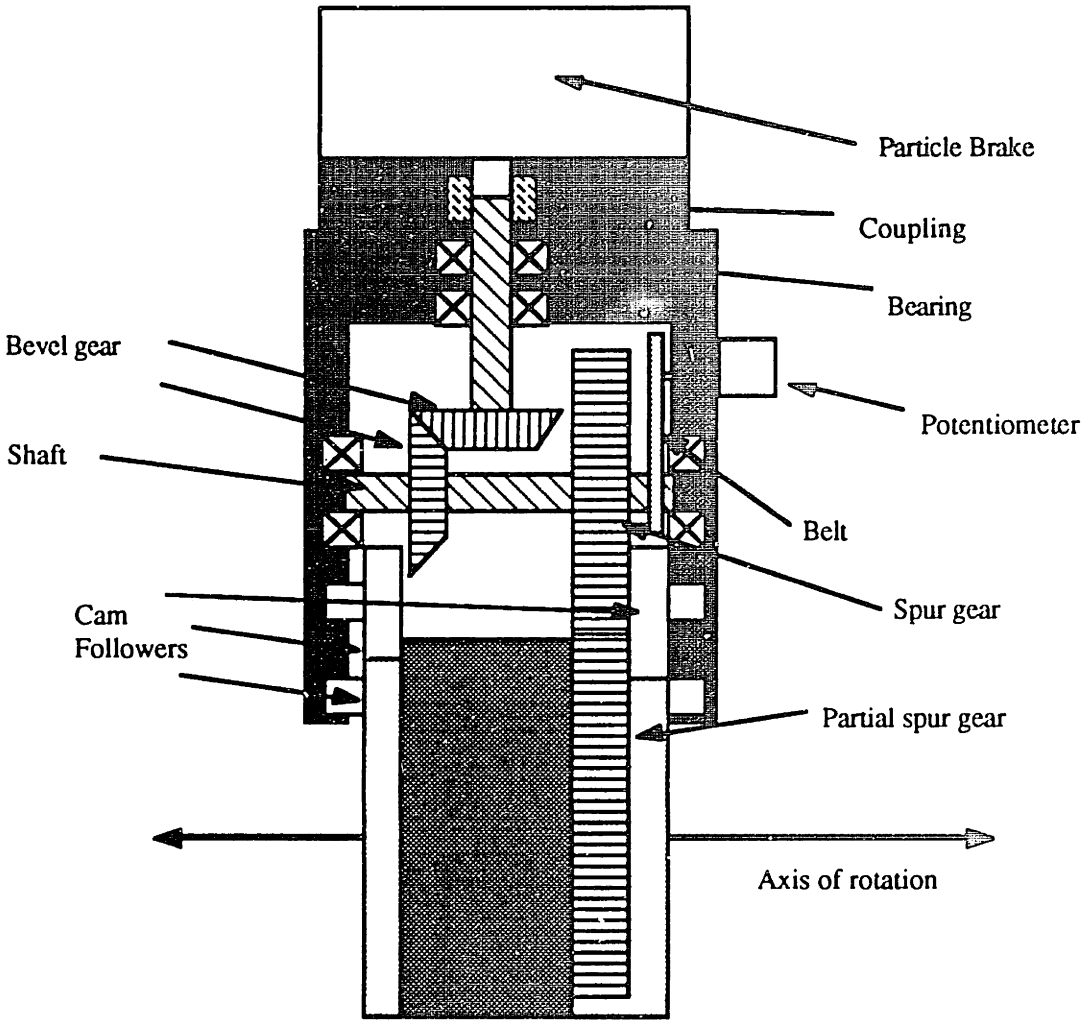

Figure #3-36. Axis #6 concept B

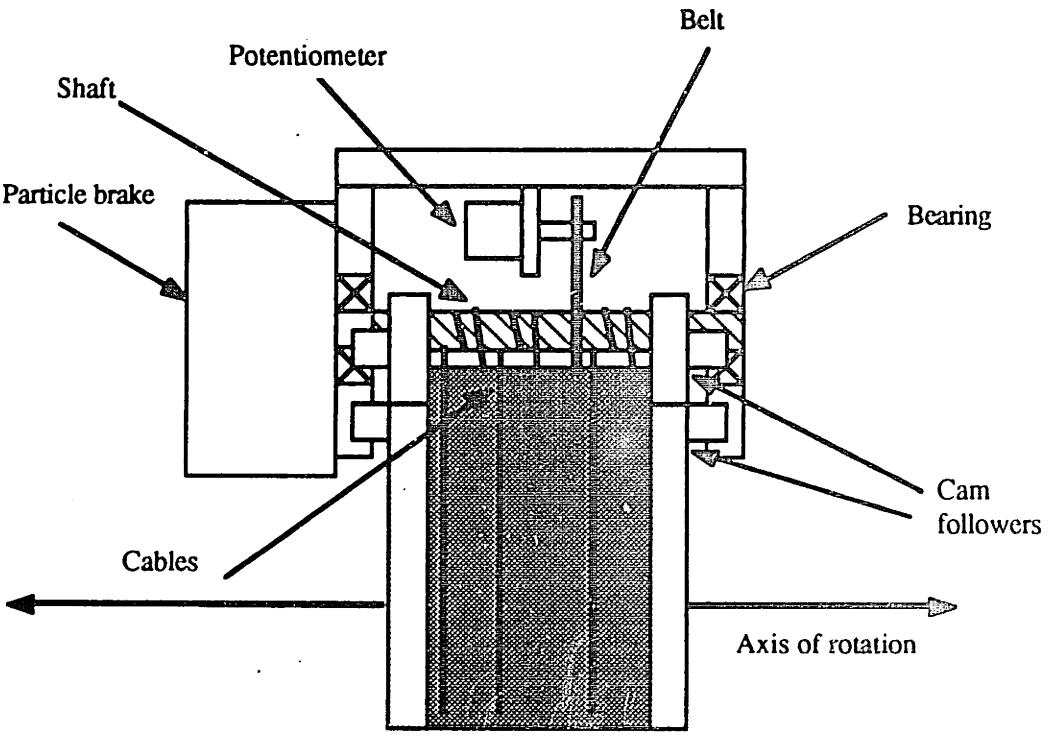

Figure #3-37. Axis #6 concept C

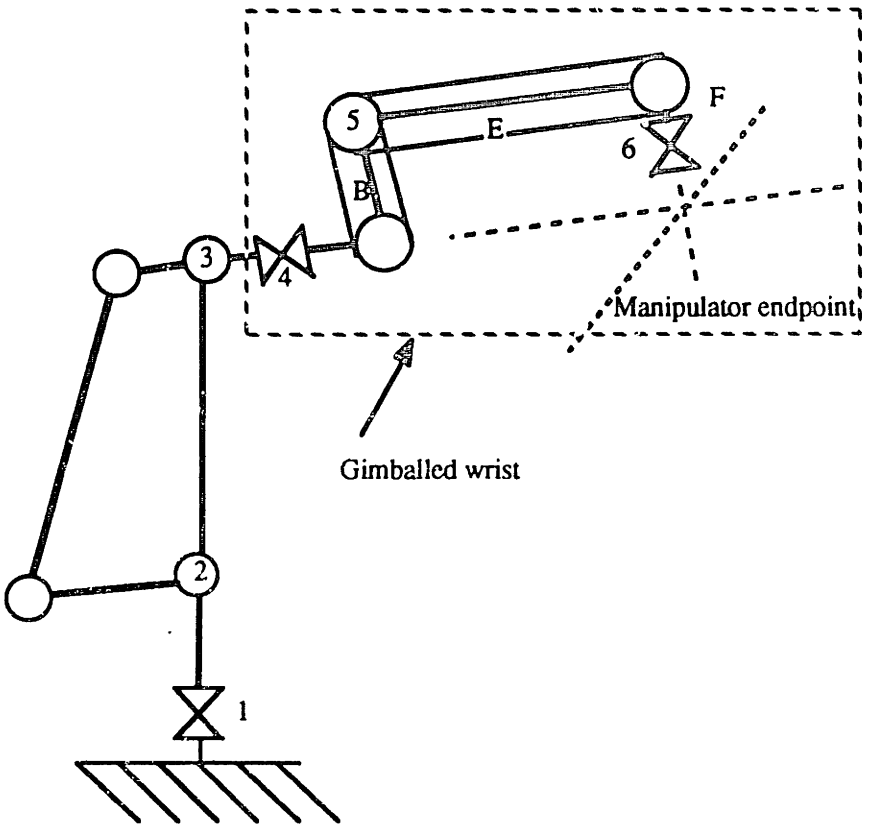

Figure #3-38. Axis #5 belt drive concept

Chapter 4
Final MED Manipulator System

This chapter presents in detail the final six-degree-of-freedom modulated-energy-dissipation (MED) manipulator system. As discussed in Chapter 1, this system will serve as a very general prototype clinical tool for measurement and differential diagnosis of movement disorders and as a means of simulating the characteristics of practical tremor-suppression orthoses with up to six degrees of freedom.

An overview of the system is shown with the subject in the loop in Figure 4-1. The MED manipulator system consists of five modules. The modules include the six-degree-of-freedom MED manipulator, a subject support chair, control electronics, and an IBM PC/AT clone with a EGA graphics display. The computer runs control algorithms which control the damping parameters and update the display while storing the required experimental data sets. Each of the system modules is discussed in turn. Figure 4-2 presents a photograph of the MED manipulator system.

Manipulator

The final manipulator linkage design is a 6R serial link device diagrammed in Figure 4-3. The three distal degrees of freedom are arranged in the form of a novel gimbal configuration. Two of the proximal degrees of freedom are mechanically coupled through a four bar mechanism providing, in effect, two rotations and a near-prismatic joint. This design is driven largely by our goal of building a system with an orthogonal Jacobian matrix to provide end-point force-velocity colinearity. The manipulandum applies its 6-dof load at a single point of attachment on the hand, wrist, or distal forearm.

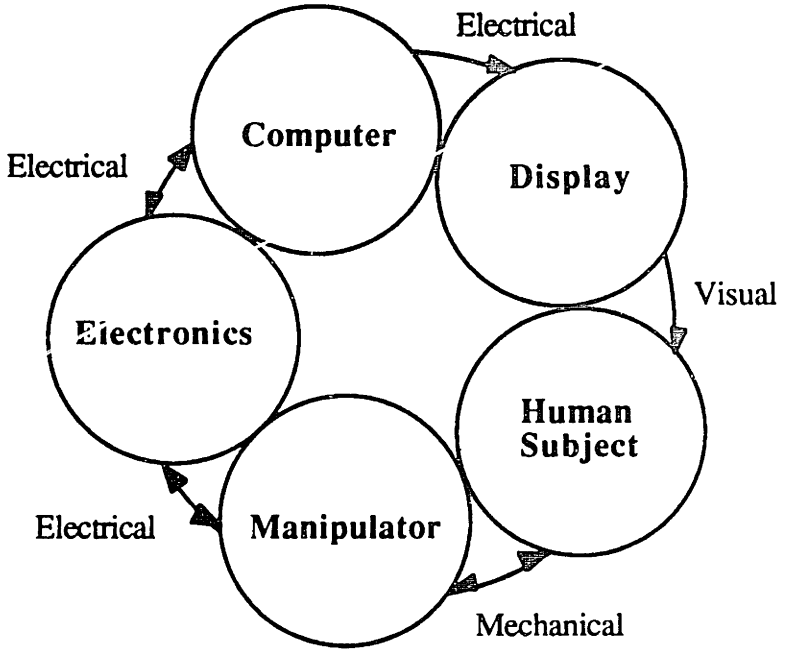

Figure #4-1. MED manipulator system overview

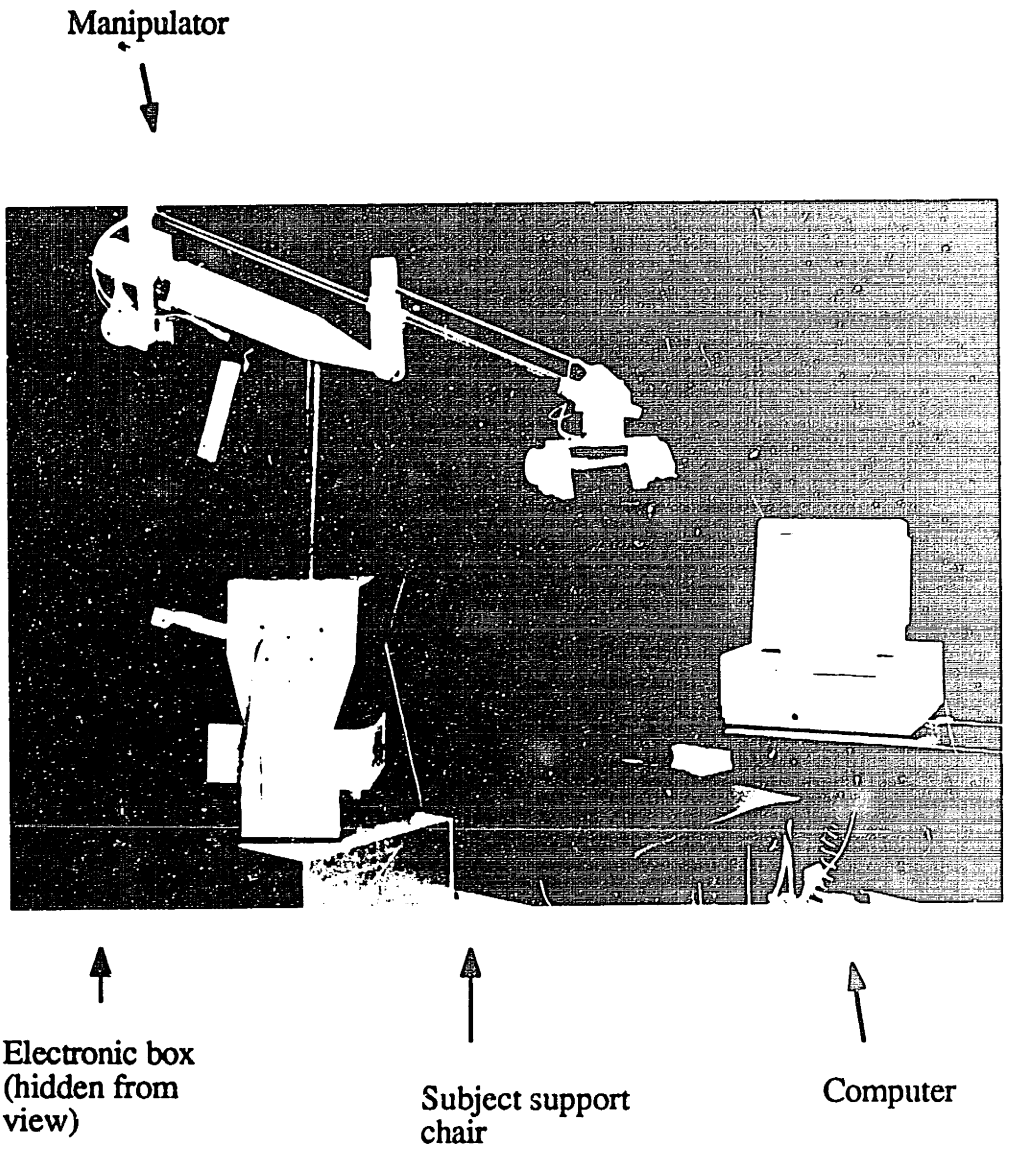

Figure #4-2. Photograph of MED manipulator system

The manipulator is discussed in the following five sections; linkage, actuators, reducers (transmission), position sensors and force-torque sensor.

Linkage

The manipulator linkage is diagrammed in more realistic detail in Figure 4-4. The axis 1 rotation produces the first rotation φ, of a spherical coordinate system, and axis 2 rotation produces the second rotation, Θ. The four-bar linkage, CEFD, is the R-2R linkage discussed in chapter three which produces the near-translational movement of the manipulator endpoint in the spherical coordinate system r direction. The upper linkage consists of three parallelogram sets which work together to produce the axis 4 (roll) and axis 5 (pitch) rotations of the manipulator endpoint. Finally, axis 6 produces the yaw rotation of the manipulator endpoint. Photographs of the MED manipulator linkage are shown in Figures 4-5, 4-6, 4-7, and 4-8.

The manipulator has added masses in two locations used as counterbalances. The two masses, labelled Lower Counterbalance and Upper Counterbalance in Figure 4-4, act to produce a net zero weight at the manipulator endpoint (that is, the human subject connected to the manipulator feels no weight load). The upper counterbalance centers the mass for both axis 3 and axis 4, i.e., the upper counterbalance acts to redistribute the mass of the upper linkage so that the center of mass is at the intersection of axes 3 and 4. The lower counterbalance redistributes the load of the entire manipulator so that the center of mass of the manipulator is at axis 2.

The need for counterbalance weights at two points indicates the manipulator can use heavier actuators for axes 1,2,3,4, and 5. This is true because each counterbalance is placed in the same location as an actuator. If the actuators were larger, we would both eliminate the need for counterbalances and increase the load capabilities of the manipulator without increased inertia. Even with the present actuators, however, the present load

capability of 60 Newtons at the manipulator endpoint is approximately three times what other tremor management devices currently deliver.

The manipulator linkage materials were mostly machined aluminum parts and graphite epoxy composite tubing. Other materials included a stainless steel counterbalance and lead counterbalances.

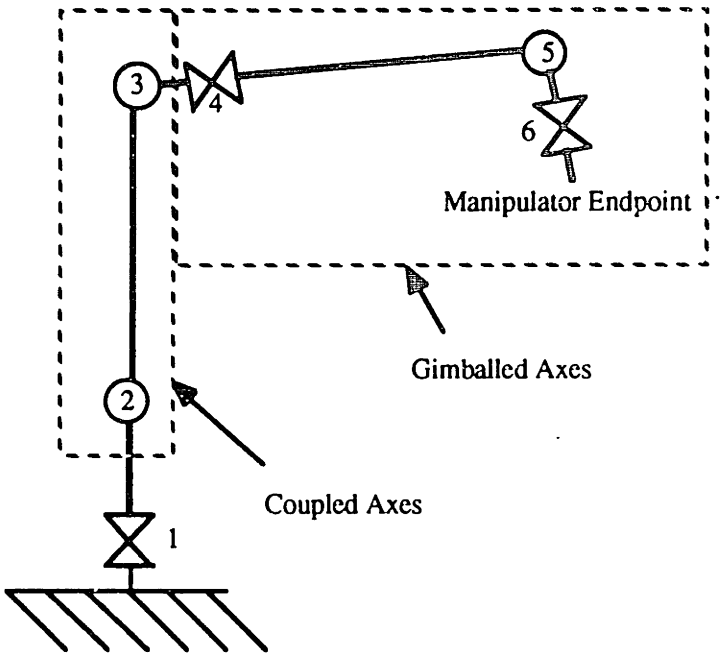

Figure #4-3. Kinematic structure of manipulator

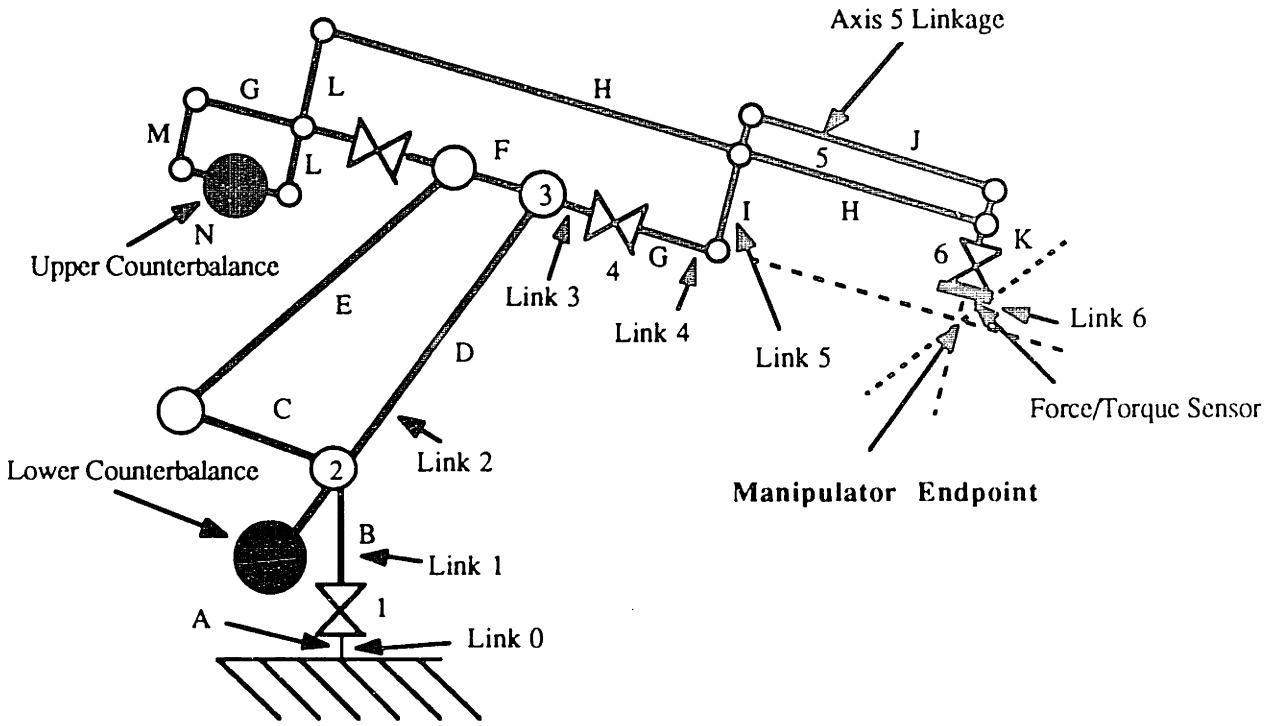

Figure 4-4. Manipulator linkage diagram

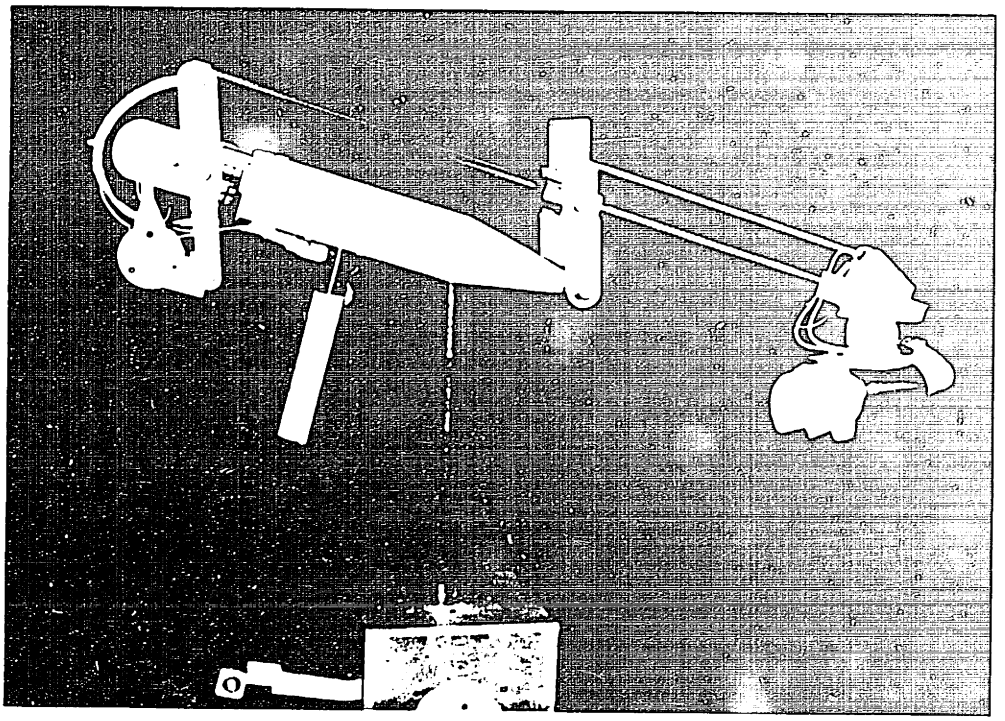

Figure #4-5. Photograph of MED maniulator

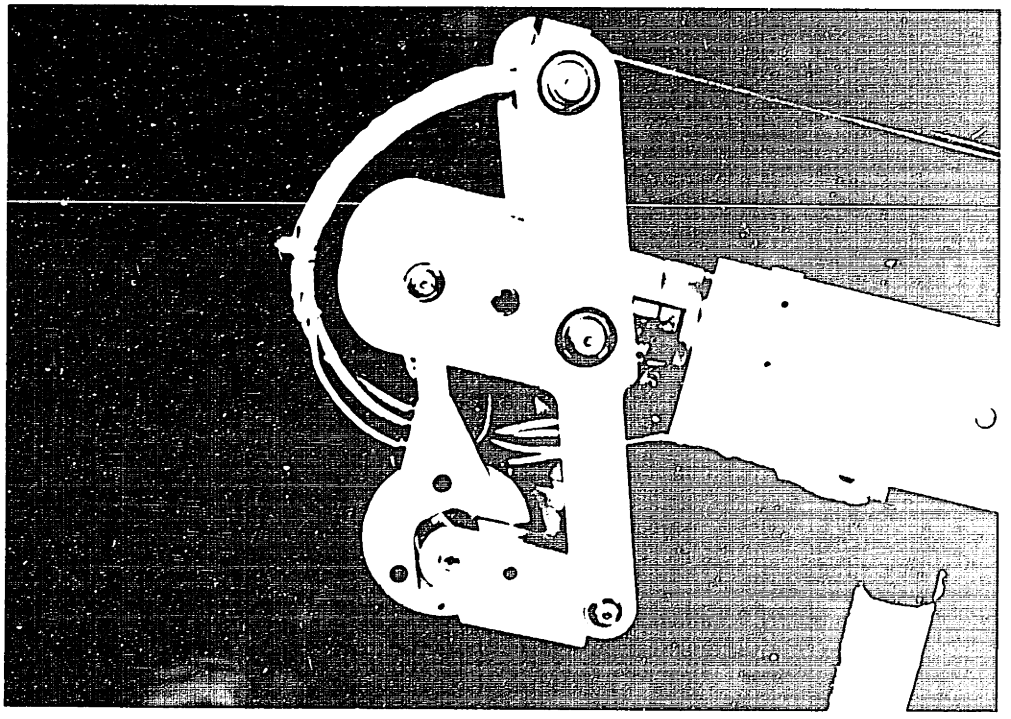

Figure # 4-6. Photograph of upper rear linkage

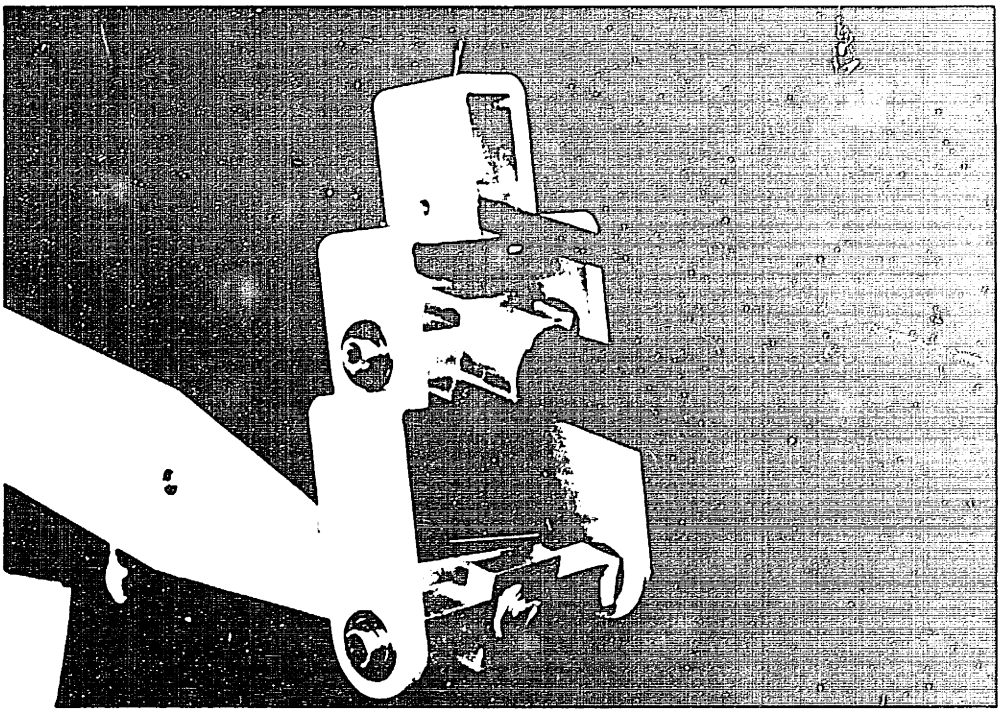

Figure #4-7. Photograph of front linkage

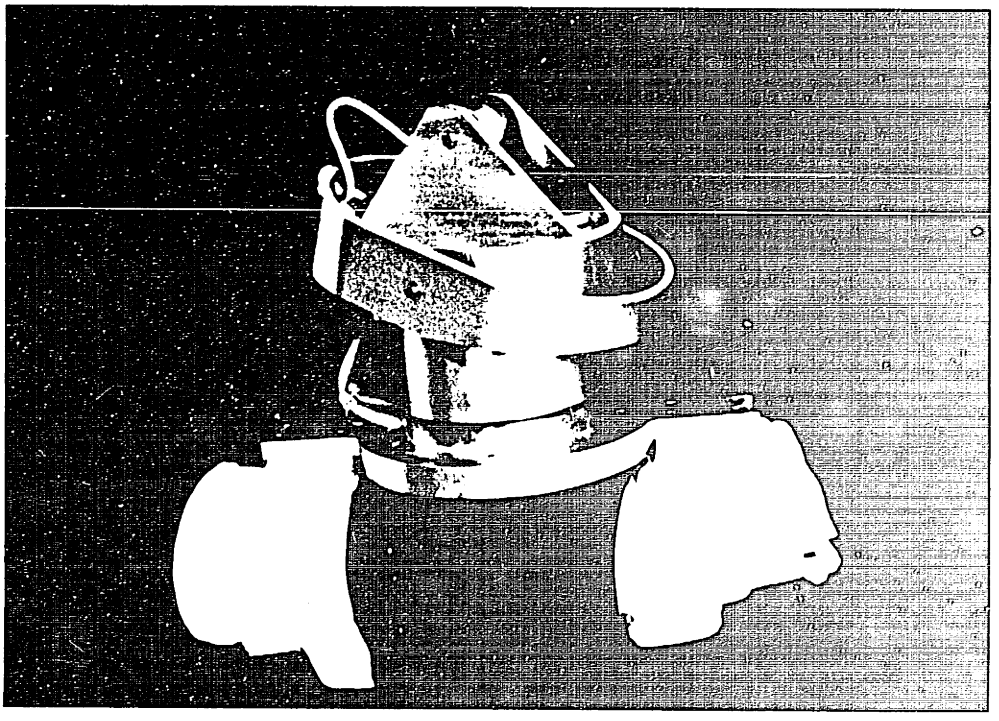

Figure # 4-8. Photograph of manipulator endpoint with limb coupler cuff

Actuators

The MED actuators chosen for this application were Placid Industries magnetic particle brakes. These actuators were chosen due to their low cost, ease of control, and proven reliability in past Newman Laboratory projects (for example Adelstein, 1981; Maki, 1982; Hausdorff, 1988).

Placid Industries model B115P was used for axes of the manipulandum. This 24 Volt particle brake has a rated torque of 115 inch-lbs at a rated current of .333 Amps, a maximum speed of 1800 RPM, and a de-energized drag[1] of 25 ounce-inches. Placid Industries model B15P was used for axes 4-6 of the manipulandum. This 24 Volt brake has a rated torque of 15 inch-lbs at a rated current of .25 Amps, a maximum speed of 2000 RPM, and a de-energized drag of 5 ounce-inches.

The actuators were located in non-traditional locations on the manipulator linkage of figure 4-4. Actuator 1 is located between link 0 and link 1 and controls the dissipative load of axis 1. Actuator 2 is located between link 1 and link C and controls the dissipative load for axis 2. Actuator 3 is located between link C and link 2 (link D) and controls the dissipative load of the translational motion in the r direction. Actuator 4 is located between link F and link L and controls the load of axis 4. Actuator 5 is located between link M and link N and controls the axis 5 load. Finally, actuator 6 is located between link K and link 6 and controls the load of axis 6.

This specific design was chosen because one actuator is connected to mechanical ground and four actuators are used as counterbalances. Actuator 1 is connected directly to ground and the only inertia it adds to the manipulator linkage is due to its rotating shaft and disk. Actuators 2 and 3 are in the same location as the lower counterbalance of Figure 4-4 and act to help counter the load of the complete manipulator linkage. The axis 4 actuator

---

1 De-energized drag is the power off "Coulomb" friction torque resulting from seals and residual magnetism.

helps to balance the load about axis 3. Finally, the link 5 counterbalance is in the same location as the upper counterbalance and acts to balance the center of mass of the upper linkage about both axis 3 and axis 4.

Reducer

The torque output of each of the first three breaks is amplified by approximately four times using cable drive transmissions. Cable drives were chosen because they best fit the design criteria of low-cost, low-backlash, and low friction. The axis 1 reducer is shown in Figure 4-9. The brake for the first axis, Z, is connected directly to a two inch aluminum capstan, Y, which is connected to an eight inch capstan, L, via a 1/8th inch diameter aircraft cable with a nylon cover procured from McMaster Carr. The eight inch capstan, L, is connected directly to link 1 of Figure 4-4, designated U in Figure 4-9.

Figure 4-10 illustrates the transmission for axes 2 and 3. To orientate the reader, the eight inch capstan, L, is shown at the bottom of the figure and is connected directly to the manipulator link 1, U. The transmission consists of two eight inch capstans connected to two separate two inch capstans via the same 1/8th inch aircraft cable used in axis 1, designated P. The axis 2 actuator's housing, O, is connected directly to one of the two inch capstans, N, which is connected to the eight inch capstan, Q, which is fixed to link 1, U. The output shaft of the axis 2 actuator is connected to the other two inch capstan, which is connected to the second eight inch capstan, S, via another aircraft cable, V. This large capstan, S, is connected directly to link C of Figure 4-4. Relative motion between the base and the output shaft of the axis 2 actuator produces the rotational motion of axis 2. The axis 3 brake's housing, W, is connected to link 2 of Figure 4-4, and designated T and R in Figure 4-10. The output shaft of this actuator is connected to the two inch capstan, X. Relative rotation between the actuator's base and output shaft produces the translational movement, r, of the manipulator endpoint.

All three transmissions used a 7 x 19 strand right lay nylon coated aircraft cable with a bare cable diameter of 1/8" and a finished cable diameter of 3/16". The coating offers a number of advantages. It cushions the cable from shock and pressure, protects the pulleys from abrasion, and seals in the lubrication while sealing out moisture, dirt and grit. In each transmission, the cable is attached at one end to a flat 8" capstan, wrapped around a 2" capstan and then again attached to the 8" capstan. As Dipietro (1988) suggested, the right lay cable was originally wound on the capstans with a left lay wrap in a figure eight circuit. This method did not work well for our design, so the cable was re-wrapped with a loop wrap. The cable has a breaking strength of 2,000 lbs and, when used in the design configuration, has a calculated life of 300,000 cycles at 110 lbs tension.

The cable drive transmissions were pre-tensioned[1] using a moveable pulley center arrangement. Pre-tensioning tensioned each cable to approximately 55 lbs, enough so the cable never became visibly slack on its low-tension side.

---

1 Pretensioning doubles the stiffness of the cable drive as long as neither cable becomes slack.

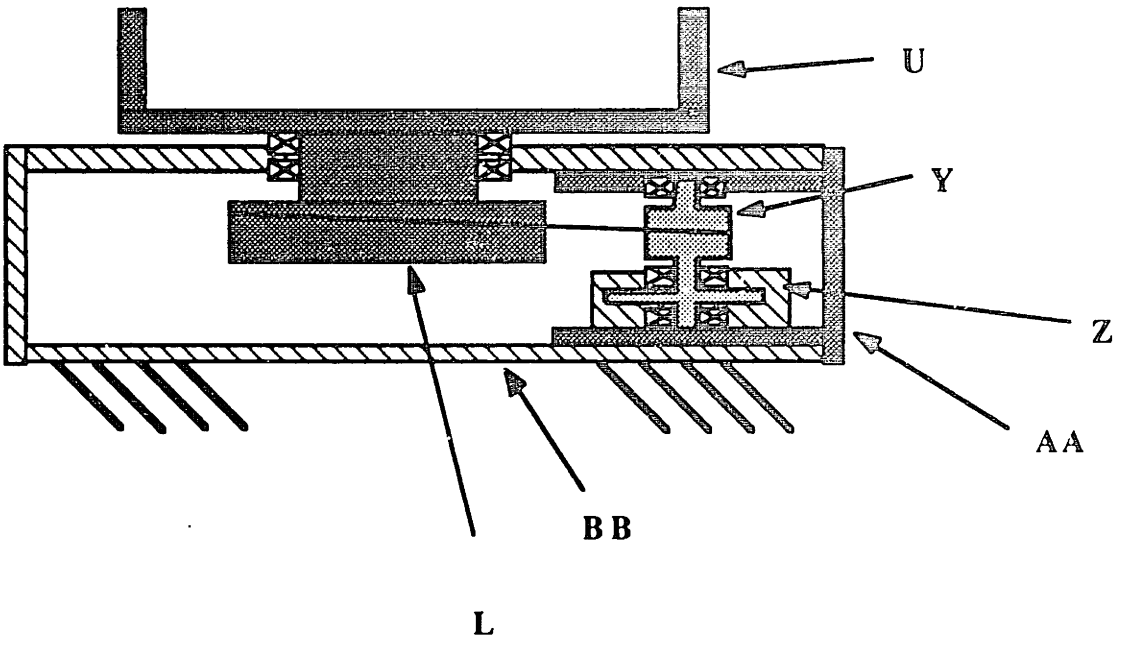

Figure # 4-9. Diagram of the axis 1 transmission

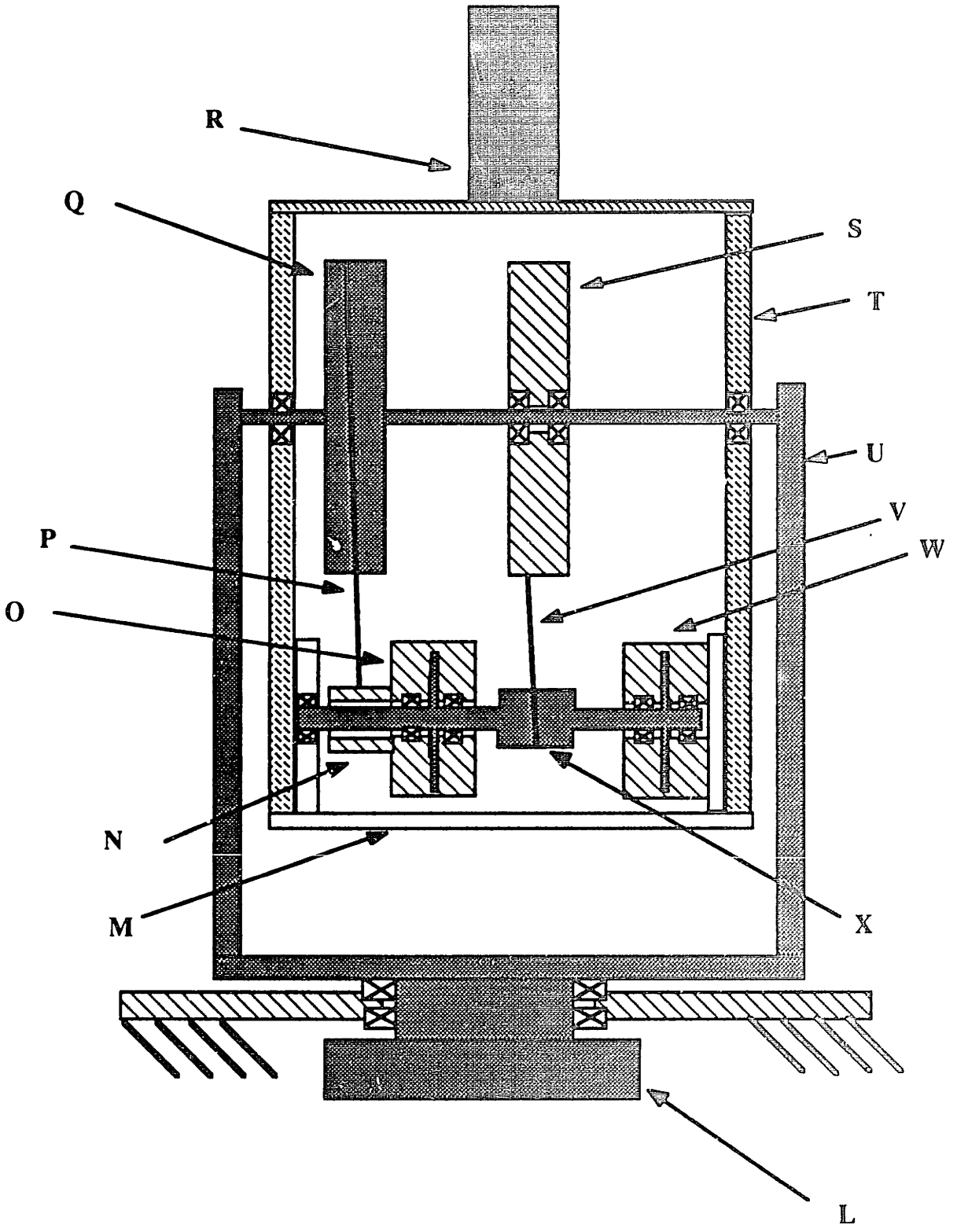

Figure # 4-10. Diagram of axes 2 and 3 transmission.

Position Sensors

Potentiometers were chosen as the position sensors for the MED manipulator and velocity signals were derived by differentiating their output. These sensors were chosen for their low cost and ease of computer I/O using an inexpensive A/D converter board. Helipot model 6186-R5K L1.0 B604M Potentiometers were chosen for this application. These conductive plastic 5K Ohm potentiometers have a manufacturers specification of 1% linearity over their near-360 degree range of operation. The potentiometers connect to the output shafts through PIC Designs No-Slip series timing belts and pulleys. The double aramid fiber core timing belts are designed and manufactured to be backlash free, operate without lubrication, and to be very quiet during operation.

Because the cable drive transmissions were not completely coupled to the two inch capstan, it is possible for the two inch capstan to slip in relation to the eight inch capstan. This necessitates moving the potentiometers downstream of the axis 1, 2, and 3 cable drives to eliminate the possibility of gradual loss of calibration. The potentiometer locations are listed in Table 4-1 with reference to the linkage in Figure 4-4.

Table #4-1

Potentiometer Locations

Refer to Figure #2 for illustration of link nomenclature

Potentiometer	Measures angle between Link	and Link
1	0	1
2	B	C
3	1	2
4	3	4
5	4	5
6	5	6

Force/Torque Sensor

The force/torque sensor was designed to attach between the final link of the manipulator and the subject's limb coupler cuff (as shown in Figure 4-4). Because of the sensor's location, the design needed to be very low in weight and small in size while still measuring loads up to the maximum capacity of the manipulator. The final force/torque sensor elastic element is the common (maltese) cross design. This elastic element design was chosen because it best fit the design criteria.

The elastic element was machined from a five inch diameter 7075-T6 aluminum rod. This particular alloy was chosen due to its high thermal conductivity, linearity, machinability and its low histeresis properties. The elastic element was designed so that the highest strain on any strain gage was 1000 microstrain for maximum forces of 23 lbs and maximum torques of 88 inch-lbs applied to the centroid of the elastic element. The dimensions of the elastic element were calculated based upon the algorithm described by Brock (1987).

The thirty-two strain gages attached to the elastic element were Omega Engineering type HMB 3/120 LG 13. These constantan foil gages have a glass reinforced phenolic resin carrier and nickel plated copper ribbon lead wires. They have a 120 Ohm nominal resistance and a temperature characteristic matched to the thermal expansion coefficient of the aluminum elastic element (23×10^{-6}).

The strain gages were installed using the eleven step method as detailed in Measurements Group, 1979. The elastic elements were degreased using CSM-1 degreaser, abraded with 400 grit silicon carbide paper thoughoughly wetted with M-Prep Conditioner A, and neutralized with M-Prep Neutralizer 5 applied with a cotton-tipped applicator. After surface preparation, the gages were secured with M-Bond 200 fast curing room temperature adhesive and M-Bond 200 Catalyst. Finally, the wire leads were soldered to terminal pads and the assembly was coated with a liquid polyurathane.

The final assembly is shown in Figures 4-11 and 4-12. Note in Figure 4-12 that the instrumentation amplifiers (discussed later) are contained within the force sensor housing resulting in important signal-to-noise ratio. The elastic element is shown in Figure 4-13. The overall dimensions, including the circuit board area, are four inches in diameter and .8 inches in thickness, an extremely small package when compared with commercial sensors. The strain gage configuration is shown in Figure 4-14 and Figure 4-15 shows the Wheatstone bridge circuits which transduce the strain into voltages representing the horizontal force and vertical force for each of the elastic element's for arms. Each arm of the elastic element cross contains eight strain gages arranged into two Wheatstone bridge circuits. In total, the eight Wheatstone bridge circuits contain the information needed to determine the three force and three torque component loads applied to the force/torque sensor.

The force torque sensor 3/8 inch Diameter rod is mounted inside the hollow output shaft of the final particle brake with a light press fit. The sensor is further secured with a set screw hub which deforms the particle brake's hollow output shaft.

Limb coupler cuff

The final limb coupler cuff design was discussed in chapter 2 and is shown connected to the housing in the force/torque sensor in Figure 4-8. The limb coupler cuff is mounted to ouput side of the force/torque sensor using four 6-32 thread screws on each end of the limb coupler cuff. The black band around the limb coupler cuff in Figure 4-8 is a counterbalance shim. The shim is used to balance the manipulator with the current limb cuff design. If heavier designs are used in the future, the shim can be replaced with a shim of lower weight so that the manipulator will again balance.

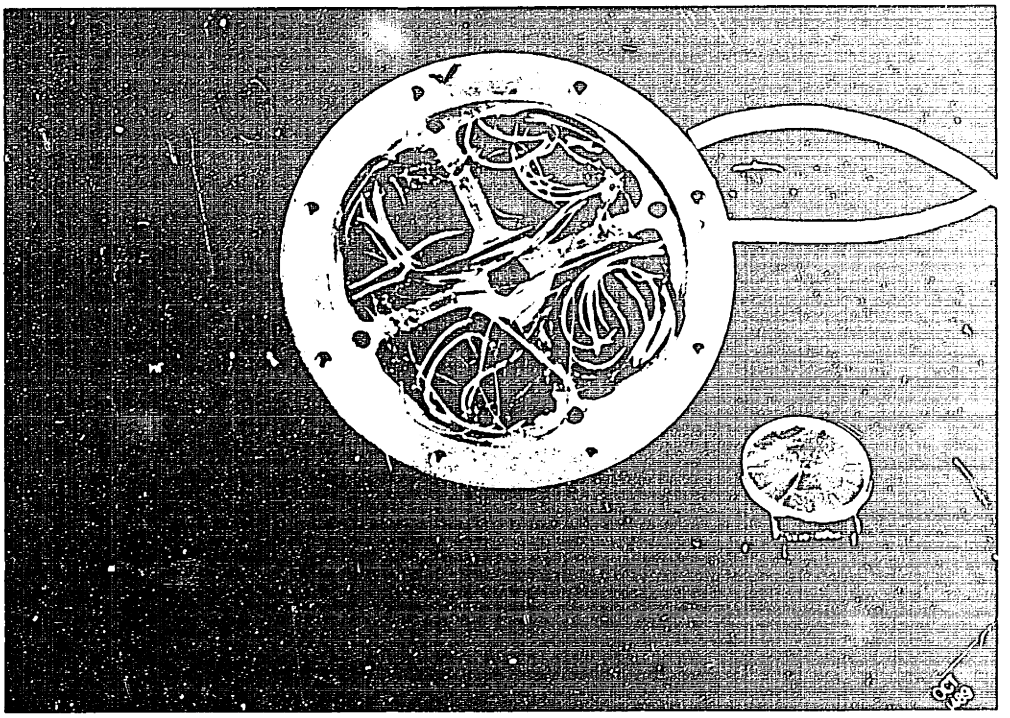

Figure 4-11. Photograph of force/torque sensor, top view

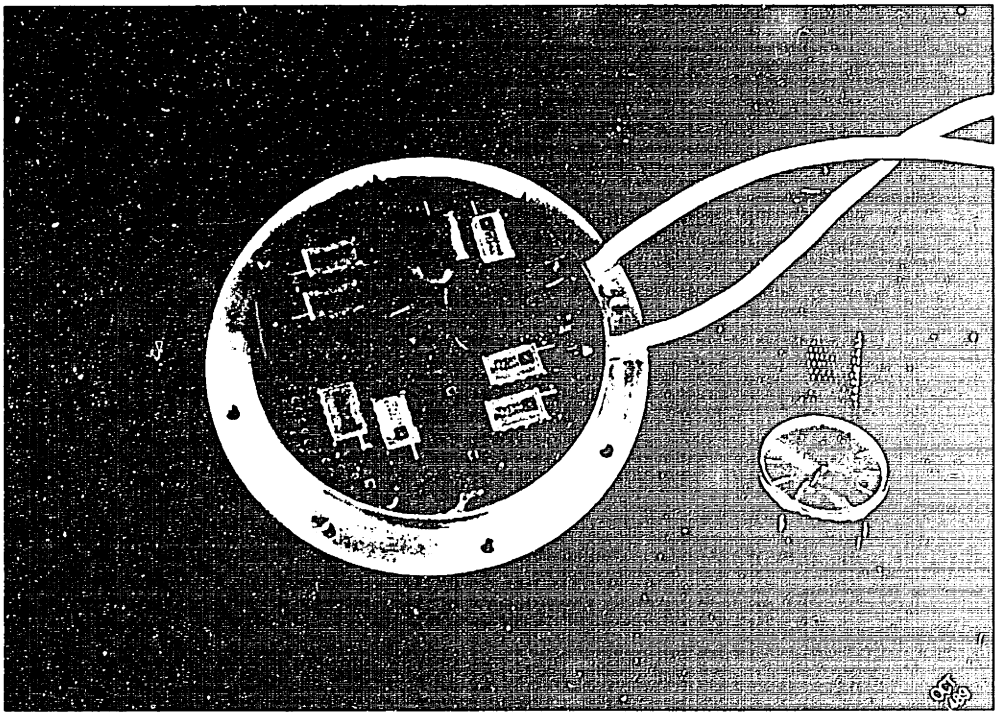

Figure #4-12. Photograph of force/torque sensor, bottom view

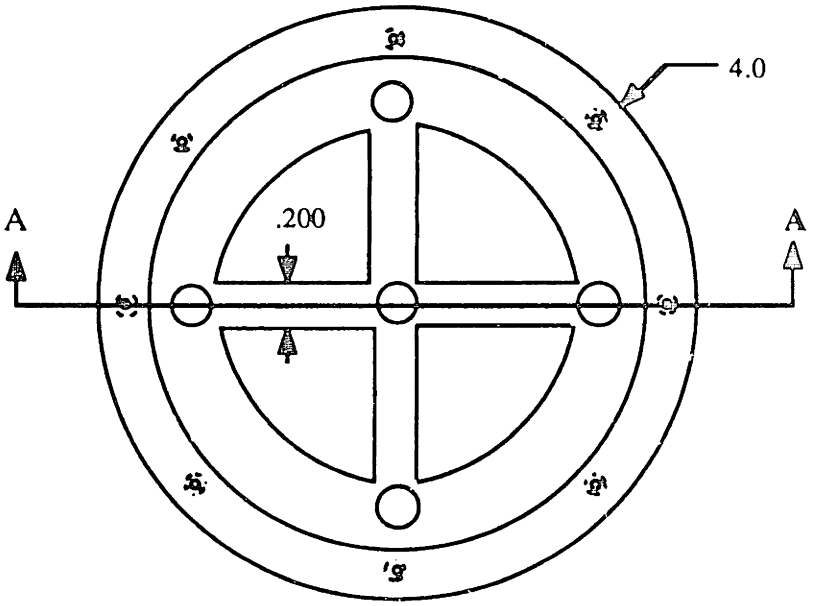

Section A-A

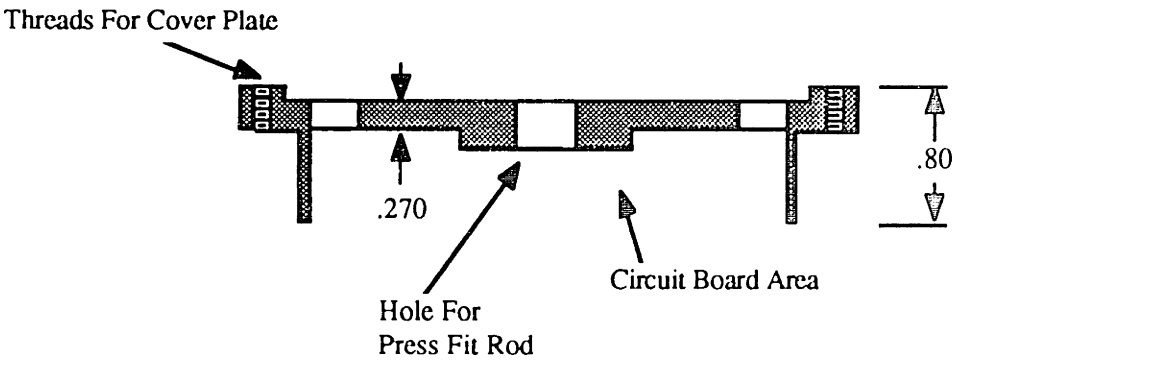

Figure #4-13. Overview diagram of force/torque sensor

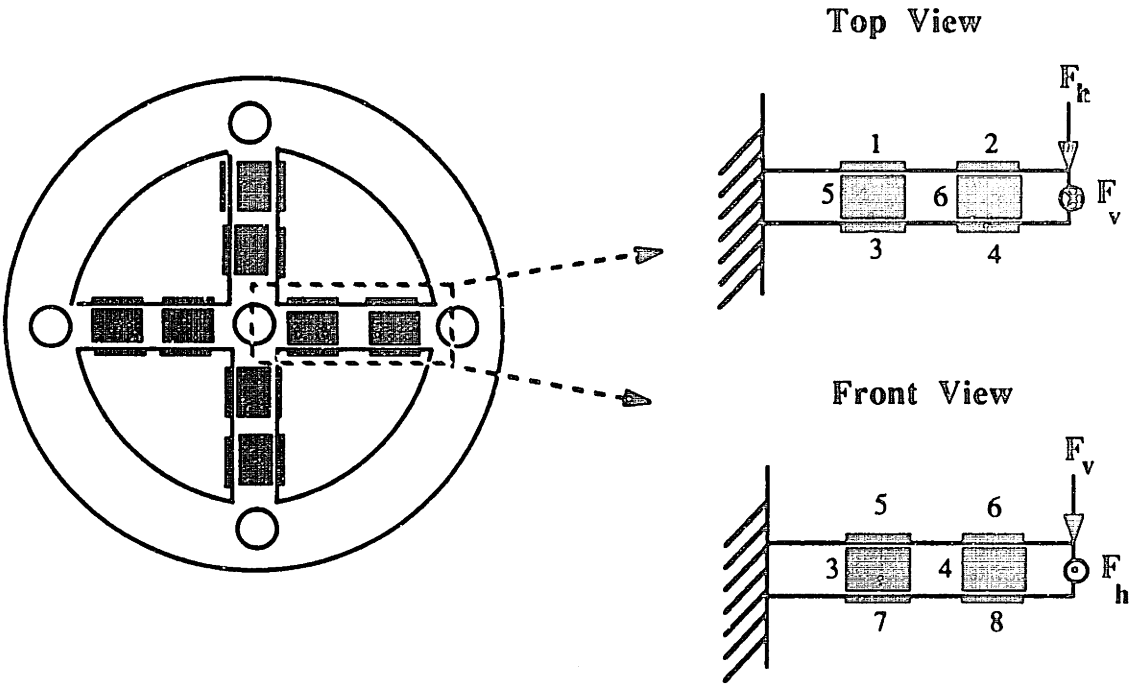

Figure #4-14. Strain gage placement diagram

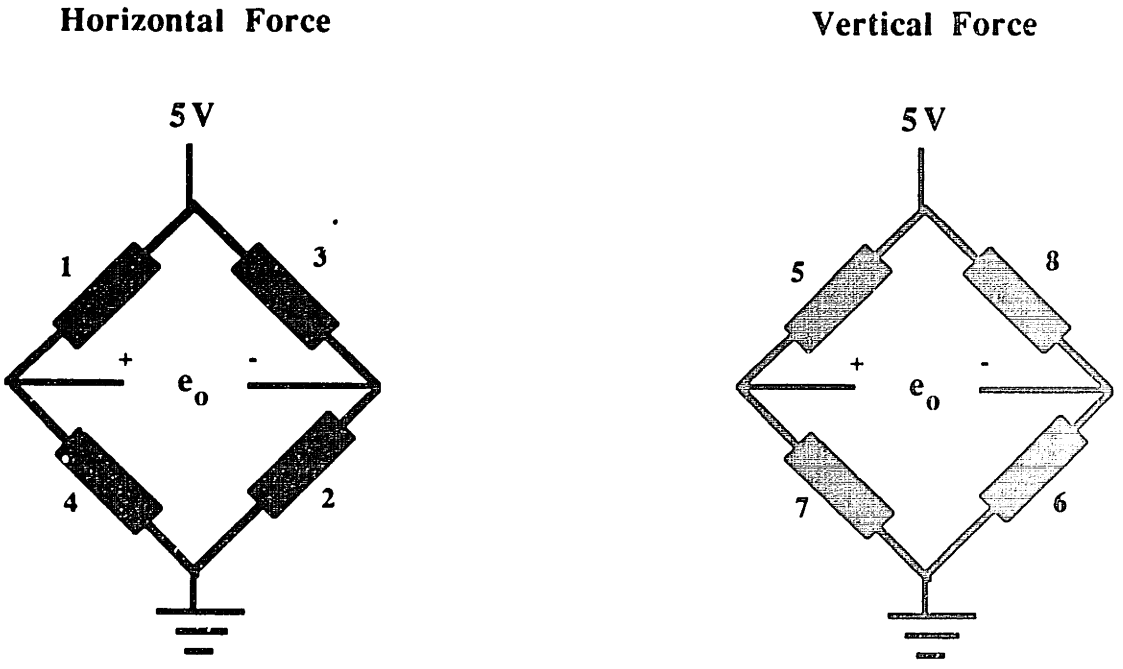

Figure #4-15. Wheatstone bridge circuits

Subject Support Chair

The experiments planned for the MED manipulator require that subjects be seated in positions which must be maintained comfortably for extended periods of time. Their disabilities differ which will require adjustment of seating position on an individual basis. In addition, it will be necessary that the base of the manipulandum and other experimental equipment be mounted rigidly but adjustably to the mechanical ground in which the subject is seated. Finally, experimental protocols may require secure, comfortable, repeatable fixation of the subject's torso to the mechanical ground.

To this end, a general purpose subject support chair and device mount was developed. The chair, pictured in Figures 4-16 through 4-21 is highly adjustable. Both the chair back and seat have adjustable angles so that a subject can comfortably sit upright or semi-reclining. The cushions of the seat are made with Comfor-foam, an open-cell visco-elastic foam, upholstered in a durable vinyl. The human subject is held firmly in the seat with a series of three belts, as shown in Figure 4-18, which can be configured in a number of ways, depending on the subject and experiment. Another attachment helpful for securing some subjects in the seat are handles as shown in Figure 4-20.

The frame of the chair, pictured in Figures 4-16 and 4-17, is made with welded square steel tube. The base of the frame has wheels and retractable machine feet which raise the base up off of the wheels. With the feet retracted, the chair is easily transportable on its wheels.

A series of modular aluminum plates with a two-inch 1/4-28 tapped holes has been developed so that it can be configured in different forms. One form, pictured in Figure 4-21, turns the aluminum plates into a tabletop. In other forms, the plates bolt securely to the chair base for use as mounts for experimental devices.

The modularity of the subject support chair allows the manipulator to be used for many subject and experiment mount applications. We envision the chair's use as a general

piece of laboratory equipment. The modularity of the chair can be expanded in many directions. One possibility is to build a base which will raise the chair a few inches vertically, thereby allowing more experiments to be performed on human legs than are possible with the chair's current height.

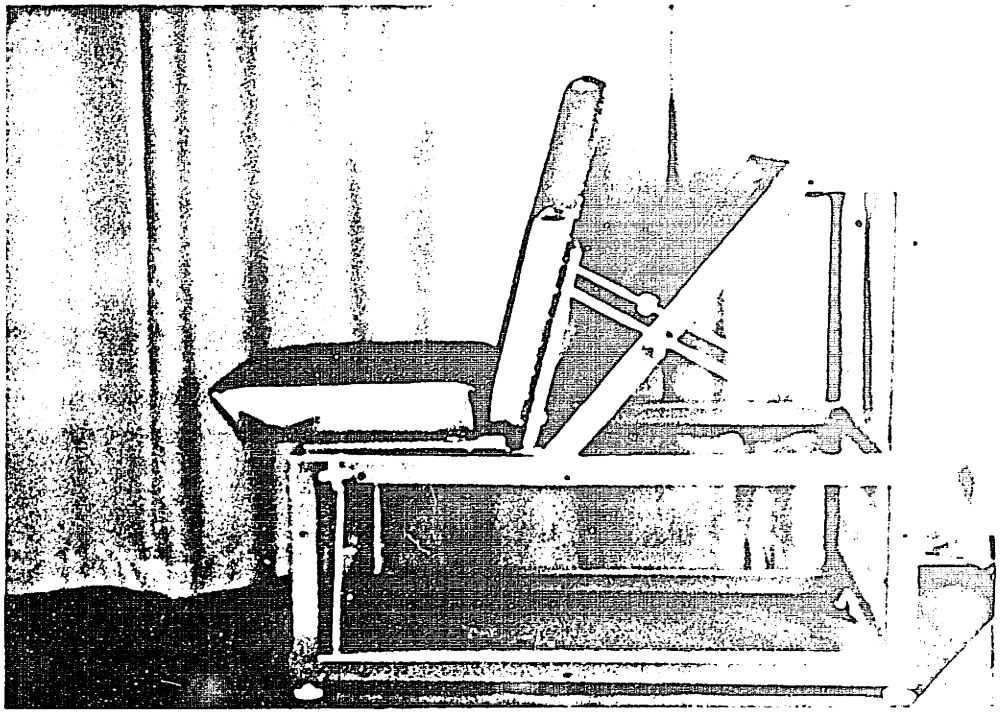

Figure #4-16. Photograph of subject support chair, upright position

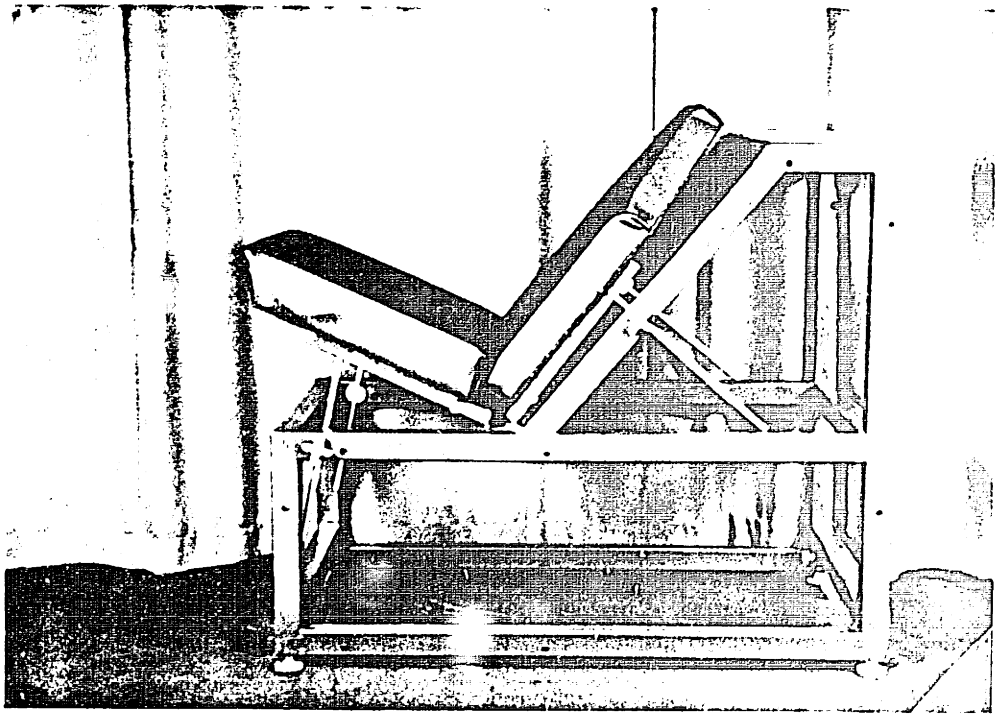

Figure #4-17. Photograph of subject support chair, reclining position

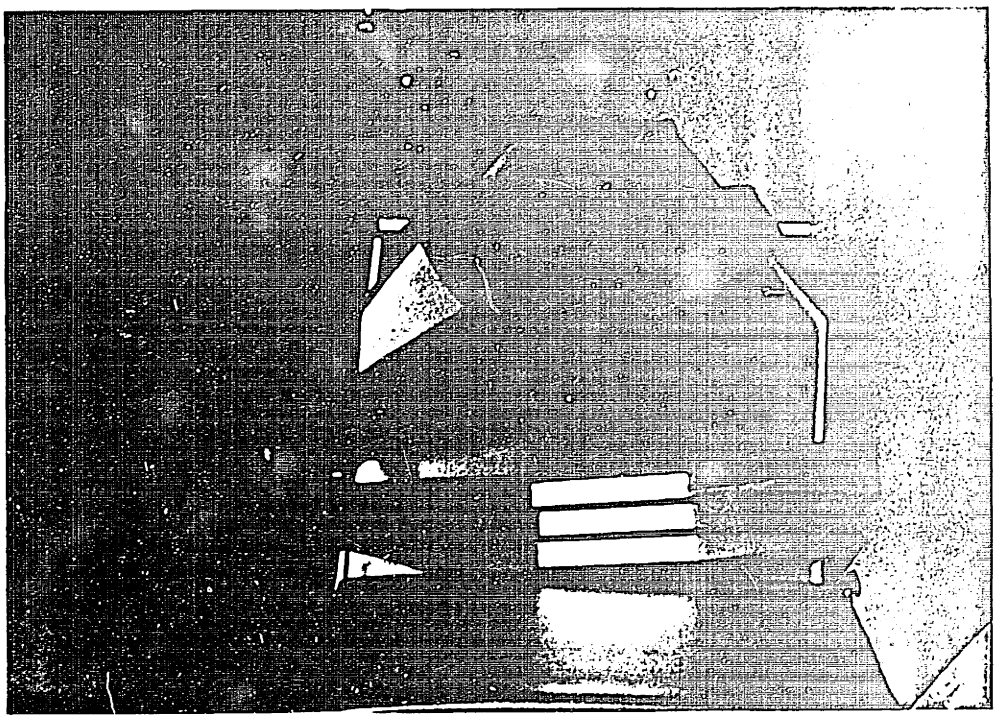

Figure #4-18. Photograph of subject support chair, support straps

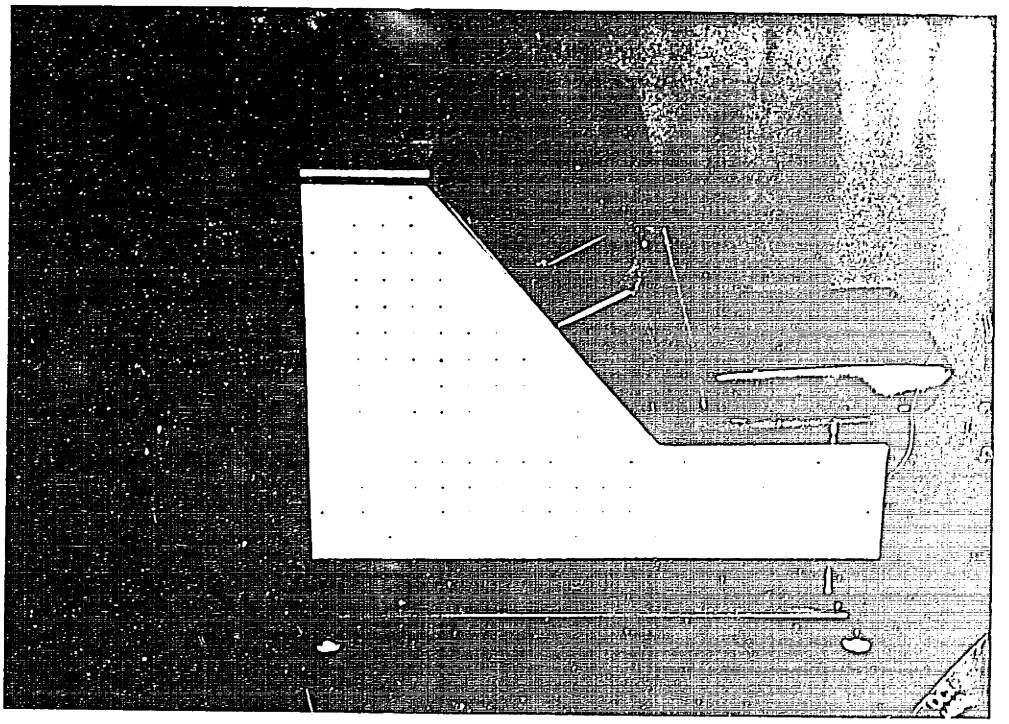

Figure #4-19. Photograph of subject support chair, attachment plate

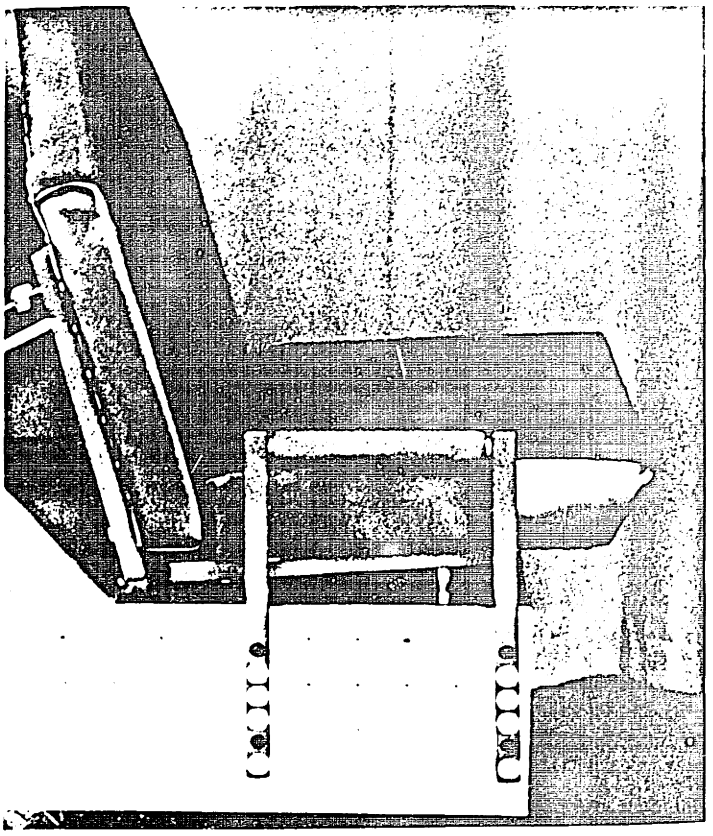

Figure #4-20. Photograph of subject support chair, handles

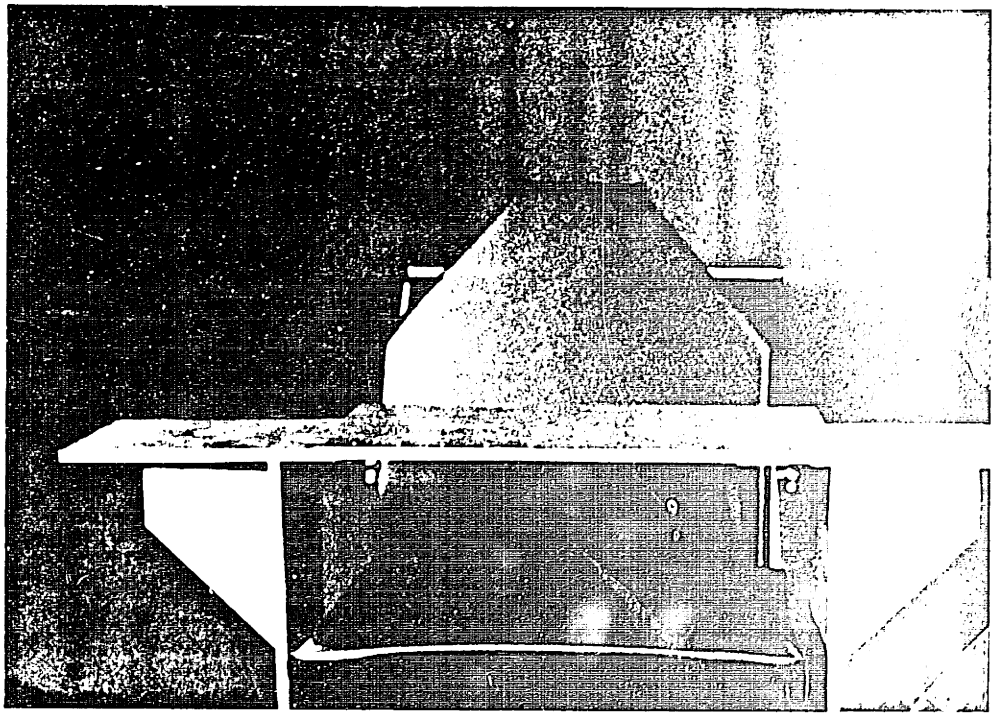

Figure #4-21. Photograph of subject support chair, table attachment

Electronics

General

The electronics used in the manipulator consist of analog circuits for the force/torque sensor, the potentiometers and the particle brakes. In the final configurations, all circuits are mounted on a single board and housed in an electronics enclosure along with the MED manipulator's power supplies.

Force/Torque sensor

The eight Wheatstone bridge circuits of the force/torque sensor are amplified at the force/torque sensor location (as seen in Figure 4-12) using the Analog Devices AD524C precision instrumentation amplifier circuit shown in Figure 4-22. The AD524C instrumentation amplifier was chosen for its high linearity, high common mode rejection, low offset voltage drift, and low noise properties.

Figure 4-22 also illustrates our method of bridge balancing. The Bridge balance resistor value is estimated using a potentiometer, and the closest single resistor value is attached at the proper location. The 10K trim pot is then adjusted to completely null the zero force signal.

The Wheatstone Bridge preamplifier electrical cabling runs through the manipulator linkage to the main electronic board where each signal is further amplified and low-pass filtered (20Hz cutoff frequency) as shown in Figure 4-23. The amplification is provided by an LM324 quad operational amplifier configured as an inverting differential amplifier. This configuration provides an additional amplification and offset adjust at the electronic box. The filter is made up of a National Semiconductor MF4 fourth-order Butterworth switched capacitor filter with the input clock frequency derived from an Analog Devices AD654 voltage-to-frequency converter. Both the filter and the converter were chosen because of their low cost and ease of use.

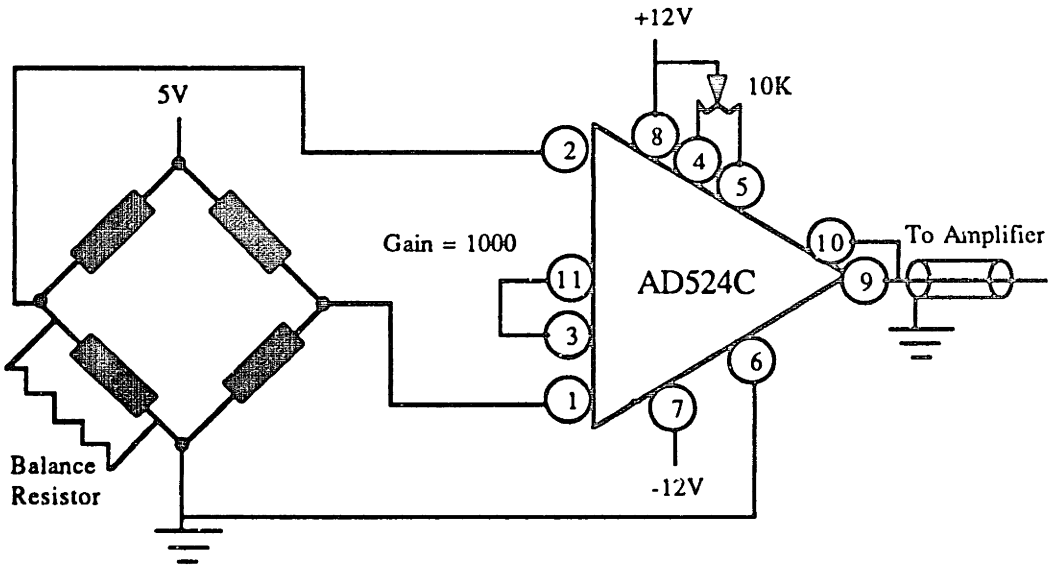

Figure #4-22. Wheatstone bridge preamplifier circuit

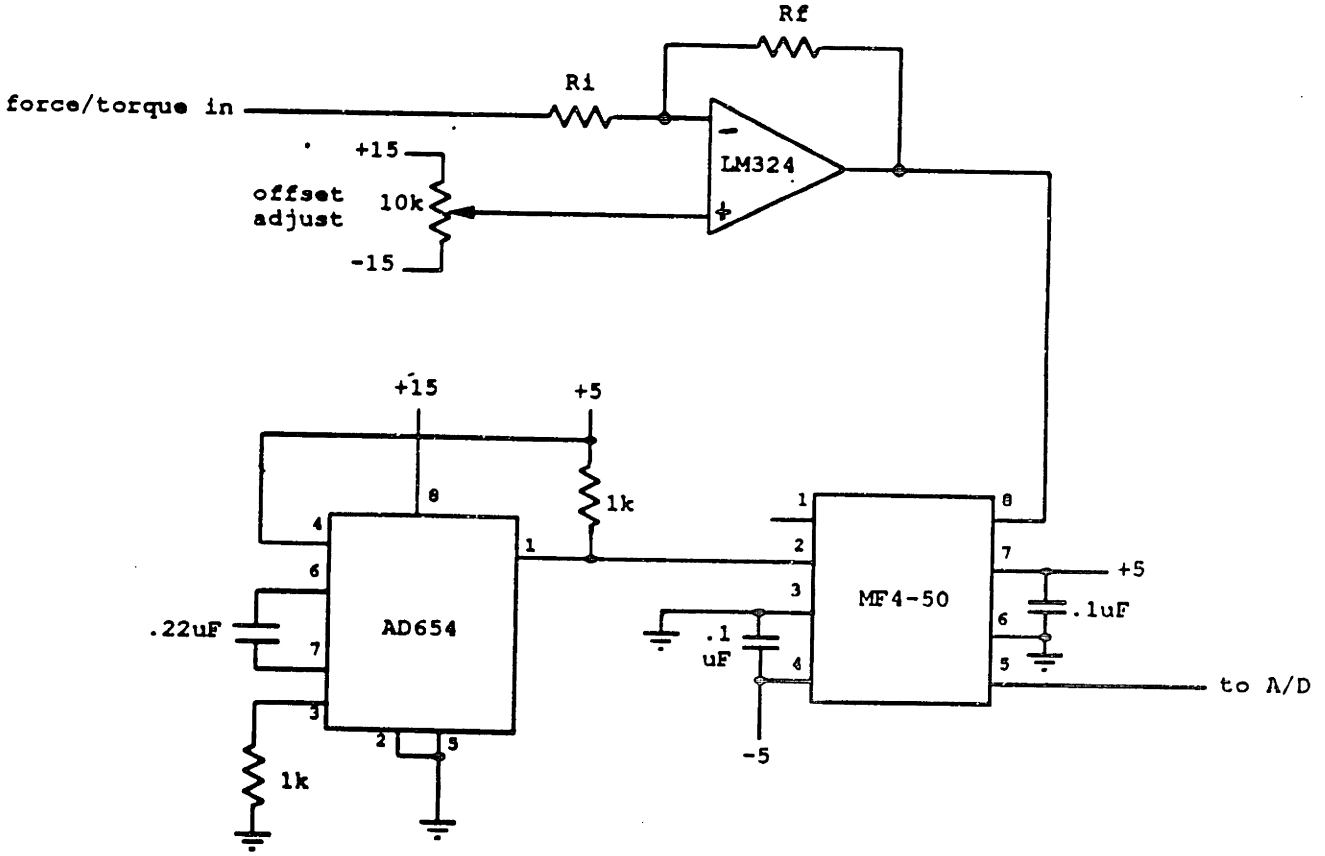

Figure #4-23. Force/torque sensor circuit diagram

Potentiometer

As noted above, position and velocity are transduced using 5K-Ohm potentiometers placed at different locations throughout the manipulator linkage. The output of each potentiometer is input into two different circuits, an amplifier circuit and differentiator circuit, to provide the manipulator position and velocity information (Figure 4-24). The amplifier circuit incorporates an offset adjust reducing the need to accurately place the angle-measuring potentiometer in zero position. The practical differentiator has two poles and a zero, which provides a low-noise velocity signal.

Particle Brake Driver Circuit

The particle brake driver electrical circuit, designed by undergraduate research assistant Stacy Ho with the assistance of Ralph Burgess went through two iterations before we were were satisfied with the design. The first design used a voltage-to-current amplifier pulse-width modulation (PWM) circuit. Although the PWM circuit was inexpensive and reliable, it was nonlinear, audibly noisy, and created electromagnetic noise which resulted in induced voltages in the signal-conditioning circuitry and microcomputer. The electromagnetic noise was greatly reduced through the use of shielding, but the continued noise and nonlinearity of the circuitry proved to be unacceptable for this application.

The circuitry was redesigned to incorporate a linear amplifier to eliminate the noise and nonlinear conditions. The new circuit is a linear voltage controlled current source (VCCS) with boosted voltage and current output (Figure 4-25). The circuit input comes from the D/A board (range 0-5V). A zero voltage input corresponds to a reverse current of 10 mA and 5 Volts corresponds to a forward current of 300 mA. (The amount of reverse current can be adjusted by varying R3.) The reverse current is used to reduce the effect of magnetic hysteresis in the brakes. We found that a very simple method of reducing the power-off friction in the brakes is to input a small reverse current through them.

The input from the D/A is attenuated by R1 and R2 to provide the correct range of output current. The current gain of the circuit may be adjusted by varying these values. Transistor Q1 provides Voltage amplification (gain determined by R7 and R6) while the push-pull output of Q2 and Q3 provides current amplification. The current through the brake is sensed by R8 and fed back to the positive input of A1 for non-inverting operation. R4 and R5 serve to shift the output of A1 to the current range of values for the operation of Q1, and C1 serves to compensate for the time constant associated with the brake, which is modeled as an inductor with resistance in series.

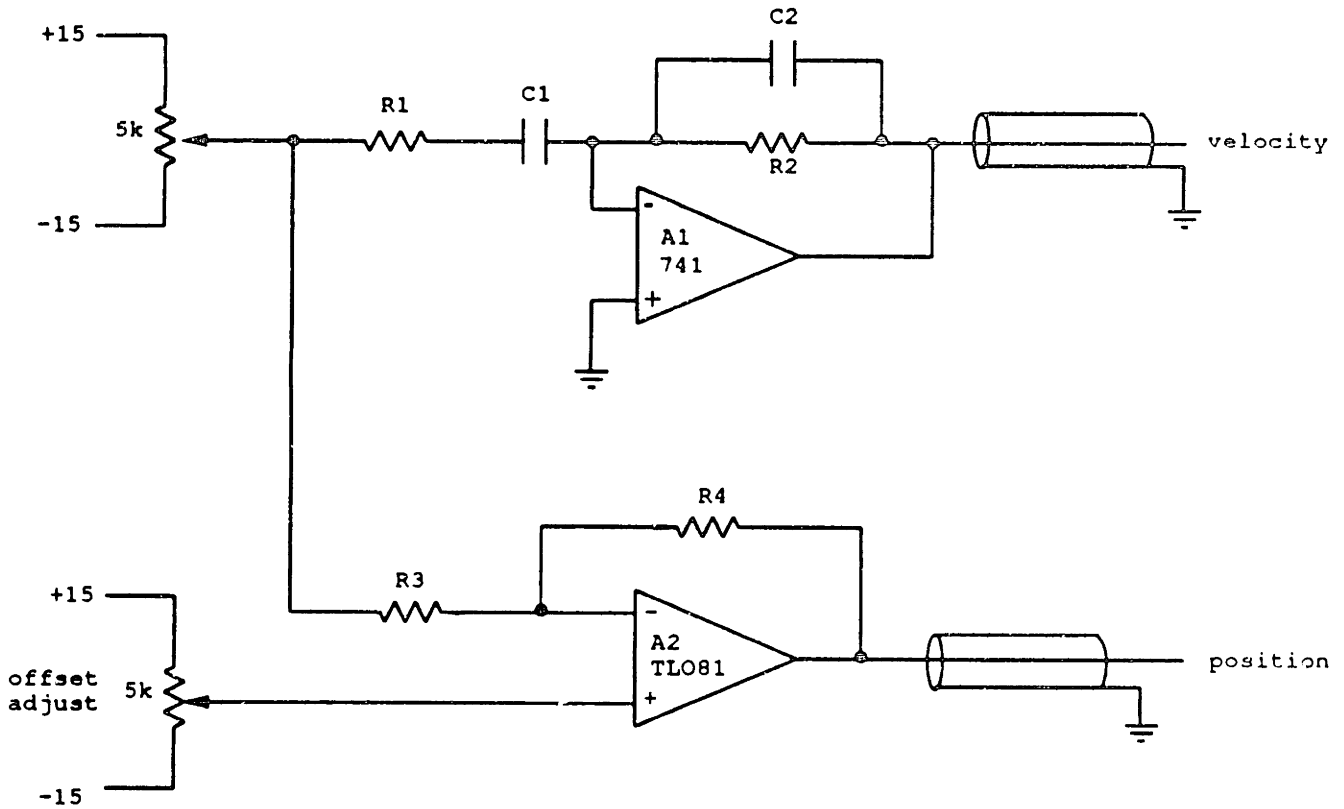

brake	R1	C1	R2	C2
1	15k	1uF	430k	.033uF
2	15k	1uF	430k	.033uF
3	15k	1uF	1.5M	.01uF
4	1.5M	.1uF	2M	.005uF
5	1.5M	.1uF	3M	.0033uF
6	1.5M	.1uF	1M	.005uF

Figure 4-24. Potentiometer circuit diagram

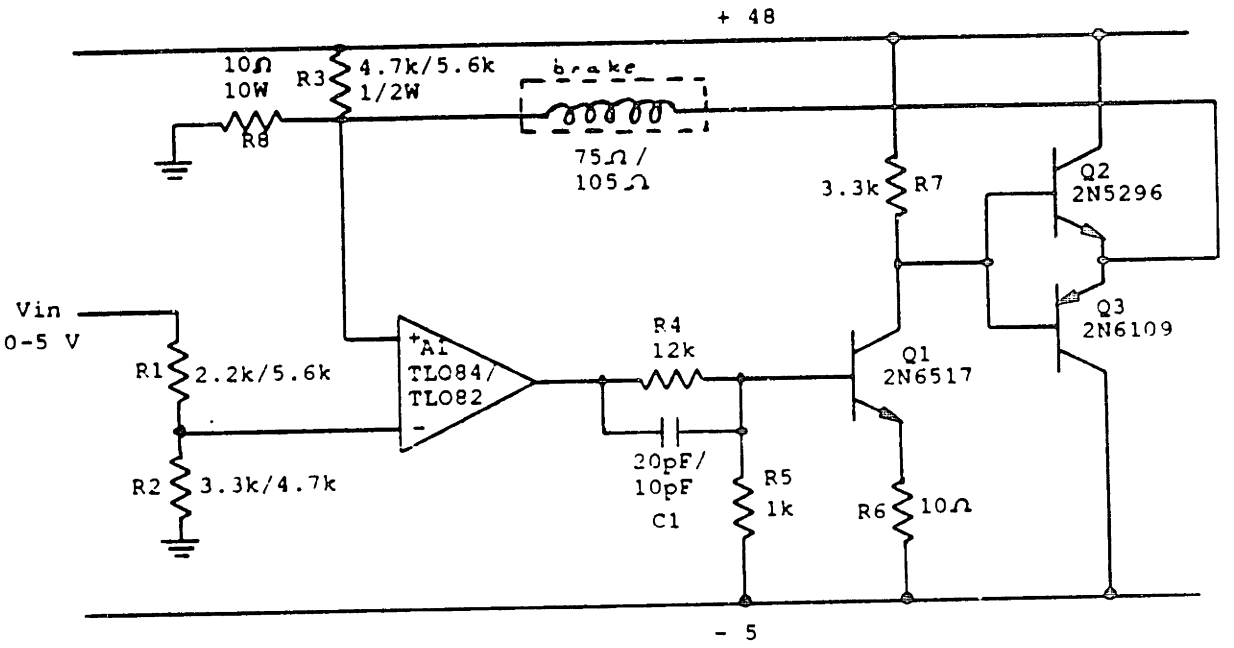

notes:

large brake value/small brake value

all resistors 1/4W unless otherwise noted

Figure #4-25. Particle brake driver circuit diagram

Electronics Housing

The power supplies and electronic signal conditioning circuitry all fit within an electronics box partly built by undergraduate research assistant Mohanjit Jolly. The first electronic box internal design had slots to accommodate ten circuit boards approximately 6" square. That enclosure and installed boards are shown in Figure 4-26. This configuration proved difficult to troubleshoot so the box was redesign to accommodate a single circuit board shown in Figures 4-27 and 4-28.

The electronics box, shown in Figures 4-29 and 4-30, contains two muffin fans to cool the electronics, a key-lock switch to prevent unauthorized use, a mushroom switch for quick emergency shutdown, a power-on light, and an assortment of cable connectors to attach to both the computer and the MED manipulator.

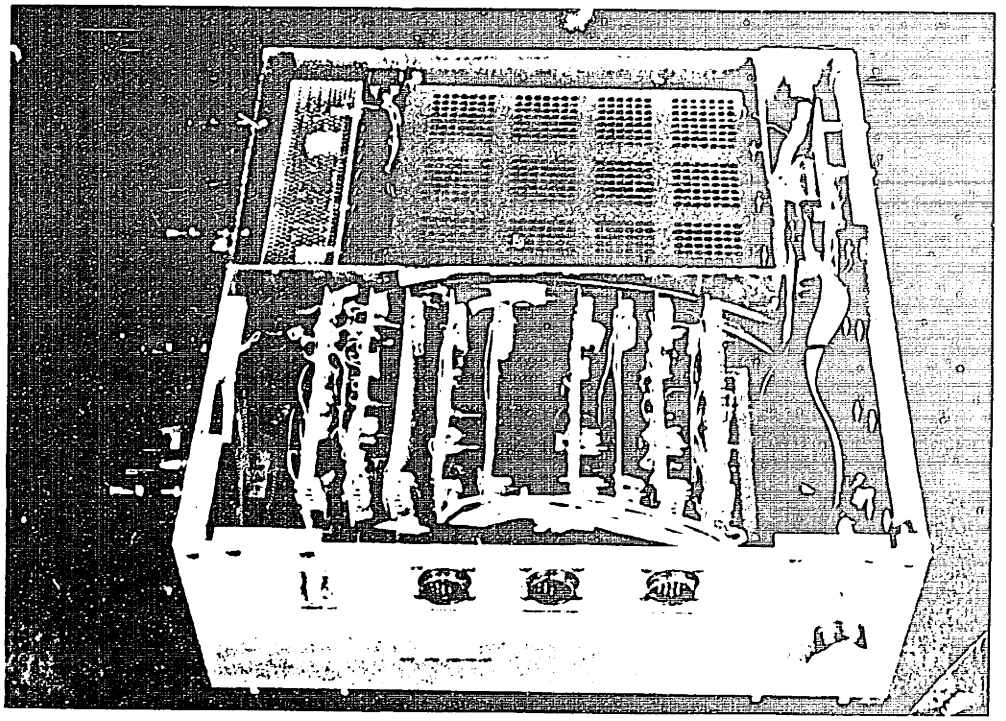

Figure #4-26. Photograph of electronic box, upright board position

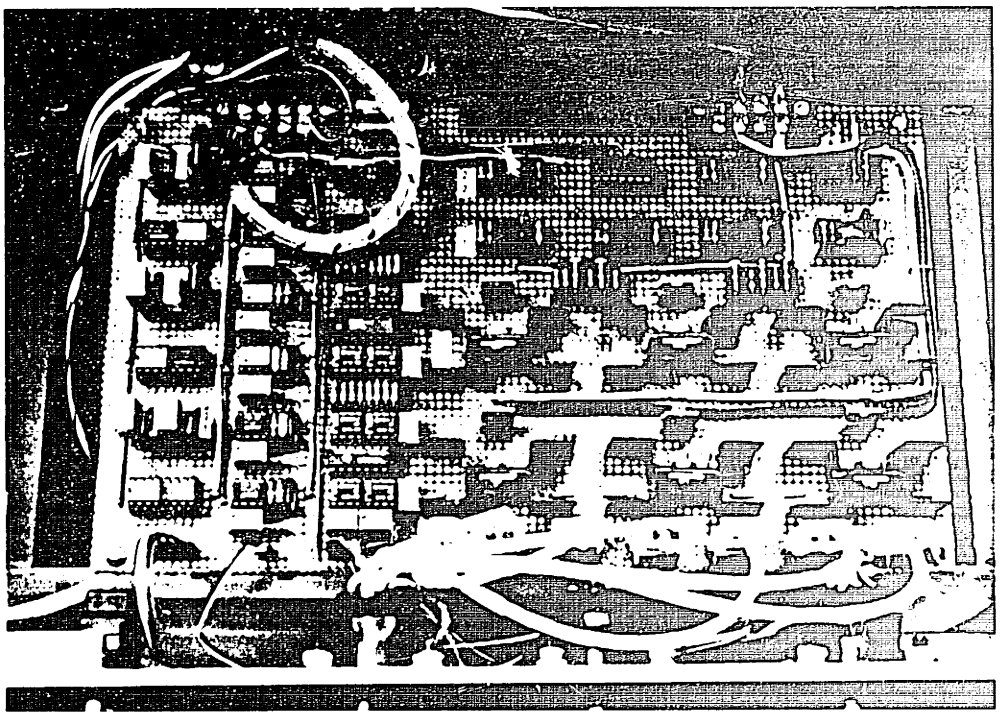

Figure #4-27. Photograph of improved electronic board in horizontal board position

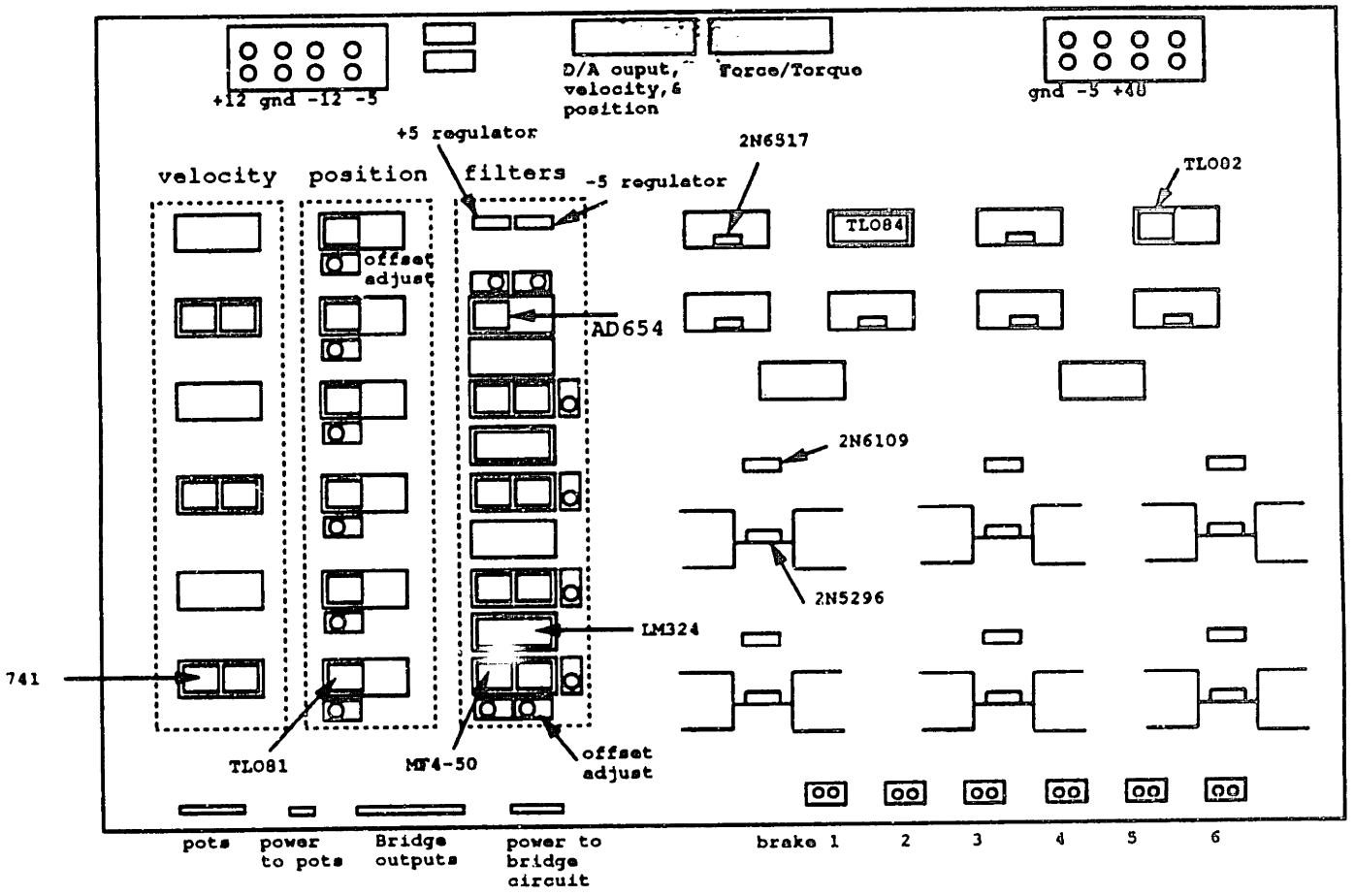

Figure #4-28. Physical layout of electronic board

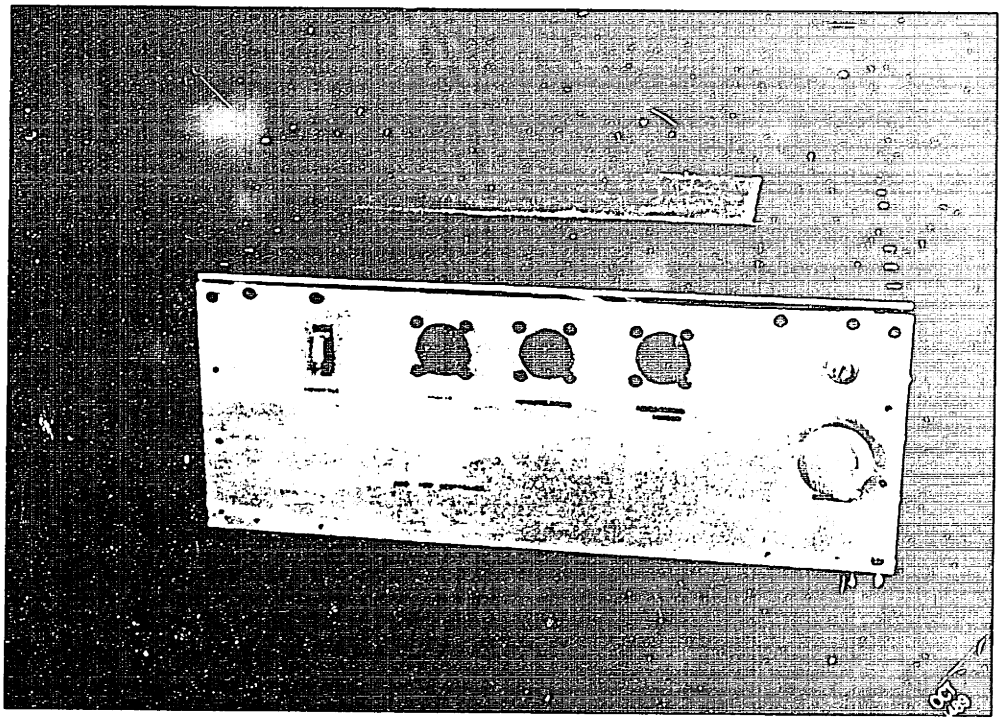

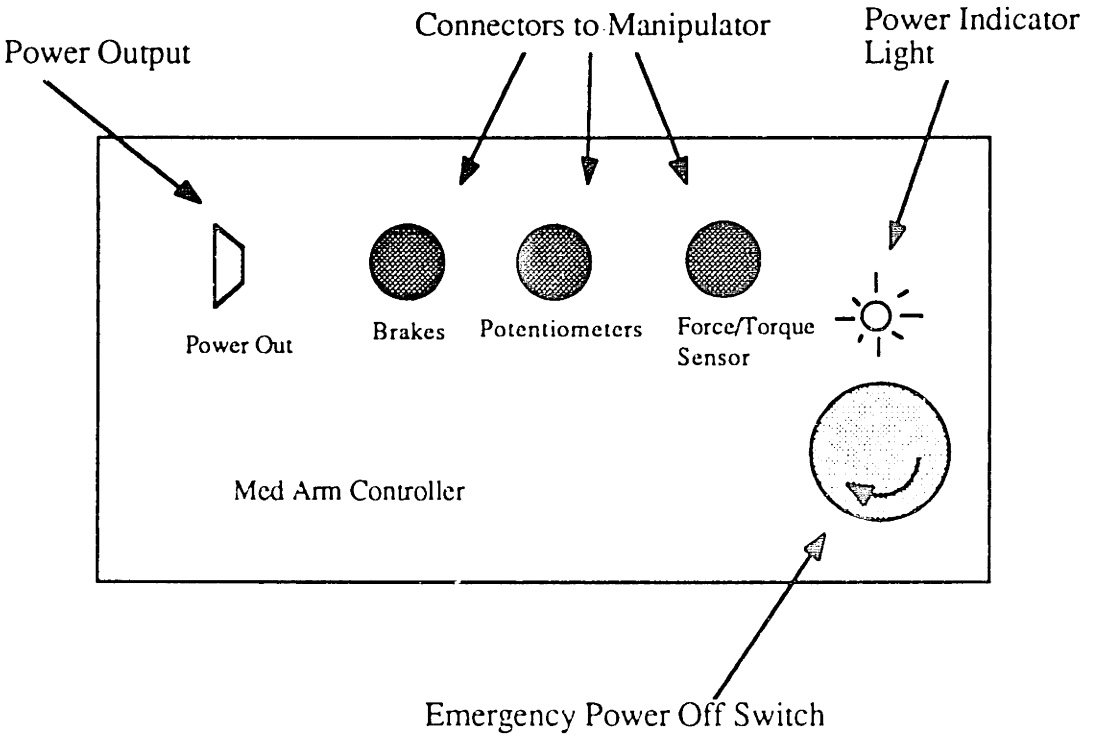

Figure #4-29. Electronic box housing, front view

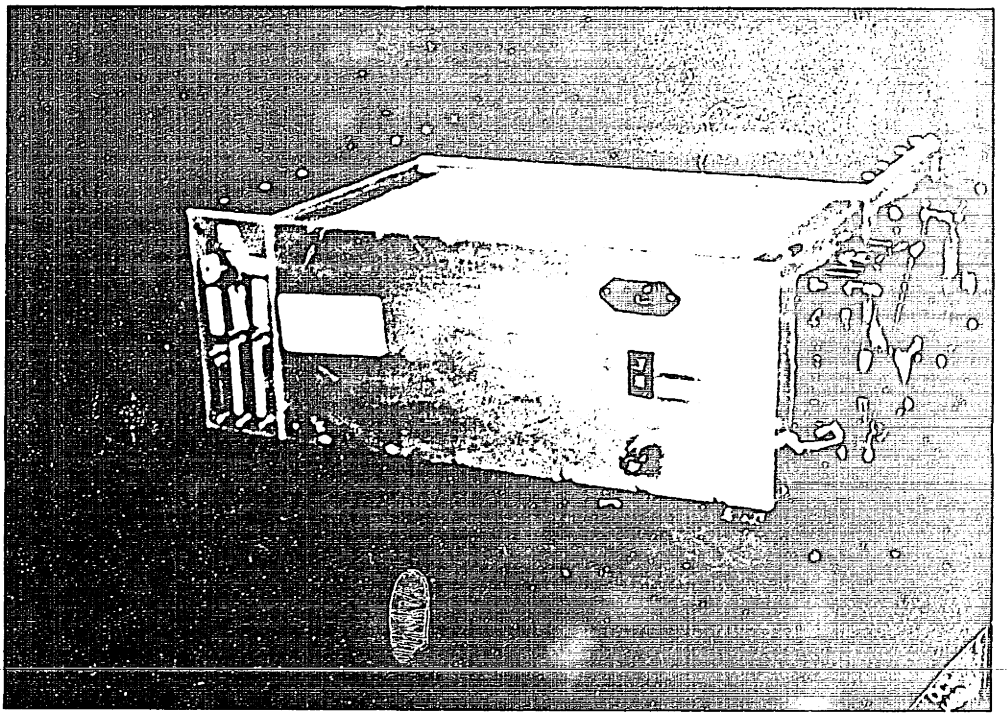

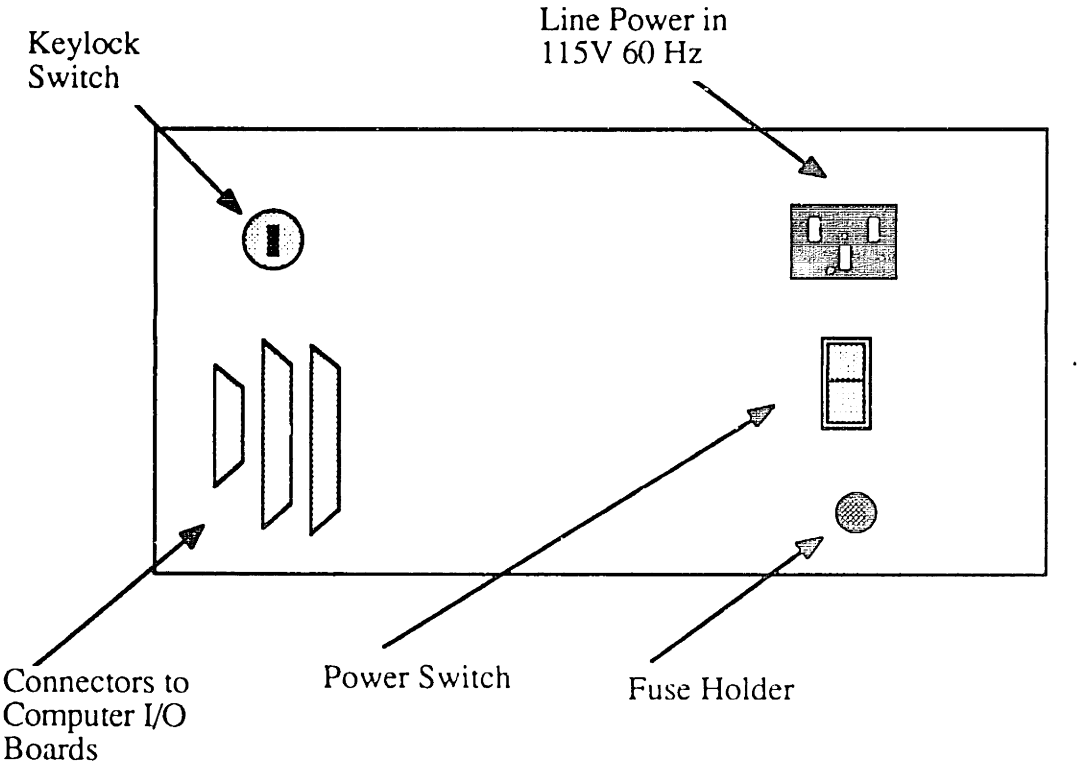

Figure #4-30. Electronic box housing, rear view

Computer Hardware

The computer used for all of the developmental and experimental work is a Leading Edge model D2 AT-compatible computer. The computer is configured with 640 kilobytes of memory, 8 megahertz clock speed, an 80287 math co-processor, and an enhanced graphics display adaptor (EGA). The computer system contains three I/O boards:

- a Data Translation DT2814 analog to digital (A/D) converter board which provides 12 bit resolution on each of the 16 single-ended analog input channels,
- a MetraByte DAS-8 A/D converter board which offers 12 bit resolution on each of the 8 single ended analog input channels and an Intel 8254 programmable interval timer, and
- a MetraByte DDA-06 digital to analog (D/A) converter which delivers 12 bit resolution on each of the 6 output channels and 24 bits of digital I/O which can be programmed for input or output.

Twenty of the twenty four A/D channels are utilized by the MED manipulator system in the following way: six position and six velocity input signals from the potentiometer signal conditioning circuitry and eight force/torque input signals from the load sensor signal conditioning circuitry. The six D/A channels are used for outputs to the particle brake controllers used to control the output torque of the particle brakes. The actual I/O mapping is shown in Table 4-2.

Table #4-2

Computer Hardware Mapping to Manipulator Functions

Data Translations A/D Board

Channel	Manipulator Function
0	Axis #1 Position
1	Axis #1 Velocity
2	Axis #2 Position
3	Axis #2 Velocity
4	Axis #3 Position
5	Axis #3 Velocity
6	Axis #4 Position
7	Axis #4 Velocity
8	Axis #5 Position
9	Axis #5 Velocity
10	Axis #6 Position
11	Axis #6 Velocity

DAS-8 A/D and Timer Board

Channel	Manipulator Function
0	Wheatstone bridge #1
1	Wheatstone bridge #2
2	Wheatstone bridge #3
3	Wheatstone bridge #4
4	Wheatstone bridge #5
5	Wheatstone bridge #6
6	Wheatstone bridge #7
7	Wheatstone bridge #8

DDA-06 D/A Board

Channel	Manipulator Function
0	Particle brake #1 control
1	Particle brake #2 control
2	Particle brake #3 control
3	Particle brake #4 control
4	Particle brake #5 control
5	Particle brake #6 control

Computer Software

All computer programs developed for the MED manipulator were written in C. The compiler used was The Microsoft® C Optimizing Compiler version 5.0 for the MS-DOS® operating system.

The computer programs are briefly described in Appendix A.

Simple Control Algorithm

The first controller designed for the manipulator is a simple open-loop viscous damping control algorithm. This controller is designed to make the manipulator end-point "feel" to the human as if a six degree-of-freedom viscous damper is attached to his arm. Because the actuators are energy-dissipating, however, the controller cannot eliminate the passive mass of the manipulator structural elements. As discussed in Chapter 2, the human does not feel the passive mass at high damping levels but increasingly feels the mass as the damping level is reduced.

The basic manipulator control algorithm is shown in Figure 4-31. Although the programs in Appendix A list variations of and support programs for the algorithm in Figure 4-31, the algorithm is representative of the method used to control the MED arm. Each of the different software modules, is represented by a box and given a module number in Figure 4-31, and explained individually below.

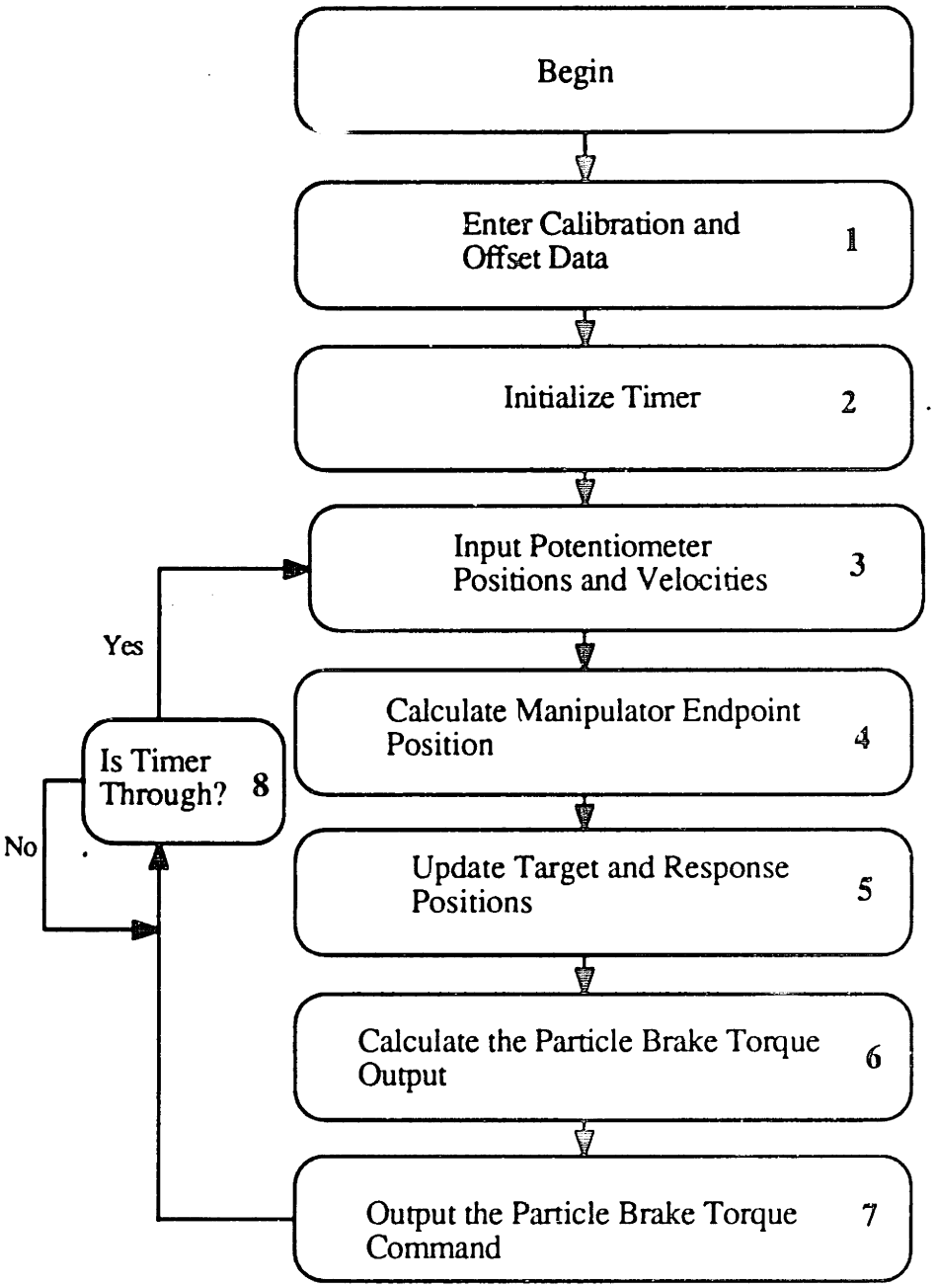

Figure #4-31 Overview of Control Algorithm

Module 1 • Enter Calibration and Offset Data

The calibration data is used to calculate the physical potentiometer positions and velocities from the voltages input into the computer. The calibration routine stores the calibration data in a data file (actual methods of calibration are discussed later) for retrieval by this module.

The offset data is used to eliminate voltage drift in the velocity measurement channels. The voltage offsets are input before running the control algorithm by program OFFSETS and stored in a data file. The control algorithm enters the offsets from the data file to be used in the calculation of the physical data.

Module 2 • Initialize Timer

The Timer initialization module initializes the timer located on the Metrabyte DAS-8 A/D and Timer Board. That board was hardware-configured so that the clock 2 output cascades into the clock 1 input and clock 1 output is connected to the interrupt input pin. The timer initialization module consists of loading the proper mode (mode 3) into clocks one and two, loading the proper count into clocks one and two, disabling the interrupts, and clearing the polling bit. This initialization sets the interrupt polling bit every $1/60^{th}$ of a second without generating a computer interrupt, allowing the computer to have a 60 Hz. control loop.

Module 3 • Input Potentiometer Positions and velocities

As Table 4-2 shows, the signals coming from the potentiometer analog circuits are digitized in the Data Translations A/D Board. The digitizing software sets the multiplexer channel for conversion, initiates conversion, and waits for the conversion complete bit to be set. Once it is set, the software inputs the digitized signal and proceeds to set the multiplexer for the next channel, thereby repeating the process for all the channels.

Module 4 • Calculate Manipulator Endpoint Position

Once the data is input, calculations are made to determine the manipulator endpoint position and velocity. The base coordinate systems used for the manipulator and computer screen are shown in Figure 4-32. Further, the Denavit-Hartenberg coordinate system notation for the manipulator is shown in Figure 4-33. This notation relates any two coordinate systems with a series of (4 x 4) transformation matrices, A_i. (Note: to emphasize the **A** matrix clearly, a leading superscript is sometimes used, and the matrix is written as ${}^{i-1}\mathbf{A}_i$. This superscript is ignored here. Also, this section assumes knowledge of coordinate system and transformation matrices. For a good general reference see Asada and Slotine, 1986.) The **A** matrix link parameters for the Med manipulator and the generalized **A** matrix are shown in Table 4-3.

The manipulator in Figure 4-33 is shown with all joint angles equal to zero (the angles are defined as zero when the X axes from all six coordinate systems align). Figure 4-34 shows the manipulator in our (arbitrary) neutral position.

The position and orientation of the manipulator endpoint are given by the product of the **A** matrices:

$$\mathbf{T}_6 = \mathbf{A}_1\mathbf{A}_2\mathbf{A}_3\mathbf{A}_4\mathbf{A}_5\mathbf{A}_6 \qquad (4\text{-}1)$$

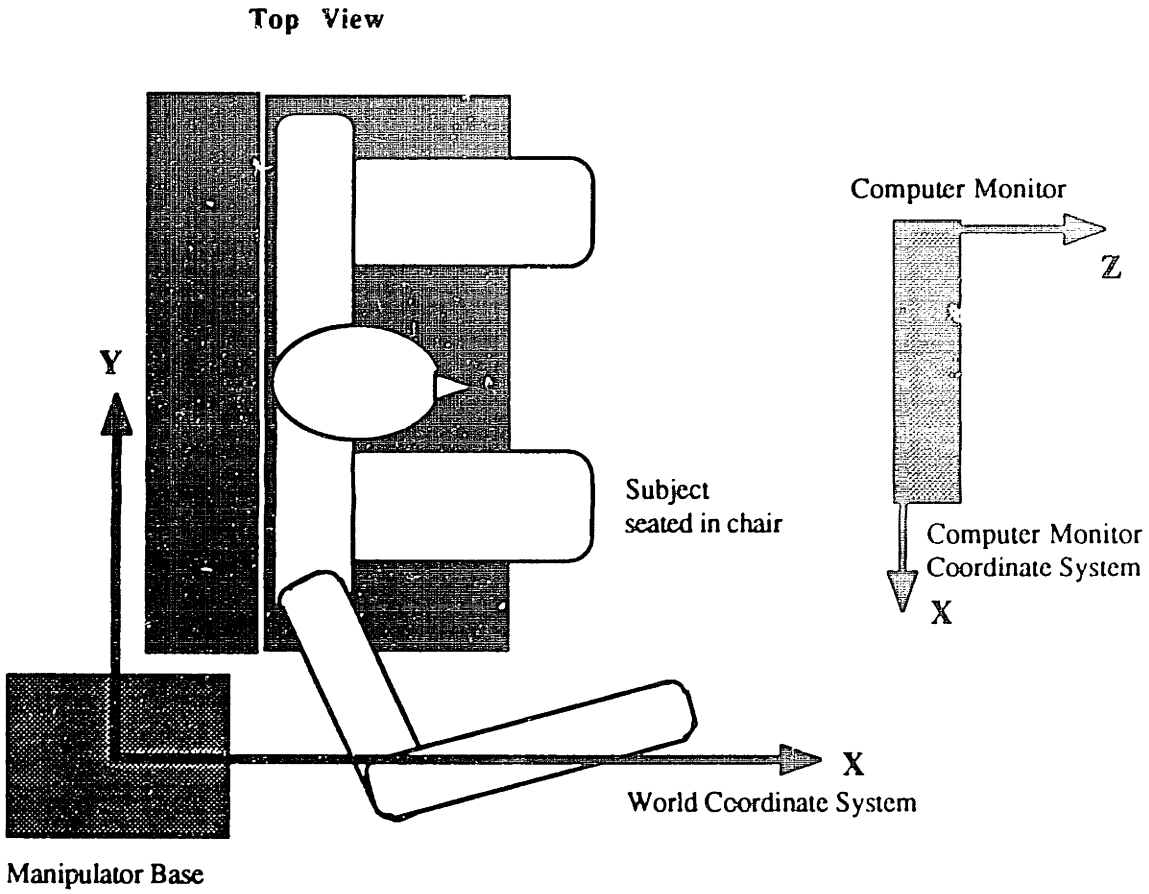

Figure #4-32. Base Coordinate systems for manipulator and computer monitor.

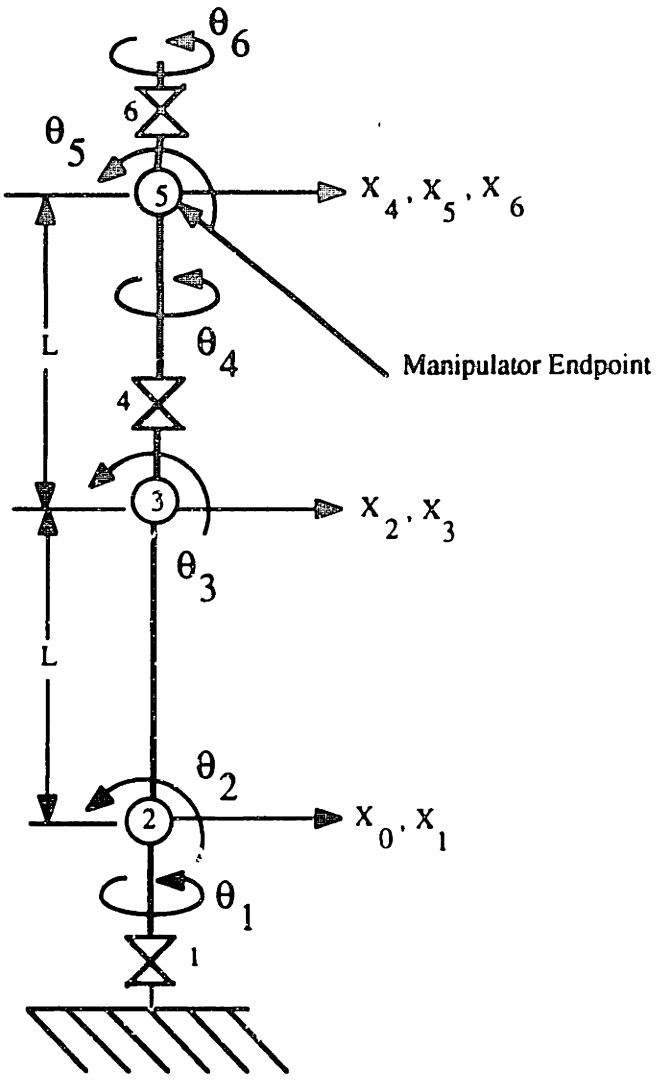

Figure #4-33. MED manipulator coordinate systems.

Table #4-3
Denavit-Hartenberg Parameters for MED Manipulator

Link	θ	α	a	d
1	θ_1	+90 degrees	0	0
2	θ_2	0	a_2	0
3	θ_3	-90	0	0
4	θ_4	+90	0	d_4
5	θ_5	-90	0	0
6	θ_6	0	0	0

For the Med Manipulator $a_2 = d_4 = l = 22.54$ inches.

$$\mathbf{A_n} = \begin{bmatrix} \cos\theta_n & -\sin\theta_n \cos\alpha_n & \sin\theta_n \sin\alpha_n & a_n \cos\theta_n \\ \sin\theta_n & \cos\theta_n \cos\alpha_n & -\cos\theta_n \sin\alpha_n & a_n \sin\theta_n \\ 0 & \sin\alpha_n & \cos\alpha_n & d_n \\ 0 & 0 & 0 & 1 \end{bmatrix}$$

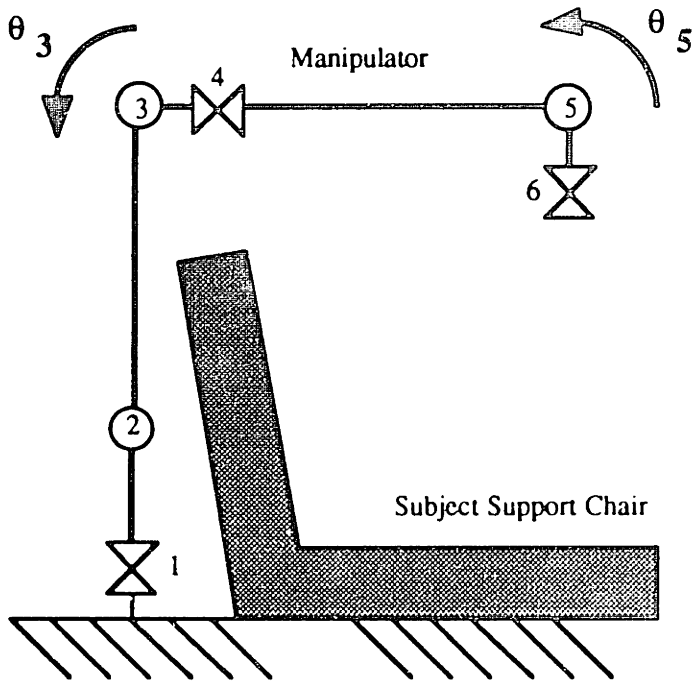

Figure #4-34. Neutral position of manipulator ($\theta_3 = \theta_5 = -90$ Degrees).

While this method of determining the manipulator endpoint position is widely used in practice and may be useful for the MED manipulator in future work, we took advantage of the manipulator's simplified geometry to determine the X, Y, and Z locations of the manipulator's endpoint. Figure 4-35 shows (schematically) the manipulator potentiometer measurements, labelled pot_i, and intermediate variables, α and ϕ, used to calculate the endpoint position. The specific equations are as follows:

$$\alpha = \pi/4 + pot_2 - pot_3 \tag{4-2}$$

$$\phi = \pi/4 + pot_3 \tag{4-3}$$

$$\theta_1 = pot_1 \tag{4-4}$$

$$R = 2L \cos\alpha \tag{4–5}$$

$$R_h = R \cos\phi \tag{4-6}$$

$$X = R_h \cos\theta_1 = R \cos\phi \cos\theta_1 \tag{4-7}$$

$$Y = R_h \sin\theta_1 = R \cos\phi \sin\theta_1 \tag{4-8}$$

$$Z = R \sin\phi \tag{4–9}$$

$$L = 22.54 \text{ inches.} \tag{4-10}$$

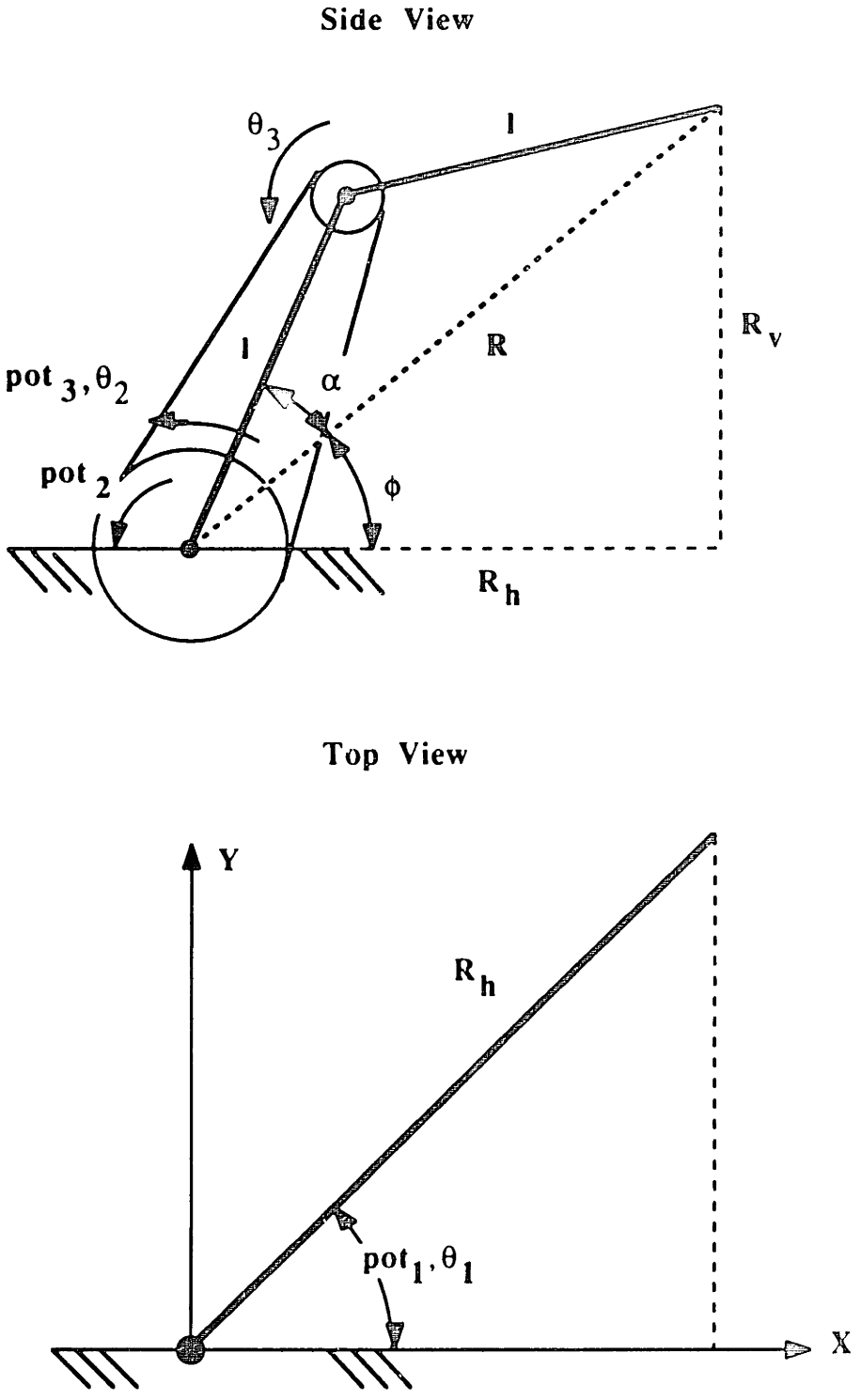

Figure #4-35. Intermediate coordinate system used to determine kinematic equations.

Module 5 • Update Target and Response Positions

This module is only used for specific manipulator tests which involve pursuit target tracking tasks. An overview of the target tracking task is given in the Chapter 6. If the user runs the control program which includes pursuit target tracking tasks, the program updates the target and response positions at this point. The tracking module was adapted from Beringhause (1988). A complete discussion on the pursuit target tracking module can be found in that reference.

Module 6 • Calculate the Particle Brake Torque output

For a viscous damper virtual environment, the ultimate relationship between force and velocity at the end of the manipulator is

$$\mathbf{f} = \mathbf{B}\mathbf{v} \tag{4-11}$$

where **f** is the force at the endpoint of the manipulator, **B** is the viscous damping matrix, and **v** is the velocity of the end of the manipulator. The control law for a force-velocity conlinear manipulator is

$$\mathbf{f} = \mathbf{B}\mathbf{v} \tag{4-12}$$

$$\tau_m = \mathbf{J_m}\mathbf{f} = \mathbf{J_m}\mathbf{B}\,\mathbf{v} \tag{4-13}$$

$$\tau_m = \mathbf{J_m}\mathbf{B}\mathbf{J_m}\mathbf{v_m}. \tag{4-14}$$

Using the above equation and calculating $\mathbf{J_m}$ and $\mathbf{v_m}$ will give the output torque to the manipulator MED actuators.

The transformation matrices, **A**, are used to derive the manipulator jacobian matrix, **J**, which relates the manipulator endpoint velocity to the manipulator joint velocities. The procedure outlined in chapter four of Paul (1981) was used to obtain the Jacobian matrix with respect to the link four coordinate system. Figure 4-36 shows the resulting Jacobian

matrix relating the velocity of the endpoint of the manipulator in link four coordinates to the manipulator joint angular velocities.

The manipulator Jacobian between endpoint velocity and actuator velocity, $\mathbf{J_a}$, can be derived by post-multiplying the joint-based Jacobian by the joint-actuator coupling matrix, **C**. The Med Manipulator coupling matrix is shown in Figure 4-37 and the actuator-based Jacobian, $\mathbf{J_m}$, is shown in Figure 4-38. The upper left 3 x 3 partition of $\mathbf{J_m}$ has orthogonal column vectors showing that the three translational directions of the manipulator can always be force-velocity colinear (if properly controlled).

$$\begin{bmatrix} l\,S_4(C_2-S_{23}) & l\,C_4(S_3-1) & -l\,C_4 & 0 & 0 & 0 \\ 0 & l\,C_3 & 0 & 0 & 0 & 0 \\ l\,C_4(S_{23}-C_2) & l\,S_4(S_3-1) & -l\,S_4 & 0 & 0 & 0 \\ S_{23}C_4 & -S_4 & -S_4 & 0 & 0 & -S_5 \\ C_{23} & 0 & 0 & 1 & 0 & C_5 \\ S_{23}S_4 & C_4 & C_4 & 0 & 1 & 0 \end{bmatrix}$$

Notes: $C_i = \cos(\theta_i)$, $S_i = \sin(\theta_i)$, $S_{ij} = \sin(\theta_i+\theta_j)$

Figure #4-36. Joint-based Jacobian matrix, **J**, in link four coordinate system.

$$\begin{bmatrix} 1/4 & 0 & 0 & 0 & 0 & 0 \\ 0 & 1/4 & 1/4 & 0 & 0 & 0 \\ 0 & 0 & -1/2 & 0 & 0 & 0 \\ 0 & 0 & 0 & 1 & 0 & 0 \\ 0 & 0 & 0 & 0 & 1 & 0 \\ 0 & 0 & 0 & 0 & 0 & 1 \end{bmatrix}$$

Figure #4-37. Med Manipulator coupling matrix, **C**.

$$\begin{bmatrix} \frac{1}{4} l S_4(C_2-S_{23}) & \frac{1}{4} l C_4(S_3-1) & \frac{1}{4} l C_4(S_3+1) & 0 & 0 & 0 \\ 0 & \frac{1}{4} l C_3 & \frac{1}{4} l C_3 & 0 & 0 & 0 \\ \frac{1}{4} l C_4(S_{23}-C_2) & \frac{1}{4} l S_4(S_3-1) & \frac{1}{4} l S_4(S_3+1) & 0 & 0 & 0 \\ S_{23}C_4 & \frac{1}{4} S_4 & \frac{1}{4} S_4 & 0 & 0 & -S_5 \\ C_{23} & 0 & 0 & 1 & 0 & C_5 \\ S_{23}S_4 & \frac{1}{4} C_4 & \frac{1}{4} C_4 & 0 & 1 & 0 \end{bmatrix}$$

Notes: $C_i = \cos(\theta_i)$, $S_i = \sin(\theta_i)$, $S_{ij} = \sin(\theta_i+\theta_j)$

Figure #4-38. Actuator-based Jacobian in link four coordinate system.

Although the above equations are widely used methods for determining manipulator endpoint velocity, we used the MED Manipulator's simple linkage geometry and the fact that the first three actuators result in an orthogonal (spherical) coordinate system to arrive at our control algorithm one axis at a time. Figure 4-39 shows the model used for determining the actuator #1 torque output. In the model, F and V represent the force and velocity on the end of the manipulator in the direction of movement of the first axis. For the viscous damper we want

$$F = bV \tag{4-15}$$

From the joint capstan's perspective,

$$\tau_1 = FR_h \tag{4-16}$$

and

$$V = \dot{\theta}_1 R_h. \tag{4-17}$$

Because of the 4:1 ratio in the cable-drive transmission in the joint,

$$\tau_1 = 4\tau_{m1} \tag{4-18}$$

and

$$\dot{\theta}_1 = \frac{\dot{\theta}_{m1}}{4}. \tag{4-19}$$

Combining the above equations, to make the endpoint feel like a viscous damper in the direction of the first joint,

$$\tau_{m1} = \frac{R_h^2}{4} b \dot{\theta}_1. \tag{4-20}$$

Variable b is given, R_h was calculated earlier, and we calculate the joint angular velocity, $\dot{\theta}_1$, from

$$\dot{\theta}_1 = \dot{pot}_1. \tag{4-21}$$

That is, the angular velocity of the joint is the same as the measured potentiometer 1 angular velocity signal.

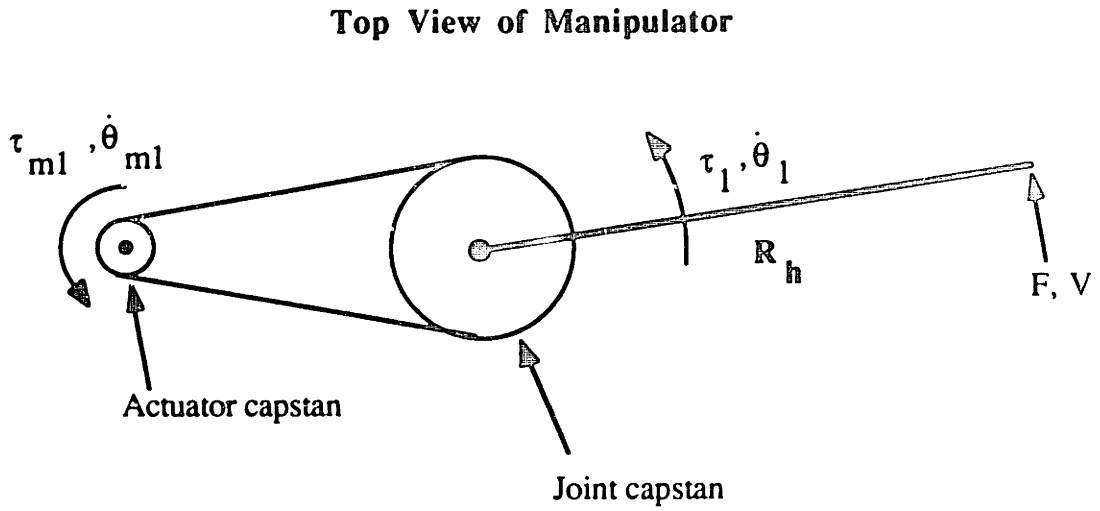

Figure #4-39. Model for determining actuator #1 torque output

Figure 4-40 shows the model used for determining actuator #2 torque output. Using the same analysis as before,

$$\tau_{m2} = \frac{R^2}{4} b \dot{\phi} \tag{4-22}$$

Variable b is given, R is calculated above, and $\dot{\phi}$ is calculated from

$$\dot{\phi} = \dot{pot}_3 \tag{4-23}$$

Figure 4-41 shows the model used for determining actuator #3 torque output. (Actuator #3 maps to the R direction movement.) For a viscous damper, we want

$$F = b \dot{R}. \tag{4-24}$$

The actuator torque output is calculated by performing the power balance

$$F\dot{R} = \tau\dot{\alpha} \tag{4-25}$$

where α is defined by 4-2.

The linear and rotational velocities are related by

$$\dot{R} = (-2L\sin\alpha)\dot{\alpha} \tag{4-26}$$

Because of the 4:1 ratio of the belt drive transmission

$$\tau_{m3} = \frac{1}{4}\tau \tag{4-27}$$

Combining the above equations, the resulting control equation is

$$\tau_{m3} = (b\,L^2\sin^2\alpha)\dot{\alpha} \tag{4-28}$$

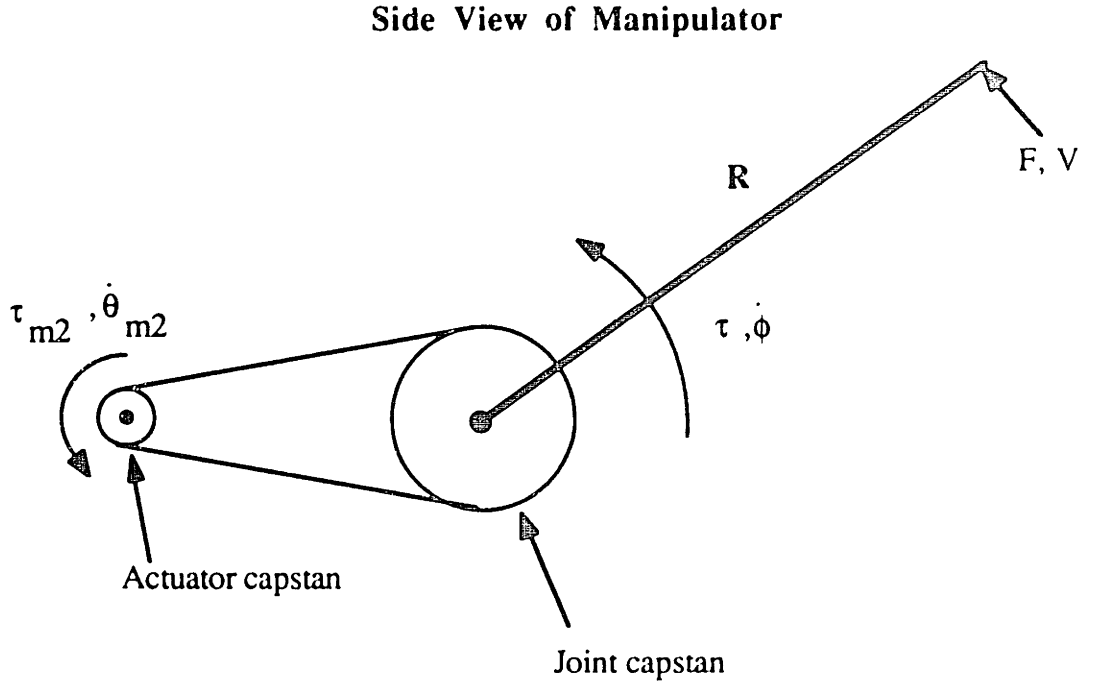

Figure #4-40. Model used for determining actuator #2 torque output

Side View of Manipulator

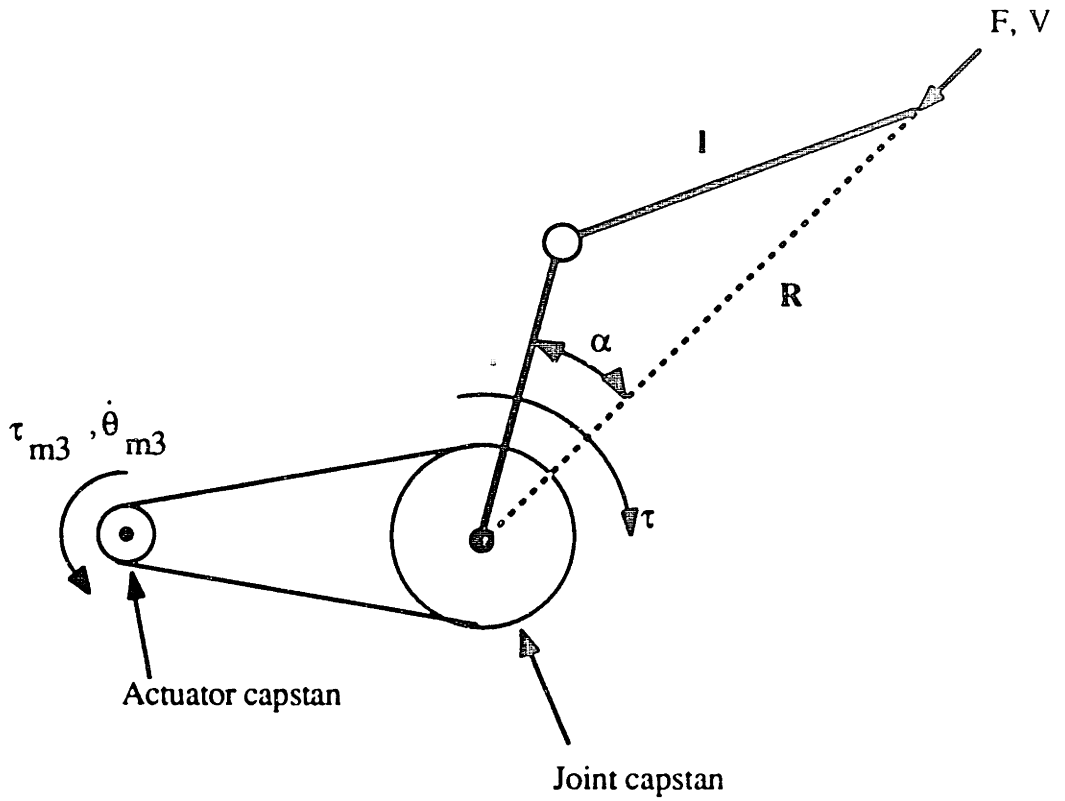

Figure #4-41. Model used for determining actuator #3 torque output

Finally, axes 4, 5, and 6 are direct drive and gimballed producing the rotation at the endpoint of the manipulator. Each of the last three axes has the control equation

$$\tau_{mi} = b_\omega \dot{pot}_i \qquad i = 4, 5, 6 \tag{4-29}$$

where b_ω is the given angular damping constant and $\dot{pot}_i$ is the input potentiometer velocity.

Module 7 • Output the Particle Brake Torque Command

Once the output torque is calculated, the Voltage representing the desired torque is output through the Metrabyte D/A converter board using the mapping shown in Table 4-2.

Module 8 • Is the Timer Through?

This module checks to see if the interrupt polling bit is set. If the bit is not set, it continues to check the bit until it is set. Once the bit is set, it clears the bit and releases control to module three.

Note that the control algorithm is embedded in an endless loop. Two methods were used to end the control algorithm. One method was to end the program after one minute (3600 loops through the $1/60^{th}$ of a second loop). The other method was to end the loop whenever a key on the keyboard was pressed by the user. Both methods were incorporated into various control programs.

Chapter 5

System Characterization

Characterization Goal

The goal of the system characterization experiments we conducted was to determine calibration values for the sensors and actuators and MED manipulator model parameters. To this end, thorough measurements of MED arm performance were made. Two kinds of experiments were undertaken, component calibration experiments and the complete manipulator experiments. The former included characterization of the force and position sensors, the particle brakes and the electronics board, while the latter determined the overall manipulator stiffness, friction, and inertial properties.

Force Sensor and Signal Conditioning Electronics

In order to generate a calibration sensitivity matrix C to relate the responses from the eight Wheatstone bridges, **W**, to the actual applied load inputs, $\mathbf{F_S}$, a standard calibration procedure was employed (see, for instance, Hull and Davis, 1981). Briefly, a set of known load types (Fx, Fy, Fz, Mx, My, Mz) were applied to the dynamometer using a laboratory calibration apparatus and computer program FCAL designed for this purpose. Figures 5-1 and 5-2 shows the force/torque sensor in the calibration apparatus with the loads Mx (moment about the X-axis) and Mz (moment about the Z-axis) applied. Each pure load type was applied in increasing increments in both the positive and negative directions.

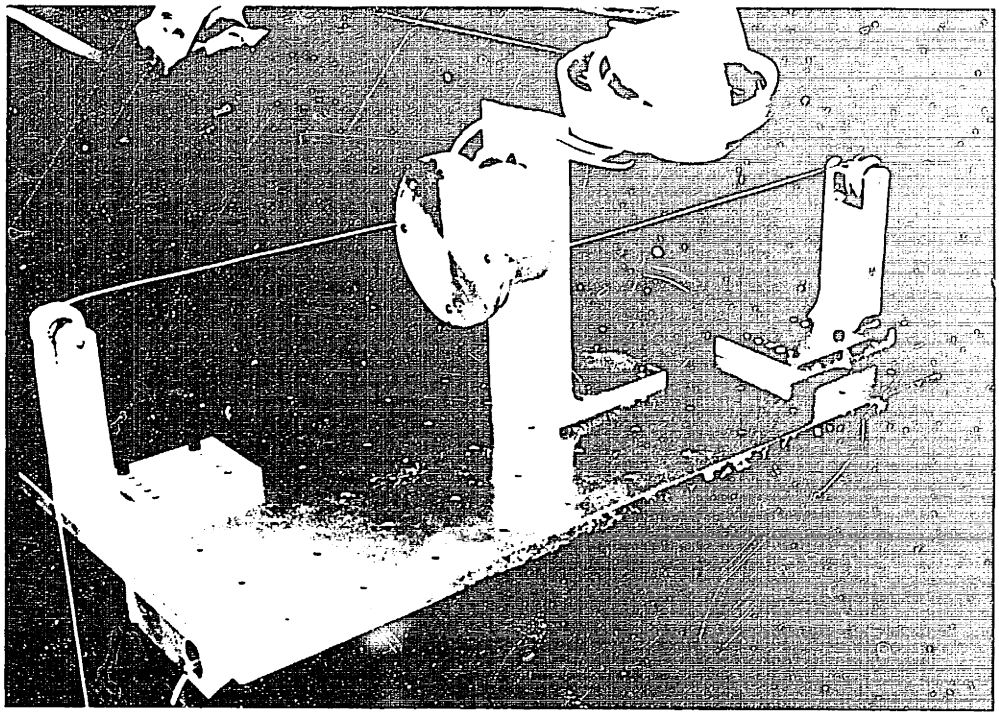

Figure #5-1. Force/torque sensor calibration in Mx direction

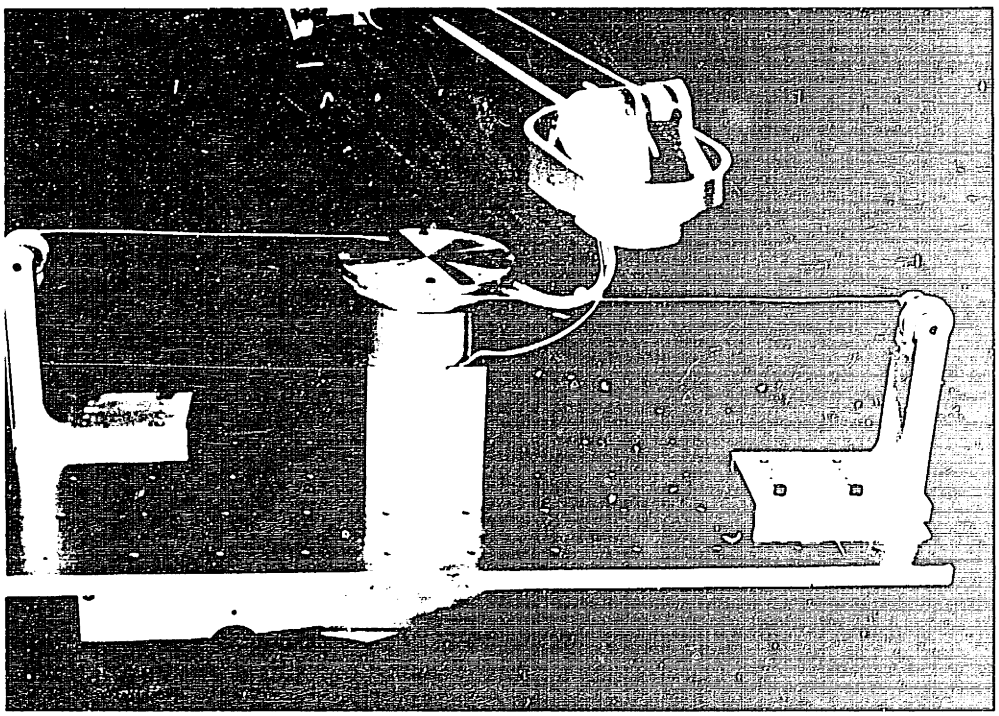

Figure #5-2. Force/torque sensor calibration in Mz direction

The loads were applied to a point in the center of the cross so the resulting calibration sensitivity matrix C, when postmultiplied by the Wheatstone bridge output Voltages, calculates the loads at this point.

The data were reduced with a least squares fit algorithm resulting in an optimal linear relation between the load inputs and the Voltage outputs of the dynamometer and signal conditioning electronics. The regression coefficients for each pure load type produced a single column in the calibration matrix, **K** (6 x 8). The final **K** matrix is shown in figure 5-3 in units of Volts/Newton and Volts/Newton-Meter. The coefficients of determination (R^2) corresponding to each element in the **K** matrix shown in figure 5-4.

$$\mathbf{K} = \begin{bmatrix} -.086 & 2.16 & -8.84 & -298.9 & -5.36 & -.622 \\ -.244 & .507 & -.465 & 1.279 & -18.46 & -164.8 \\ -2.008 & .054 & -6.059 & 1.353 & -297.46 & 8.912 \\ -.78 & -.301 & -.363 & 7.558 & -5.05 & -167.9 \\ .085 & -2.039 & -8.310 & 298.65 & 5.22 & -2.87 \\ .046 & -1.016 & -.298 & 3.119 & 4.85 & -162.98 \\ 2.294 & .067 & -5.861 & -8.324 & 298.4 & 4.689 \\ .717 & -.095 & -1.114 & -31.504 & 2.134 & -167.64 \end{bmatrix}$$

Figure #5-3. Force/Torque sensor calibration matrix x 10^3

$$\begin{bmatrix} .446 & .999 & .999 & .9999 & .963 & .410 \\ .439 & .941 & .979 & .948 & .997 & .999 \\ .994 & .031 & .999 & .425 & .999 & .630 \\ .929 & .838 & .994 & .998 & .996 & .999 \\ .725 & .999 & .999 & .9997 & .855 & .934 \\ .0373 & .987 & .986 & .9903 & .994 & .999 \\ .9923 & .633 & .999 & .946 & .9998 & .884 \\ .894 & .329 & .997 & .9998 & .979 & .999 \end{bmatrix}$$

Figure #5-4. Coefficients of Determination for the calibration matrix

Almost all of the coefficients of determination, R^2, are very close to one, suggesting a strong linear relationship between $\mathbf{F_s}$ and $\mathbf{W}$. The coefficients of the $\mathbb{K}$ matrix with corresponding low coefficient of determination values (components 1,1; 1,6; 2,1; 3,2; 3,4; 6,1; and 8,2), are themselves very small. These $\mathbb{K}$ matrix coefficients have low R^2 values probably because the electrical noise is large as compared to the signal. (The noise in the signal adds randomness to the linear relation between $\mathbf{F_s}$ and $\mathbf{W}$.)

We can derive the the matrix of sensitivity coefficients by use of the matrix algebra equations (Strang, 1976):

$$\mathbf{W} = \mathbf{K}\,\mathbf{F_s} \tag{5-1}$$

$$\mathbf{K}^t\,\mathbf{W} = \mathbf{K}^t\,\mathbf{K}\,\mathbf{F_s} \tag{5-2}$$

$$(\mathbf{K}^t\,\mathbf{K})^{-1}\,\mathbf{K}^t\,\mathbf{W} = \mathbf{F_s} \tag{5-3}$$

Finally, define the Force/torque sensor calibration sensitivity matrix, **C**, as

$$\mathbf{C} = (\mathbf{K}^t\,\mathbf{K})^{-1}\,\mathbf{K}^t \tag{5-4}$$

Where **C** is the psuedo-inverse of the **K** matrix (optimal inverse in the least squares sense). then

$$\mathbf{Fs} = \mathbf{C}\ \mathbf{W}. \tag{5-5}$$

Equation 5-4 allows us to calculate **C** From our data points. After we have obtained the **C** matrix from our system calibration experiments, we can calculate **Fs** using equation 5-5 and the measured voltages, **W**. Figure 5-5 shows the **C** matrix in units of Newtons/Volt and Newton-Meters/Volt calculated from the **K** matrix of Figure 3-3.

$$C = \begin{bmatrix} -125.6 & 26.966 & 80.613 & -665.76 & -34.28 & -43.364 & 64.8778 & 689.59 \\ -10.98 & 678.056 & -28.367 & -73.93 & -.1566 & -650.72 & 22.5185 & 39.27 \\ -40.019 & 4.83 & -26.759 & -6.61 & -40.014 & -3.990 & -26.4734 & 4.417 \\ -1.69 & 4.78 & -.158 & -.451 & 1.7118 & -4.52 & .1434 & .121 \\ .894 & -.165 & -2.254 & 4.81 & .2907 & .2372 & 1.2183 & -4.9779 \\ .195 & -2.576 & .206 & -1.24 & .0579 & -.4424 & .0472 & -1.7524 \end{bmatrix}$$

Figure #5-5. Force/torque sensor calibration matrix

The final test of the system's accuracy is its ability to calculate loads. Nonlinearity in the dynamometer's response to loading decreases the accuracy of the instrument by producing errors. To assess the accuracy of the dynamometer and related data processing matrices detailed above, eighteen pure load values were applied to the force/torque sensor and the force estimate was calculated using equation 5-5.

Table 5-1 shows the results of this system test. The results suggest that the pure force directions are accurate to within approximately 1.3 Newtons for low level forces and 2.3 Newtons for higher level loads. The cross coupling of the forces (calculated loads which are not actually applied) is a maximum of 11% for low level forces reducing to less than 1% for higher level loads.

The moment directions are even more accurate. For low level moments, the calculated load is within .1 NM of the applied load increasing to within .2 NM for high level loads. The cross-coupling for the moment terms is within 1% for all loads.

The cross-coupling between the moments and forces is more difficult to assess other than to recognize that the worst cross-coupling occurs when the My load is applied. When the 7.1 NM My load is applied, the Fx force calculation is 7.2 N which is distinctly higher than other cross-coupling terms.

An attempt was made to increase the accuracy of the calculated loads. The coefficients of the **K** matrix which had low coefficients of determination were reduced to zero and the **C** matrix was recalculated. The new **C** matrix was then used to recalculate the loads of Table 5-1. These results are shown in table 5-2. Although a statistical analysis was not performed on the data, the calculated loads in Table 5-2 are very close to the loads in Table 5-1.

Table #5-1

Applied Load vs. Calculated Load

	Calculated Load (Fs^t)					
Input Load	Fx	Fy	Fz	Mx	My	Mz
4.448 N Fx	**3.182**	.2119	.3309	.0074	.0018	-.0055
44.48 N Fx	**45.66**	2.377	.2161	.0108	-.027	-.0206
-44.48 N Fx	**-42.15**	.3569	-.2298	-.0053	-.0114	.0475
8.896 N Fy	-.6408	**9.44**	-.5827	.0033	.0148	.0344
88.964 N Fy	2.3463	**90.05**	-.9867	.0093	-.0379	-.0817
-17.739 N Fy	3.16	**-18.34**	-1.70	-.0104	-.0657	-.0383
8.896 N Fz	-1.3931	1.0561	**9.522**	.0858	.0423	-.0047
62.275 N Fz	-1.767	2.4626	**63.1**	.1101	.0517	.0008
-88.964 N Fz	-.7241	3.649	**-87.8**	.1118	.0481	-.0035
2.0337 NM Mx	1.37	-.466	-.347	**2.01**	-.0325	.0039
7.11804 NM Mx	-.645	.091	-.979	**7.062**	-.0346	.0126
-1.01686 NM Mx	-1.133	1.056	-.6804	**-1.09**	.0146	.0051
2.0337 NM My	2.395	.7813	-.4655	.0094	**1.965**	.0115
7.118 NM My	7.2124	2.314	-.7864	-.0025	**6.94**	.0016
-1.0168 NM My	.931	-.473	-1.005	-.0055	**-1.111**	.0217
1.01686 NM Mz	1.9829	-.3735	-.6638	-.0002	-.0552	**1.041**
2.0337 NM Mz	3.2115	-.3726	-.884	-.0088	-.0883	**2.007**
-3.559 NM Mz	1.3876	1.2718	-.2968	.0025	-.0262	**-3.57**

Table #5-2

Applied Load vs. Calculated Load For Second C Matrix

	Calculated Load (Fs^t)					
Input Load	Fx	Fy	Fz	Mx	My	Mz
4.448 N Fx	**3.1697**	-.1988	-.3283	.0054	.0019	-.0039
44.48 N Fx	**45.164**	-5.906	.174	-.0347	-.0237	.0048
-44.48 N Fx	**-43.07**	8.78	-2.097	.0418	.0043	.0234
8.896 N Fy	-1.027	**9.147**	-.6155	.0011	.0177	.0361
88.964 N Fy	-2.2505	**88.03**	-1.315	-.0043	-.0031	-.0639
-17.739 N Fy	4.14	**-20.58**	-1.64	-.0254	-.0735	-.0372
8.896 N Fz	-1.636	2.172	**9.516**	.0928	.0441	-.0064
62.275 N Fz	-2.149	3.85	**63.08**	.1194	.0545	-.0013
-88.964 N Fz	-.97	4.31	**-87.8**	.11	.049	-.004
2.0337 NM Mx	1.5677	-.8169	-.419	**2.01**	-.0385	.0052
7.11804 NM Mx	-.1636	1.0487	-1.23	**7.070**	-.0538	.0128
-1.01686 NM Mx	-1.5226	2.35	-.64	**-1.08**	.0201	.0028
2.0337 NM My	2.663	-.4565	-.4693	.0014	**1.963**	.0141
7.118 NM My	8.0327	-2.4239	-.8006	-.0337	**6.897**	.0107
-1.0168 NM My	1.051	-1.317	-1.005	-.0112	**-1.112**	.0231
1.01686 NM Mz	2.274	-2.034	-.64	-.01	-.058	**1.044**
2.0337 NM Mz	3.57	-2.6295	-.8381	-.0217	-.0911	**2.01**
-3.559 NM Mz	1.178	.3427	-.3915	-.0073	-.0249	**-3.56**

Position Sensor and Signal Conditioning Electronics

A block diagram of the position and velocity calculation is shown in Figure 5-6. The potentiometer voltage is used to derive two signals, one to determine the position of the axis and one to determine the velocity of the axis. The potentiometer signal, A, is processed by the analog electronics gain stage, the D/A converter, and the calibration gain and offset stage (software multiply) resulting in a value in physical units (radians). The signal is also operated on by a second set of analog electronics which, in effect, differentiates and amplifies the signal (the differentiation is represented in the figure by the Laplace operator, s). This signal is then digitized and multiplied by the calibration gain b_2 thereby generating a value in radians/second. This section describes the methods used to determine b_0, b_1 and b_2.

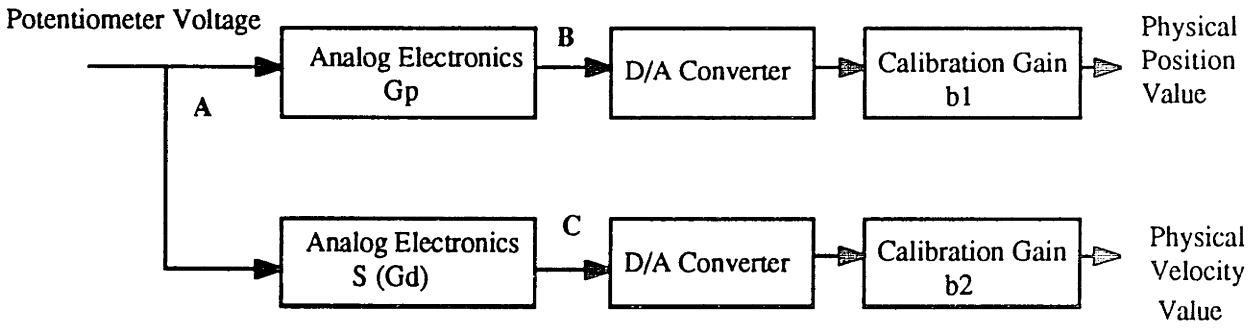

Figure #5-6. Overview of position and velocity calculation

Positions were calibrated using the program PCAL and a Wedge Innovations digital level[1]. The computer program prompts the investigator to move an individual axis through a given set of orientations using the digital level as a reference. At each angle, he presses a key on the computer keyboard to "enter" that value. At the end of a calibration

1 The digital level produces a digital readout of the angle away from horizontal and is accurate to 0.1 degrees.

run for a single axis, the computer has stored the set of specified angles through which it has moved and the measured A/D value corresponding to each. PCAL performs a least squares fit on the data, calculating the slope estimator, b_1 (units of radians/LSB), the offset estimator, b_0, and the coefficient of determination, R^2, for the equation angle = b_0 + (b_1)(A/D value in LSB's) (5-6).

. The coefficient values for all six axes are given in Table 5-3 for the most recent calibration. Note in the table that the coefficients of determination are very close to one, indicating a very good linear fit to the data.

Table #5-3

Results from Potentiometer Position Calibration

Axis	b_0	b_1	R^2
1	1.849905	-.000874	.999947
2	1.568	-.000771	.999975
3	-1.139934	.000528	.999459
4	-5.037	.002459	.999933
5	-.9872	.000487	.999787
6	-1.99874	.000948	.999525

The value of the velocity gain b2 was calculated from the equation

$$b_2 = \frac{(G_p)(b_1)}{G_d} \tag{5-7}$$

The value for Gp was calculated by substituting a function generator sine wave output for the potentiometer voltage input into the electronic board and dividing the measured output amplitude by the measured input amplitude. This was repeated for four input amplitudes and Gp was computed as the average ratio. The resulting values for Gp are given in Table 5-4.

The sine wave output from a function generator was also used to calculate the analog electronics velocity gain, G_d. The sine wave amplitude and frequency were used to calculate the maximum value of the derivative of the input signal (for the actual system the potentiometer is the input signal and its derivative is the velocity signal). This value was compared to the peak output value from the differentiator electronics (point C in Figure 5-6) to obtain an equivalent differentiator gain. This gain was calculated for four different frequency values up to 4 Hz (well below the cutoff frequency of the low pass portion of the filter). The gains were then averaged resulting in the calculated velocity gain, Gd, shown in Table 5-4 along with the results of the b_2 calculation (from equation 5-7) for each axis.

Table #5-4

Velocity Gain

axis	Gp	Gd	b2
1	.55	.54	1.019
2	.604	.54	1.119
3	.913	1.87	.448
4	.1569	.195	.805
5	1.017	.31	3.281
6	.527	.0936	5.63

Particle Brake and Electronics

The particle brake and brake driver electronics were put through two sets of tests. The first set was intended to test the speed of response of the brake torque to the drive voltage from the D/A, and the second was intended to test the linearity of the relationship between break torque and the voltage from the D/A converter.

To measure speed of a square wave from a function generator substituted for the D/A output[1] to the electronic board. The voltage across the brake's current sense resistor and the square wave voltage input were then compared on a dual trace oscilloscope screen shown in Figures 5-7 and 5-8 for the large and small particle brakes. Interestingly, the large and the small particle brakes have virtually identical fast settling times of 125 microseconds on the upside and 750 microseconds on the downside. The upside and downside transients are significantly different because the positive voltage rail is 48 Volts while the negative rail is only at -5 Volts. Although the rise time on the downside is very low, it could be further lowered by increasing the negative rail voltage.

The torque vs input Voltage experiments were performed with both the large and small particle brakes. The experimental setup was similar to the force/torque transducer calibration, with the cables and weights adjusted so that a pure torque was applied to the brake output shaft. (Brakes were not installed in the MED manipulator for these tests.) The D/A output, in LSBs, was then set to zero and weights were applied to the cables until the torque applied to the brake was greater than the braking torque producing shaft rotation. This torque level was recorded and the D/A output was then incremented by 100 LSBs and weights were again applied until shaft slip. This process continued in increments of 100 LSBs up to 4000 LSBs out of the D/A maximum of 4095 LSBs. Then, the D/A output was decreased in decrements of 100 LSBs until the output was back to zero.

---

1 A computer program also could have been written which would output a square wave to the electronics board. Using the function generator saved some program development time.

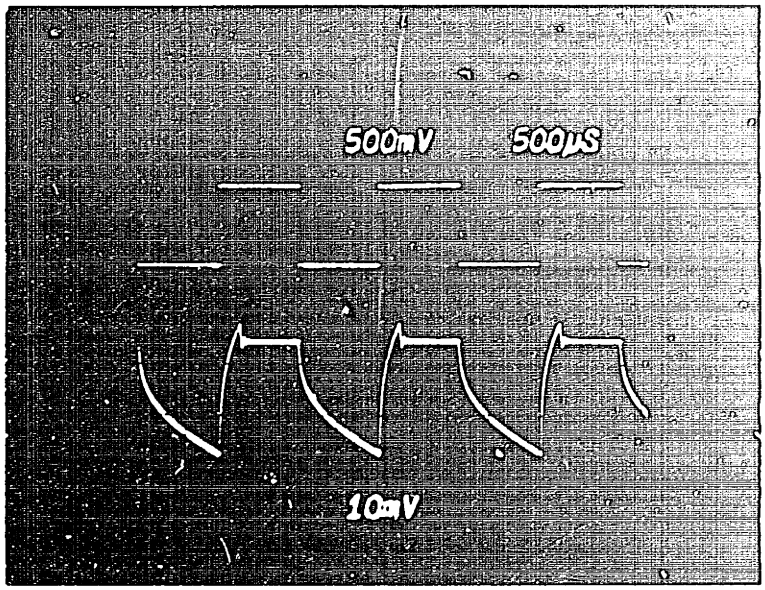

Figure 5-7. Current sense ouput and Voltage input for large brake

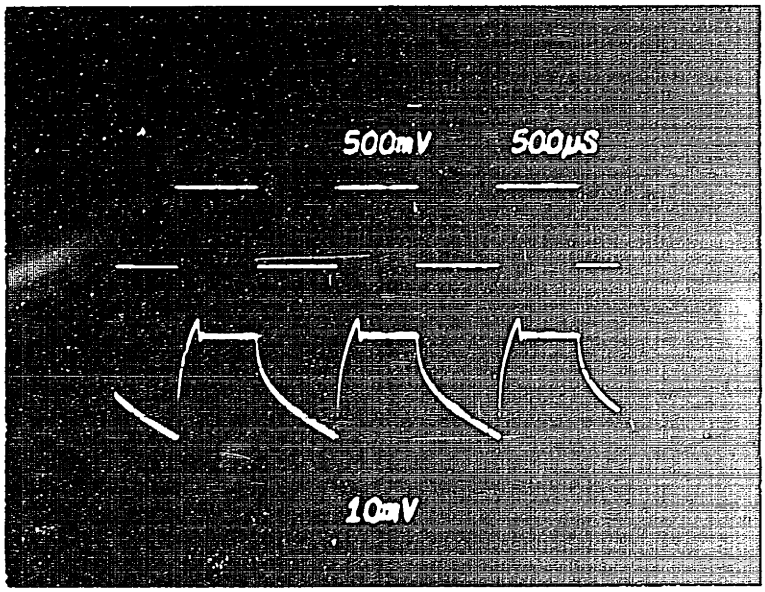

Figure 5-8. Current sense output and Voltage input for small brake

Test results for the small brake are shown in Figure 5-9. The difference between the torque as the D/A level was increased (the bottom section of the curve) and the torque as the D/A level was decreased is the magnetic hysteresis in the brake. Results for the large brake looked qualitatively the same. The results of a linear least square fit on the data shows the following equation for the small particle brake:

$$\text{Torque} = -.0624 + 5.276 \times 10^{-4} \text{ (D/A output-120) Nm} \qquad (5\text{-}8)$$

(remember that the D/A output level of 120 is the zero current level in the brake)

The result for the large brake was

$$\text{Torque} = -.0813 + 2.77 \times 10^{-3} \text{ (D/A output-120) Nm.} \qquad (5\text{-}9)$$

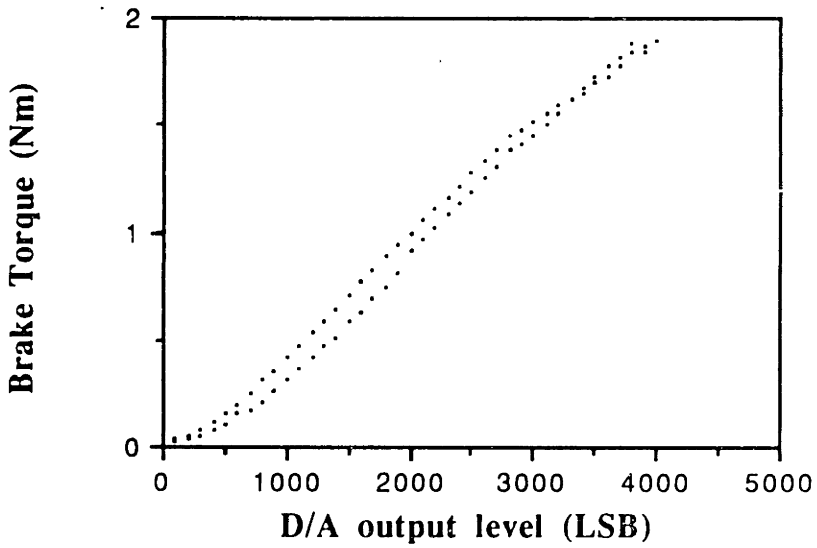

Figure #5-9. Small brake output level vs. D/A output level

Passive Properties of Complete Manipulator

The goal of the passive parameter tests was to obtain an estimate of the manipulator endpoint stiffness, inertia, and coulomb friction. Each of these parameters is dependent on position, velocity, and acceleration of the endpoint, suggesting a complex set of experiments and calculations to determine the parameters as a function of manipulator state. Our initial experiments were only intended to give rough parameter estimates.

The stiffness of the manipulator endpoint was measured at two different manipulator orientations. During each test, the brakes were fully powered (D/A outputs were all at 4095 LSBs). Weights were applied to the endpoint of the manipulator, via a cable and pulley. By moving the pulley and adjusting the weights, a series of loads was applied to the manipulator endpoint in the X, Y, and Z directions. The deflection of the endpoint of the manipulator in the direction of the load was measured using a dial indicator with a one inch travel and .001 inch resolution. The indicator was fixed in the room frame of reference. This method measured the stiffness of the entire manipulator structure and base including the links, the cable drives, the particle brake shafts and particles, and the subject support chair mounting structure (all the way through the feet on the chair).

The force-deflection curves resulting from these experiments are shown in Figures 5-10 and 5-11 for the two different manipulator orientations and the results are summarized in Table 5-5. The table coefficients result from a least squares fit of the data. As can be seen from the graphs, the manipulator is stiff in both orientations, with a minimum (worst case) stiffness of 3.3 Newtons/mm.

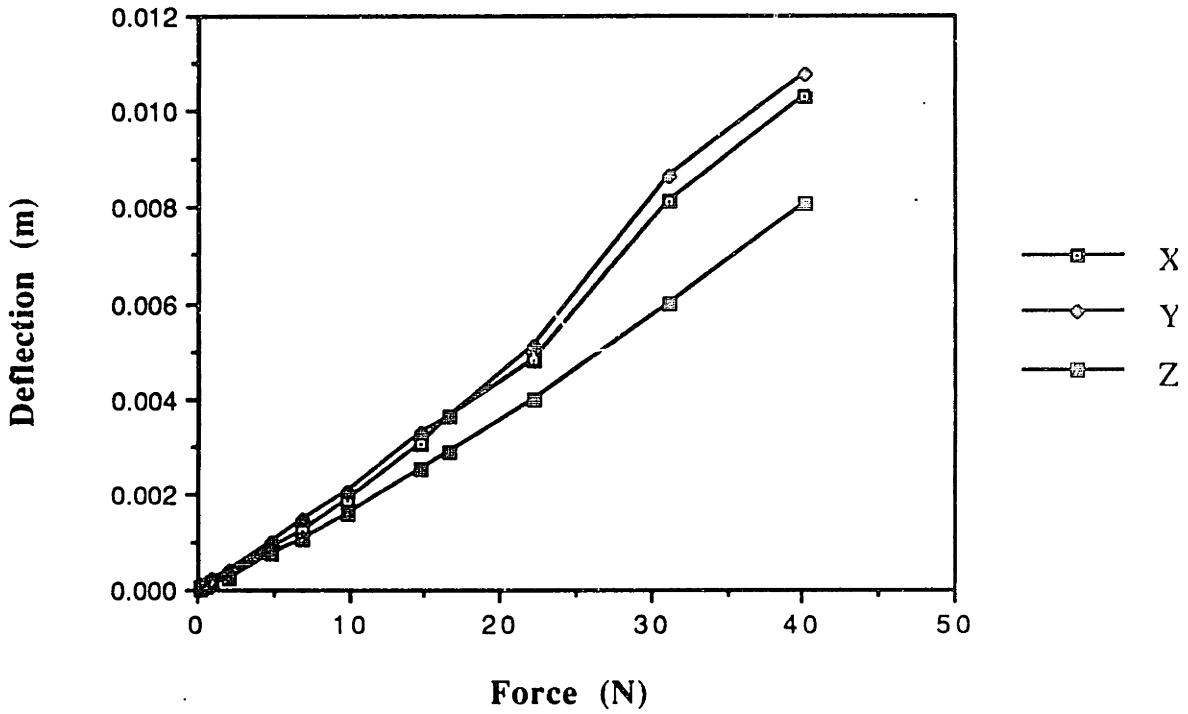

Figure #5-10. Force-deflection curve for first manipulator orientation

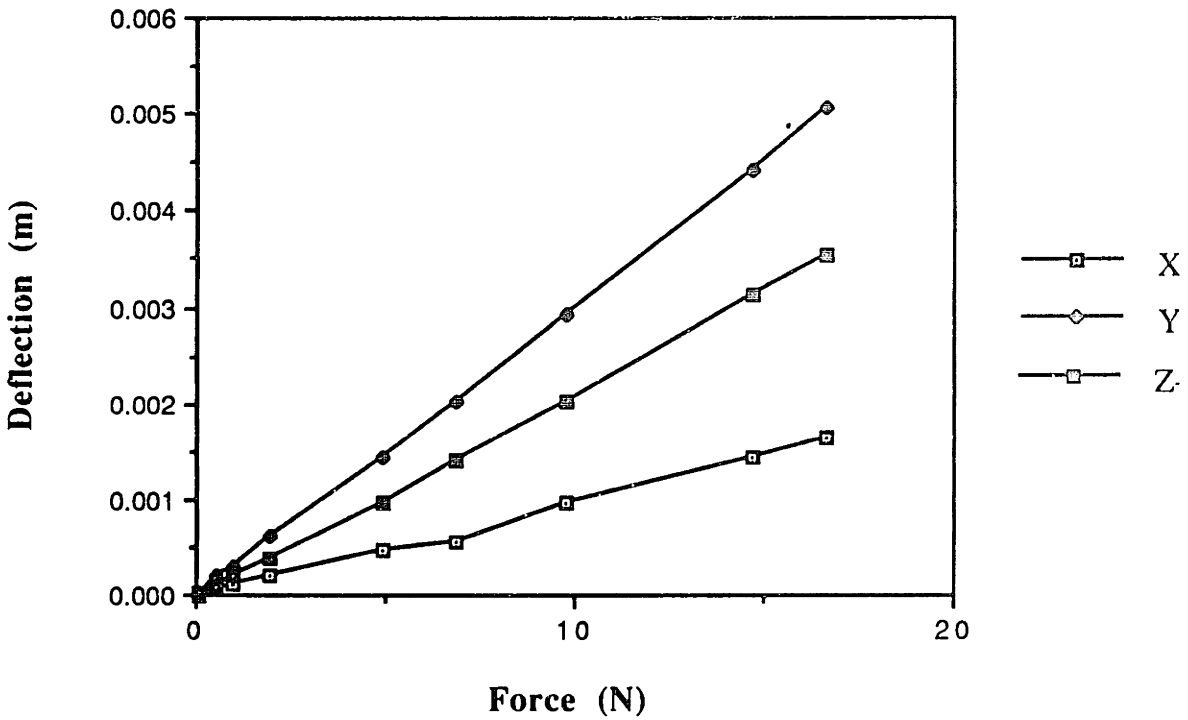

Figure #5-11. Force-deflection curve for second manipulator orientation

Table #5-5

Stiffness experiment summary

Orientation (degrees)						Stiffness (Newtons/meter x10^{-4})		
m_1	m_2	m_3	m_4	m_5	m_6	K_x	K_y	K_z
1.6	-6.7	-27.4	-4.4	44.9	6.6	.385	.368	.503
-.7	-40.9	-37.4	.8	32.8	-7.3	1.02	.33	.469

The effective inertia of the manipulator endpoint was estimated using the same cable pulley arrangement we used in the stiffness experiments. In the inertia test, however, the brakes were all off and the measurement was of the manipulator endpoint acceleration. This experiment is shown diagrammatically in Figure #5-12.

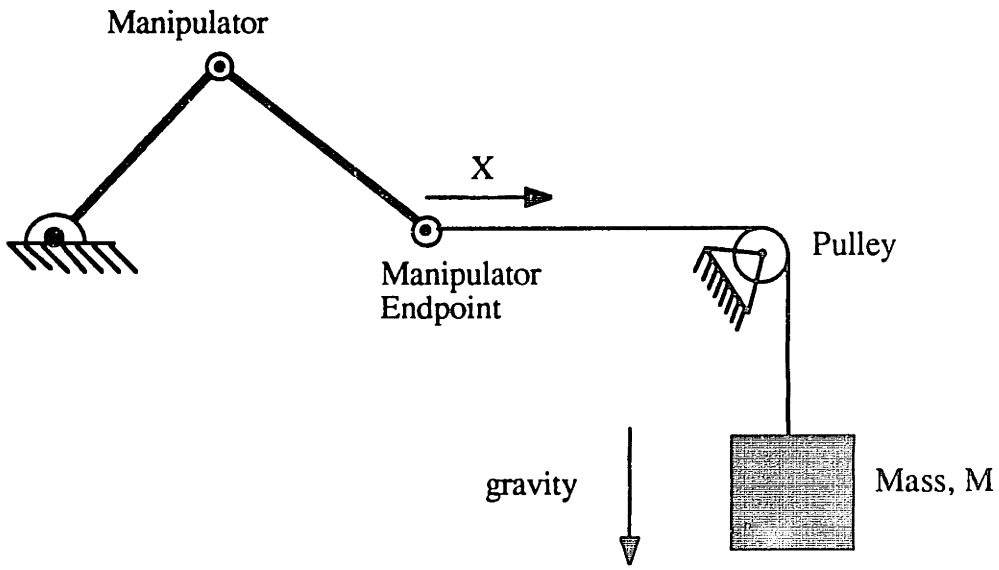

Figure #5-12. Diagram of manipulator inertia experiment

The effective mass of the end of the manipulator, m_e, is calculated from Newton's second law:

$$Mg = (m_e + M)\,\ddot{x} \tag{5-10}$$

We ignore the coulomb friction force because it is small. Rearranging,

$$m_e = \frac{Mg}{\ddot{x}} - M \tag{5-11}$$

The acceleration, $\ddot{x}$, is measured using the Newman Laboratory's Selspot camera system, TRACK software, and one light emitting diode (LED) array mounted on the end of the manipulator (for a complete discussion on the system see Antonsson and Mann, 1989). The track software smoothed the data and the acceleration output from the software differentiation was used as the $\ddot{x}$ value in equation 5-11.

For a large range of its workspace, the manipulator the X, Y, and Z direction effective masses were well below 5 Kg, 3 Kg, and 5 Kg respectively. It is important to remember here that these are the masses, not the weights the subject feels at the endpoint, (the manipulator is completely counterbalanced). A similar inertia would be felt if a weight were hung from the ceiling by a cord. In this case, the feeling of pushing on the suspended mass (for small ranges of motion) in the horizontal plane would be like the feeling of pushing on the counterbalanced manipulator.

The power-off friction in the manipulator was measured using the same experimental set-up as above minus the acceleration measurement. In this case, weights were added to the end of the cable until the force overcame the friction in the manipulator and the manipulator joints moved. The measured maximum friction at the manipulator endpoint was 110 grams in axis #3 with the friction in axes #1 and #2 much lower at

approximately 35 grams. Axes #4, #5, and #6 are direct drive axes, so the friction in the axis is mostly from the friction in the particle brake. This friction is given by the manufacturer to be .0353 Nm (.31 in-lbs).

Chapter 6

Experimental Protocol

The 6-dof MED manipulator was developed for the primary purpose of studying the effects of MED loads on whole-arm tremor. This chapter discusses the protocol for the initial testing of the device.

Experimental Goal

The goal of the first experiments with the MED arm was to test its compliance with performance expectations. This required meeting the following objectives:

- Measure changes in tremor and purposeful movement which result from use of the MED arm as damping levels are adjusted;
- Test the hypothesis that the MED arm allows the subject purposeful movement while reducing the tremor component of movement in 6-dof; and
- Demonstrate the use of the arm as a damped orthosis emulator.

Measures Used to Reduce Cumulative Experiment Effects

The possibility of learning and fatigue must be accounted for in experimental design. If learning effects are present, a subject performs significantly better on later experimental trials than on the first trial in spite of constant experimental conditions. Conversely, fatigue[1], discouragement or boredom could cause degraded task performance in later experiments. Although these effects tend to counteract each other, one may dominate. Good experimental procedure dictates that in order to correlate changes in

---

1 The term fatigue is kept purposely vague. We include all possible systemic fatigue factors.

tremor and purposeful movement to changes in damping levels, all other parameters should be held constant. Although human system parameters will inevitably vary over the days experiments, experimental design can help to reduce the confounding effects of learning, fatigue, discouragement, and boredom.

The learning effect has been modeled as a steep ascent in the amount learned in early trials and diminishing learning as they continue (Berringhause, 1988). That is, the learning is very rapid early in the experiment but additional learning is very small after a large number of experiments.

The learning effect can be mitigated to a degree with a combination of easy to learn experiments and practice time with the device before data is collected. Easy to learn experiments should result in lowering the time constant of the learning function, while practice time results in moving up the learning function to a fairly flat point before the experiments begin. Easy-to-learn experiments combined with short, simple sessions, conversation, and an informal atmosphere may also reduce the subject's discouragement and boredom.

Arm muscle fatigue can be minimized with short experiments and rest periods between sessions. Keeping experiment time to approximately one minute with the subject resting for four minutes is similar to the protocol used successfully by Berringhause (1987).

Most important, randomization of the order of the experiments can minimize the misinterpretation of the data. Randomizing the damping levels will tend to keep damping levels uncorrelated with human parametric changes caused by cumulative experiment effects. This will eliminate the possibility of attributing increased tremor levels to lower damping when the increased tremor is in fact caused by fatigue, boredom, or some other factor related to cumulative effects.

Finally, cumulative effects can be minimized through selection of subjects who are expected to learn the experiments quickly and should not fatigue prematurely.

Experiments

This section describes an ideal testing protocol for two sets of experiments , which will be described as Abstract and Functional. Initial experiments deviated slightly from this protocol.

While the Functional experiments were designed to determine how well the subjects performed during activities of daily living, the Abstract pursuit target tracking experiments are meant to permit a more precise quantitative analysis of subjects' task performance.

Subject Selection

The pool of disabled subjects from which ours were chosen included individuals with adventitious and inherited intention tremors.[1]. We require that intention tremor be present in major arm joints during voluntary movement of the arm. Also, test subjects were medically stable, have good vision (as corrected) and occulomotor control (to perform the target tracking experiments), and have normal cognitive function. Sex, age, and ethnic/socioeconomic backgrounds of subjects are irrelevant criteria from which to select subjects (these criteria do not affect a subject's experimental results).

Abstract Experiments

In the abstract pursuit target tracking task experiment, two icons appear on the screen. One, the target rectangle (Figure 6-1), moves around the computer screen in a seemingly random pattern. The other icon, the response cross, moves around the screen as the MED arm end effector moved. The subject's limb is coupled via the limb coupler cuff discussed in Chapters 2 and 4. Movement of the subject's limb causes movement of the manipulator and, therefore, movement of the response cross on the computer screen. The subject is asked to try to move the limb being tested in such a way as to make his response

---

1 These include Multiple Sclerosis, Joseph's Disease, Friedreich's Ataxia, familial essential tremors, and sequelae of head injuries resulting in lesions of the cerebellum or brain stem.

cross appear inside the target (Figure 6-2) throughout the trial. The viscous resisting force of the MED arm is expected to reduce the tremor motion while allowing the subject's purposeful movement.

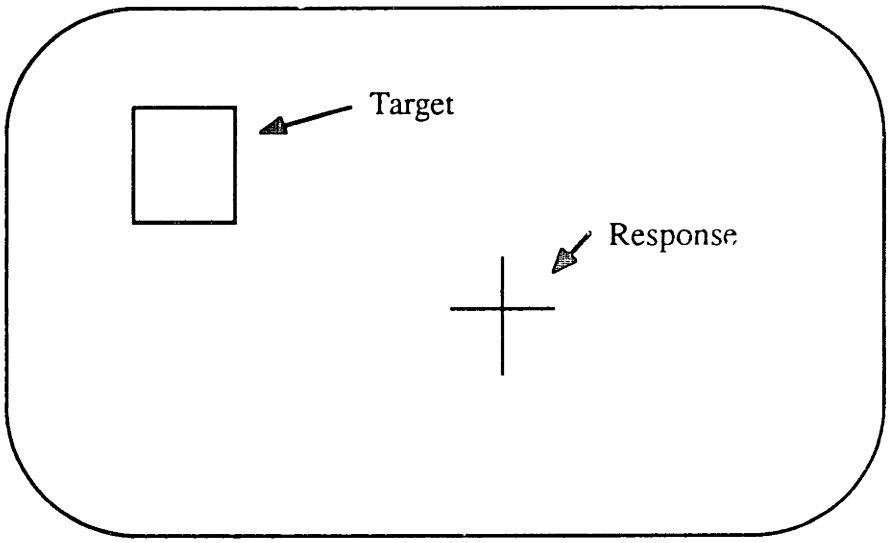

Figure #6-1. Computer tracking task display

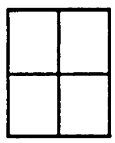

Figure #6-2. Perfect match between target and response

Because the tracking experiments are only two dimensional, we determined which two of the six manipulator degrees of freedom to map into X-Y movement of the response cross on the computer screen. The most intuitive mapping represents the subjects' frontal (vertical) plane (manipulator Y-Z plane) as the screen plane. In this mapping, when the

subject moves his/her arm up, the response cross moves up. When the subject moves his/her arm left, the response cross moves left. If the subject moves his arm forward or backward, the response cross does not move (the subject is still damped in these directions, however).

A total of four abstract experiments is performed by each subject, all with vertical plane mapping. In each experiment, one of four damping levels, designated level 0 to level 3, is used. The subject is allowed to move with the manipulator at different damping levels. He then is asked to choose the damping level that "feels" best to him according to whatever criteria he selects. This damping level is defined as level 2. Level 1 damping is less and level 3 damping is greater than level 2[1]. At Level 0, no active damping is present; the subject is resisted only by the passive manipulator inertia and friction.

The computer monochrome monitor is used to present the tracking display (Figure 6-3). The display driver software was developed by Steve Beringhause and used successfully in previous tracking tasks in two dimensions (Beringhause, 1988). The reference explains the Microsoft C programs in detail; only a brief a brief discussion is presented here.

The investigator must first determine what range of manipulator movement to map to the screen. The scaling program instructs the investigator to move the manipulator to the points he wishes to correspond to the response cross' upper left and lower right limits. This sets up the amplification and offset from the desired workspace of the manipulator to the workspace of the screen.

The target rectangle moves in the X and Y directions according to positions in a pre-determined function with the highest frequency content of .5 Hz. The function is created from a program which computes the X and Y values by summing five sine waves with

---

1 Ideally, we would like to suggest that level 3 damping is a particular percentage higher than level 2 and level 1 is a particular percentage lower than level 2. The problem with an algorithm like this is that level 2 damping may be close to the maximum damping level so that we cannot guarantee a particular percentage increase for level 3 damping.

frequencies of .5, .42, .27, .19, .12, and .08 Hz. With these five frequencies, the target will repeat approximately every seventeen minutes.

During the experiment, target x, y (in screen coordinates) and response y, z (in manipulator coordinates) values are written to a hard disk file after each tracking experiment is completed. Discussion on use of this data can be found in Chapter 7.

Instructions are given before the start of the each experimental session. The subject is instructed to keep his response cross inside the moving target rectangle by moving his hand in the vertical plane.

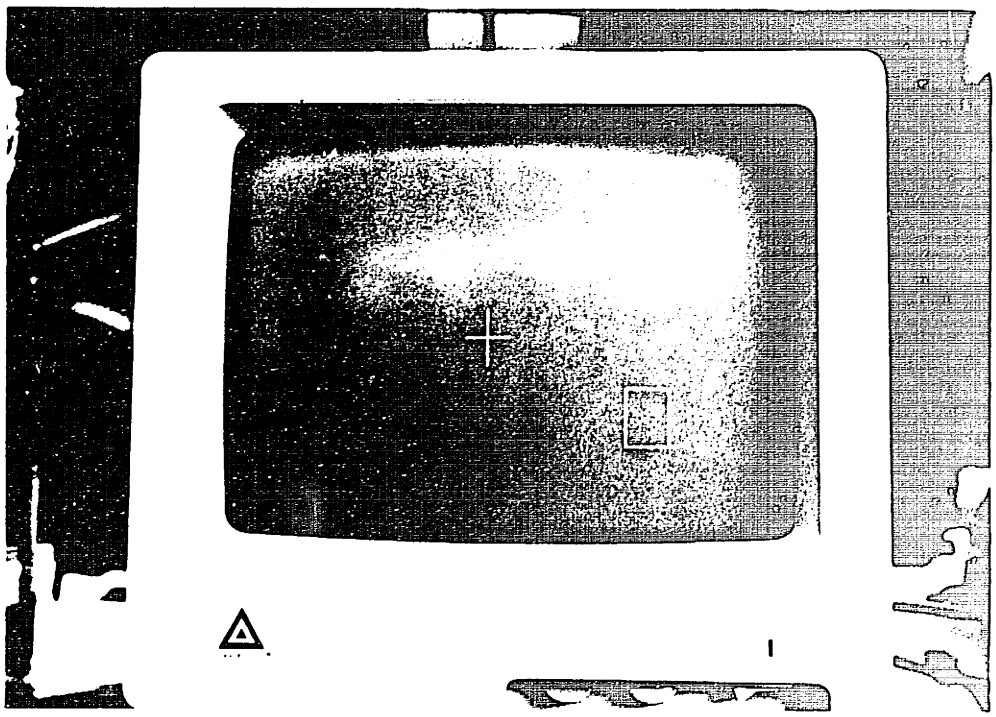

Figure #6-3. Photograph of target and response

Functional Experiments (performed by neurologist)

A set of functional experiments was developed by Dr. Mindy Aisen at the Burke Rehabilitation Center with the help of a standard clinical rating scale (Fahn, Tolosa, and Marin, 1988). Each experiment involves a simple clinical assessment task:

- The tremor-at-rest assessment includes the neurologist asking the subject to relax his arms on a table. The postural tremor is analyzed with the subject's arms fully extended at shoulder height. Finally, the action tremor evaluation has the subject moving his extended finger from the tip of his nose to the finger of the neurologist.

- The subject's handwriting is tested by asking the subject to write his full name with a pen on a standard sheet of white paper. Next, the subject is asked to perform the Archemedes spiral test (Figure 6-4). In this test, the subject is asked to connect the outside mark with the inside mark without crossing the lines of the spiral.

- For the water pouring test, the clinician asks the subject to pour water from one disposable cup (Dixie style with 8 cm height) filled to within 1 cm of the top into another cup.

- For the drinking/eating soup test, the subject is asked to attempt to eat "soup" (water) with a spoon. If this is not possible, the subject is asked to try drinking the "soup" out of a glass with one hand. Finally, if the subject is unable to bring a glass to his mouth with one hand, the subject is asked to try the same with two hands.

- The keyboard experiment has the subject spelling his name out on a large QWERTY keyboard (key size approximately 3 cm square with 7 cm between centers).

As with the abstract experiments, each task is undertaken at the same damping values used in abstract experiments (for the preliminary experiments discussed in Chapter 8, we used similar but different levels). Each task is performed at the four different damping levels before the next task is undertaken.

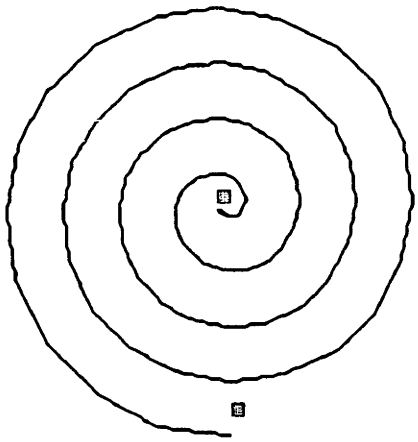

Figure #6-4. Archemedes Spiral test

Testing Procedure

A testing session lasts approximately one hour including breaks. Although the experimental protocol is detailed below, all aspects of the protocol are flexible enough to accommodate unexpected changes and differences among subjects in their schedule, motivation, and medical condition.

The informed consent form (Appendix B) for the human subject experiments is signed and the subject is asked to complete (with help as needed) Questionnaire #2 in Appendix B. This questionnaire is intended for recording the subject's observations of how tremor affects his activities of daily living. The possibility of direct personal benefit of participation in the experiments is specifically downplayed when informed consent is obtained to reduce the chance of false hopes and disappointment. While the subject completes his questionnaire, the clinician is asked to complete Questionnaire #1 (Appendix B). This questionnaire targets aspects of the subject's medical history relating to tremor as well as a clinical/tremor evaluation on the day of testing.

For the first two subjects, an adjustable limb-coupler attachment was used which accommodated each subject's right arm. For future tests, the subject's arm will be measured for his limb-coupler attachment and a pattern will be developed for the orthoplast cuff. The orthoplast material will be cut to size and immersed in hot water and the warm, pliant orthoplast will then be molded onto the subject's arm. After shaping, the limb coupler cuff will be fitted with velcro straps and the MED arm attachment plate. Finally, the subject's arm will be inserted into the limb coupler and the limb coupler will be attached to the manipulator end effector.

The subject is comfortably seated in the subject support chair and seat-belt harnesses help keep the him secure. During the abstract experiments, the subject faces the computer screen from a distance of approximately .8 Meters. The functional experiments have the subject facing a table on which most of the experiments are performed. During both sets of experiments, the electronic equipment is kept behind the subject to help eliminate the potential for distraction.

Before the experiments begin, the subject is allowed to move his arm coupled to the manipulator and damping levels are adjusted. The subject identifies the preferred damping level which is defined as level 2 (see the Abstract Experiments section above for more details)

The experiments begin with the set of abstract experiments followed by the set of functional trials. The sequence of four damping levels within each set of experiments is fully randomized for each subject, but no damping level is repeated. Practice runs are permitted at the start of each new experiment. The experiment begins when the subject is satisfied that he is familiar with the task and the feel of the new damping level.

Each experiment takes approximately one minute to perform, and a break of five minutes is given between tests. Between the abstract and functional experiments, a longer break is given for the subject to relax in order to reduce the potential for boredom.

After both sets of trials are finished, the subject is asked to complete the post-test Questionnaires #3 and #4 (in the appendix). These questionnaires evaluate the subject's reaction to the MED arm. Also, if the M.I.T. investigators are not present during future experiments, we will request that the clinician complete Questionnaire #5 (in the appendix) to record his/her evaluation of the MED arm.

Chapter 7

Data Analysis Methods

This chapter discusses the data analysis methods used for the preliminary MED arm experiments. Our data analysis methods have been used with successful results in previous studies (Adelstein, 1981; Beringhause, 1988).

Abstract Experiments

Adelstein (1981) includes both an overview of pursuit target-tracking analyses and details on the specific methods outlined here. Many methods have been used to quantify results from pursuit target-tracking tremor experiments. Simple measures include peak-to-peak amplitudes of the oscillations, average rectified peak magnitudes, and accumulated tremor (integrated rectified limb travel over a duration of time). More complex measures include tremor variance and mean square power.

This research used data analysis methods developed by Adelstein (1981). The data reduction results in quantitative measures of both tracking fidelity and tremor magnitude. Both are important because increased external loading to reduce tremor magnitude may also reduce tracking fidelity. For instance, the tremor would be reduced to zero if the subject's arm was tied to a rigid structure but the subject would be unable to move his arm and tracking fidelity would also be zero.

One measure of tracking fidelity is defined in terms of the transfer function defining the input-output relation (for a constant parameter linear system model) calculated by dividing the target-response cross-power density function by the target auto-power spectrum. Optimum tracking performance results in transfer function of magnitude one and

zero phase lag for all frequencies. The degradation of tracking performance can be analyzed by identifying the deviation from the optimum.

One measure of tremor magnitude is quantified by looking at the auto-power specra of the residual portion of the subject's response. The residual is the portion of the response signal not linearly related to the target signal. The ideal tremor power density (amplitude of the residual auto-spectrum) is zero for all frequencies (not attained even by normal individuals).

Simpler measures for tracking fidelity and tremor magnitude are also suggested by Adelstein. A simple measure of tracking fidelity is the signal-to-noise ratio defined as the square root of the area under the cross-power density curve divided by the square root of the area under the tremor magnitude curve. A simple measure of tremor magnitude is tremor power defined by the area under the residual response spectrum.

Specific Calculation Steps

While an overview of the processing is described above, this section describes the processing steps in detail including the actual programs used to perform the processing. For a more detailed discussion, see Adelstein (1981).

(1) The pursuit target tracking program STCONTROL is executed. This program controls the manipulator and the target and response icons. The program has a sampling rate of 60 Hz and samples for a period of 60 seconds for a total of 3600 data frames.

(2) The data is then reconfigured using the program TFORM. This program queries the researcher as to whether he wants to process the data from the x direction (horizontal screen coordinate) or in the y direction[1] (vertical on the screen). Next, the single degree of freedom target, t(t), and response, r(t), data is placed in the proper format for the spectral processing step (3).

(3) The spectral processing was performed using the program SPECTRAL adapted by Ivan Baiges from Dov Adelstein's DEC computer programs. This program uses a Fast Fourier Transform (FFT) to perform a spectral analysis on the data using a Cooley-Tukey algorithm. SPECTRAL first computes the auto-power spectrum of the target signal, $G_{tt}(f)$, the auto-power spectrum of the response signal, $G_{rr}(f)$, and the cross-power density between the target and response signals, $G_{tr}(f)$. The constant-parameter linear transfer function, $H_{tr}(f)$, is then calculated:

$$H_{tr}(f) = \frac{G_{tr}(f)}{G_{tt}(f)} \qquad (7\text{-}1)$$

---

1 The present method of data analysis uses only one dimensional processing. We envision the use of more complex processing methods in the future.

The tremor quantification comes from the residual portion of the response not linearly related to the input target, $\Delta r(t)$. The residual signal is defined as the difference between the response, r(t), and the response of the linear system output, $\hat{r}(t)$. At any time,

$$\Delta r(t) = r(t) - \hat{r}(t). \tag{7-2}$$

The residual auto-power spectrum is calculated by multiplying the auto-power spectrum of the response by one minus the coherence between the tracking and response signals[1]. This result is derived by Adelstein (1981).

The auto-power spectrum for the residual portion of the response, $G_{\Delta r \Delta r}(f)$, is calculated by SPECTRAL:

$$G_{\Delta r \Delta r}(f) = G_{rr}(f)\left[1 - \gamma_{tr}^2(f)\right] \tag{7-3}$$

where $\gamma_{tr}^2(f)$ is the coherence and is defined by

$$\gamma_{tr}^2(f) = \frac{|G_{tr}(f)|^2}{G_{tt}(f)\, G_{rr}(f)} \tag{7-4}$$

and,

$$0 \le \gamma_{tr}(f) \le 1. \tag{7-5}$$

Tremor, T(f), is then defined as zero in the frequency range of the target spectrum (0 to .5 Hz. for our experiments) and $G_{\Delta r \Delta r}(f)$ for all other frequencies.

After computations have been made, SPECTRAL puts the results of the system transfer function and tremor power spectrum in data files.

---

1 The coherence is a measure of the linearity of the relationship between the target and response signals. A completely linear response, i.e. one without noise and/or non-linear components at any frequency, will result in a coherence of 1 at that frequency, while a completely nonlinear response will result in a coherence of 0. The power-spectra of the residual will be lower the more linear the relationship between the tracking and response signals.

(4) Next, the post-processing program VALUE is run. This program numerically integrates the area under the tremor power-spectra to arrive at the value of integrated tremor, T. The program further calculates the signal-to-noise ratio, R, defined here as:

$$R = \frac{\sqrt{\int_0^{f_c} |G_{tr}(f)|\, df}}{\sqrt{\int_{f_c}^{\infty} T(f)\, df}} \qquad (7\text{-}6)$$

Where f_c is the maximum frequency content of the target signal.

(5) Finally, the post-processing program COMBINE is executed. This program takes the data from the SPECTRAL output files and combines it into one file for simplicity in file management. Data from this file is then transfered to a Macintosh Plus personal computer (using the commercial program LAP-LINK) and plotted (using the commercial program CRICKET GRAPH).

After the processing is complete for the first direction, either x or y, the researcher then goes back through steps 2 through 5 again for the other movement direction.

Functional Experiments

The analysis methods for the functional experiments were also borrowed directly from previous research (Fahn, Tolosa, and Marin, 1988). Each task was associated with a distinct method of data analysis. Tasks and score definitions are summarized in Table 7-1. All tasks are scored by the Neurologist[1] except the subject's subjective evaluation. After the functional experiments are complete, the subject is asked for his own evaluation of his performance with damping relative to the base case of no damping. This evaluation describes his impression of his performance on all the tasks. The subjective evaluation is then scored as shown in the table. The subject is then given a global score obtained by a simple addition of the individual scores for each task (including the subjective score). This global score is then used overall as the measure of effectiveness of the device loading.

---

1 The score for each task is based on the Neurologist's visual "measurement."

Table 7-1

Summary of Functional Experiments Evaluation Scores

Task	score	Description
Tremor Amplitude	0	No tremor
	1	Tremor amplitude less than .5 cm
	2	Tremor amplitude .5 to 1 cm
	3	Tremor amplitude 1 to 2 cm
	4	Tremor amplitude greater than 2 cm
Handwriting	0	Normal
	1	Slightly untidy
	2	Legible but significant tremor
	3	Illegible
	4	Unable to keep pencil on paper
Archimedes Spiral	0	Normal
	1	Crosses lines occasionally/slightly tremulous
	2	Crosses lines frequently
	3	Great difficulty/many errors
	4	Unable to perform
Pouring	0	Normal
	1	Very careful, but no water spilled
	2	Spills under 10% of the water
	3	Spills 10-50% of the water
	4	Unable to perform without spilling most water
Drinking "soup"	0	Normal
	1	No water spilled with one hand
	2	No water spilled with two hands
	3	Spills under 10% of the water with two hands
	4	Unable to perform without spilling more than 10% of the water
Keyboard	0	Normal
	1	Very careful, but hits all keys
	2	Has difficulty hitting under 10% of the keys
	3	Has difficulty with 10-50% of the keys
	4	Unable to perform
Subjective	-3	Marked (50-100%) improvement over base-case
	-2	Moderate (25-49%) improvement over base-case
	-1	Mild (10-24%) improvement over base-case
	0	Unchanged
	+1	Mild (10-24%) worsening
	+2	Moderate (25%-49%) worsening
	+3	Marked (50-100%) worsening

Chapter 8

Results

The results of initial experiments with the MED manipulator conducted with two tremor-disabled subjects and one able-bodied subject are discussed in this chapter. All three subjects had only their right arm tested.

Subject N

Subject N is a normal, able-bodied subject, tested for control purposes. This subject is a 27 year old male with no history of neurological problems. Because N's functional tests resulted in the same score for all damping levels, we only report the abstract experiment results below.

Abstract Testing Results

Figures 8-1 and 8-2 show the tremor magnitude for N in the X (horizontal) and Y (vertical) direction respectively. Note that although the magnitude of "tremor" is very small, the plots of the N show a measurable signal out to approximately three Hertz. This result is due to our definition of tremor as the residual signal not accounted for in a linear system. Our results indicate that, albeit small, N's tracking response has a nonlinear component.

The damping level numbers in the legend of the graph were described in the system characterization chapter. Briefly, the first number is the viscous damping level used for the first three axis which result in translational motion of the manipulator end point and the second number is the viscous damping level used for the last three axes which result in rotational motion of the manipulator end point. Although there is a spread in the data,

especially at low frequencies, the "tremor" in the normal subject does not seem to change due to the damping applied to the subject's arm.

Figures 8-3 and 8-4 show the transfer function magnitude for the normal subject in the X and Y direction respectively. The transfer function has a magnitude of approximately one and, again, the damping levels do not seem to create a systematic change in the magnitude.

Figures 8-5 and 8-6 show the transfer function phase angle corresponding to the Figures 8-3 and 8-4 above. There is a very small phase delay for frequencies up to .25 Hz which increases to 15 degrees for frequencies in the .45 to .7 Hz range. Again, nothing systematic seems to occur as the damping level is adjusted.

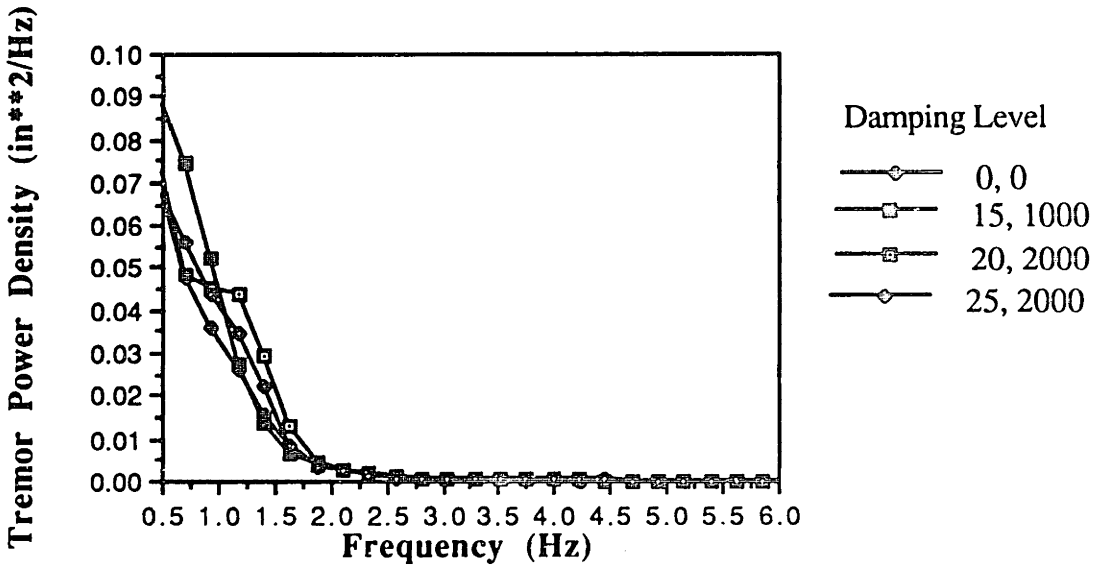

Figure #8-1. Subject N's tremor power density in the X-direction

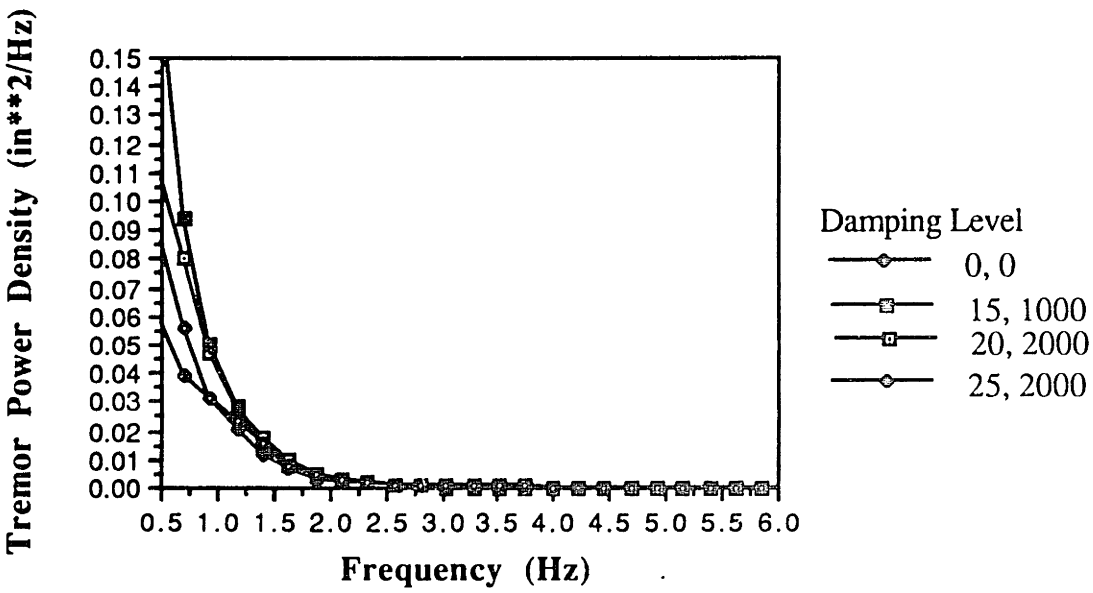

Figure #8-2. Subject N's tremor power density in the Y-direction

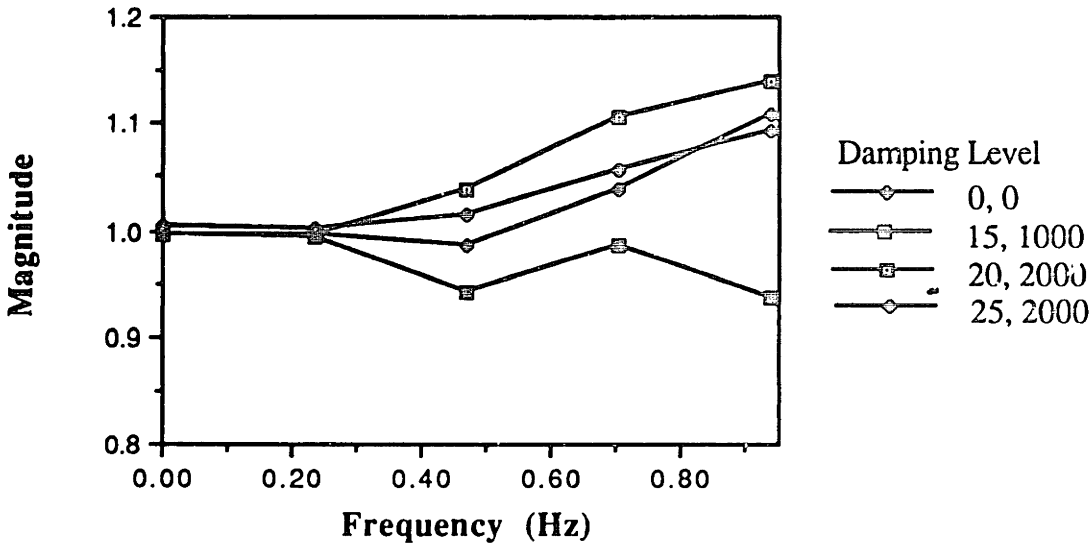

Figure #8-3. Subject N's transfer function magnitude in the X-direction

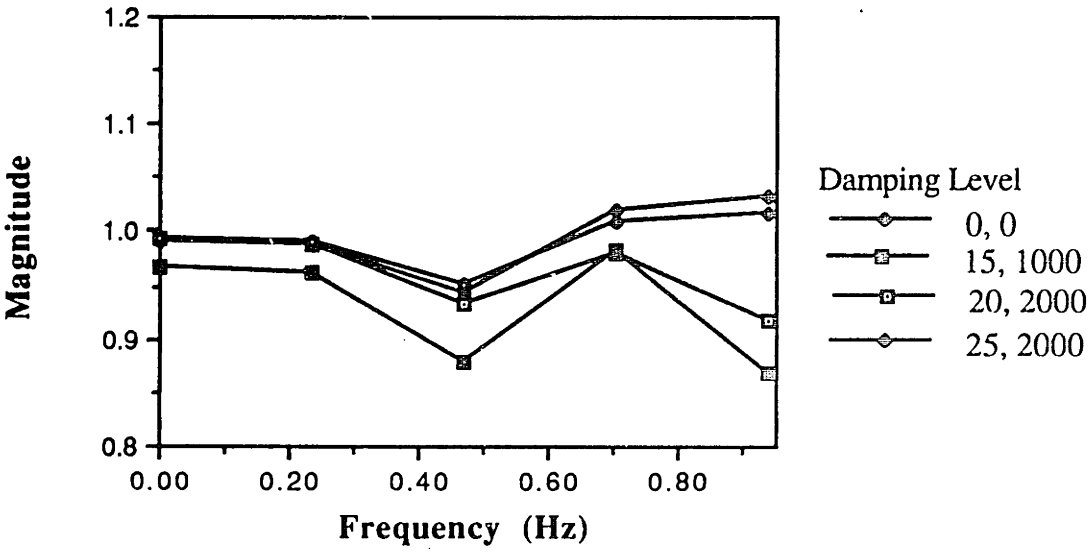

Figure #8-4. Subject N's transfer function magnitude in the Y-direction

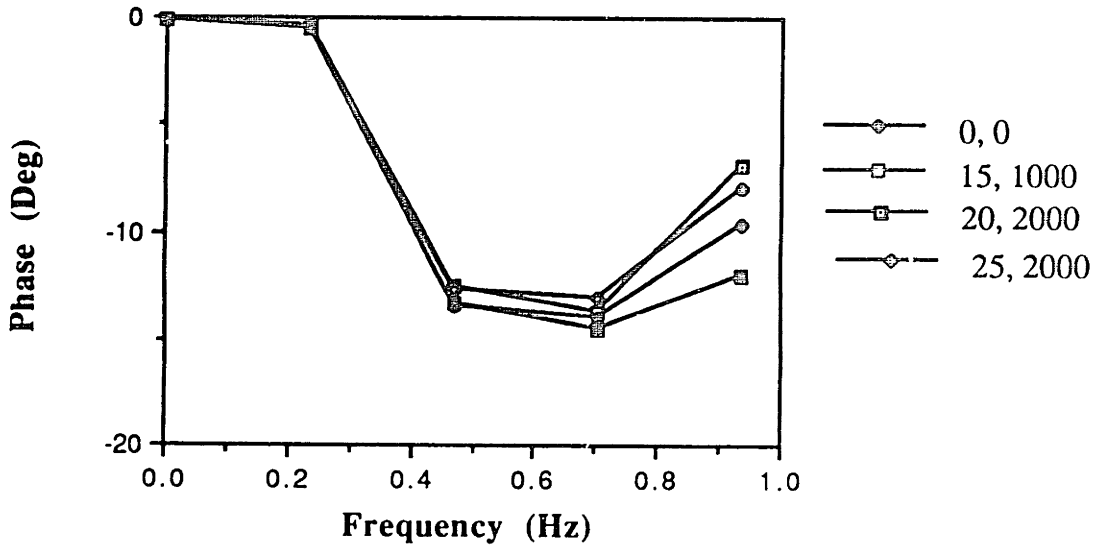

Figure #8-5. Subject N's transfer function phase in the X-direction

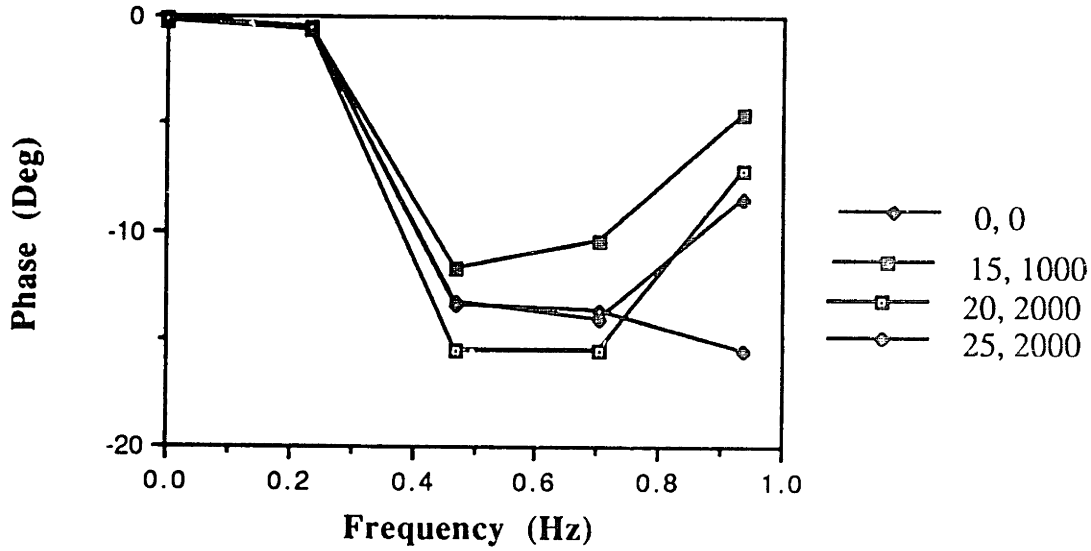

Figure #8-6. Subject N's transfer function phase in the Y-direction

Subject A

Subject A is a tremor-impaired 29 year old right-handed male with a history of head trauma resulting from a car accident in 1981. The subject was in a coma for approximately six months following the accident and, upon awakening, was paralyzed on the left side. As he regained function on his left side, tremor started (in 1983) on his right side. He has been given numerous medications without success and, at the time of the study, was not taking any medication for his tremor. Tremor in his lower extremities causes imbalance during walking resulting in his confinement to a wheelchair. A motor exam displayed severe tremor of the head, trunk, arms, and legs. The tremor is much worse on the right than on the left and his arms are much worse than his legs. The tremor in his arms has been diagnosed as "severe action tremor." The subject's strength is normal with the right side stronger than the left side.

The subject said he was able to perform 22 out of the possible 84 tasks described on the subject observation questionnaire (Questionnaire 2 in Appendix B). Of the tasks he is able to perform, summarized in Table 8-1, most are restricted by his tremor. For instance, he brushes his teeth with an electric toothbrush, shaves with an electric razor, dials the operator for assistance in reaching another, and drinks with a straw.

Functional Testing Results

Functional task results at different damping levels are shown in Table 8-2. Note that as the damping level increases, the Total Score decreases for each of the functional tests. Because the lower score means higher functional ability, this result suggests that increasing the viscous damping helps subject A function at a higher level.

The results from the functional tests are reclassified by functional task in Table 8-3. While most of the tasks benefit from the increase in viscous damping, the handwriting task and the drawing task scores remained the same. This result comes about for two reasons. First, the manipulator is not designed to damp motion of the subject's fingers, which play a major role in these tasks. Second, the limb-coupler cuff obstructs the ability of the subject

to hold the pen comfortably. Either the writing and drawing tasks should be changed to require pen movement over a larger area (so the manipulator can have an effect on the motion) or these tasks should be eliminated in future experiments. If the writing and drawing results were eliminated in the present results, subject A's score would be 19, 12, 10, and 9 as the damping level increases from 0, 0 to 30, 2000.

Abstract Testing Results

Figures 8-7 and 8-8 show the tremor power density for the X and Y directions, respectively. Subject A has a level of tremor an order of magnitude above that of the normal subject (Figures 8-1 and 8-2). Subject A also has a distinct tremor peak at approximately 1.2 Hz for two of the experimental runs. Other than the observation that the X direction peak at zero damping was reduced at all other damping levels, there does not seem to be a simple monotonic relationship between damping level and the reduction of tremor. We must caution here, however, as we are evaluating an extremely small sample of data. Also, we may be looking in vain for the tremor to continue to be reduced as we increase the damping parameter value. For instance, subject A may have "optimal damping" somewhere in the 15, 1000 range (as shown by the reduced tremor power and increased signal-to-noise ratio in Table 8-4) so that any reduction or increase in damping parameter value would result in increased tremor.

Table 8-4 lists the tremor peak frequency (if there is a peak), tremor power, and signal-to-noise ratio for subject A in both the X and Y directions. Again, damping does not seem to affect these values in a monotonic manner and 15, 1000 yields the best results.

Why the discrepancy between the functional tests and the abstract tests? Many possible explanations exist. One explanation is that these abstract tests (or data reduction methods) are not a proxy for functional performance. Another is that our functional tasks are not scored as accurately as we need to see variation with damping similar to the results of the abstract tasks. Other explanations include the possibility that our very small sample

of tests is not representative, and a more complete set might have shown a better correlation between functional performance and abstract performance indices.

Subject A's transfer function, Figures 8-9 and 8-10 for magnitude and Figures 8-11 and 8-12 for phase in the X and Y directions, also behave in a seemingly non-systematic manner as the damping level was adjusted. Also, most of the experiments resulted in the same plot shape except the plot for the transfer function magnitude in the X direction at zero damping (which corresponds to the unique tremor density peak in the X direction noted earlier). These results suggest that the increased damping is not decreasing purposeful tracking performance defined by the transfer function magnitude and phase. In fact, for many frequencies, the worst lag and greatest attenuation occur in the undamped case.

Post-Test Questionnaire Results

Subject A's post-testing questionnaire results were mostly positive. He said that he was better able to control his arm when it was in the device, the device reduced his tremor, and the device felt "good, except the wrist was held too tight." Also, "It restricts the wrist". This suggests more work needs to be done in making the limb-coupler cuff more comfortable, and possibly restoring the human wrist flexion/extension and radial/ulna deviation motions which are locked in the present limb coupler cuff.

Subject A felt the device did not make him very tired but "Its a good workout. It is just like going to the gym. You would get tired if you were in it too long." He further added that when we increased the damping level, his tremor was reduced but it took more effort to move the device. This suggests that many more load types should be attempted that restrict tremor more selectively relative to purposeful movement.

If he would change anything, Subject A would like the device to be made smaller so that he could "carry it around on my back, in a backpack."

Table 8-1

Subject A Observations on His Functional Disability Due to Tremor

Rating Scale 0-10 Causes no problems = 0 Functionally impossible = 10

Of the 84 tasks on the questionnaire, the subject had answers lower than 10 on the 22 following tasks:

Task	Rating	Notes
Putting on socks	5	
Putting on pants	3.5	
Putting on shirt	9	
Putting on coat	6	
Pulling a zipper	2	
Tucking in clothes	9	
Adjusting clothes	9	
Turning taps (bathroom)	9	
Brushing teeth	7	Electric toothbrush
Shaving	0	Electric razor
Applying ointments to skin	5	
Loading spoon from plate	0	
Stirring with spoon	8	
Unloading spoon into mouth		(Oatmeal = 0, Soup = 10)
Drinking from glass		Uses a straw
Passing dishes	5	
Open/shut cupboards	0	If he gets his wheelchair in the right position
Unlock doors	5	
Open doors with handle	0	
Dialing telephone		Calls the operator for assistance
Holding telephone receiver	4	Sometimes starts hitting his head
Retrieving money from pockets	9	

Table 8-2

Functional Testing Results Summary Subject A

Damping Level Axes 1-3	Axes 4-6	Functional Test	Score
0	0	Resting Tremor	2
		Postural Tremor	3
		Action Tremor	3
		Handwriting	2
		Drawing: Archimedes Spiral	2
		Pouring	4
		Drinking/Eating Soup	4
		Keyboard	3
		Total Score	23
5	700	Resting Tremor	1
		Postural Tremor	2
		Action Tremor	2
		Handwriting	3
		Drawing: Archimedes Spiral	2
		Pouring	4
		Drinking/Eating Soup	1
		Keyboard	2
		Total Score	17
15	1000	Resting Tremor	3
		Postural Tremor	1
		Action Tremor	2
		Handwriting	2
		Drawing: Archimedes Spiral	3
		Pouring	3
		Drinking/Eating Soup	0
		Keyboard	1
		Total Score	15
30	2000	Resting Tremor	2
		Postural Tremor	2
		Action Tremor	1
		Handwriting	2
		Drawing: Archimedes Spiral	2
		Pouring	3
		Drinking/Eating Soup	0
		Keyboard	1
		Total Score	13

Table 8-3

Functional Testing Results By Functional Task Subject A

Functional Test	Damping Level Axes 1-3	Axes 4-6	Score
Resting Tremor	0	0	2
	5	700	1
	15	1000	3
	30	2000	2
Postural Tremor	0	0	3
	5	700	2
	15	1000	1
	30	2000	2
Action Tremor	0	0	3
	5	700	2
	15	1000	2
	30	2000	1
Handwriting	0	0	2
	5	700	3
	15	1000	2
	30	2000	2
Drawing: Archimedes Spiral	0	0	2
	5	700	2
	15	1000	3
	30	2000	2
Pouring	0	0	4
	5	700	4
	15	1000	3
	30	2000	3
Drinking/Eating Soup	0	0	4
	5	700	1
	15	1000	0
	30	2000	0
Keyboard	0	0	3
	5	700	2
	15	1000	1
	30	2000	1

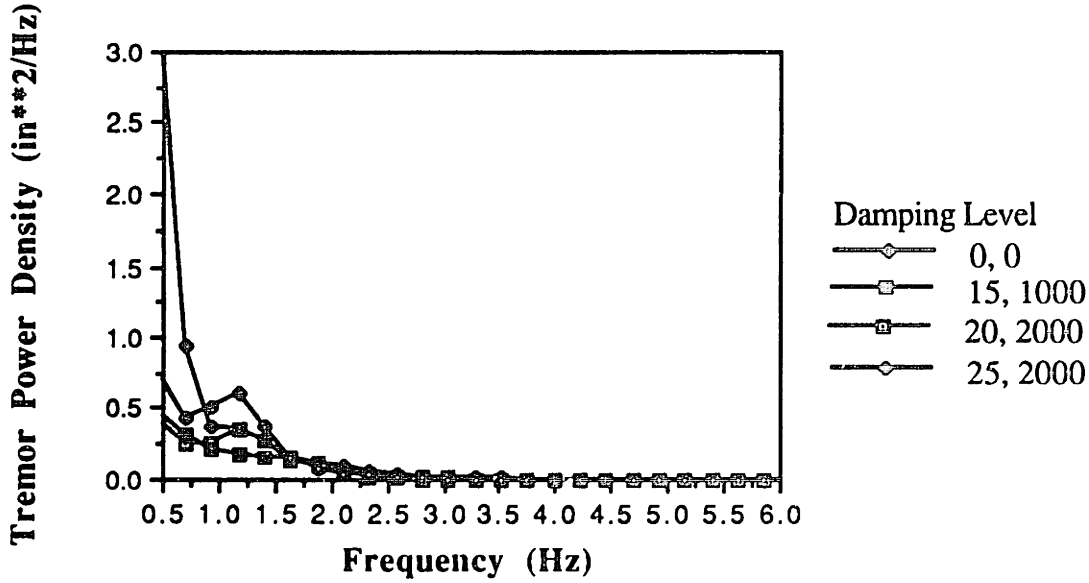

Figure #8-7. Subject A's tremor power density in the X-direction

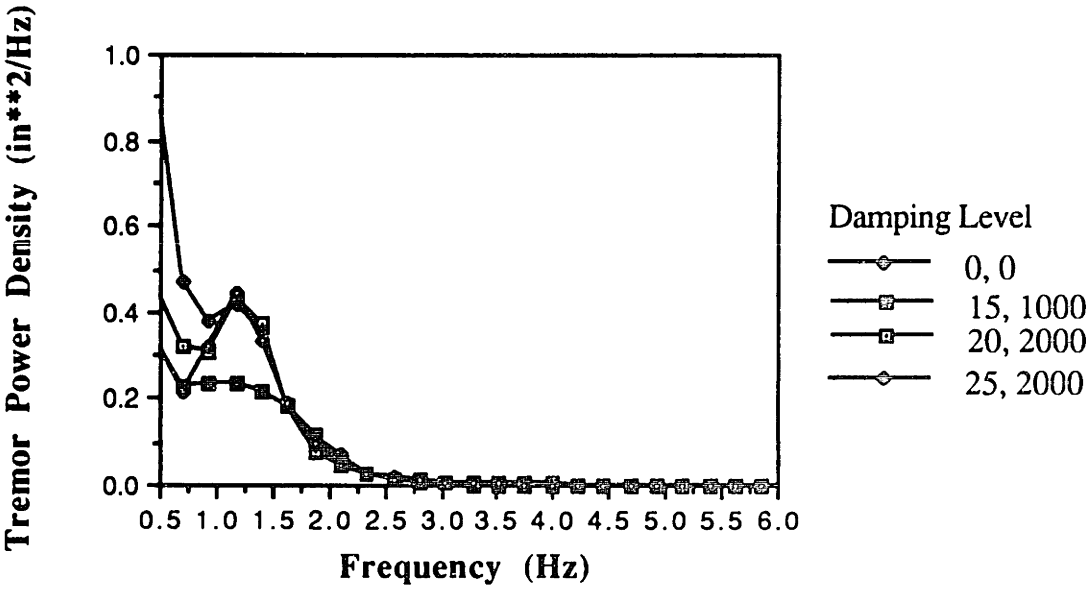

Figure #8-8. Subject A's tremor power density in the Y-direction

Table 8-4

Summary Table for Subject A's Abstract Experiment Performance

Direction	Damping Level	Tremor Peak Frequency	Tremor Power	Signal to Noise Ratio
X	0, 0	1.2 Hz	.491 in**2	65
	15, 1000	No Peak	.260	115
	20, 2000	1.2	.333	91
	25, 2000	No Peak	.494	67
Y	0, 0	1.2	.380	37
	15, 1000	.9	.294	52
	20, 2000	1.2	.395	41
	25, 2000	1.2	.436	37

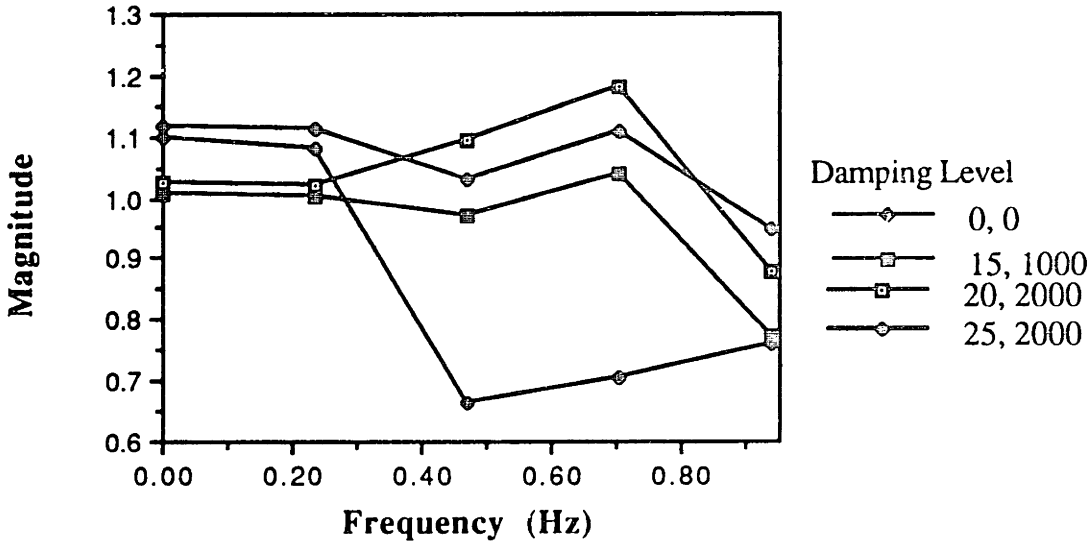

Figure #8-9. Subject A's transfer function magnitude in the X-direction

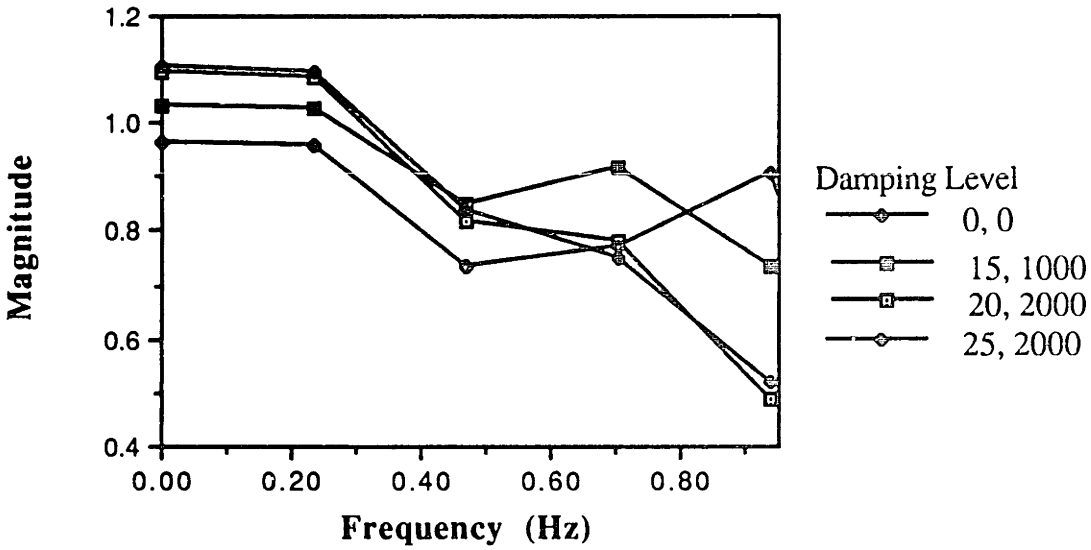

Figure #8-10. Subject A's transfer function magnitude in the Y-direction

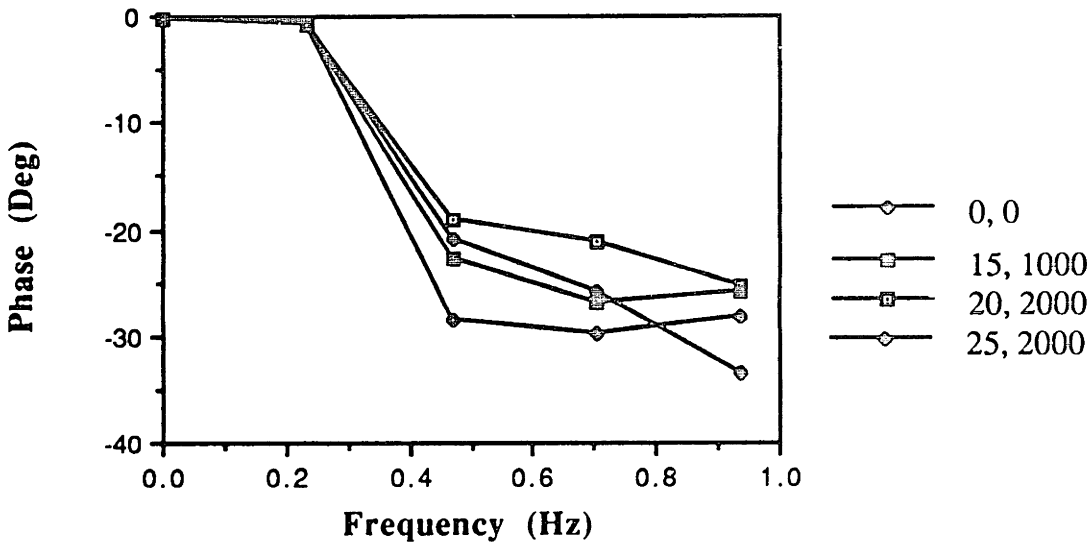

Figure #8-11. Subject A's transfer function phase in the X-direction

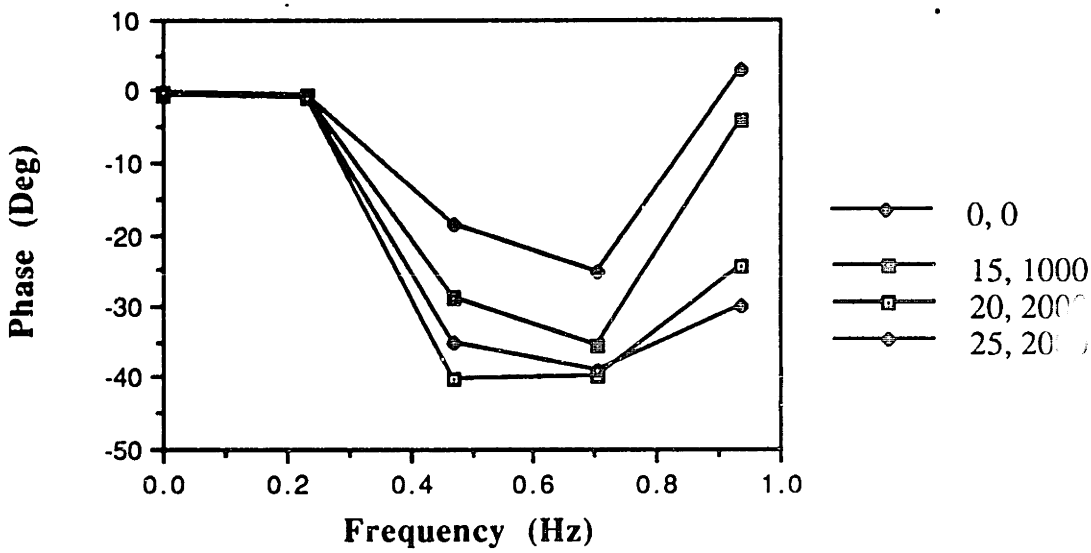

Figure #8-12. Subject A's transfer function phase in the Y-direction

Subject B

Subject B is a 47 year old male with Multiple Sclerosis. His diagnosis came in 1974 when he complained of difficult gait and tremor. He has dysarthria and spacticity of his legs and trunk resulting in confinement to a wheelchair. He has tremor in his head, neck, trunk, and right arm. His left arm has little to no tremor. His difficulties have been progressively worse since his diagnosis.

Like subject A, Subject B is almost completely functionally disabled by his tremor and other symptoms. The subject said he was able to perform only 13 out of the possible 84 tasks described on the subject observation questionnaire (Questionnaire 2 the Appendix B). Of the few tasks he is able to perform, summarized in Table 8-5, most are performed only with his left arm (which is not disabled by tremor). As with subject A, subject B uses an electric toothbrush and drinks with a straw.

Functional Testing Results

Functional test results for subject B are shown in Table 8-6. While all the total scores with damping are lower than the total score without damping, subject B did best with a small level of damping (5, 500). This may suggest that there is an optimal level of damping for the functional tasks for subject B.

Table 8-7 groups the results by functional test. Note that the subject had no resting tremor, little postural tremor, and significant action tremor in all of the tests, with the action tremor somewhat reduced by the presence of viscous damping. Although the handwriting, drawing and pouring tests resulted in reduced tremor with damping, the optimal level of damping for these tests seems to be at a low damping level (5, 500), with some reversal of the effect at higher damping. The drinking/eating soup and keyboard task showed a mild improvement for all levels above zero damping.

Abstract Testing Results

Figures 8-13 and 8-14 show the tremor power density for the X and Y directions. Subject B has a tremor signature that is both distinct from subject A and invariant with changing damping level. Tremor peak frequency for subject B is approximately 2.6 to 3 Hz. and, other than the distinct plot at the zero damping level in the X direction, all magnitudes were approximately the same between 1.5 and 6 Hz.

Table 8-8 lists the tremor peak frequency, tremor power, and signal-to-noise ratios for subject B. The tremor peak frequency rises slightly with levels above zero damping along with the tremor power. The change in the signal-to-noise ratio seems to inversely follow the inverse of tremor power quite well as the damping levels are changed.

Again, there does not seem to be any relationship between the results of the functional tasks and the results of the abstract tasks, suggesting that more tests should be performed to get statistically significant results or that other abstract tests must be explored to identify those more predictive of function.

The transfer function magnitude is shown in Figures 8-15 and 8-16 for the X and Y directions. All the results are grouped closely around magnitude one for low frequencies and reduce down to the .5 range at approximately .5 Hz. The tight grouping along with the absence of correlation with damping level suggests that the transfer function magnitude is not affected by the damping level.

The transfer function phase is shown in Figures 8-17 and 8-18 for the X and Y directions. Like the transfer function magnitude, the transfer function phase in the X direction is tightly grouped and the magnitude is uncorrelated to the damping level. The transfer function phase for the Y direction is more scattered and there seems to be some correlation between the phase delay and the damping level. This result suggests that there may be some degradation of purposeful movement for subject B in the Y direction. Again, more testing needs to be performed to determine the statistical significance of the data.

Post-Test Questionnaire Results

Subject B's post-testing questionnaire results suggested a conservative optimism regarding the device. He felt that he was better able to control his arm when using the device. Also, he felt the device was smooth and reasonably comfortable, but the limb-coupler cuff irritated the tissue in his thumb and he had difficulty seeing what he was writing during the functional experiment writing tasks.

Subject B felt the appearance of the device does not matter if it works, but believes the present device impractical for home use because he would need another room (he lives in an apartment and believes our MED arm system is too large for it) and he would need someone to transfer him from his wheelchair to the device.

Finally, the subject felt moderately optimistic about the future of devices such as the MED manipulator because he "was able to do most tasks better (with the machine) than without the machine."

Table 8-5

Subject B Observations on His Functional Disability Due to Tremor

Rating Scale 0-10 Causes no problems = 0 Functionally impossible = 10

Of the 84 tasks on the questionnaire, the subject had answers lower than 10 on the 13 following tasks:

Task	Rating[1]	Notes
Brushing teeth		Uses an electric toothbrush with left hand
Brushing hair		Uses his left hand
Washing hair		Uses his left hand
Loading spoon into mouth		Uses soup spoon in left hand
Unloading spoon into mouth		Uses left hand
Stirring with a spoon		Tenuous at best with left hand
Drinking from glass		Uses a straw
Pull open/push shut cupboards/drawers		If wheelchair positioned properly
Open doors with handle		If wheelchair positioned properly
Dialing telephone		Uses pushbutton phone with left hand
Holding telephone receiver		Sometimés a problem
Retrieving wallet from bag		Okay
Open/close windows		Okay

Other Comments

It is somewhere between difficult and impossible for subject B to do anything. He uses his right arm for almost nothing.

---

1 This subject did not like a numerical rating scale. He prefered to answer all the questions with brief answers.

Table 8-6

Functional Testing Results Summary Subject B

Damping Level Axes 1-3	Axes 4-6	Functional Test	Score
0	0	Resting Tremor	0
		Postural Tremor	1
		Action Tremor	3
		Handwriting	3
		Drawing: Archimedes Spiral	3
		Pouring	4
		Drinking/Eating Soup	4
		Keyboard	2
		Total Score	20
5	500	Resting Tremor	0
		Postural Tremor	1
		Action Tremor	2
		Handwriting	1
		Drawing: Archimedes Spiral	1
		Pouring	3
		Drinking/Eating Soup	3
		Keyboard	1
		Total Score	12
15	1500	Resting Tremor	0
		Postural Tremor	1
		Action Tremor	2
		Handwriting	2
		Drawing: Archimedes Spiral	1
		Pouring	4
		Drinking/Eating Soup	3
		Keyboard	1
		Total Score	14
25	2000	Resting Tremor	0
		Postural Tremor	1
		Action Tremor	2
		Handwriting	2
		Drawing: Archimedes Spiral	2
		Pouring	4
		Drinking/Eating Soup	3
		Keyboard	1
		Total Score	15

Table 8-7

Functional Testing Results By Functional Task Subject B

Functional Test	Damping Level Axes 1-3	Axes 4-6	Score
Resting Tremor	0	0	0
	5	500	0
	15	1500	0
	25	2000	0
Postural Tremor	0	0	1
	5	500	1
	15	1500	1
	25	2000	1
Action Tremor	0	0	3
	5	500	2
	15	1500	2
	25	2000	2
Handwriting	0	0	3
	5	500	1
	15	1500	2
	25	2000	2
Drawing: Archimedes Spiral	0	0	3
	5	500	1
	15	1500	1
	25	2000	2
Pouring	0	0	4
	5	500	3
	15	1500	4
	25	2000	4
Drinking/Eating Soup	0	0	4
	5	500	3
	15	1500	3
	25	2000	3
Keyboard	0	0	2
	5	500	1
	15	1500	1
	25	2000	1

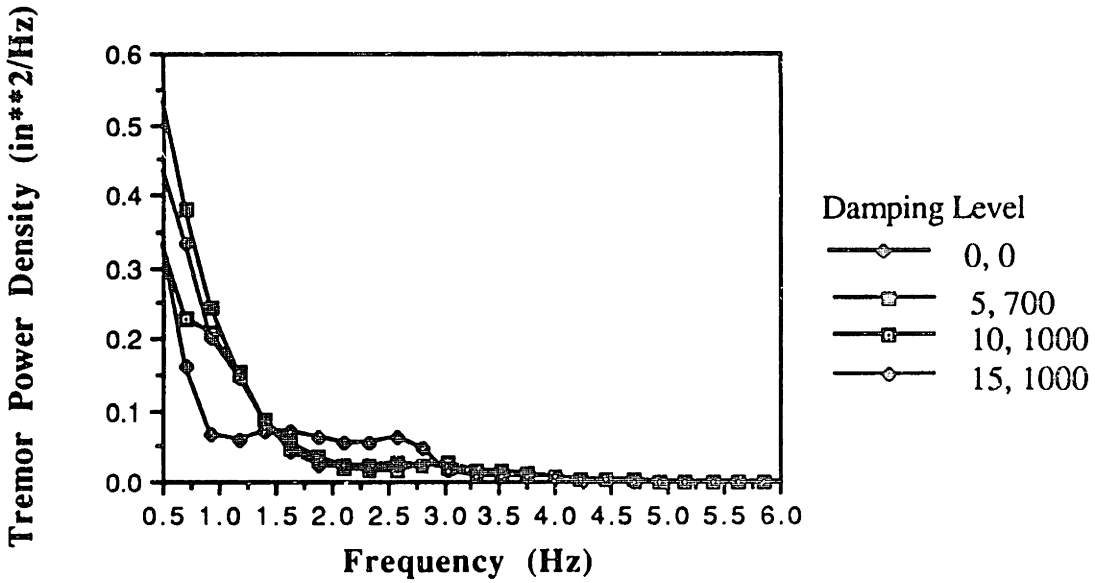

Figure #8-13. Subject B's tremor power density in the X-direction

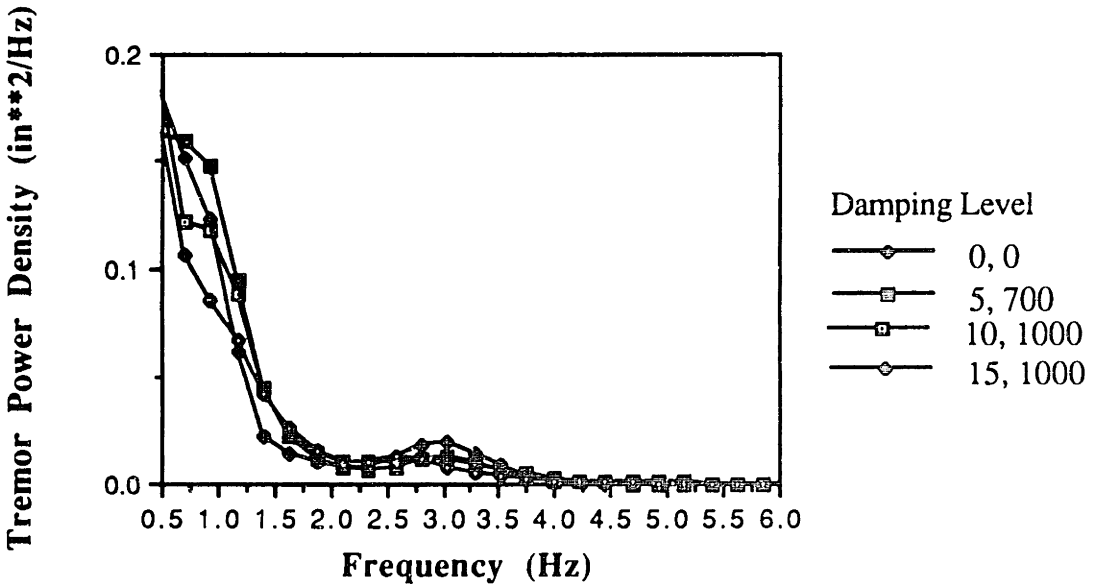

Figure #8-14. Subject B's tremor power density in the Y-direction

Table 8-8

Summary Table for Subject B's Abstract Experiment Performance

Direction	Damping Level	Tremor Peak Frequency	Tremor Power	Signal to Noise Ratio
X	0, 0	2.6 Hz	.164 in**2	179
	5, 700	2.6	.225	133
	10, 1000	3.0	.191	154
	15, 1000	2.8	.197	152
Y	0, 0	2.6	.086	166
	5, 700	2.8	.114	121
	10, 1000	3.0	.1	137
	15, 1000	3.0	.096	142

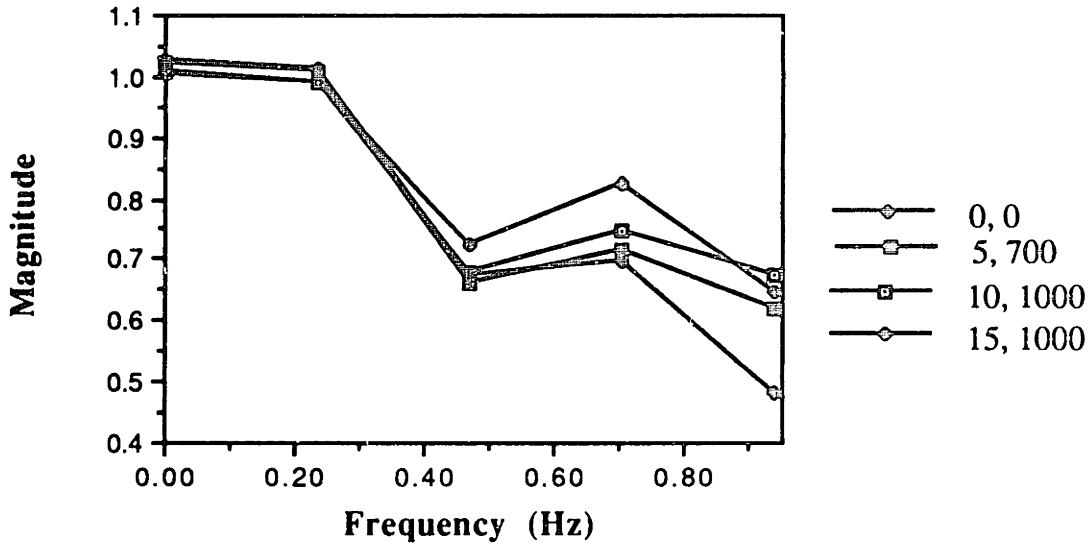

Figure #8-15. Subject B's transfer function magnitude in the X-direction

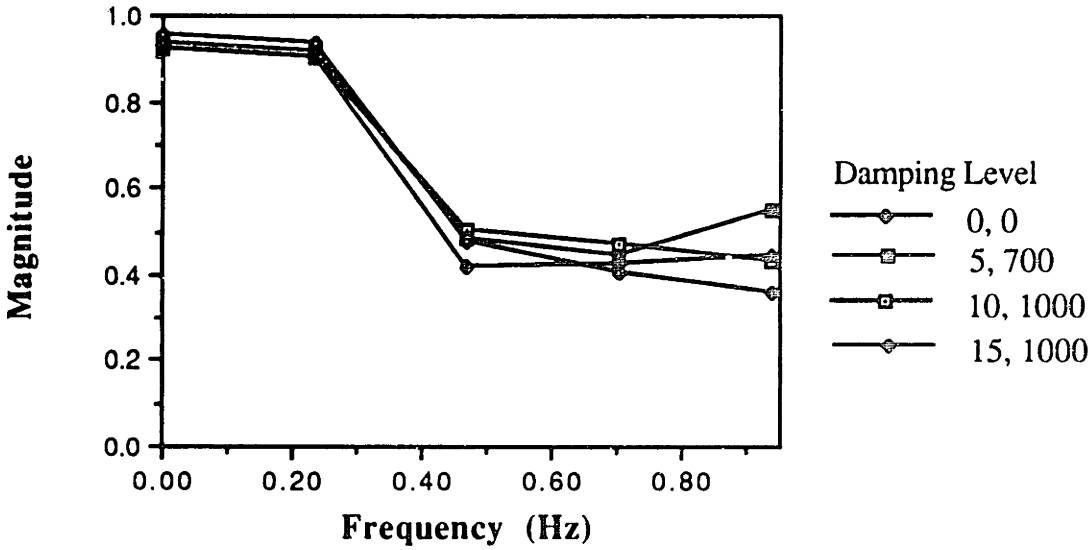

Figure #8-16. Subject B's transfer function magnitude in the Y-direction

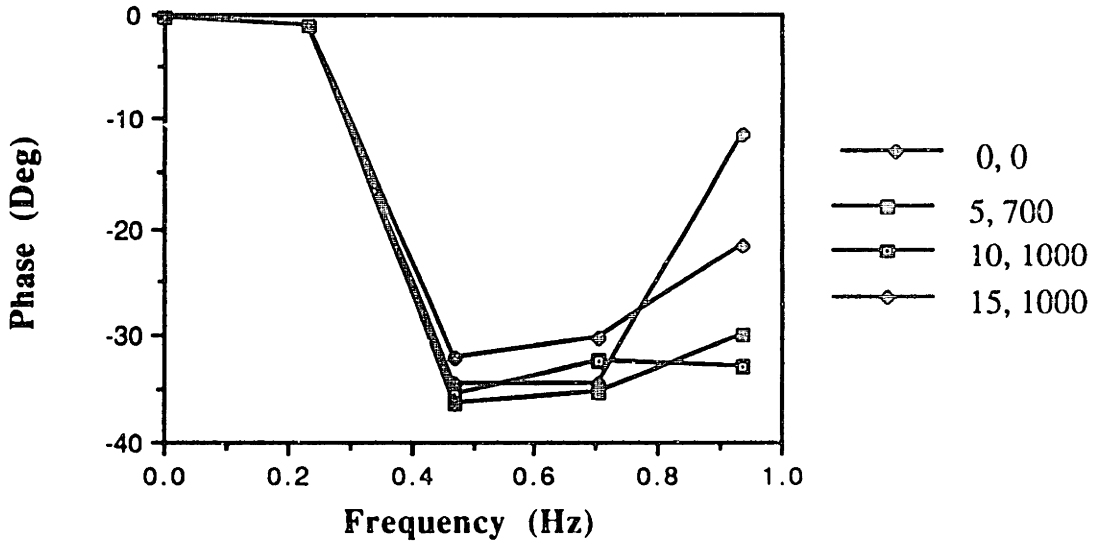

Figure #8-17. Subject B's transfer function phase in the X-direction

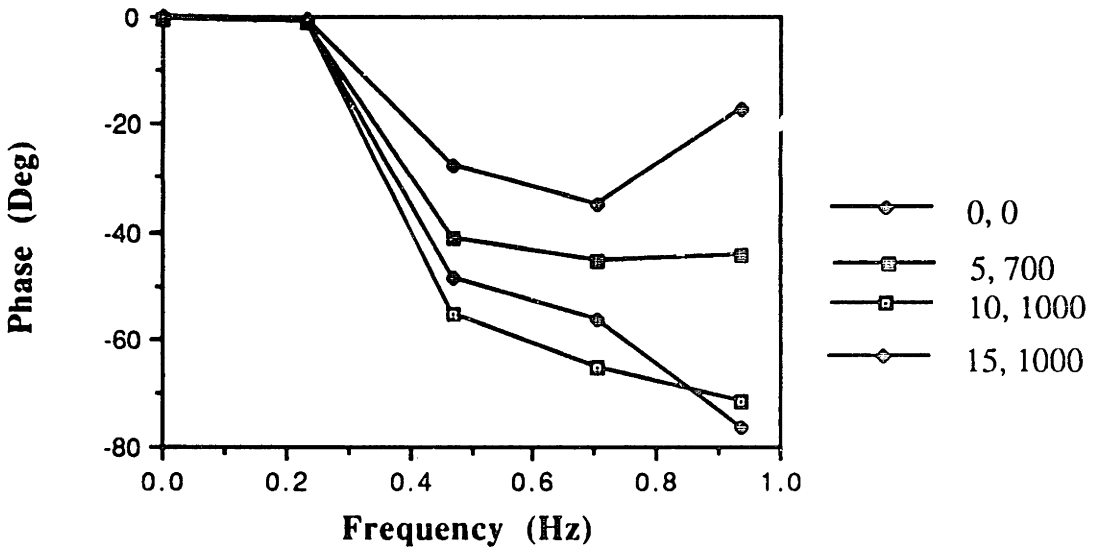

Figure #8-18. Subject B's transfer function phase in the Y-direction

Summary and Discussion of Results

Both subject A and subject B had reduced (i.e. improved) scores in the functional tests when damping was increased above the zero level. Subject A's results show that his score continued to improve (the score went down) as the damping level increased. Subject B, however, had a large score improvement when the damping levels were adjusted from 0-5,500 but as the damping parameter values were increased above this level, his overall functional test score declined.

When comparing specific functional tests, neither subject showed improvement in the resting tremor or postural tremor tests. In the action tests, however, both subjects showed improvement. Again, in the handwriting and drawing tests, neither subject showed improvement. Mild improvements were seen in the pouring test and the eating/drinking soup tests showed major improvements for subject A and minor improvements for subject B, as the damping level was increased. Finally, in the keyboard tests, both subjects showed significant improvement as we increased the damping level.

In the abstract pursuit-target-tracking-task experiments, both subject A and subject B showed significantly larger tremor power densities than did subject N. Subject B, for instance, showed over twenty times subject N's tremor power density magnitude for much of the frequency range. While subject N showed no peak frequencies and had a significant attenuation slope, subject A showed significant peaks in the 1 Hz range and subject B showed a peak in the 2.5-3 Hz range.

While all three subjects showed consistent transfer function magnitude plots across the entire damping range, the intersubject similarities were few. Subject N stayed within the .85-1.15 range of magnitude, while subject B had a significantly reduced magnitude, down to approximately .5 at its lowest point. Subject A had a reduced magnitude at

increased frequency in the Y direction, but in the X direction, he had a magnitude of above 1 for most of the damping levels at most of the frequencies.

The transfer function phase plots, on the other hand, showed consistent intersubject patterns, but subjects A and B had significantly greater phase delays than did subject N.

Chapter 9

Accomplishments and Further Work

Summary

This thesis has described the analysis, development, and testing of a six-degree-of-freedom MED manipulator system used as an orthosis simulator for the study of whole-arm tremor. Our theoretical analysis includes the development of a general theory for modulated-energy-dissipation spatial devices (manipulators). The development includes examples of both revolute and cartesian manipulators.

The manipulator linkage design is a 6R serial link device. The three distal degrees of freedom are arranged in the form of a novel gimbal configuration. Two of the proximal degrees of freedom are mechanically coupled through a four bar mechanism providing, in effect, two rotations and a near-prismatic joint. This design was driven largely by our goal of building a system with a diagonal Jacobian matrix partitions to provide end-point force-velocity colinearity. The manipulandum applies its 6-dof load at a single point of attachment to the human forearm. The orthosis simulator system incorporates the MED manipulator, control electronics, control software run on a PC/AT computer, a display for target tracking experiments, and a specially designed subject support chair.

Initial experimental results have been obtained with two tremor-impaired subjects and one able-bodied subject. While the results from the viscous loading experiments are not statistically significant, they appear to validate the concept of loading the arm of a tremor subject with MED loads.

Specific Accomplishments

This program of analysis, design, and research contributes theoretically and experimentally to the development of controlled orthotics meant to reduce the difficulty encountered by tremor-disabled individuals in performing the tasks of daily living. Specifically, our research extends previous work in three ways:

1) It is directed toward managing tremor in six degrees of freedom,
2) It is more theory-based than previous work directed at MED device design, and
3) It develops a novel linkage design based upon the theory developed.

Recommendations For Further Work

The work discussed in this thesis answers few of the many questions related to MED manipulator design, linkage development, and tremor management. Recommendations for further work along these dimensions are included here.

Theoretical Development

The theory developed in chapter 3 is for the quasi-static case (we did not consider the inertial forces) with only one connection to the human arm except in the case of human joint space. This theory should be extended to the more dynamic case of linkage inertia and the more complex case of more than one connection to the human arm in the analysis. Asada and Youcef-Toumi (1987) have researched the area of invariant inertia tensors in robot manipulators and West (1986) has researched the area of braced manipulators which is a very similar concept to bracing the human arm. Their results are probably useful to the further development of MED manipulator theory.

Manipulator System Development

Linkage Development

The present theory suggests that to achieve force-velocity colinearity with simple MED manipulators, the manipulator linkage must produce orthogonal partitions of the actuator Jacobian matrix (the Jacobian matrix between actuator space and endpoint space). Further work should be undertaken to identify a set of manipulator designs which can achieve this desired end and attractive designs should be evaluated for possible development and use in future generations of MED manipulators. Cable drives, for instance, may be a way to couple axes and reduce the inertia of the device by moving the actuators to the base of the manipulator.

Display Development

Although the MED arm opposes tremor in six degrees of freedom, only two degrees of freedom were measured in the pursuit target tracking experiment. From the data analysis viewpoint, it would be interesting to analyze pursuit tracking of a target in at least three degrees of freedom. Choosing two-degree-of-freedom pursuit tracking tasks was motivated primarily by equipment and time constraints. It is very difficult for a person to perceive more than two degrees of freedom on a personal computer screen.

Various possible three degree-of-freedom display methods were considered including using size, rotation, tie lines, or color changes of the planar icons to unambiguously represent the third direction on the screen, using an RS-232C serial port connection to a Silicon Graphics IRIS workstation (as is done in the man-machine systems lab in this department) for high resolution pictorial representation of the icons; and using a physical object manipulated by a human as the target to eliminate the computer screen altogether.

All possible multi-degree-of-freedom display alternatives should be fully investigated (as part or all of a Masters or Ph.D. project). To this end, Willis (1990) is currently investigating three-degree-of-freedom pursuit target tracking tasks on an Amiga personal computer and is using our MED arm as a computer input device.

Specific Improvements on Current System

Possible improvements for the current MED manipulator system include the following:

1) Machining grooves in the pulleys will prevent the cables from rubbing and keep cables round. This should reduce coulomb friction and increase transmission stiffness and fatigue life.

2) The transmission box at the base of link 2 contains a electrical cable connected to the floating axis 2 particle brake (marked O in Figure 4-10) which rotates 720 degrees with respect to ground. Although we have not experienced any broken cables, it may be beneficial to substitute slip rings in the place of the electrical cable.

3) Many parts on the manipulator can be reduced in size and/or fabricated with new materials to make the manipulator lighter. Plastic composites have been dominating the recreational equipment materials industry for a number of years (Dreger, 1986; Dann, 1982). If the MED manipulator is redesigned using modern plastics, the manipulator would be approximately 1/3 lighter. Dvorak (1987) discusses many designs which have been made lighter and smaller using new material technology. Finite element analysis could be performed on the major structural parts of the manipulator to determine optimal materials, shapes, and sizes.

4) The computer/controller can be updated with a faster set of hardware so that closed loop control can be performed. One possible method of speeding up the computer is installing a single-board computer on the PC/AT bus to achieve parallel processing (see examples in Zheng and Chen, 1985; Ozguner and Kao, 1985).

5) The present position sensors are potentiometers. If a higher accuracy is desired, optical encoders should be considered. The digital optical encoders do not have the electromagnetic noise problems inherent in the analog nature of

potentiometers. While the present force/torque sensor is as accurate as commercial sensors, the design should be evaluated using a finite element analysis to optimized the sensitivity to all load types and possibly reduce the number of strain gages in the system.

Experimental Studies

Many tremor-impaired subjects should be tested with the current orthosis simulator. First, enough subjects should be tested with each of several tremor types to allow statistically significant results for the current viscous loading algorithm.

After complete knowledge of viscous loading is obtained, other load profiles should be considered based on tremor mechanism models (see Adelstein, 1981 or 1989 for an excellent summary of these). Load profiles of force output as a function of velocity squared, acceleration, and/or position are some of the many load types which can be considered.

Another dimension of research which should be considered is determining the functional difference between assistive devices having different numbers of axes, e.g., Does a patient need 6-dof or can he make do with a simpler device? Can tremor be better managed with a device of fewer degrees of freedom? The results from testing with different mechanical constraints could have differences because of such issues as leverage against a device (see West, 1986 for applications in the robotics field), the workspace chosen (small vs. large, vertical vs. horizontal), or the cognitive demand for the tremor-impaired subject of moving in a small number of degrees-of-freedom vs a large number.

A related experimental issue is the importance of force-velocity colinearity. As discussed in Chapter 3, simple testing with Adelstein's (1989) device yielded qualitative results suggesting an angle between force and velocity of more than ten degrees reduced the tracking performance of able-bodied subjects. Quantitative tests should be performed on both able-bodied and tremor-impaired subjects to determine tracking performance degradation, if any, as the force and velocity vector directions are changed.

Finally, the present MED manipulator system should be made available for other research groups interested in mechanical interactions between humans and machines, called virtual environments or telepresence by some (we discuss this area in Chapter 3). The main reason our device should be considered for these areas is that it is inherently safe, an attribute which should not be underestimated. As with our research, this attribute comes at the cost of reduced loading possibilities.

Another very promising area of research is in musculo-skeletal rehabilitation. Present commercial "dynamometer" exercise devices limit the rehabilitation workspace to one-degree-of-freedom. Our device could prove useful in rehabilitating multi-joint muscles or joints with more than one-degree-of freedom such as the biceps muscle or shoulder joint. The benefits of our device come with the reduced amount of time needed to set the device up for a particular treatment and with the increased complexity of movement offered with our device. Our device does, however, offer these advantages at the cost of only allowing energy dissipating loading of the human arm (the magnitude of this cost, however, is undetermined).

Bibliography

1) Adelstein, B.D., (1981), "Peripheral Mechanical Loading and the Mechanism of Abnormal Intention Tremor," S.M. Thesis, Department of Mechanical Engineering, MIT.

2) Adelstein, B.D., (1989), "A Virtual Environment System for the Study of Human Arm Tremor," Ph.D. Thesis, Department of Mechanical Engineering, MIT, June.

3) Adelstein, B.D., and M.J. Rosen, (1981), "The Effect of Mechanical Impedance on Abnormal Intention Tremor," Proceedings, 9th Annual Northeast Bioengin. Conf., Piscataway, New Jersey, March.

4) Adelstein, B.D., and M.J. Rosen, (1984), "Design of a Two-Degree-of-Freedom Manipulandum for Tremor Research," Proceedings, 6th Annual IEEE EMB Conf., Los Angeles, CA, pp 47-51.

5) Adelstein, B.D., and M.J. Rosen, (1987), "A Two-Degree-of-Freedom Loading Manipulandum for the Study of Human Arm Dynamics," Proceedings, ASME Winter Conf., Boston, MA, December.

6) American Academy of Orthopaedic Surgeons, (1975), Atlas of Orthotics, The C.V. Mosby Company, Saint Louis."

7) Antonsson,E.K. and Mann,R.W., (1989) "Automatic 6dof Kinematic Trajectory Acquisition and Analysis," Journal of Dynamic Systems and Control, Vol 111, March, pp 31-39.

8) As Complexity Rises, Tiny Flaws in Software Pose a Growing Threat," (1987), The Wall Street Journal, January 28, p1.

9) Asada, H., and Slotine, J.-J. E., (1986), Robot Analysis and Control, John Wiley and Sons, New York.

10) Asada, H., and Youcef-Toumi, (1987), Direct Drive Robots, Theory and Practice, The MIT Press, Cambridge, Massachusetts, pp 209-229.

11) Atkinson, W.D., Bond, K.E., and Wilson, K.R., (1977), "Computing With Feeling," Comput. & Graphics, Vol. 2, pp 97-103.

12) Baiges, I., (1988), "Tremor Analysis Software User's Instructions," unpublished manual, Department of Mechanical Engineering, M.I.T., May.

13) Barry Wright Corporation, Products For Flexible Automation, 700 Pleasant Street, Watertown, MA, 02172.

14) Beckwith, T.G., Buck, N.L., and Maragoni, R.D., (1982), Mechanical Measurements, pp 427-428, Addison Wesley, Reading.

15) Bejczy, A.K., and Salisbury, J.D., (1980), "Kinesthetic Coupling Between Operator and Remote Manipulator," Advances in Computer Technology, ASME, vol. 1, August.

16) Bennett, L., (1971-1974), Transferring Load to Flesh. Bull. Prosthetic Research.:
Part II. Analysis of Compressive Stress, BPR 10-16:45-63, Fall 1971.
Part III. Analysis of Shear Stress, BPR 10-17:38-51, Spring 1972.
Part IV. Flesh Reaction to Contact Curvature, BPR 10-18:60-67, Fall 1972.
Part V. Experimental Work, BPR 10-19:88-103, Spring 1973.
Part VI. Socket Brim Radious Effects, BPR 10-20:103-117, Fall 1973.
Part VII. Gel Liner Effects, BPR 10-21:23-53, Spring 1974.

17) Beringhause, S., (1988) "Viscously Damped Joystick for Proportional Control by Tremor Patients," S.M. Thesis, Department of Mechanical Engineering, M.I.T.

18) Brock, L.B., (1987) "Enhancing the Dexterity of a Robot Hand Using Controlled Slip," S.M. Thesis, Department of Mechanical Engineering, MIT, May.

19) Brookes-Smith, C.H.W., and J.A. Colls, (1939), "Measurement of Pressure, Movement, Acceleration and Other Mechanical Quantities by Electrostatic Systems," J. Sci. Inst. (London) 14:361.

20) Carter, B.C., J.F. Shannon, and J.R. Forshaw, (1945), "Measurement of Displacement and Strain by Capacity Methods," Proc. Instn. Mech. Engrs. 152:215.

21) Chaplin, J., Lueders, M., and Zhao, Y., (1987), "Three-Point Hitch Dynamometer Design and Calibration,: Applied Engineering in Agriculture, vol. 3, no.1, pp. 10-13.

22) Chesmond, C., (1982), Control Systems Technology, Edward Arnold Ltd., London.

23) "Chip by Intel Contains Flaw In Calculating," (1989), The Wall Street Journal, October 27, p.1.

24) Colgate, J.E., 1983, "The Design of a Dynamics Measuring Device," S.M. Thesis, M.I.T.

25) Corell, R.W. and Wijnschenk, M.J., 1964, "Design and Development of the Case Research Arm Aid," Report No. EDC 4-64-4, Case Institute of Technology and Highland View Hospital.

26) Dann, R.T., (1982), "Recreational Equipment: Technology Makes Good Times Better," Machine Design, pp. 54-62.

27) Denavit, J., and Hartenberg, R.B., (1955), "A Kinematic Notation for Lower-Pair Mechanisms Based on Matrices," ASME J. Appl. Mech., Vol. 23, pp 215-221.

28) Deringer, T.J., (1984), "The Real Challenge in Robotic Systems," Proceedings of the Human Factors Society, 28th Annual Meeting, San Antonio Texas, pp 107-111.

29) Dreger, D.R., (1986), "Plastics Dominate Sports, Recreational Equipment," Machine Design, pp. 76-82, December 11.

30) Dvorak, P.J., (1987), "Mechanical Components: Getting Lighter and Smaller," Machine Design, pp. 120-127, April 9.

31) Desmedt, J.E. Editor, (1978), Progress in Clinical Neurophysiology Volume 5: Physiological Tremor, Pathological Tremors and Clonus, Karger, New York.

32) Diffrient, N., Tilley, A.R., and Bardagjy, J.C., (1974), Humanscale 1/2/3, MIT Press, Cambridge.

33) Diffrient, N., Tilley, A.R., and Harman, D., (1981), Humanscale 1/2/3, MIT Press, Cambridge.

34) Dipietro, D.M., (1988), "Development of an Actively Compliant Underwater Manipulator," S.M. Thesis, Department of Mechanical Engineering, MIT.

35) Dubois, M., (1981), "Six Component Strain Gage Balances for Large Wind Tunnels", Experimental Mechanics, vol. 21, no. 11, pp 401-407.

36) Dunfee, D.E., (1979), "Suppression of Intention Tremor by Mechanical Loading," S.M. Thesis, Department of Mechanical Engineering, Massachusetts Institute of Technology, February.

37) Ewald, B., (1979), "The Development of Electron Beam Welded Strain Gaged Wind Tunnel Balances", Journal of Aircraft, vol. 16, no. 5, pp 349-352.

38) Fahn, S., Tolosa,E., and Marin, C., (1988) "Clinical Rating Scale for Tremor," from Parkinson's Disease and Movement Disorders, edited by Jankovic and Tolosa, Urban & Schwarzenberg, Baltimore-Munich, pp 225-234.

39) "Faults and Failures," (1987), IEEE Spectrum, August, p.17.

40) Findley, L.J., and Capildeo, R.C., (1984), Movement Disorders: Tremor, Oxford University Press, New York.

41) Fornoff, H. and Thornton, W.G., 1973, "Experimental Evaluation of Remote Manipulator Systems," Remotely Manned Systems: Exploration and Operation in Space, Proceedings of the First National Conference, California Institute of Technology, Pasadena, CA.

42) Franke, E.K., (1951), "Mechanical Impedance of the Surface of the Human Body," J. Applied Physiol., vol. 3, pp 582-590.

43) Gibson-Harris, S., (1987), "Looking For Trouble," Mechanical Engineering, June, pp 36-38.

44) Girard, D., (1986), "Development of Multicomponent Force Transfer Standards By ONERA for French BNM,: in Mechanical Problems in Measuing Force and Mass, ed. H. Wieringa, pp 1-12, Martinus Nijhoff, Dordrecht.

45) Goodwin, R.J., (1975), "An Extended Octagonal Ring Transducer or Use in Tillage Studies," J. of Agric. Eng. Res., vol. 20, pp 347-352.

46) Gray, W.E., and Pieper, D.L., (1973), "Implications of Non-Space Applications," Remotely Manned Systems: Exploration and Operation in Space, Proceedings of the First National Conference, California Institute of Technology, Pasadena, CA.

47) Hausdorff, J.M., (1988), "Gait Orthosis Combining Controllable Damping and Muscle Stimulation," S.M. Thesis, Department of Mechanical Engineering, MIT.

48) Hetenyi, M., (1950), Handbook of Experimental Stress Analysis. New York: John Wiley & Sons, Inc., 1950, p 287.

49) Hogan, N., (1980), "Mechanical Impedance Control in Assistive Devices and Manipulators," Proceedings of the Joint Automatic Control Conference, San Francisco, August, Vol. 1.

50) Hogan, N.,(1985),"The Mechanics of Multi-Joint Posture and Movement Control," Biological Cybernetics, vol. 52, pp 315-331.

51) Hollerbach, J.M., (1983), "Wrist-Partitioned Inverse Kinematic Accelerations and Manipulator Dynamics, Int. J. Robotics Res., Vol 2.

52) Hollerbach, J.M., (1985), "Optimum Kinematic Design for a Seven Degree of Freedom Manipulator," Presented at the ASME WAM, Miami.

53) Huang, S. (1989), S.B. Thesis, Department of Mechanical Engineering, MIT.

54) Hull, M.L., and Davis, R.R., (1981), "Measurement of Foot Pedal Loads During Bicycling: I. Instrumentation," Journal of Biomechanics, Vol. 14, No. 12, pp 443-457.

55) Hunt, N.L., (1985), "Design of an Electrical Orthosis Joint Brake" S.M. Thesis, Department of Mechanical Engineering, MIT.

56) Johnson, E.G. and Corliss, W.R., 1967, "Teleoperators and Human Augmentation," NASA special report SP-5047.

57) Joyce, G.C., and P.M.H. Rack, (1974), "The Effects of Load and Force on Tremor at The Normal Human Elbow Joint," J. Physiol., Vol. 240, pp 375-390.

58) JR^3 Inc., 22 Harter Avenue, Suite 13, Woodland, CA 95695.

59) Kapandji, I.A., (1982), The Physiology of the Joints. Volume 1: Upper Limb, Churchill Livingstone, New York.

60) Karchak, A., Jr. and Allen, J.R., 1968, "Investigation of Externally Powered Orthotic Devices", Final Project Report V.R.A. Grant Rd-1461-m-67, Attending Staff Association of the Rancho Los Amigos Hospital, Inc., Downey, CA.

61) Karnopp, D., (1982), "Active Damping in Road Vehicle Suspension Systems," Vehicle System Dynamics, Vol. 12, pp 291-316.

62) Kazerooni, H., (1989), "Human/Robot Interaction via the Transfer of Power and Information Signals Part I: Dynamics and Control Analysis," Presented at the IEEE International Conference on Robotics and Automation, Scottsdale, Arizona, May.

63) Kenjo, T., and Nagamori, S., (1985), Permanent-Magnet and Brushless DC Motors, Clarendon Press, Oxford.

64) Krishna, C.M., and Shin, K.G., (1987), "Performance Measures for Control Computers,"IEEE paper# 0018-9286/87/0600-0467$01.00.

65) Leifer, L., (1981), "Rehabilitative Robots," Robotics Age, Vol. 3, No. 3, May/June.

66) Lord Corporation, Industrial Automation Division, 407 Gregson Drive, Cary, North Carolina 27511.Langer, B.F., (1943), "Design and application of a magnetic strain gage," SESA Proc. 1, 2:82.

67) Lovelace, E.C.F.,(1988), "The Design and Construction of a Test Bed for Semi-Active Loading of Arm Orthoses," S.B. Thesis, Department of Mechanical Engineering, MIT, May.

68) Luh, J.Y.S., Fisher, W.D., and Paul, R.P., (1983), "Joint Torque Control by a Direct Feedback for Industrial Robots," IEEE Transactions on Automatic Control, AC-28: 153-161, February.

69) Machine Design, (1986) Fluid Power Reference Issue, September 18.

70) Maki, B.E., (1982), "Modification of Spastic Gait Through Mechanical Damping," S.M. Thesis, Department of Mechanical Engineering, MIT.

71) Mansfield, J.M., (1988), "The Design of a Lightweight Elbow Prosthesis Emulator," S.M. Thesis, Department of Mechanical Engineering, MIT.

72) Margolis, D., (1982), "The Response of Active and Semi-Active Suspensions to Realistic Feedback Signals," Vehicle System Dynamics, Vol. 11, No. 6, pp. 267-282, December.Mark, J. W., and W. Goldsmith, (1955), "Barium titanate strain gages," SESA Proc. 13, 1:139.

73) Mason, W.P., and R.N. Thurston, (1957), "Use of piezoresistive materials in the measurement of displacement, force, and torque," J. Acoustical Soc. Am. 29.

74) McGorry, R., (1989), "Active Dynamometry in Quantitative Evaluation and Rehabilitation of Musculoskeletal Dysfunction," Assistive Technology, Vol. 1, no. 4, pp. 91-99.

75) Measurents Group, Inc., (1979), "Strain Gage Installations with M-Bond 200 Adhesive," Micro-Measurents Division, PO Box 2777, Raleigh, NC, 27611.

76) Millward, A. and Rossiter, J., (1983), "The Design of a Multi-Purpose Multi-Component Strain Guage Dynamometer," Strain, vol. 19, pp 27-30.

77) Molland, A.F., (1978) "A five-Component Strain Gauge Wind Tunnel Dynamometer," Strain, Vol. 14, no. 1, pp 7-13.

78) Mussa-Ivaldi, F.A., Hogan, N., and Bizzi, E., (1985),"Neural, Mechanical, and Geometric Factors Subserving Arm Posture in Humans," The Journal of Neuroscience, Vol. 5, No. 10, pp 2732-2743, October.

79) Nader, R., (1967), "The Engineer's Professional Role: Universities, Corporations, and Professional Societies," Engineering Education, February, pp 450-454.

80) NASA, 1987, "Controller for a High-Power, Brushless dc Motor," NASA Tech Briefs MFS-28168, Marshall Space Flight Center, Alabama.

81) Nickel, V.L., 1964, "Investigation of Externally Powered Orthotic Devices," Final Project Report V.R.A. Grant RD-518, Attending Staff Association of the Rancho Los Amigos Hospital, Inc., Downey, CA.

82) Nyborg, W.L., (1975), Intermediate Biophysical Mechanics, Cummings Publishing Company, Reading MA, chapter 12.

83) Ono, K. and Gatamura, Y., (1986)," A New Design for 6-Component Force/Torque Sensors," in Mechanical Problems in Measuring Force and Mass, ed. H. Wieringa, pp. 39-48, Martinus Nijhoff, Dordrecht.

84) Oomens, C.W.J., Grootenboer, H.J., and Van Campen, D.H., (1983), "A Non-Linear Two-Phase Model for Skin and Subcutaneous Fatty Tissue," 1983 Biomechanics Symposium, The American Society of Mechanical Engineers, pp 121-124.

85) Otway, H., and Haastrup, P., (1989), "On the Social Acceptability of Inherently Safe Technologies," IEEE Transactions on Engineering Management, Vol. 36, No. 1, pp 57-60.

86) Ozguner, F., and Kao, M.L., (1985), "A Reconfigurable Multiprocessor Architecture for Reliable Control of Robotic Systems," IEEE paper #CH2152/0000/0802$01.00.

87) Papadopoulos, J.M., (1987),"Forces in Bicycle Pedalling," Biomechanics in Sport, ASME.

88) Paul,R.P., (1981), Robot Manipulators: Mathematics, Programming, and Control MIT Press, Cambridge.

89) Paul,R., Renaud, M., and Stevenson, C.N., (1983) "A Systematic Approach for Obtaining the Kinematics of Recursive Manipulators Based on Homogeneous Transformations," Robotics Research, Brady and Paul, ed., M.I.T. Press, Cambridge, pp 707-726.

90) Perry, C.C., and H.R. Lissner, (1962), "The Strain Gage Primer," 2nd. ed. New York, McGraw-Hill Book Co., p 157.

91) Phillips, J.R., and Johnson, K.O., (1981), "Tactile Spatial Resolution. III. A Continuum Mechanics Model of Skin Predicting Mechanoreceptor Responses to Bars, Edges, and Gratings," Journal of Neurophysiology, Vol. 46, No. 6, December, pp 1204-1224.

92) Pieper, D.L., (1968), "The Kinematics of Manipulators Under Computer Control," Doctoral Dissertation, Stanford University.

93) Quinn, T.P., and Mote, C.D., (1988), "Optimal Design of an Uncoupled Six Degree of Freedom Dynamometer," Dept. of Mech. Eng., UC Berkeley.

94) Rahimi, M., (1984), "System Safety Approach To Robotic Safety," Proceedings of the Human Factors Society, 28th Annual Meeting, San Antonio Texas, pp 102-106.

95) Redford, J.B., (1980), Orthotics Etcetera, Second Edition, Williams & Wilkins, Baltimore.

96) Regan, K. and Reuber, M., (1985) "3-D Force-Sensing Robot Hand," in Proceedings of the 1985 ASME International Computers in Engineering Conferenceand Exhibition, ed. R. Raghavan, S.M. Rogde, vol. 1, pp 165-167, ASME, New York, August.

97) Riley, P.O., and M.J. Rosen, (1987), "Evaluating Manual Control Devices for Those with Tremor Disability," Journal of Rehab. Res. and Develop., pp 99-110, Spring.

98) Ripperger, E.A., (1954), "A piezoelectric strain gage," SESA Proc. 12, 1:117.

99) Robson, J.G., (1959), "The Effect of Loading on The Frequency of Muscle Tremor," J. Physiol., Vol. 149, pp 29-30.

100) Rosen, M.J., (1986), personal conversation.

101) Russo, M.A., Current S.M. Research, Department of Mechanical Engineering, MIT.

102) Salisbury, J.K., (1980),"Active Stiffness Control of a manipulator in Cartesian Coordinates," IEEE Conf. Decision and Control, Albuquerque, New Mexico, November.

103) Schultz, M.J., (1987), "Proliferating Hospital Testing Devices," IEEE paper #0278-6648/87/1200-0012$01.00.

104) Schwartz, M. M., 1984, Composite Materials Handbook, McGraw Hill, New York, pp. 7.85-7.98. Schwartz, M. M., 1984, Composite Materials Handbook, McGraw Hill, New York, pp 7.85-7.98.

105) Shaw, M.C., (1984), Metal Cutting Principles, Clarendon Press, Oxford.

106) Sheingold, D.H., editor, (1980), Analog-Digital Conversion Notes, Analog Devices, Norwood, Massachusetts, pp 115-118.

107) Shigley, J.E., and Mitchell, L.D., (1983), Mechanical Engineering Design, McGraw-Hill Book Company, New York.

108) Showers, D.C., and Strunck, M.L., (1985), "Sheet Plastics and Their Applications in Orthotics and Prosthetics," Orthotics and Prosthetics, Vol. 38, No 4, pp 41-48.

109) Simonson, E., Snowden, A., Keys, A., and Brozek, J., (1949), "Measurement of Elastic Properties of Skeletal Muscle in Situ," J. Applied Physiol., Vol. 1, pp 512-525.

110) Smith, M.J., (1988), "Tactile Interface for 3-Dimensional Computer-Simulator Environments: Experimentation and the Design of a Brake-Motor Device," S.M. Thesis, Department of Mechanical Engineering, MIT, June.

111) Spotts, M.F., (1985), Design of Machine Elements, Prentice-Hall, Inc., New Jersey.

112) Stapleton, S.R., (1982), "Damped Arm Restraint for Tremor Patients," S.B. Thesis, Department of Mechanical Engineering, MIT, May.

113) "Subway Door Problem No Open and Shut Case," (1987), The New York Times, April 19, p E6.

114) Takase. K., Inoue, H., Sato, K., Hagihara, S., (1974) "The Design of an Articulated Manipulator with Torque Control Ability," proc. IRIR4, Tokyo, Japan.

115) Tani, Y., Hatamura, Y., and Nagao, T., (1983), "Development of Small Three Component Dynamometer for Cutting Force Measurement," Bulletin of the Japanese Society of Mechanical Engineers, vol. 26, no. 214, pp 650-658.

116) Tenney, C.G., and Lisak, J.M., (1986), Atlas of Hand Splinting, Little, Brown and Company, Boston.

117) "The Case Against Active Robotics in Rehabilitation," Cybex Division of Lumex, Inc. advertisement. Cybex, 2100 Smithtown Avenue, Ronkonkoma, NY 11779.

118) Thompson, B.S., and Sung, C.K., (1985), "The Design of Robots and Intelligent Manipulators Using Modern Composite Materials," Mechanism and Machine Theory, vol. 20, no. 6, pp. 471-482, 1985.

119) Townsend, W.T., (1988), "The Effect of Transmission Design on Force-controlled Manipulator Performance," Ph.D. Thesis, Department of Mechanical Engineering, MIT.

120) TRAX, (1986), "The Roto-Lok® Rotary Drive System," TRAX Instrument Corporation promotional brochure, 10100 Cochiti Road SE, Albuquerque, NM, 87123.

121) Vilis, T. and J. Hore, (1977), "Effects of Changes in Mechanical State of Limb on Cerebellar Intention Tremor," J. Neurophysiol., Vol. 40, pp 1214-1224.

122) Vijaykumar,R., Tsai,M.J., and Waldron,K.J., (1985) "Geometric Optimization of Manipulator Structures For Working Volume and Dexterity," IEEE paper number CH2152-7/85/0000/0228$1.00.

123) Von Gierke, H.E., Oestreicher, H.L., Franke, E.K., Parrack, H.O., and Von Wittern, W.W., (1952)," Physics of Vibrations in Living Tissues," J. Applied Physiol., vol 4, pp 886-900.

124) Vukobratovic, M., Hristic, D. and Stoljiljkovic, Z., 1975, " Application of Active Exoskeletons in the Rehabilitation of Handicapped Persons," Proceedings of 5th Symp. on External Control of Extremities, ETAN, Yugoslavia, Dubrovnik.

125) Vykukal, H.C., 1971, "Exoskeletal Techanology," Technology and the Neurologically Handicapped, a conference sponsored by NASA and the United Cerebral Palsy Foundation, Ames Research Center, Moffet Field, CA.

126) Vykukal, H.C., King, R.F., and Vallotton, W.C., 1973, "An Anthropomorphic Master-Slave Manipulator System," Remotely Manned Systems: Exploration and Operation in Space, Proceedings of the First National Conference, California Institute of Technology, Pasadena, CA.

127) Watson, P.C. and Drake, S.H., (1978), "Method and Apparatus for Six Degree of Freedom Force Sensing," U.S. Patent No. 4,094,192, June 13.

128) West, H., (1986), "Kinematic Analysis for the Design and Control of Braced Manipulators," Ph.D. Thesis, Department of Mechanical Engineering, MIT, June.

129) Wheatstone, C. (1843), "An account of several new instruments and processes for determining the constants of a voltaic circuit," Phil. Trans. Roy. Soc., (London) 133:303.

130) Whitbeck, C., (1987), "The Engineer's Responsibility For Safety: Integrating Ethics Teaching Into Courses In Engineering Design," Presented at the ASME Winter Annual Meeting, Boston, December.

131) Whitney, D.E., (1969), "Resolved Motion Rate Control of Manipulators and Human Prostheses," IEEE Transactions on Man-Machine Systems, Vol. 10, No. 2, June, pp 47-53.

132) Willis, D.M. Jr., (1991) S.M. Thesis work in progress, Department of Mechanical Engineering, MIT.

133) Wire Rope Users Manual, Second Ed., (1981), American Iron and Steel Institute, Washington, D.C., 1981.

134) Woolnough, R., (1988), "The Viper: Developers Pushed by Impending Sense of Danger," Electronic Engineering Times, March 14, pp 55-60.

135) Wong, J., (1990), S.B. Thesis, Department of Mechanical Engineering, MIT, May.

136) Wunderly,G.,andHull,M.L.,(1985),"ANewElectromechanical Binding/Dynamometer for Actively Controlled Snow Ski Binding Systems," Skiing Trauma and Safety, STP 938, ASTM, Philadelphia, pp. 249-259.

137) Zheng, Y.F., and Chen, B.R., (1985), "A Multiprocessor for Dynamic Control of Multilink Systems," IEEE paper #CH2152-7/85/0000/0295$01.00.
Papadopoulos, J.M., (1987),"Forces in Bicycle Pedalling," Biomechanics in Sport, ASME.

Appendix A
Computer Program Descriptions

This appendix summarizes the programs used to help calibrate and control the manipulator and experiment on human subjects. The programs are broken into four broad categories; low-level programs to diagnose problems with the manipulator, calibration programs to give physical meaning to the electrical signals entering the computer, control programs to control the manipulator and perform experiments on human subjects, and data reduction programs to manipulate and evaluate the human subject experiment data.

Low-level programs

check

This program allows the researcher access directly to the I/O data. The researcher can choose from any of three methods of viewing the data from the A/D converters in real time or choose to output data through any of the D/A output lines. The user chooses one of the four functions by pressing the correct option number.

Option one allows the user to view the raw input data from the A/D converters in units of LSBs. The computer inputs the data from all twenty A/D converters used by the manipulator and displays the data on the computer screen. The computer then inputs the data again and displays the new data on the computer screen. The effect is similar to having nineteen digital multi-meters displaying voltages with approximately a one Hertz refresh rate.

Options two and three give the researcher the same information as option one, but with different units. The units for option two is voltage and the units for option three is physical values corresponding to the voltages (radians, radians/second, etc.).

Finally, option four allows the researcher to output data, in LSBs, through any of the six D/A channels.

This program proved to be one of the most useful programs during the manipulator development, used to diagnose an assortment of problems including broken wires, electrical shield problems, and cold solder joints.

stiff

This program makes the manipulator stiff. It does this by energizing each of the particle brakes to one-half of maximum.

flabby

This program makes the manipulator flabby. It does this by turning off all the particle brakes.

Calibration Programs

fcal (force calibration)

This program is used to calibrate the force/torque sensor. The sensor should be mounted to the calibration apparatus before executing this program. The program is run once for each pure load (Fx, Fy, Fz, Mx, My, Mz) and the output from the program is one column of the force/torque sensor calibration matrix, $\mathbb{K}$, and the corresponding coefficients of determination, R^2. See the system characterization chapter for a more complete description of the calibration.

pcal (potentiometer calibration)

This program is used to calibrate the potentiometer positions. The program allows any combination of potentiometers to be calibrated. For instance, if axis three is dissassembled for maintenance, it will need to be recalibrated before the manipulator is controlled again. This program will allow the researcher to calibrate only axis three. The program calculates the slope and offset coefficients and puts the data in data file pcal.dat in the format:

axis 1 offset axis 1 slope axis 2 offset axis 2 slope ...axis 6 offset axis 6 slope

offsets

This program enters the voltages corresponding to each the velocity and force/torque channel and puts the information in the data file offsets.dat in the format

velocity #1 #2 #3 #4 #5 #6 force/torque #1 #2 #3 #4 #5 #6 #7 #8

This data is collected when the manipulator is not moving. The data is used to subtract out small voltage drifts which may occur in the system.

Control Programs

dampval

This program allows the researcher to update the values of the damping coefficients for each of the six axes. The data is written to the data file dampval.dat in the format:

b_1 b_2 b_3 b_4 b_5 b_6

control

This program controls the manipulator and allows the values of the damping coefficients to be changed. The damping values are changed by pressing a key representing the axis number and the direction (higher or lower). For instance, pressing the *1* key will make b_1 decrement by one unit while pressing the *shift 1* key will make b_1 increment by one unit.

scontrol (save control)

This program controls the manipulator and saves the data from the 19 input channels for 20 seconds at a 60 Hz. sampling rate. The program does not produce a target.

target

This program produces the data file for the pursuit target tracking task using a summation of sine waves for each of the two degrees of freedom. This program allows the user to adjust the offset angle and direction for each of the axes. This allows the user a very large number of independent target trajectories. The output file is named target.dat and each row of the target file has the format:

Target X *Target Y*

Each row of the data file is a single data point, and the program enters 3600 rows, enough for 60 seconds worth of data at a 60 Hz. control frequency. The target data is in computer screen coordinate in units of pixels. The computer screen is 640 pixels in the horizontal direction, X, and 350 pixels in the vertical direction, Y.

scaling

This program produces the mapping file from manipulator coordinates to computer screen coordinates. The program asks the researcher to move the end of the manipulator to where he would like the response cursor to appear in the upper left corner of the computer screen. Then, the program asks the researcher to move the end of the manipulator to where he would like the lower right corner to be. The data is stored in data file scaling.dat in the format:

max left position *max right position* *max top position* *max bottom position.*

Left, right, top, and bottom refer to the computer monitor positions. The value of each of the four parameters is the manipulator value which corresponds to the maximum length of travel in the direction of the parameter.

tcontrol (tracking control)

This program controls the MED manipulator and performs a two degree-of-freedom pursuit target tracking task in the manipulator Y and Z directions but does not save the data for later use. The program is intended to be used as a human subject practice program used for the subject to learn the task.

The program first enters data from a series of files. The target is entered from the data file target.dat, scaling data is entered from the file scaling.dat, potentiometer calibration data is entered from the file pcal.dat, offset data is entered from the file offset.dat, and damping values are entered from the file dampval.dat.

The target is a rectangle and the response is a + cursor. The program begins by allowing the subject to move the response icon around the screen while the manipulator is controlled. This allows the subject time to get acquainted with the damping level and the mapping from the movement of his arm to the movement of the response on the computer screen.

When any key on the computer keyboard is pressed, the target moves through the sequence dictated by the data from the file target.dat and the response moves to the point corresponding to the scaled manipulator endpoint position. After 60 seconds the end of the target data is reached and the program returns control to the computer operating system.

stcontrol (save tracking control)

This program is the same program as **tcontrol** except this program saves the target and response data along with the damping values in the data file track.dat in the format: The first row of the data file lists the damping levels for the experiment,

$$b_1 \quad b_2 \quad b_3 \quad b_4 \quad b_5 \quad b_6$$

Each of the remaining (3600) rows lists the time for the given data set and the data set

time i *target x* *target y* *response x* *response y*

where, for instance, *target x* refers to the x position of the target at time *i*. The data is in the computer screen coordinate system in units of pixels.

fstcontrol (force save tracking control)

This program is very similar to **stcontrol** except that this program saves the force sensor data in addition to the target and response position data. The force data is saved in the file force.dat in the format

Wheatstone output *#1* *#2* *#3* *#4* *#5* *#6* *#7* *#8*

tform

This program converts the file track.dat into the set of data files spectral requests to perform the spectral analysis. The program firsts asks the researcher whether he would like to form the X data or the Y data (only one dimension of data can be analyzed at once). There are three output data files from this program. Data file input_1.data has the following format for each of its 3600 rows:

target x or target y (depending on the direction the user requests)

Data file output.data has the following format for each of its 3600 rows:

response x or response y (again depending on the direction the user requests)

Data file time.data has in the first of its two rows:

sampling period

and in the second row:

nsize nseg npts nbits

The definitions of each of these parameters can be found in Baiges, 1988.

spectral

Fortran program written by Ivan Baiges. The program performs the spectral analysis algorithm developed by Adelstein, 1981. (For a complete description of the spectral software see Baiges, 1988.) The program inputs data from the files input_1.data, output.data, and time.data. The program produces the following data files:

AUTO_1.DATA	The input power spectrum
AUTO_Y.DATA	The output power spectrum
CROSS_AM.DATA	The cross power spectrum amplitude
CROSS_PH.DATA	The cross power spectrum phase
TRANS_AM.DATA	The system transfer function amplitude
COHER.DATA	The ordinary coherence function
TREMOR.DATA	The tremor power spectrum
FREQ.DATA	The frequencies used

More complete descriptions of these data files can be found in the reference.

combine

The spectral analysis software outputs a eight data files. This program takes the important information and combines it into one data file, spectral.dat. Each row of the output data file has the following format:

frequency tremor power transfer function amplitude transfer function phase

value

This program was adapted from the Baiges program **score**. The program is a spectral analysis postprocessor which calculates the tremor power, mean frequency, and signal-to-noise ratio which are all discussed in the data analysis chapter. The program uses data from the files tremor.data, frequ.data, cross_am.data, and auto_1.data. The results of the processing are only printed to the screen (they are not stored).

Appendix B

Human Subject Documents

This appendix includes the human subject informed consent form and subject questionnaires

Informed Consent Statement

Project Title: Suppression of abnormal involuntary movements by application of mechanical loads

Tremor Studies

We are interested in testing new methods of suppressing tremors and other unintentional movements in people who could use their limbs more effectively if these movements were reduced. We hope to determine whether such movements may be reduced by providing a brace for the affected limb which resists the muscles' "attempts" to move it in an undesirable way.

You may be asked to participate in one or two experiments. In Experiment One you will be asked to view a computer screen. Two markers will appear on the screen. One will move as your limb moves. The other will serve as a target and may move in an unpredictable way. Your limb will be fitted comfortably to an apparatus which measures its position and in some experiments resists your tremor. You will be asked to try to move your limb so as to make your marker keep up with the target. The resistance, when present, may make it easier for you to perform this task. Surface sensors measuring electrical activity of your muscles may also be applied.

Experiment Two has two parts. In the first, you will be asked to perform a task similar to playing a simple car racing video game. The computer screen will show a "wheelchair" (symbol) located at the bottom of the screen. Also on the screen will be a "track". Again, your limb will be fitted to an apparatus which measures its position and you will be asked to try to move the limb being tested in such a way as to make the "wheelchair" drive along the "track."

In the second part Experiment Two you will actually drive a powered wheelchair along a track marked with tape. on the laboratory floor. The track will be marked with masking tape. You will control the chair using a device identical to the one used in Part One. Again, in some experiments, it will apply a force which resists tremor. You will be asked to try to move the limb being tested in such a way as to steer the wheelchair along the track. The resistance, when applied, may make it easier for you to perform this task. Surface

sensors measuring electrical activity of muscles may also be applied in this experiment.

Both experiments will be performed repeatedly for a few minutes at a time. Between trials, you may rest as long and as frequently as necessary for your comfort. An experimental session will last at least an hour, counting breaks, but beyond that point their length and scheduling will be suited to your capacity and convenience.

Data from our equipment and other information obtained during experiments will be kept in a confidential file. If this information is used for education or published reports, your name will be withheld. Short sequences of video tape may be taken for our records if you consent, but this material will not be used for education or publication if you request that it be kept confidential.

Although much of the equipment we will be use is electronic in nature, no shock hazard is present. You may withdraw from participation in this study at any time. You are encouraged to ask questions and make comments or suggestions at any time. Your ideas will help us.

The goal of these studies is limited. We will not build a practical tremor-suppressing device for you to use in normal activities. If these experiments are successful, the design of such devices will have been helped by your participation. There are, at present, more conventional methods of treatment which might be appropriate for your movement disorder. It has not been conclusively demonstrated that the techniques to be tried in these experiments are useful alternatives to present methods of treatment.

I have fully explained to _____ the nature and
Subject/Parent/Guardian
purpose of the above procedure and will answer all questions to the best of my ability.

_____ _____
Date Investigators Signature

I have been satisfactorily informed of the above-described procedure and I agree to participate in these experiments.

In the unlikely event of physical injury resulting from participation in this research, I understand that medical treatment will be available from the M.I.T. Medical Department, including first aid, emergency treatment and follow-up care as needed, and that my insurance carrier may be billed for the cost of such treatment. However, no compensation can be provided for medical care apart from the foregoing. I further understand that making such medical treatment available, or providing it, does not imply that such injury is the investigator's fault. I also understand that by my participation in this study I am not waiving any of my legal rights*.

I understand that I may also contact the Chairman of the Committee on the Use of Humans as Experimental Subjects, Dr. George Wolf (MIT room 56-213, 253-6781), if I feel I have been treated unfairly as a subject.

*Further information may be obtained by calling the Institute's Insurance and Legal Affairs Office at 253-2822.

_____

Subject/Parent/Guardian

_____ _____

Date Witness to Signature

Questionnaires

Included on the attached pages are five questionnaires:

1) The first questionnaire is for the subject's clinician to fill out regarding the subject's medical history.

2) The second questionnaire is for the subject to fill out regarding his/her interpretation of how tremor affects Activities of Daily Living.

3) The third questionnaire is for the subject to fill out after he/she has experienced use of any of the devices we will be testing. The questionnaire is intended to help us design future devices.

4) The fourth questionnaire is for the subject to fill out after he/she has experienced use of one particular device, named the MED arm.

5) The fifth questionnaire is for the clinician to fill out after he/she has used the device in the clinic without our presence.

1
Clinician's Observations

Subject's Name _____

Clinician _____

Subject Data:

Sex: Male ___ Female ____ Age _____

Diagnosis:

Movements Affected By Tremor:

Previous Therapy and Results:

#2
Subject's Observations

Name _____

Does your tremor cause problems on a regular basis?
Please Rate 0-10 (Causes no problems= 0, Makes independent function impossible= 10). If a question does not apply to you, mark N/A.

Dressing

Shoes ____
Socks ____
Pants ____
Shirt ____
Coat ____
Tie ____
watch ____

Do and undo
Buttons ____
Zipper ____

Clothes on body
Tuck in ____
Adjust ____

Grooming

Turn taps ____

Plug in and out ____
Towel dry ____
Unscrew/replace toothpaste tube ____
Squeeze tube ____
Apply to brush ____
Wash hair ____
Apply bandage to cut ____
Apply ointments to skin generally ____

Brush teeth ____

Brush hair ____
Comb hair ____
Apply makeup ____
Shave ____

Preparing meals

Hold saucepan ____
lift lids ____
Stir contents of pan ____
Cut meat ____
Pull of lids ____
Use corkscrew ____
Pick up pans with handles ____

Pour ____
Shake ____
Undo milk container ____
Slice bread ____
Screw off lids ____

Pick up pans without handles ____
Peal banana ____
Peal orange ____

Eating

load spoon from plate or bowl ____
Unload spoon into mouth ____
Use fork for impaling ____
Use knife for cutting ____
Use knife for spreading ____
Stir with spoon ____
drink from glass ____
pouring from container ____
lift dishes ____
pass dishes ____

Cleaning dishes

Squeeze detergent ____
Stack china ____
Scrape dishes ____
Pour detergent ____
Rub dishes ____
Dry dishes with cloth ____

Reading

Get book or magazine from shelf ____
Hold book or magazine steady ____
Turn pages ____

Writing

write with pencil/pen ____
pick up paper from table ____
place in envelope ____
Type ____
Stamp envelope ____
fold paper ____
Seal envelope ____
Cut with scissors ____

Housework

Ironing ____
Folding clothes ____
Vacuum floor ____
Washing clothes ____
Sweep/mop floor ____

cupboards and drawers

Pull open/push shut ____

Other daily tasks

Unlock doors ____
Open doors with handle ____
Dialing telephone _____
Holding telephone receiver ____
Retrieve money, etc. from pockets ____
Retrieve wallet from pocket ____
Retrieve wallet from purse ____
Open/close windows ____
Wind and/or set watch ____
Replace lightbulb ____
Nailing with hammer ____

Comments

How would you feel about a device you could attach to your arm that would reduce the shaking in your arm?

3
Impressions of Assistive Device

Name _____

How did the device feel?

Was it comfortable?

What would you change or add to the device?

Were the connections to your arm comfortable?

Were you better able to control your arm when this device was resisting your tremor?

4

Impressions of MED arm

Name _____

Some of the following questions ask you to rate the question numerically from 0-10.
0= very negative
5= neutral
10= very positive

Please rate your overall impression of using the device (0-10): _____
Comments:

Please rate the appearance of the device (0-10): ____
Comments:

In those activities where you used the device, how do you feel it affected your performance?
(0-10): ____
Comments:

If you could improve the device in any way, what changes would you recommend?

Would you use this device at home for any activities? Y/N _____
If yes, in what activities?

Additional comments:

5
Clinical Evaluation Survey

Subject's Name _____

Clinician _____

Subject Data

Sex: Male · Female · Age ____

Diagnosis:

Briefly summarize how the device was used with this patient and what you were trying to accomplish:

What were the results?

Were any modifications or peripherals added to the device? Y/N: ____

Comments:

Please list the activities in which the client used the device. Indicate whether or not you feel the application was appropriate. For the appropriate activities, indicate how useful you think the arm was:

Activity	Appropriate (Y/N)	not useful=0 Useful=10